

**Characterization and functional analysis of the  
Artemisinin resistance protein Kelch13 in  
*Plasmodium falciparum***

**- DISSERTATION -**

**with the aim of achieving a doctoral degree at the  
Faculty of Mathematics, Informatics and Natural Sciences**

**Department of Biology  
Universität Hamburg**

**submitted by  
Sarah Scharf**

**Hamburg, 2021**

**Vorsitz der Prüfungskommission: Prof. Dr. Julia Kehr**

**1. Gutachter der Dissertation: Prof. Dr. Tim-Wolf Gilberger**

**2. Gutachter der Dissertation: Dr. Tobias Spielmann**

**Datum der Disputation: 25. Juni 2021**

# Eidesstattliche Versicherung

Hiermit erkläre ich an Eides statt, dass ich die vorliegende Dissertationsschrift selbst verfasst und keine anderen als die angegebenen Quellen und Hilfsmittel benutzt habe.

Sarah Scharf

Hamburg, 21. April 2021

Sarah Scharf

# Language certificate

I am a native speaker, have read the present PhD thesis and hereby confirm that it complies with the rules of the English language.

A handwritten signature in cursive script, appearing to read 'L. Welsh', with a horizontal line underneath the name.

Dr Laura Welsh  
Gold Coast, Australia  
19 April 2021

## Summary

The infectious disease malaria kills more than 400,000 people every year, mainly children younger than 5 years. The human malaria parasite *Plasmodium falciparum* is a unicellular parasite that belongs to the genus Apicomplexa. The parasite is transmitted to humans through the bite of an *Anopheles* mosquito. The following asexual reproduction of the parasite in erythrocytes of the human host cause the symptoms of the disease. Artemisinin and its derivatives (ART) are currently the most important agents for the control and treatment of malaria and are typically administered with a partner drug as an Artemisinin based combination therapy. ART are activated in the parasite by hemoglobin degradation products that result from host cell cytosol that the intracellular parasite endocytoses during blood stage growth. Alarmingly, since 2008, parasites with lower susceptibility to the drug (resistance) have emerged in Southeast Asia which has led to treatment failures and threatens recent success of malaria control. Artemisinin resistant parasites have single point mutations in a protein named Kelch13. The potential molecular mechanism of resistance was recently cleared up: less endocytic uptake of hemoglobin in resistant parasites leads to less hemoglobin that is available for digestion in the parasite and hence less artemisinin activation.

To gain insight into the function and cellular location of Kelch13, former studies performed dimerization induced quantitative DIQ-BioID experiments with Kelch13 wild type parasites and proteins in close proximity to Kelch13 were identified. These proteins co-located with Kelch13 in an unknown compartment. Beside proteins such as UBP1 and Eps15, most of the other Kelch13 compartment proteins were *Plasmodium* specific (designated as Kelch13 interaction candidates (KICs)). To better understand the involvement of the Kelch13-defined compartment in ART resistance, it was assessed in this thesis whether other Kelch13 interacting candidates (KICs) were also involved in resistance which would substantiate their involvement in the Kelch13 pathway. These experiments showed that the disruption of three of the non-essential KICs (MCA2-TGD, KIC4-TGD and KIC5-TGD) led to reduced susceptibility to ART. It was shown recently that inactivation of UBP1, Eps15 and KIC7 resulted in decreased susceptibility of the parasites to ART and together with the results of the KIC-TGD cell lines it can be concluded that the Kelch13 compartment is involved in ART resistance.

Furthermore, it is demonstrated in this thesis that the MCA2-TGD and KIC5-TGD parasites showed impaired fitness levels and that KIC7 and UBP1 are essential for parasite survival in ring as well as in trophozoite stages. Inactivation of KIC7 via knock sideways resulted in a similar phenotype to that of UBP1 inactivation when stage-specific parasite development was monitored using Giemsa smears, in support of a similar function of these proteins in parasite development. In contrast to KIC7 and UBP1, the data presented here also confirm previous findings that Kelch13 is essential for parasite survival in

ring stages only. Moreover, the data presented in this thesis shows that inactivation of KIC7 leads to increased vesicle formation or accumulation in the parasite, supporting the hypothesis that endolysosomal transport of vesicles to the digestive vacuole might be impaired after KIC7 inactivation. Additionally, the data indicate that less hemozoin is present upon KIC7 inactivation, giving further evidence that KIC7 is involved in endocytosis.

To further investigate the resistance causing mechanism and to assess how mutations in the Kelch13 protein influence ART resistance, it was determined whether a changed interaction profile of parasites with a resistance-conferring Kelch13 mutation could lead to resistance. Using DIQ-BioID experiments with the Kelch13 mutant parasites the interaction profile of mutated and wild type Kelch13 was compared. However, no notable differences were observed in the two cell lines, indicating that mutating Kelch13 does not change a specific interaction of the protein. Rather it was shown using quantitative immunoblot analysis and fluorescence intensity quantification that mutated Kelch13 is less abundant in the cell compared to wild type Kelch13. Moreover, using episomally expressed complementation constructs, it was shown in this thesis that increased Kelch13 abundance in resistant parasites leads to the loss of resistance. These findings indicated that Kelch13 protein levels influence resistance and gave evidence that mutated Kelch13 reduces its abundance and hence the overall Kelch13 activity per cell.

In order to better understand the cellular function of Kelch13 and to investigate the functions of the individual domains of Kelch13, constructs consisting of different Kelch13 domain combinations were episomally expressed on the resistant Kelch13 mutant background. The importance of the domains for the cellular localization of Kelch13 was determined by fluorescence microscopy and the ability of constructs to maintain the function of Kelch13 was assessed by determining the resistance level, assuming that a functional construct reverts the parasites to sensitivity. These experiments indicated that the *Plasmodium* specific N-terminus of Kelch13 promotes function and that the conserved C-terminus containing the Kelch propeller domain does not display a role in protein function but rather might act as a regulator of Kelch13 stability. Semi-quantitative Western Blot analysis indicated that episomal constructs containing the Kelch propeller domain have significantly higher abundance in the cell than constructs lacking the Kelch propeller domain. These findings suggest a function of the Kelch propeller domain as a regulator of protein abundance of Kelch13.

The data presented in this this thesis show that proteins of the Kelch13 defined compartment are involved in artemisinin resistance and that resistance is influenced by Kelch13 abundance. Furthermore, the data indicate that the N-terminal part of Kelch13 fulfills the function of the protein and the C-terminal part is a regulatory domain and influences Kelch13 abundance.

## Zusammenfassung

Die Infektionskrankheit Malaria tötet jedes Jahr mehr als 400.000 Menschen, wobei meistens Kinder unter 5 Jahren betroffen sind. Der menschliche Malariaerreger *Plasmodium falciparum* ist ein einzelliger Parasit, der zur Gattung der Apicomplexa gehört. Der Parasit wird durch den Stich einer *Anopheles* Mücke auf den Menschen übertragen. Die anschließende ungeschlechtliche Vermehrung des Parasiten in den Erythrozyten des menschlichen Wirts verursacht die Symptome der Krankheit. Artemisinin und seine Derivate (ART) sind derzeit die wichtigsten Medikamente zur Kontrolle und Behandlung von Malariainfektionen und werden typischerweise mit einem Partnerpräparat als Artemisinin-basierte Kombinationstherapie verabreicht. ART werden im Parasiten durch Hämoglobin-Abbauprodukte aktiviert, die aus dem Zytosol der Wirtszelle stammen, welches der intrazelluläre Parasit während des Wachstums im Blutstadium durch Endozytose aufnimmt. Alarmierender Weise sind seit 2008 in Südostasien Parasiten mit geringerer Anfälligkeit gegenüber dem Medikament (Resistenz) aufgetreten, wodurch es zu Behandlungsfehlern kommt und die bisherigen Erfolge der Malariakontrolle bedroht werden. ART-resistente Parasiten weisen Punktmutationen in einem Protein namens Kelch13 auf. Der mögliche molekulare Resistenzmechanismus wurde kürzlich aufgeklärt: Eine geringere Hämoglobinaufnahme in resistenten Parasiten führt zu einer geringeren Hämoglobinverdauung in der Zelle und damit zu einer geringeren ART-Aktivierung.

Um einen Einblick in die Funktion und die zelluläre Lokalisation von Kelch13 zu erhalten, wurden in früheren Studien mit Kelch13 Wildtyp Parasiten Dimerisierungs-induzierte quantitative BioID (DiQ-BioID) Experimente durchgeführt und Proteine in unmittelbarer Umgebung von Kelch13 identifiziert. Diese Proteine wurden gemeinsam mit Kelch13 in einem unbekanntem Kompartiment lokalisiert. Neben Proteinen wie UBP1 und Eps15 sind die meisten der anderen Proteine des Kelch13-Kompartiments *Plasmodium*-spezifisch (bezeichnet als Kelch13-Interaktionskandidaten (KICs)). Um die Beteiligung des Kelch13-definierten Kompartiments an der ART-Resistenz besser zu verstehen, wurde in dieser Arbeit untersucht, ob andere Kelch13-Interaktionskandidaten ebenfalls an der Resistenz beteiligt sind, was die Beteiligung am gleichen zellulären Prozess wie Kelch13 untermauern würde. Diese Experimente zeigten, dass die Trunkierung der Gene von drei der nicht-essentiellen KICs (MCA2-TGD, KIC4-TGD und KIC5-TGD) zu einer verminderten Anfälligkeit gegenüber ART führte. Kürzlich wurde gezeigt, dass die Inaktivierung von UBP1, Eps15 und KIC7 zu einer verminderten Anfälligkeit der Parasiten gegenüber ART führte und zusammen mit den Ergebnissen der KIC-TGD-Zelllinien kann daraus geschlossen werden, dass das Kelch13-Kompartiment an der ART-Resistenz beteiligt ist.

Des Weiteren wurde in dieser Arbeit gezeigt, dass die MCA2-TGD- und KIC5-TGD-Parasiten eine eingeschränkte Fitness aufweisen und dass KIC7 und UBP1 für das Überleben der Parasiten sowohl im Ring- als auch im Trophozoitenstadium essentiell sind. Die Inaktivierung von KIC7 durch Knock

Sideways führte zu einem ähnlichen Phänotyp wie die Inaktivierung von UBP1, wenn die stadienspezifische Parasitenentwicklung mit Giemsa-Ausstrichen analysiert wurde, was eine ähnliche Funktion dieser Proteine in der Parasitenentwicklung vermuten lässt. Im Gegensatz zu KIC7 und UBP1, bestätigen die in dieser Arbeit vorgestellten Daten zudem auch frühere Erkenntnisse, dass Kelch13 für das Überleben der Parasiten ausschließlich in Ringstadien essentiell ist. Zudem zeigte sich, dass die Inaktivierung von KIC7 zu einer vermehrten Akkumulation von vesikulären Strukturen im Parasiten führt, was die Hypothese unterstützt, dass der endolysosomale Transport von Vesikeln zur Verdauungsvakuole nach KIC7-Inaktivierung beeinträchtigt sein könnte. Zusätzlich deuten die Daten darauf hin, dass nach KIC7-Inaktivierung weniger Hämозoin vorhanden ist, was ein weiteres Indiz dafür ist, dass KIC7 an der Endozytose beteiligt ist.

Um den Resistenz-verursachenden Mechanismus weiter zu untersuchen und besser zu verstehen, wie Mutationen im Kelch13-Protein die ART-Resistenz beeinflussen, wurde ermittelt, ob ein verändertes Interaktionsprofil von mutierten Kelch13-Parasiten zur Resistenz führen könnte. Anhand von DIQ-BioID-Experimenten mit Parasiten, die eine ART-Resistenz vermittelnde Mutation in Kelch13 tragen, wurde das Interaktionsprofil von mutiertem und Wildtyp-Kelch13 verglichen. Es wurden jedoch keine nennenswerten Unterschiede in den beiden Zelllinien festgestellt, was darauf hinweist, dass die Mutation in Kelch13 keine spezifische Interaktion des Proteins verändert. Vielmehr wurde in dieser Arbeit mittels quantitativer Immunoblot Analyse und Quantifizierung der Fluoreszenzintensität gezeigt, dass mutiertes Kelch13 im Vergleich zu Wildtyp-Kelch13 weniger häufig in der Zelle vorkommt. Darüber hinaus wurde in dieser Arbeit mit Hilfe von episomal exprimierten Komplementierungskonstrukten gezeigt, dass eine erhöhte Kelch13 Proteinmenge in resistenten Parasiten zum Verlust der Resistenz führt. Diese Ergebnisse wiesen darauf hin, dass der Kelch13-Proteinspiegel die Resistenz beeinflusst und gaben Hinweise darauf, dass mutiertes Kelch13 die Kelch13-Proteinmenge und damit die gesamte Kelch13-Aktivität pro Zelle reduziert.

Um die zelluläre Funktion von Kelch13 besser zu verstehen und die Funktionen der einzelnen Domänen von Kelch13 zu untersuchen, wurden Konstrukte, die aus verschiedenen Kelch13-Domänenkombinationen bestehen, episomal auf dem resistenten mutierten Kelch13 Hintergrund exprimiert. Die Wichtigkeit der Domänen für die zelluläre Lokalisation wurde mittels Fluoreszenzmikroskopie bestimmt und die Fähigkeit der Konstrukte, die Funktion von Kelch13 aufrechtzuerhalten, wurde durch die Messung des Resistenzniveaus bestimmt, wobei davon ausgegangen wurde, dass ein funktionelles Konstrukt die Parasiten sensitiv gegenüber ART werden lässt. Diese Experimente zeigten, dass der *Plasmodium*-spezifische N-Terminus von Kelch13 für die Funktion des Proteins wichtig ist und dass der konservierte C-Terminus, der die Kelch-Propeller-Domäne enthält, keine Rolle bei der Proteinfunktion spielt, sondern möglicherweise als Regulator der Kelch13-Stabilität fungieren könnte. Semi-quantitative Western Blot Analysen gaben Hinweise darauf,

dass episomale Konstrukte, die die Kelch-Propeller-Domäne enthalten, signifikant höhere Kelch13-Proteinmengen aufweisen als Konstrukte, denen die Kelch-Propeller-Domäne fehlt. Diese Ergebnisse deuten auf eine Funktion der Kelch-Propeller-Domäne als Regulator der Proteinmenge von Kelch13 hin.

In dieser Arbeit wurde gezeigt, dass Proteine des Kelch13-definierten Kompartiments an der Artemisinin-Resistenz beteiligt sind und dass die Resistenz durch die Proteinmenge von Kelch13 beeinflusst wird. Außerdem deuten die hier vorgestellten Daten darauf hin, dass der N-terminale Bereich von Kelch13 die Funktion des Proteins erfüllt und der C-terminale Bereich eine regulatorische Domäne ist und die Kelch13-Proteinmenge beeinflusst.

# Table of contents

<b>Summary</b>	<b>iv</b>
<b>Zusammenfassung</b>	<b>vi</b>
<b>Table of contents</b>	<b>ix</b>
<b>List of figures</b>	<b>xiv</b>
<b>List of Tables</b>	<b>xvii</b>
<b>Abbreviations</b>	<b>xviii</b>
<b>1 Introduction</b>	<b>20</b>
<b>1.1 Malaria: a worldwide public health problem</b>	<b>20</b>
1.1.1 Historical background of the disease	20
1.1.2 Epidemiology of malaria	21
1.1.3 Human-pathogen <i>Plasmodium</i> species	22
1.1.4 Diagnosis of malaria	25
1.1.5 Transmission and Prevention	25
<b>1.2 <i>Plasmodium falciparum</i>: the malaria causing parasite</b>	<b>26</b>
1.2.1 The life cycle of <i>Plasmodium falciparum</i>	26
<b>1.2.1.1 The liver stage</b>	<b>27</b>
<b>1.2.1.2 Asexual blood stage development</b>	<b>27</b>
<b>1.2.1.3 Gametocytogenesis</b>	<b>29</b>
<b>1.2.1.4 The mosquito stage</b>	<b>30</b>
<b>1.3 Treatment of malaria infections</b>	<b>31</b>
1.3.1 Vaccine development	31
<b>1.3.1.1 Transmission-Blocking Vaccines</b>	<b>31</b>
<b>1.3.1.2 Anti-Infection Vaccines</b>	<b>32</b>
<b>1.3.1.3 Blood-Stage Vaccines</b>	<b>32</b>
1.3.2 Antimalarial drugs	33
<b>1.3.2.1 Quinine</b>	<b>33</b>
<b>1.3.2.2 Antifolates</b>	<b>33</b>
<b>1.3.2.3 Artemisinin (ART) - the front-line drug against malaria</b>	<b>34</b>
<b>1.4 The biology of <i>Plasmodium falciparum</i> parasites</b>	<b>35</b>
1.4.1 Cellular biology and protein export of <i>P. falciparum</i> parasites	35

1.4.2 Endocytosis in <i>P. falciparum</i> and the endolysosomal pathway .....	37
<b>1.5 Artemisinin resistance.....</b>	<b>38</b>
1.5.1 Emergence and distribution of ART resistance.....	38
1.5.2 Proteins associated with ART resistance.....	40
1.5.3 Kelch13 – the major ART resistance marker protein.....	41
1.5.4 The Kelch repeat superfamily .....	42
1.5.5 Potential ART resistance mechanisms .....	42
<b>1.6 Preliminary data on Kelch13 function and its role in ART resistance.....</b>	<b>43</b>
1.6.1 Studying Kelch13 function and role in resistance.....	44
1.6.2 Kelch13 defines an unknown compartment containing multiple unknown proteins .....	44
1.6.3 The role of Kelch13 and Kelch13 compartment proteins in endocytosis .....	46
<b>1.7 Aims of this thesis .....</b>	<b>48</b>
<b>2 Material and Methods .....</b>	<b>49</b>
<b>2.1 Material .....</b>	<b>49</b>
2.1.1 Bacterial and <i>Plasmodium</i> strains .....	49
2.1.2 Chemicals .....	49
2.1.3 DNA- and protein-ladders .....	51
2.1.4 Kits .....	51
2.1.5 Antibodies.....	51
2.1.6 Fluorescence dyes.....	52
2.1.7 Enzymes and polymerases.....	52
2.1.8 Oligonucleotides.....	52
2.1.9 Plasmids.....	52
2.1.10 Labware and disposables.....	53
2.1.11 Software and bioinformatics tools.....	54
2.1.12 Technical devices .....	54
2.1.13 Solutions and buffers for biochemical experiments .....	55
2.1.14 Solutions and buffers for microbiological culture.....	56
2.1.15 Solutions and buffers for molecular biological experiments.....	57
2.1.16 Solutions and buffers for cell biological experiments.....	58
<b>2.2 Methods .....</b>	<b>61</b>
2.2.1 Microbiological Methods .....	61
2.2.1.1 Sterilization of solutions and devices .....	61
2.2.1.2 Production of competent <i>E. coli</i> .....	61
2.2.1.3 Transformation of chemo-competent <i>E. coli</i> .....	61

---

2.2.1.4 Cultivation and storage of <i>E. coli</i> .....	61
2.2.2 Molecular biological Methods.....	62
2.2.2.1 Polymerase chain reaction.....	62
2.2.2.2 Agarose gel electrophoresis.....	63
2.2.2.3 PCR-product and plasmid purification.....	63
2.2.2.4 Restriction digest.....	64
2.2.2.5 Gibson assembly.....	64
2.2.2.6 Plasmid isolation .....	65
2.2.2.7 Sequencing of plasmid DNA.....	65
2.2.2.8 DNA precipitation .....	65
2.2.2.9 Nucleic Acid quantification.....	65
2.2.2.10 Genomic DNA isolation.....	65
2.2.3 Cell biological Methods .....	66
2.2.3.1 Continuous culture of <i>P. falciparum</i> .....	66
2.2.3.2 Cryo-stabilates of <i>P. falciparum</i> .....	66
2.2.3.3 Thawing procedure of <i>P. falciparum</i> cryo-stabilates .....	66
2.2.3.4 Blood smears and Giemsa staining.....	67
2.2.3.5 Transfection of <i>P. falciparum</i> .....	67
2.2.3.6 Selection for transgenic parasite cell lines using SLI.....	68
2.2.3.7 Sorbitol synchronization of <i>P. falciparum</i> .....	68
2.2.3.8 Percoll gradient of <i>P. falciparum</i> infected erythrocytes.....	68
2.2.3.9 Saponin lysis of <i>P. falciparum</i> infected erythrocytes.....	69
2.2.3.10 Biotin labeling of proteins using DIQ-BioID.....	69
2.2.3.11 Flow cytometry growth assay.....	70
2.2.3.12 Stage specific experiments upon knock sideways induction.....	70
2.2.3.13 In-vitro ring stage survival assay <sup>0-3h</sup> (RSA).....	71
2.2.3.14 Immunofluorescence assay (IFA) of transgenic parasites .....	71
2.2.3.15 Knock sideways induction.....	72
2.2.3.16 DiCre induction .....	72
2.2.4 Biochemical Methods.....	72

2.2.4.1 Western Blot analysis .....	72
2.2.5 Microscopy .....	74
2.2.5.1 Live cell and fluorescence microscopy .....	74
<b>3 Results</b>	<b>76</b>
<b>3.1 Functional analysis of Kelch13 compartment proteins</b> .....	<b>76</b>
3.1.1 Ring stage survival assays with KIC-TGDs.....	76
3.1.2 Impact of KIC-TGDs on parasite growth.....	77
3.1.3 Stage-specific phenotype after Kelch13, UBP1 and KIC7 inactivation.....	78
3.1.4 KIC7 inactivation leads to increased numbers of PI4P positive circular structures.....	87
<b>3.2 Investigation of the resistance causing mechanism</b> .....	<b>90</b>
3.2.1 DIQ-BioID with ART resistant K13C580Y <sup>endo</sup> parasites.....	90
3.2.2 Interactome comparism of K13WT <sup>endo</sup> and K13C580Y <sup>endo</sup> .....	92
3.2.3 Kelch13 abundance in K13C580Y <sup>endo</sup> parasites is reduced compared to K13WT <sup>endo</sup> parasites	93
<b>3.3 Functional analysis of Kelch13</b> .....	<b>95</b>
3.3.1 Kelch13 protein level influences resistance .....	95
3.3.2 Functional analysis of the Kelch13 domains.....	103
3.3.3 Influence of individual domains of Kelch13 for its abundance in the cell.....	123
<b>3.4 Functional analysis of a new K13C580Y<sup>endo</sup> integration cell line with a shortend homology region</b> .....	<b>128</b>
<b>4 Discussion</b>	<b>136</b>
<b>4.1 Kelch13 complex proteins are involved in resistance and endocytosis</b> .....	<b>136</b>
<b>4.2 Reduced Kelch13 protein level leads to resistance</b> .....	<b>139</b>
<b>4.3 Functional analysis of the Kelch13 domains</b> .....	<b>140</b>
4.3.1 Technical considerations .....	144
4.3.2 Further experiments to investigate the function of the Kelch13 domains.....	145
<b>4.4 Prevalence of Kelch13C580Y, resistance and fitness cost</b> .....	<b>147</b>
<b>4.5 A new Kelch13C580Y integration cell line with shortened homology region</b> .....	<b>148</b>
<b>4.6 Conclusion</b> .....	<b>149</b>
<b>5 References</b>	<b>150</b>
<b>Publications</b>	<b>168</b>
<b>Danksagung</b>	<b>169</b>
<b>Appendix</b>	<b>170</b>
<b>Appendix 1</b> .....	<b>170</b>

<b>Appendix 2 .....</b>	<b>171</b>
<b>Appendix 3 .....</b>	<b>176</b>
<b>Appendix 4 .....</b>	<b>176</b>
<b>Appendix 5 .....</b>	<b>179</b>
<b>Appendix 6 .....</b>	<b>180</b>
<b>Appendix 7 .....</b>	<b>180</b>

## List of figures

Figure 1. Map of malaria case incidence rate (cases per 1000 population at risk) by country in 2018 (WHO, 2019 a).....	21
Figure 2. Global trends in a) malaria case incidence rate (cases per 1000 population at risk), b) mortality rate from 2000 - 2019 (WHO 2020).....	22
Figure 3. The Incidence of <i>Plasmodium falciparum</i> and <i>Plasmodium vivax</i> Malaria in 2017. ....	24
Figure 4. Life cycle of <i>Plasmodium falciparum</i> parasites.....	26
Figure 5. Invasion process of merozoites in erythrocytes. ....	28
Figure 6. Asexual blood stage development of <i>P. falciparum</i> . ....	29
Figure 7. Sexual stage development of <i>P. falciparum</i> in the human host. ....	30
Figure 8. Schematic illustration of <i>P. falciparum</i> organelles, membranes and host cell modifications.....	35
Figure 9. Host cell cytosol uptake in <i>P. falciparum</i> .....	38
Figure 10. Frequency distribution of Kelch13 wild-type alleles in Asia (A) and worldwide (B).....	40
Figure 11. Schematic illustration of Kelch13.....	42
Figure 12. DIQ-BioID experiment with endogenously tagged K13WT <sup>endo</sup> parasites. ....	45
Figure 13. Kelch13-defined complex is involved in endocytosis and resistance.....	47
Figure 14. The Kelch13 complex proteins are involved in ART resistance. ....	48
Figure 15. Ring stage survival Assay with KIC-TGD parasites. ....	77
Figure 16. FACS based growth analysis with KIC-TGD parasites.....	78
Figure 17. Stage-specific phenotypes after inactivation of KIC7. ....	80
Figure 18. Stage-specific phenotypes after inactivation of UBPI. ....	82
Figure 19. Stage-specific phenotypes after full inactivation of Kelch13 (1xNLS).....	84
Figure 20. Stage-specific phenotypes after partial inactivation of Kelch13 (3xNLS). ....	86
Figure 21. Localisation of SidM positive structures upon KIC7 knock sideways.....	89
Figure 22. Consequences on PI4P-positive membranes and vesicular structures after inactivation of KIC7. ....	90
Figure 23. Inducible dimerization of K13C580Y <sup>endo</sup> with mCherry-FRB-BirA*.....	91
Figure 24. Scatter plot of K13C580Y <sup>endo</sup> DIQ-BioID. ....	92
Figure 25. Interactome comparison of K13WT <sup>endo</sup> and K13C580Y <sup>endo</sup> . ....	93
Figure 26. Quantitative Western Blot analysis of K13WT <sup>endo</sup> and K13C580Y <sup>endo</sup> . ....	94
Figure 27. Fluorescence intensity quantification of K13WT <sup>endo</sup> and K13C580Y <sup>endo</sup> foci. ....	95
Figure 28. Functional analysis of endogenous K13C580Y <sup>endo</sup> parasites episomally expressing K13WT <sup>epi</sup> . ....	96
Figure 29. Functional analysis of endogenous K13C580Y <sup>endo</sup> parasites episomally expressing K13C580Y <sup>epi</sup> .....	98

Figure 30. Functional analysis of endogenous K13C580Y <sup>endo</sup> parasites episomally expressing K13R539T <sup>epi</sup> .....	100
Figure 31. Functional analysis of endogenous K13C580Y <sup>endo</sup> parasites episomally expressing K13E252Q <sup>epi</sup> .....	102
Figure 32. Schematic illustration (not to scale) of the domains of Kelch13. ....	103
Figure 33. Functional analysis of endogenous K13C580Y <sup>endo</sup> parasites episomally expressing mCherry-L-BTB-KD <sup>epi</sup> .....	104
Figure 34. Functional analysis of endogenous K13C580Y <sup>endo</sup> parasites episomally expressing mCherry-L-Linker-BTB-KD <sup>epi</sup> .....	106
Figure 35. Functional analysis of endogenous K13C580Y <sup>endo</sup> parasites episomally expressing mCherry-L-BTB <sup>epi</sup> .....	108
Figure 36. Functional analysis of endogenous K13C580Y <sup>endo</sup> parasites episomally expressing mCherry-L-CC-BTB-KD <sup>epi</sup> .....	110
Figure 37. Functional analysis of endogenous K13C580Y <sup>endo</sup> parasites episomally expressing mCherry-L-CC-BTB <sup>epi</sup> .....	113
Figure 38. Functional analysis of endogenous K13C580Y <sup>endo</sup> parasites episomally expressing mCherry-L-PSR-CC-BTB <sup>epi</sup> .....	114
Figure 39. Functional analysis of endogenous K13C580Y <sup>endo</sup> parasites episomally expressing mCherry-L-PSR107aa-CC-BTB <sup>epi</sup> .....	116
Figure 40. Functional analysis of endogenous K13C580Y <sup>endo</sup> parasites episomally expressing mCherry-L-PSR-CC <sup>epi</sup> .....	118
Figure 41. Functional analysis of endogenous K13C580Y <sup>endo</sup> parasites episomally expressing mCherry-L-PSR-CC-L-KD <sup>epi</sup> .....	120
Figure 42. Functional analysis of endogenous K13C580Y <sup>endo</sup> parasites episomally expressing mCh-L-PSR-CC-2aaBTB-2xmyc-loxP-T2A <sup>epi</sup> .....	122
Figure 43. Side-by-side comparison of RSA results of endogenous K13C580Y <sup>endo</sup> parasites episomally expressing different K13 domain constructs. ....	123
Figure 44. Western Blot based quantification of the abundance of different Kelch13 domain constructs. ....	125
Figure 45. Effect of mDHFR domain on relative cellular abundance of episomal Kelch13 constructs lacking the Kelch domain.....	127
Figure 46. Integration strategy for N-terminal tagging of K13C580Y <sup>endo</sup> .....	129
Figure 47. Functional analysis of endogenously tagged K13C580Y_HR260 <sup>endo</sup> parasites. ....	130
Figure 48. Localization of endogenously tagged K13C580Y_HR260 <sup>endo</sup> .....	131
Figure 49. Functional analysis of K13C580Y_HR260 <sup>endo</sup> parasites. ....	133
Figure 50. Fluorescence intensity quantification of Kelch13 foci of different cell lines with endogenously tagged Kelch13. ....	135

---

Figure 51. Host Cell Cytosol Uptake (HCCU) in <i>P. falciparum</i> .....	137
Figure 52. Model of artemisinin resistance. ....	139
Figure 53. Overview of the functional analysis of endogenous K13C580Y <sup>endo</sup> parasites episomally expressing constructs consisting of different Kelch13 domain combinations. ....	142
Figure 54. Schematic illustrations (not to scale) of pSLI-N-sandwich-loxP_K13C580Y and pSkipFlox_mChK13.....	146
Figure 55. Schematic illustration of episomally expressed constructs for Kelch13 domain-specific DIQ-BioID. ....	147

## **List of Tables**

Table 1. Overview of analyzed K13WT <sup>endo</sup> DIQ-BioID hits. ....	46
Table 2. PCR mix for FirePol DNA polymerase (10 µl batch). ....	62
Table 3. Conditions for analytic PCRs. ....	62
Table 4. PCR mix for Phusion DNA Polymerase (50 µl batch).....	63
Table 5. PCR conditions for preparative purpose. ....	63

# Abbreviations

<i>A.</i>	<i>Anopheles</i>	h	hour
ACTs	Artemisinin Combination Therapies	HBsAg	hepatitis B surface antigen
AIV	Anti-Infection Vaccines	HCC	host cell cytosol
AMA1	apical membrane antigen	HCCU	host cell cytosol uptake
AP2	adaptor protein complex 2	hDHFR	human dihydrofolate reductase
ART	Artemisinin	G	Golgi-apparatus
ATP	adenosinetriphosphate	HSP101	heat shock protein 101
BACK	BTB and C-terminal Kelch	HSPGs	heparin sulfate kinase 6
BirA*	promiscuous biotin ligase BirA*	hpi	hours post infection
BSV	Blood Stage Vaccines	IFA	immunofluorescence assays
BTB	Broad-complex, Tramtrack and Bric-à-Brac	IRS	indoor residual spraying
CC	coiled-coil containing region	ITNs	insecticide-treated mosquito nets
CDPK6	calcium-dependent protein kinase 6	K13	Kelch13
ConA	ConcanavalinA	KBTBD	Kelch repeat and BTB domain-containing
<i>crt</i>	chloroquine resistance reporter gene	KEAP1	Kelch-like ECH-associated protein 1
CSP	circumsporozoite protein	KIC	Kelch13 interacting candidates
DAPI	4',6-diamidino-2-phenylindole	KLHDC	Kelch-domain containing
DDT	Dichloro-diphenyl-trichloroethane	KLHL	Kelch-like
DNA	deoxyribonucleic acid	KREP	Kelch-repeat domains forming a six-bladed $\beta$ -propeller
DG	dense granules	KS	knock sideways
DHA	dihydroartemisinin	M	micronemes
DHFR	dihydrofolate reductase	MAHRP1	Maurer's clefts associated histidine rich protein
DIC:	differential interference contrast	MC	Maurer's clefts
DIQ-BioID	dimerization induced quantitative BioID	MCA2	metacaspase 2
dNTPs	deoxyribonucleotide triphosphates	mCh	mCherry red fluorescent protein
DV	digestive vacuole	mDHFR	murine dihydrofolate reductase
EBAs	erythrocyte binding antigens	<i>mdr1</i>	multidrug resistance transporter gene
EEA1	early endosome antigen 1	min	minutes
eIF2 $\alpha$	eukaryote translation initiation factor 2 $\alpha$	MSPs	merozoite surface proteins
EMA	European Medicines Agency	mut	mutation
EMP1	erythrocyte membrane protein 1	MW	molecular weight
endo	endogenous	MyoC	MyosinC
epi	episomal	N	nuclei
ER	endoplasmatic reticulum	NLS	nuclear localization signal
EXP	exported protein	ns	not significant
FDR	false discovery rate	PCR	polymerase chain reaction
FV	food vacuole	<i>P.</i>	<i>Plasmodium</i>
R	rhoptries	PI3K	phosphatidylinositol-3-kinase
GFP	green fluorescent protein	PI(3)P	phosphoinositol-3-phosphate
GMS	Greater Mekong Sub-region	PR	pre-rhoptries
GSK	GlaxoSmithKline	PSR	<i>Plasmodium</i> -specific region

PTEX	<i>Plasmodium</i> translocon of exported proteins	Sec61	ER translocon
PV	parasitophorous vacuole	SLI	selected-linked integration
PVM	parasitophorous vacuolar membrane	SLI-TGD	selected-linked integration gene disruption
QC	chloroquine	SNAREs	soluble N-ethylmaleimide-sensitive-factor attachment receptor
PI(3,4)P <sub>2</sub>	phosphoinositol-3,4-biphosphate	SPB1	skeleton binding protein 1
PI(3,5)P <sub>2</sub>	phosphoinositol-3,5-biphosphate	SR	survival rate
PI4P	phosphatidylinositol-4-phosphate	SV	secretory vesicles
PM	plasma membrane	TBV	Transmission-Blocking Vaccines
POZ	Poxvirus and Zinkfinger	TGN	trans-Golgi network
PPM	parasite plasma membrane	TRX2	thioredoxin 2
RON	rhopty neck protein	UBP1	Ubiquitin carboxyl-terminal hydrolase 1
rpm	rounds per minute	UPR	unfolded protein response
RSA	Ring-stage Survival Assay	VAC	vacuolar-like compartment
Rab5	Ras related protein in brain 5	VPS45	Vacuolar Protein Sorting 45
rapa	rapalog	WHO	World Health Organisation
RBC	red blood cell	WT	wild type
RDTs	rapid diagnostic tests	WRAIR	Walter Reed Army Institute of Research
RE	recycling endosome	yDHODH	yeast dihydroorotate dehydrogenase gene
REX1	ring exported protein 1		
RFP	red fluorescent protein		
RH	reticulocyte binding like homologs		
SDS PAGE	Sodium dodecyl sulfate polyacrylamide gel electrophoresis		

# 1 Introduction

## 1.1 Malaria: a worldwide public health problem

Malaria is a vector-borne disease caused by unicellular protozoan parasites of the genus *Plasmodium*. The disease is found in 87 countries (WHO, 2020) and distributed in tropical and subtropical areas including Latin America, Africa, Southeast Asia and the Indian subcontinent. Malaria remains one of the most important global public health problems as well as a heavy social and economic burden in low-income countries. The epidemiology, occurrence and mortality of the complex disease varies among the affected countries and is dependent of the disease-causing *Plasmodium* species. *Plasmodium* parasites are classified into the phylum Apicomplexa and today more than 200 *Plasmodium* species are known that, depending on the species, infect specific mammals, birds or reptiles. Five *Plasmodium* species can infect humans: *P. falciparum*, *P. knowlesi*, *P. ovale*, *P. malariae* and *P. vivax*, of which *P. falciparum* is the most virulent.

### 1.1.1 Historical background of the disease

Malaria is one of the most concerning infection diseases worldwide and no tropical disease claims as many human lives every year as malaria. Malaria was first reported 2700 BC in a classical work of Chinese medicine (Arrow et al., 2004). Hippocrates recognized the disease characterized by various attacks of fever and diagnosed malaria based on its symptoms (Cox, 2002). In 1880, the French military doctor Charles Alphonse Laveran, who was stationed in Algeria, identified the causative agent of malaria and described the single-cell parasite in blood smears from malaria patients (Laveran, 1881). Later on, Ronald Ross provided evidence, that the pathogen is transmitted by Anopheles mosquitos (Ross, 2002). Laveran and Ross were awarded with the Nobel Prize for Medicine and Physiology for their findings (Ronald Ross in 1902, Charles Alphonse Laveran in 1907). In the beginning of the 20th century, the commitment of the western world to combat malaria was strong because Europe and the United States of America were threatened by the disease (Regenass-Klotz, 2009). With the availability of the antimalarial chloroquine (QC) and the effective insecticides such as DDT for vector control, by 1951 the United States were considered malaria-free (WHO, 2008) and the World Health Organization (WHO) launched the WHO Global Malaria Eradication Program in 1955. The program showed concrete results and contributed to a massive decrease in malaria cases in countries such as India and Sri Lanka in 1963, followed by an increase of malaria cases to concerning levels after efforts ceased (Chareonviriyaphap et al., 2000, Abeyasinghe et al., 2012). In countries such as Haiti and Nicaragua, the measures were only partially effective and the elimination campaign was not seriously implemented in Africa (Molineaux and Gramiccia, 1980). The worldwide success of the Malaria Eradication Program was limited by emerging drug as well as insecticide resistance, ongoing wars and extreme climatic

conditions, which led to a new alignment turning the Global Eradication Program to a Malaria Control Program in 1978 (Rosenthal et al., 2019, WHO 2020). In 1982, the WHO certified 24 endemic countries as malaria-free, but in the 1990s the number of deaths per year due to malaria increased to the highest in human history (Rosenthal et al., 2019). With the beginning of the 21st century, funding for malaria research increased and new programs, such as the Global Fund for AIDS, Tuberculosis, and Malaria (the Global Fund), were established. A combination of the development of diagnostic tests, effective drugs, insecticide usage for indoor spraying and the widespread usage of bed nets, led to reduced malaria cases by more than 40 % from 2000 until today and reduced deaths by more than 60 % worldwide (WHO, 2020). Between 2000 and 2019, the WHO announced 21 countries malaria free for three consecutive years and certified 10 of them as malaria free. Unfortunately, malaria parasites developed resistance against the current first-line anti-malaria drug and malaria cases in high-burden areas plateaued in recent years (WHO, 2020). This situation increases the urgency to better understand the physiology of the parasite and to develop new drugs (Holmes et al., 2017).

### 1.1.2 Epidemiology of malaria

In 2019, the WHO estimated that a total number of 229 million malaria cases in 87 countries occurred worldwide (WHO, 2020). Ninety-three percent of all reported malaria cases occur in African Regions, three percent in Southeast-Asia and two percent in the Eastern Mediterranean Regions (WHO, 2019 a). With an estimated 215 million malaria cases annually, Africa is the major area for the disease. The largest number of infections were recorded in Nigeria (27 %), the Democratic Republic of the Congo (12 %) and Uganda (5 %) (WHO, 2020). Prevention and treatment of *Plasmodium* infections succeeded in Southeast Asia, leading to 73 % less cases from 2000 to 2019. The overall malaria case reduction can also be observed in parts of the Eastern Mediterranean Region (e.g., Iran) and in parts of the Western Pacific Region (e.g., China and Malaysia). Alarmingly, malaria infection rates in Venezuela increased from 2000 to 2019 from 35 500 to 467 000 (WHO, 2020) (Figure 1).

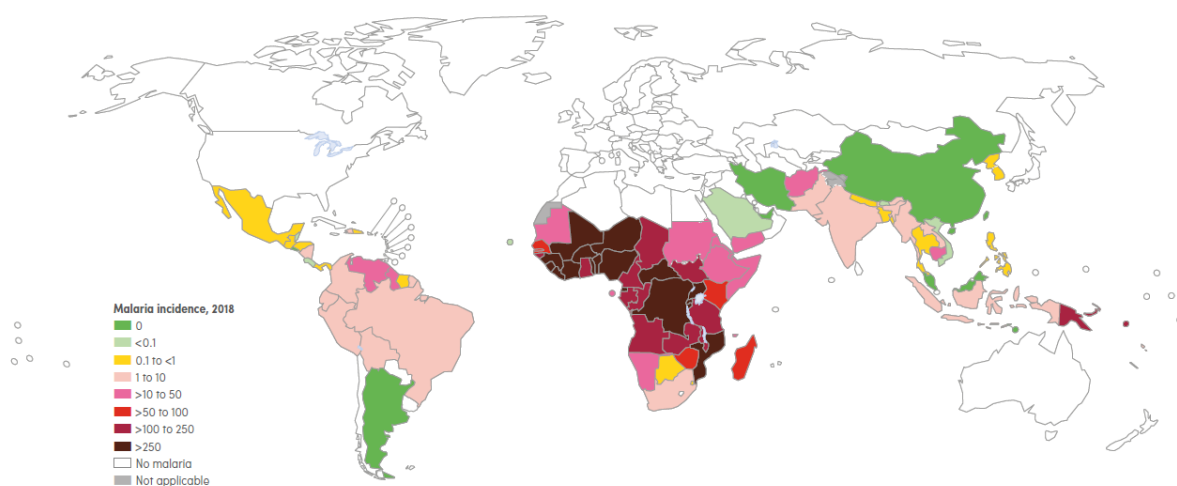
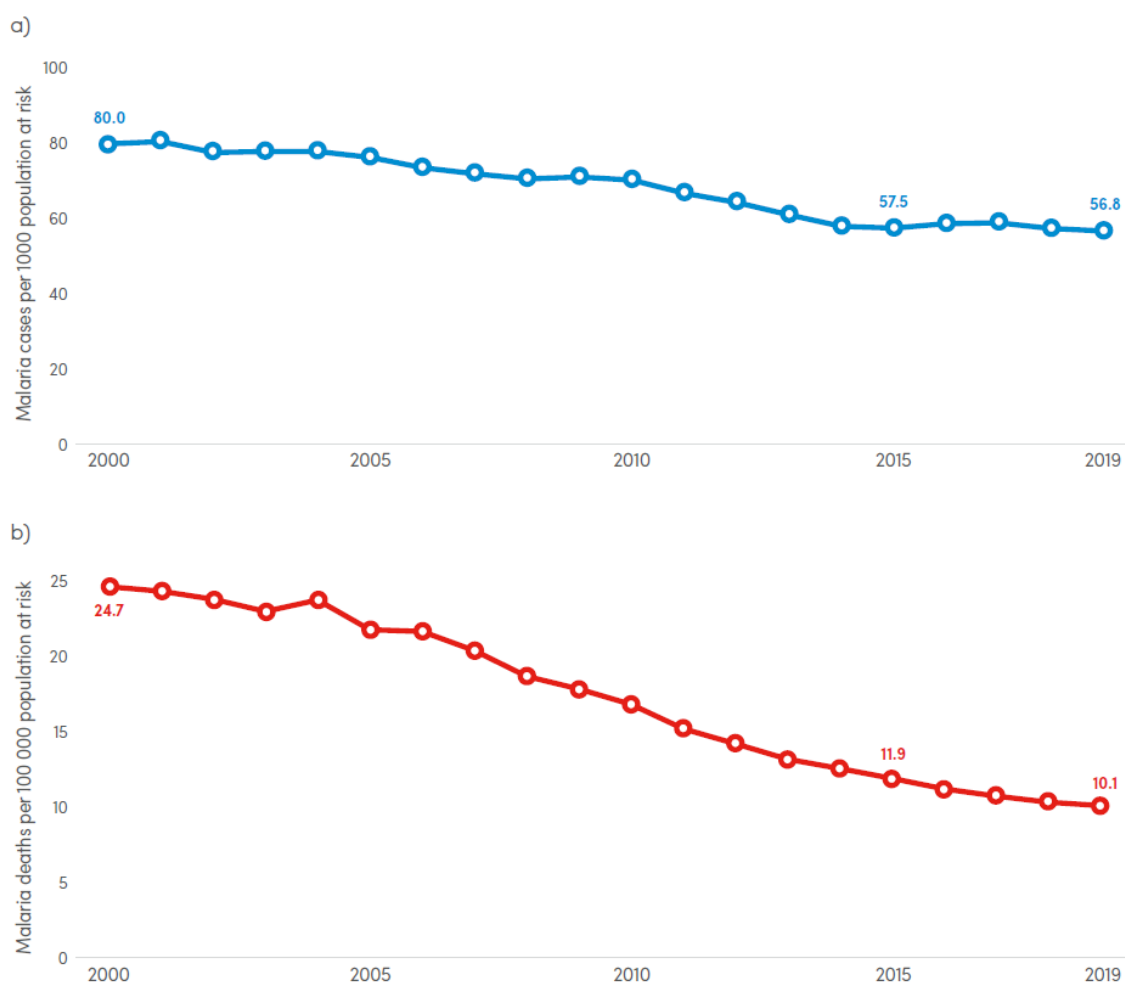


Figure 1. Map of malaria case incidence rate (cases per 1000 population at risk) by country in 2018 (WHO, 2019 a).

Globally, malaria caused 409 000 deaths in 2019 of which 67 % were among children under 5 years. According to estimations, ninety-five percent of all malaria deaths occurred in 31 countries, primarily concentrated in low-income countries and especially in Africa. In total, the global trends in the malaria case incidence rate (Figure 2a) and mortality rate (Figure 2b) declined from 2000 to 2019. In this time period, deaths per 100 000 people at risk decreased from 25 to 10 and overall malaria cases per 100 000 was reduced by 29 % from 80 to 57 (WHO, 2020). Africa is the continent most threatened by malaria worldwide, and children and pregnant women are particularly affected. Every third pregnant women become infected with malaria during her pregnancy with consequential damage for the unborn babies, such as low birth weight (Guyatt and Snow, 2004).



**Figure 2.** Global trends in a) malaria case incidence rate (cases per 1000 population at risk), b) mortality rate from 2000 - 2019 (WHO 2020).

### 1.1.3 Human-pathogen *Plasmodium* species

*Plasmodium falciparum* is the most important causative agent of malaria and the most virulent *Plasmodium* species. *P. falciparum* infections are responsible for 99 % of the lethal malaria cases worldwide (WHO, 2018 a). Geographically, *P. falciparum* is distributed in tropical and subtropical

regions with particularly strong occurrence in sub-Saharan Africa (Price et al., 2020) (Figure 3a). Due to the high transmission rate of *P. falciparum* in Africa, levels of acquired immunity are high, leading to frequently asymptomatic malaria infections in adults (WHO, 2019 a). Children and travellers that are exposed the first time to *P. falciparum* infections often develop severe malaria. In 2018, *P. falciparum*-caused malaria was estimated in 24 million children in sub-Saharan Africa. The most virulent property of *P. falciparum* is the ability to modify the infected erythrocyte surface, leading to cytoadherence of the infected red blood cells to the endothelium, which can cause impaired tissue perfusion, microvascular obstruction and even organ damage (Zekar and Sharman, 2021). If the brain is affected, this can lead to cerebral malaria, a major reason for severe complications. A further common complication associated in infections with *P. falciparum* is severe anaemia.

*Plasmodium vivax* is the globally most widespread human malaria parasite and the predominant malaria-causing species in Southeast Asia (Boissiere et al., 2020). In 2017, malaria infections caused by *P. vivax* were detected in 49 countries in South America, Eastern Africa Regions, Asia and the Pacific Islands (Price et al., 2020) (Figure 3b). Malaria infections caused by *P. vivax* parasites proceed with milder symptoms and lower mortality rates than *P. falciparum* infections (Elgoraish et al., 2019). In contrast to *P. falciparum*, *P. vivax* parasite infections occur in regions with lower environmental temperatures (Greenwood et al., 2008). *P. vivax* parasites are responsible for 70 to 80 million malaria cases worldwide (Daron et al., 2020) and in 2019 the proportion of *Plasmodium vivax* infection compared to all estimated cases decreased from 7 % to 3 % (WHO, 2020). *P. vivax* infects only reticulocytes and only Duffy antigen positive red blood cells are affected (Mercereau-Puijalon et al., 2010). The Duffy antigen is a protein that is needed for *P. vivax* to invade erythrocytes (Price et al., 2020). Sub-Saharan African countries are usually not at risk of *P. vivax* infections which can be explained by the absence of the Duffy antigen on red blood cell surfaces (Chitnis et al., 1996). In contrast to *P. falciparum*, *P. vivax* parasites are able to form dormant stages (termed hypnozoites) which survive long time periods and can be activated even years after the primary infection (Shortt et al., 1948, Krotoski et al., 1982, Mikolajczak et al., 2015). When activated, hypnozoites give rise to a new infection (White et al., 2011).

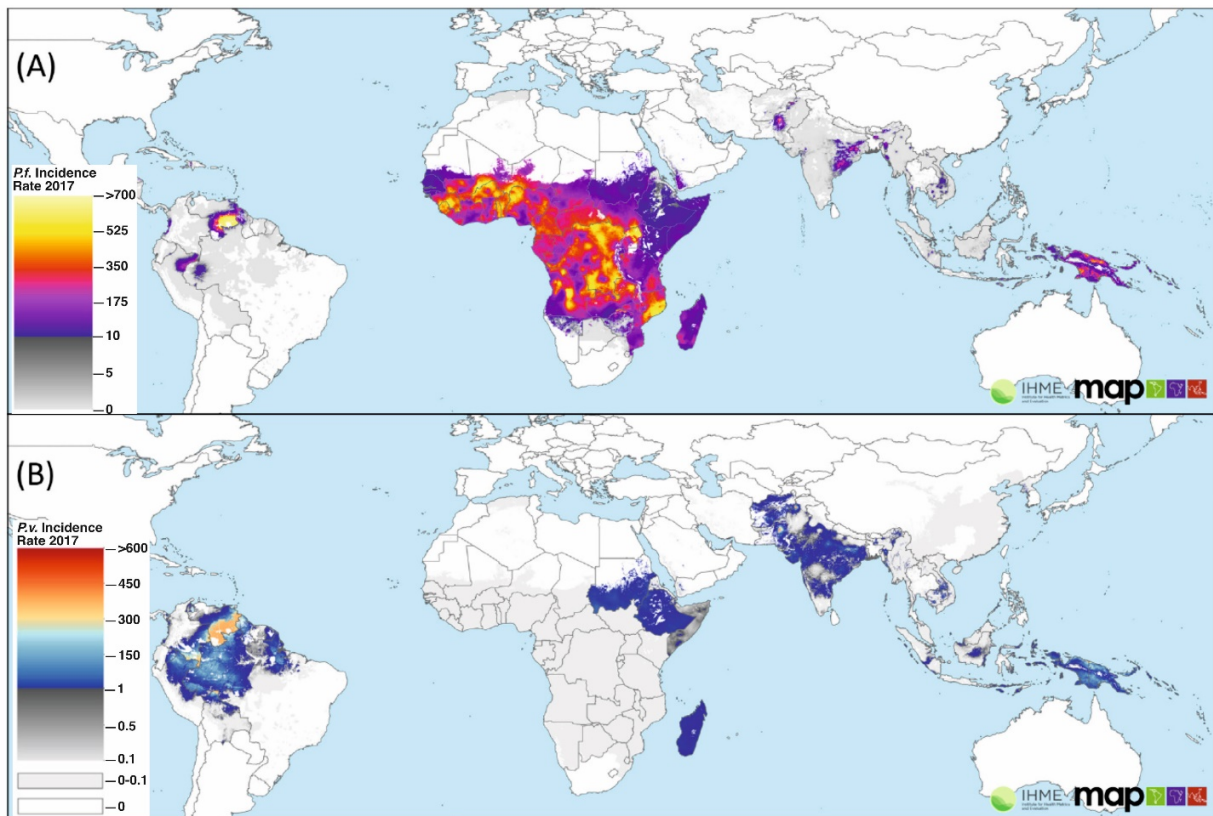


**Figure 3. The Incidence of *Plasmodium falciparum* and *Plasmodium vivax* Malaria in 2017.** Cases per 1000 people per annum of *P. falciparum* (A) and *P. vivax* (B). Color code shows incidence rate from high (yellow for *P.f.*, red for *P.v.*) to low (white) (modified from Price et al., 2020).

Malaria infections caused by *P. malariae* and *P. ovale* are significantly less frequent than *P. falciparum* and *P. vivax* infections. *P. malariae* infections occur mainly in tropical regions in Africa and co-infections with *P. malariae* and *P. falciparum* were encountered (Autino et al., 2012). *P. ovale* parasites are present in Asia, on some islands of the western Pacific region and in Africa (Collins and Jeffery, 2005) and are able to form dormant liver stages (hypnozoites) which can cause a relapse of the disease after months or even years (Greenwood et al., 2008). *Plasmodium knowlesi* was first isolated in 1931 and is primarily a zoonotic parasite infecting macaques, but in 1965 the first case of human malaria infection with *P. knowlesi* has been documented in Malaysia (Chin et al., 1965) and since then, *P. knowlesi* infections in humans have been reported in Southeast Asia (Malaysia, Indonesia, Vietnam Thailand, Singapore, Myanmar, Singapore and Cambodia). *P. knowlesi* can be transmitted in monkey-to-human, human-to-monkey and monkey-to-monkey infections (Singh and Daneshvar, 2013) but so far, there is no evidence of natural human-to-human transmission (Brock et al., 2016; Singh et al., 2004). The pathophysiology of *P. vivax*, *P. ovale* and *P. malariae* is rarely fatal and infections with these *Plasmodium* species are causing usually mild symptoms (Rahimi et al., 2014). Human *P. knowlesi* infections can cause severe symptoms such as acute respiratory distress, renal failure, shock and hyperbilirubinemia (William et al., 2011).

### 1.1.4 Diagnosis of malaria

Effective malaria management depends on the reachability of medical centres for people living in rural and urban areas. Delays in the detection of malaria result in high parasitemia in the patients and severe malaria cases which can lead to death. The nonspecific nature of the symptoms of malaria, e.g., high fever, headache, weakness, chills, sweats, dizziness and body aches, require specific and accurate diagnostic options to avoid over-treatment, non-treatment or misdiagnosis (Tangpukdee et al., 2009). Common techniques to diagnose malaria infections include the identification of the malaria causing parasite or antigens in patient blood samples, which is mainly done by rapid diagnostic tests (RDTs), by microscopy or molecular methods like polymerase chain reaction (PCR) (Holland and Kiechle, 2005). In recent years, the development of RDTs was of major interest. According to the WHO, RDTs allow fast diagnosis within 15 – 30 minutes, are simple in the handling as well as in interpreting and most important, can be used in areas with no diagnostic laboratories (WHO, 1996). RDTs detect malaria parasite specific proteins (antigens) of one or several *Plasmodium* species. The accuracy to distinguish between *Plasmodium* species is dependent on the single tests that are used. In 2020, 200 different malaria RDTs were available on the market and in 2019 615 million RDTs were used for diagnosis worldwide (WHO, 2020).

### 1.1.5 Transmission and Prevention

Malaria is transmitted through the bites of female *Anopheles* mosquitos. Globally, more than 400 different *Anopheles* species are known, of which approximately 30 species are of special importance for the transmission of human malaria (WHO, 2020). *A. gambiae* and *A. arabiensis* are the most dominant vector species in Africa (Schmidt et al., 2019). The diversity of *Anopheles* species in Southeast Asia is much larger than in Africa and represents 30 *Anopheles* species. The vectors *A. dirus*, *A. minimus* and *A. eprioticus* are responsible for most malaria cases in Southeast Asia (Obsomer et al., 2013). Female *Anopheles* mosquitoes lay their eggs in shallow freshwater ponds and organic material, such as algae and bacteria, is used as nutrition source for the larvae (Merritt et al., 1992). Due to the climatic requirements of the mosquitoes, malaria transmission is dependent climate conditions. *Anopheles* mosquito abundance is increased during humid seasons during which malaria transmission peaks (Jetten et al., 1996). Other climate conditions, such as dry seasons, limit mosquito populations and consequently the occurrence of malaria infections is reduced. Ectotherm *Anopheles* mosquitos as well as *Plasmodium* species are sensitive to temperature, which influences the speed of development of the parasite stages in the mosquito and therefore the transmission rate (Paaijmans et al., 2010). The optimal temperature for *Anopheles* mosquitos ranges from 20 – 30 °C (Beck-Johnson et al. 2013).

The malaria transmission rate in endemic countries depends on malaria vector control strategies such as insecticide-treated mosquito nets (ITNs), indoor residual spraying (IRS) and the reduction of mosquito breeding sites by controlling water levels. According to the WHO, the worldwide usage of ITNs from people that are at risk of malaria increased from 2 % to 46 % in the time period between 2000 and 2019.

Most ITNs were used in Sub-Saharan African countries like Nigeria, the Democratic Republic of the Congo and Ethiopia, whereas Nigeria announced the availability of at least one bed in 68 % of all households (WHO, 2020). The regular use of INTs is a major reason contributing to the significant decrease of malaria deaths (Greenwood et al., 2008).

## 1.2 *Plasmodium falciparum*: the malaria causing parasite

### 1.2.1 The life cycle of *Plasmodium falciparum*

The life cycle of *P. falciparum* consists of different development phases which can be defined in three main stages: the liver stage (see 1.2.1.1), the blood stage (see 1.2.1.2 and 1.2.1.3) and the mosquito stage (see 1.2.1.4) (Figure 4).

*Plasmodium falciparum* sporozoites can be transmitted to the human host by the bite of a female *Anopheles* mosquito (Figure 4, step 1). The sporozoites reach the blood stream and are transported to the liver where a single asexual replication cycle takes place and merozoites are formed in merosomes (Figure 4, step 2 - 8) without causing clinical symptoms in the human host. With the release of the merozoites into the blood stream, the erythrocytic development phase of the parasite begins. The invasive merozoite stage invades erythrocytes (Figure 4, step 9) and parasite development from ring to trophozoite and schizont stage takes place (Figure 4, step 10 - 12). This results in up to 32 new daughter merozoites that are again released into the blood stream (Figure 4, step 13) and can invade new erythrocytes. A small proportion of the intra-erythrocytic parasites undergo gametocytogenesis resulting in the production of sexual parasite stages (Figure 4, step 14), which can be taken up by the mosquito by the next blood meal where the parasite multiplies to produce sporozoites that can again infect a new human host (Figure 4, step 15).

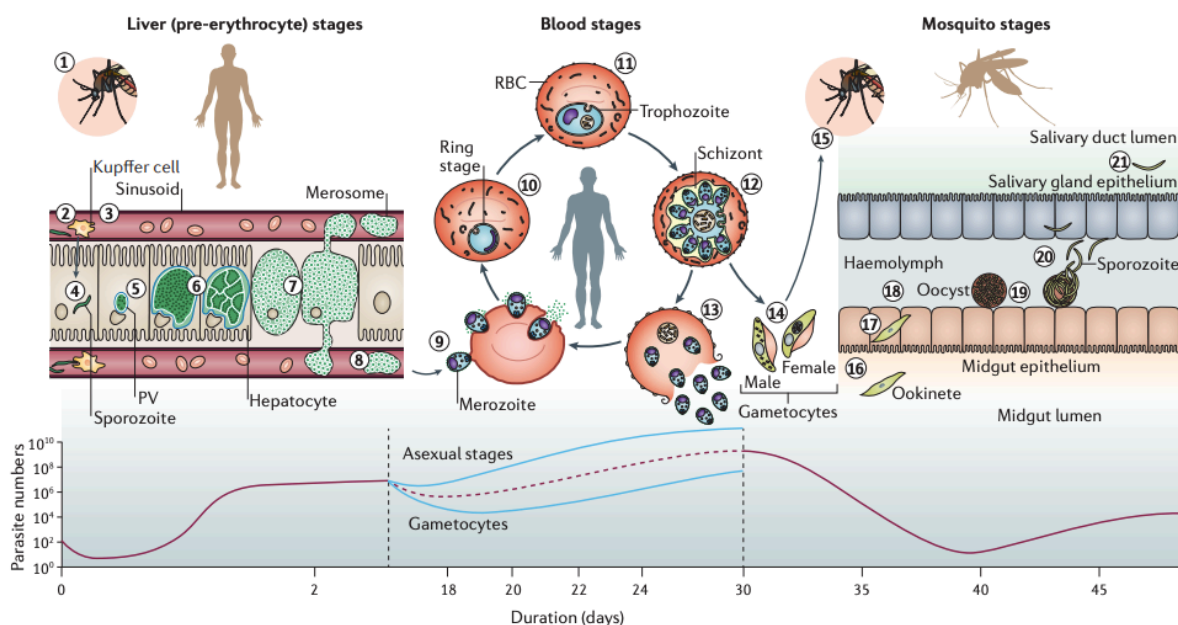


**Figure 4.** Life cycle of *Plasmodium falciparum* parasites. 1 - 8: pre-erythrocytic parasite development in the human liver. 9 - 14: blood stage development. 15 - 21: sexual parasite development in the mosquito stage. Bottom graph shows the parasite numbers present during the different stages (De Niz et al., 2016).

### 1.2.1.1 The liver stage

The hepatic stage is clinically silent and does not cause symptoms in the human host. The average duration of this phase is 5.5 days (Bartoloni and Zammarchi, 2012). The infection of the human host begins with the injection of sporozoites under the skin by the blood meal of a female *Anopheles* mosquito (Figure 4, step 1). The majority of the highly motile sporozoites reach the blood vessels and enter the blood stream but some sporozoites either stay in the skin or are rapidly eliminated by the lymph system of the human host (Yamauchi et al., 2007). Once in the blood stream, the sporozoites are transported to the liver where they migrate through the liver sinusoid and the Kupffer cells (Figure 4, step 2 – 3) and reach the hepatocytes. The invasion of the sporozoites into the hepatocytes is initiated by the binding of HSPGs (heparin sulfate kinase 6) and the activating of CDPK6 (calcium-dependent protein kinase 6) (Coppi et al., 2007). The invasion process also involves the CSP (circumsporozoite protein) that binds to heparin sulphate proteoglycans and the human CD81 receptor on the hepatocyte surface (Prinzon-Ortiz et al., 2001). Inside the hepatocyte, the parasite transmigrates and forms a parasitophorous vacuole (PV) in which it replicates asexually through several rounds of mitotic nuclear division resulting in the formation of a multinucleated cell. This process is defined as schizogony and leads to the formation of new merozoites (De Niz et al., 2016). Finally, the merozoites are released from the host cell into the blood stream in membrane-bound structures, the so called merozoites (Sturm et al., 2006) (Figure 4, step 4 – 8).

### 1.2.1.2 Asexual blood stage development

Free merozoites released from the liver into the bloodstream invade red blood cells in a process that takes no longer than two minutes. A rapid invasion strategy is necessary so that the merozoites are not exposed for long to the immune system of the human host. The merozoite is an oval-shaped and polar parasite 1-3 micrometers in size. At the apical pole of the merozoites are specialized structures, which are essential for the invasion process (De Niz et al., 2016). These secretory organelles are the rhoptries, the micronemes and the dense granules (Figure 5 A). The primary contact of the merozoite with the red blood cell (RBC) is mediated by the binding of a low affinity interaction of merozoite surface proteins (MSPs) to the surface of the erythrocyte (Wright and Rayner, 2014) (Figure 5 A). The initial attachment is followed by a re-orientation process of the merozoite to orientate with the apical pole of the merozoite towards the RBC (Figure 5 B). Attachment to the surface of the RBC is promoted by ligands that are secreted from the micronemes and the rhoptries such as the reticulocyte binding like homologs (RH) and the erythrocyte binding antigens (EBAs) (O'Donnell et al., 2000) (Figure 5 B). The parasite ligand Rh5 binds to the basigin receptor of the RBC leading to calcium influx into the RBC being invaded (Wright and Rayner, 2014; Weiss et al., 2016). Next, rhoptry neck proteins (RONs) are secreted from the rhoptries and are inserted into the host cell membrane where they form a complex (Besteiro et al., 2009). The RON complex forms a tight junction together with the apical membrane antigen (AMA1) which is then pulled around the merozoite surface as moving junctions using the actin-myosin motor

(Figure 5 D) (Lamarque et al., 2014; Bargieri et al., 2013; Hehl et al., 2000; Triglia et al., 2000). During invasion, the plasma membrane of the RBC is invaginated and, together with intercalated parasite proteins and lipid material from the rhoptries, form the parasitophorous vacuolar membrane (PVM) which, encloses the parasite in a parasitophorous vacuole (Figure 5 E, F) (Cowman and Crabb, 2006).

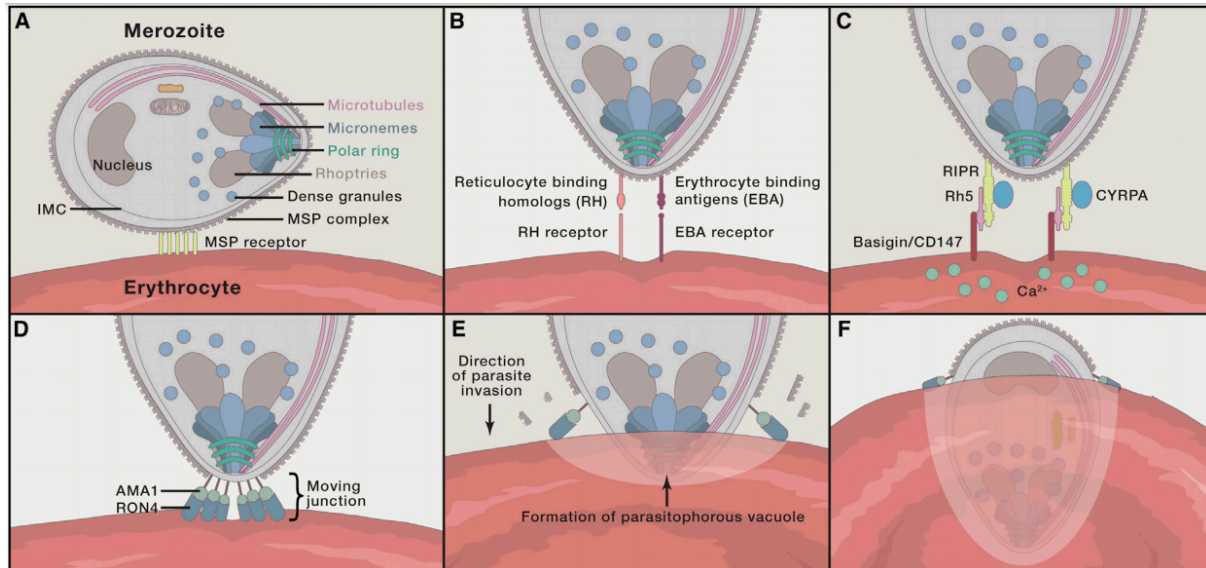


**Figure 5. Invasion process of merozoites in erythrocytes.** (A) – (F) shows sequence of events of merozoite invasion into the red blood cell (modified from Cowman et al., 2016).

During invasion, the plasma membrane of the red blood cell is invaginated and, together with intercalated parasite proteins and lipid material from the rhoptries, forms the PVM, which encloses the parasite in a parasitophore vacuole (Cowman and Crabb, 2006). Once inside the RBC, the parasite is called a ring form (Figure 6) that can change its shape between a disc-shaped and an amoeboid form (0 - 18 hours post infection (hpi)) (Gruring et al., 2011). At the early ring stage, the metabolic activity of the parasite is presumed to be low, and the parasite starts to remodel the host cell by exporting parasite proteins to the cytosol of the RBC (Figure 6). This includes the establishment of membranous structures in the host cell termed the Maurer's clefts (MC) (Atkinson and Aikawa, 1990) in the erythrocyte. Maurer's clefts are membranous organelles that are involved in the sorting of exported proteins in the host cell. In the erythrocytic phase more than 400 different kinds of parasite proteins are thought to be exported by *P. falciparum* parasites into the host cell (Marti et al., 2005). Around 18 hours after invasion, ring stage parasites mature to the trophozoite stage (18 - 32 hpi) (Figure 6) (Gruring et al., 2011). One of the most prominent host cell modification in this development stage is the formation of the so-called knobs on the surface of the RBC. Knobs are important for the cytoadherence of infected RBC to the endothelium of the blood vessels (Crabb et al., 2010) to avoid clearance by the host immune system in the spleen (Leech et al., 1984; Nagao et al., 2000; Watermeyer et al., 2016). In the trophozoite stage, the parasite grows rapidly, and the digestive vacuole (DV) appears (Figure 6). The DV is a lysosomal-like organelle with low pH, in which the erythrocyte hemoglobin that the parasite endocytoses is degraded. During proteolysis of hemoglobin the toxic heme moiety is released as a byproduct that is detoxified by crystallization to hemozoin. Hemozoin crystals can be seen by the so-called 'malaria pigment'

(Wunderlich et al., 2012). Uptake of hemoglobin from the host cell provides space for the parasite to grow and a fraction of the acquired amino acids are used as nutrient supply for the parasite (Krugliak et al., 2002). After the trophozoite stage, the parasites develop to the schizont stages (Figure 6) during which new daughter merozoites are formed in a process termed 'schizogony' (Nilsson et al., 2015; Greenwood et al., 2008; Rug et al., 2014). During cytokinesis, replication of DNA occurs followed by cell division of the multinuclear schizonts. In the parasite, the microtubular system organizes the formation of 8 - 32 daughter cells. Additionally, in this stage the apical organelles needed for invasion (see above in 1.2.1.2), are required for daughter cell formation (Keeley and Soldati; 2004; Baum et al., 2006; Kono et al., 2012). 48 hours post invasion, asexual blood stage development (Figure 6) is completed and the newly formed daughter merozoites are released into the blood stream (emergence of merozoites out of the RBC is termed 'egress'). RBC rupture induces clinical symptoms of the disease such as specific fever attacks.

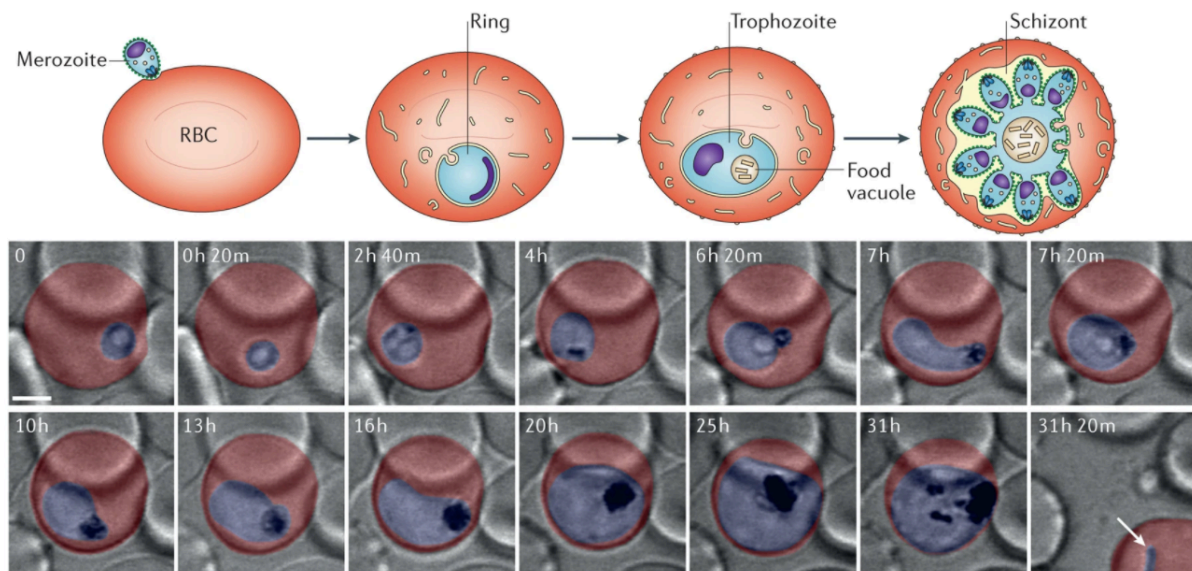


**Figure 6. Asexual blood stage development of *P. falciparum*.** (Top panel) Scheme of merozoite invasion and parasite development in the erythrocyte from ring to trophozoite and schizont stage. (Bottom panel) Time-laps imaging for 31 hours and 20 minutes starting with a late ring stage parasite. Timepoint 0 corresponds to the late ring stage. The parasite (blue) develops in the red blood cell (red). The formation of the digestive vacuole (black because of its hemozoin content) can be observed in trophozoite (2h to 20h) and schizont stage (25h - 31h). Arrow shows newly invaded parasite (De Niz et al., 2016).

### 1.2.1.3 Gametocytogenesis

During each replication cycle in erythrocytes, a small proportion (approximately 10 %) of the parasites commit to sexual differentiation and develop into male and female gametocytes (Bruce et al., 1990). This process is defined as gametocytogenesis and includes the escape from the peripheral circulation in the bloodstream and migration into the extravascular space of the bone marrow, where the parasites within 8 to 10 days grow into mature gametocytes (Figure 7) (Josling and Llinas, 2015; Brancucci et al., 2017). During this process, gametocytes can be distinguished by their shape and are categorized into 5 consecutive stages (I-V) (Nilsson et al., 2015; De Niz et al., 2016). Stage V gametocytes migrate again

into the circulatory system of the blood vessels (De Niz et al., 2018) (Figure 7) where they can be taken up by *Anopheles* mosquitos.

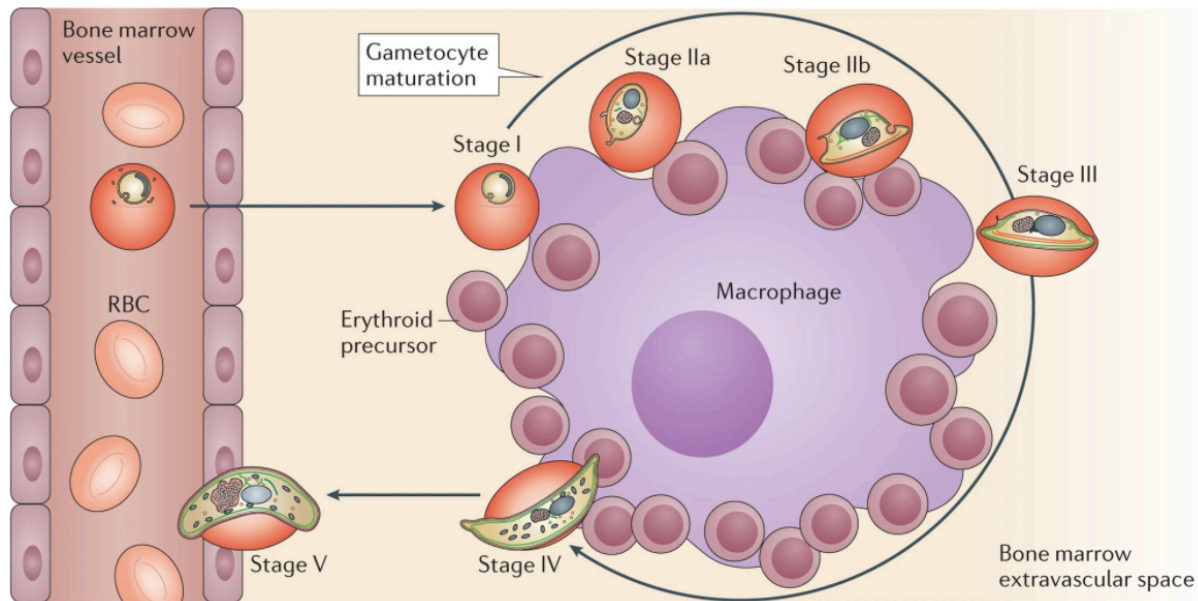


**Figure 7. Sexual stage development of *P. falciparum* in the human host.** Gametocyte maturation is defined as stage I - V and takes place in the extravascular space of the bone marrow (De Niz et al., 2016).

#### 1.2.1.4 The mosquito stage

During the blood meal of a female *Anopheles* mosquito on a *P. falciparum*-infected human host, micro- and macrogametocytes are taken up into the gut. First, the gametocytes differentiate into mature gametes in the midgut of the mosquito. This process is driven by the natural environmental conditions of the mosquito's midgut (pH, temperature) (Billker et al., 1997; Billker et al., 1998). In the case of male gametocytes, gamete formation involves the rapid replication of the DNA (from 1 N to 8 N) and development into 8 motile microgametes. The female gametocytes develop into fertile and haploid macrogametes (Guttery et al., 2015). Microgametes and macrogametes fuse together in the midgut of the mosquito to form a diploid zygote. The zygote develops into an invasive and tetraploid ookinete by meiosis that is again haploid. The ookinetes penetrate the intestinal wall of the mosquito and migrate underneath the basal lamina of the anopheles mosquito. After 10 to 12 days, an oocyst is formed in which asexual replication of the mosquito stage parasite takes place. In this process, hundreds of sporozoites are formed during sporogony (Aly et al., 2009), which are released into the hemolymph after rupture of the oocyst. Some of the sporozoites reach the mosquito's salivary glands, through which they can be transferred back into the human during the mosquito's next blood meal (Nilsson et al., 2015).

## 1.3 Treatment of malaria infections

### 1.3.1 Vaccine development

The development of an effective vaccine against infection with the human malaria parasite *Plasmodium falciparum* is a major global health priority. While malaria control and elimination programs succeeded in the containment of the disease in the last decades, this success is threatened by emerging drug as well as insecticide resistance. Sustainable control or even elimination of *P. falciparum* malaria would therefore be greatly aided by a vaccine. Malaria vaccine development has proven to be extremely complex and difficult. A challenge for vaccine development is the genetic diversity of surface proteins expressed by the parasite, including antigenic variation and polymorphisms. Furthermore, basic research to understand the molecular mechanism underlying immune response to malaria infections has to be extended to improve malaria vaccine development (Kurtovic et al., 2019). Current vaccine candidates can be classified into three major groups based on their points of attack: Transmission-Blocking Vaccines (TBV), Anti-Infection Vaccines (AIV) and Blood Stage Vaccines (BSV) (Duffy and Gorres, 2020).

#### 1.3.1.1 Transmission-Blocking Vaccines

Malaria Transmission-Blocking Vaccines (TBVs) directly act against mosquito infecting parasite stages (gametes and zygotes) and have the potential to prevent the propagation of malaria through the community (Carter et al., 2000). TBVs contain surface antigens from sexual parasite stages in order to induce antibody production against these stages in the human host. During the blood meal of a mosquito on a TBV-treated human, the mosquito absorbs not only the malaria parasite but also the antibodies against it. These mosquitoes are called immunized, and the absorbed antibodies prevent the development of the parasite in the mosquito. Consequently, these immunized mosquitoes can no longer transmit malaria parasites to other human hosts. TBVs can thus prevent the transmission and further spread of malaria (Carter and Chen, 1976; Duffy and Gorres, 2020). However, TBVs cannot protect people already infected with malaria from contracting the disease. Because of this, it will be a great challenge to explain the concept of a vaccine that does not directly protect the vaccinated person but only prevents the spread. In addition, this approach makes it difficult to obtain funding from commercial companies, as the use of TBVs only makes sense in malaria-endemic countries and does not provide direct protection for, for example, travelers or military personnel (Carter et al., 2000). Antigens against sexual parasite stages were identified in animal models with monoclonal antibodies. Promising antigen candidates can be differentiated in two groups according to the respective parasite stage that produces the antigens: gamete surface proteins (including Pfs230 and Pfs48/50) and Ookinete surface proteins (including Pfs25 and Pfs28) (Kaslow, 1997; Grotendorst et al., 1984; Duffy and Gorres, 2020). The production of recombinant proteins of these antigens is challenging but to date, Pfs25 is the most promising TBV candidate that is further investigated in clinical trials (Barr et al., 1991; Duffy and Gorres, 2020).

### 1.3.1.2 Anti-Infection Vaccines

GlaxoSmithKline (GSK) and the Walter Reed Army Institute of Research (WRAIR) developed the Anti-Infection Vaccines (AIVs) RTS,S in 1987 (Nussenzweig et al., 1967). RTS,S is a pre-erythrocytic stage vaccine which induce immune response against the major circumsporozoite protein (PfCSP) and consist of a recombinant central repeats and the C-terminal domain of PfCSP fused with the hepatitis B surface antigen (HBsAg) (Draper et al, 2018). In 2015, the European Medicines Agency (EMA) approved the usage of the malaria vaccine RTS,S/AS01E (Mosquirix<sup>TM</sup>), which is the first vaccine against malaria tested in Phase 3 clinical trials and the first that is used in pilot immunization programs in malaria endemic countries (Laurens, 2020). Children treated with 3-dose RTS,S vaccine acquire high antibody titers, nevertheless RTS,S efficacy is limited against clinical malaria (RTS,S Clinical Trial Partnership, 2015). Clinical studies confirmed moderate effect of the vaccine and showed reduced clinical *P. falciparum* malaria episodes of 46 % in young African children and of 27 % in babies (infants of the age of 6 weeks to 17 months) (WHO, 2018 b). Other clinical trials with RTS,S confirmed the relative low clinical efficiency rate which points out the need to further investigate RTS,S and to test different pre-erythrocytic stage vaccine candidates (Mahmoudi and Keshavarz, 2017). In 2019, the WHO launched RTS,S/AS01E pilot implementation programs in Ghana, Kenya and Malawi to examine the optimal vaccine distribution mechanism in the public health system and to asses safety standards (Greenwood et al., 2017; WHO report of GACVAS, 2017).

### 1.3.1.3 Blood-Stage Vaccines

The asexual parasite stage is the disease-causing development stage and consequently an attractive vaccine target. Blood-Stage Vaccines (BSVs) target intra-erythrocytic asexual parasite stages and mainly attack the merozoite stage by preventing invasion of new red blood cells. The attack of free merozoite by BSVs is made difficult by the short time (only seconds) between the release of the merozoites and the invasion of new erythrocytes (Sirima et al., 2011; Duffy and Gorres, 2020). The merzoite surface proteins 1, 2 and 3 (MSP1, MSP2 and MSP3), the apical membrane antigen 1 (AMA1) and the erythrocyte binding antigen 175 (EBA175) are proteins expressed on the surface of merozoites and were major antigen targets of BSVs. However, clinical trials with these antigens did not show any efficacy with these targets (Sagara et al., 2009; Chitnis et al., 2015). Invasion pathways in *Plasmodium* parasites are redundant which hampers the development of BSVs, but one BSV candidate, the *P. falciparum* reticulocyte-binding protein homolog 5 (PfRH5), may avoid this issue due to its limited polymorphism (Crosnier et al., 2011). PfRH5 was tested with promising results in pre-clinical studies in monkeys, where PfRH5 based antigen presentation conferred immunity and resulted in limited parasitemia (Douglas et al., 2015) and was also tested in clinical trials demonstrating only low RH5 specific responses that were induced in humans after immunization (Payne et al., 2017).

### 1.3.2 Antimalarial drugs

Malaria has been treated with natural products that were found in the traditional medicine of tropical and subtropical countries for thousands of years. Today's malaria treatment and drug development against this disease is to a considerable part based on chemicals derived from natural ingredients of plants with antimalarial effects that are found in roots, leaves or barks. Antimalarial are, beside antibiotics, the most important standard treatments of infectious diseases in tropical and subtropical countries. The population of malaria parasites is exposed to enormous drug pressure and resistance against antimalarial drugs is common (Wicht et al., 2020).

#### 1.3.2.1 Quinine

Quinine, a quinoline-containing alkaloid, was the first and likely most successful antimalarial drug. It was discovered in 1820 and was extracted from the bark of the cinchona tree. Quinine and its derivatives chloroquine (QC), mefloquine and lumefantrine are active against asexual blood stages of *Plasmodium* parasites (Achan et al., 2011). QC acts specifically in the digestive vacuole of the parasite and interferes with the detoxification of heme by inhibiting the polymerization of heme molecules (Goldberg et al., 1990). The high efficacy as well as the widespread availability of QC made it into one of the most important drugs against a tropical infectious disease (Wellems and Plowe, 2001). In the beginning of the 1950s, QC was the frontline drug against malaria, but its efficacy became jeopardised by emerging chloroquine resistance in *P. falciparum* and *P. vivax* parasites the late 1950s. Resistance in *P. falciparum* independently emerged in Columbia and the Cambodia-Thailand border (Payne, 1987). In the following years it occurred in South America, Southeast Asia and India and in the late 1970s also in Africa (White, 2004). QC resistant parasites show less QC accumulation in the digestive vacuole (Verdier et al., 1985). This is caused by a point mutation in the *Plasmodium falciparum* chloroquine resistance reporter gene (*pfcr1*) which leads to increased transport of QC out of the digestive vacuole (Bray et al., 1998; Fidock et al., 2000). Since the late 1980s, resistance to the chloroquine derivative lumefantrine and mefloquine was also reported (White, 1999). Resistance to these drugs is associated with the P-glycoprotein homolog encoding the *Plasmodium falciparum* multidrug resistance transporter gene (*pfmdr1*) (Price et al., 2004).

#### 1.3.2.2 Antifolates

Proguanil and atovaquone are used as an antimalarial combination therapy (Malarone™) with a high efficiency due to their synergistic effects (Tse et al., 2019). Atovaquone is known to inhibit mitochondrial electron transport by blocking the cytochrome *bc<sub>1</sub>* complex (Fry and Pudney, 1992). The antifolate proguanil was first reported in 1945 and described as one of the first anti-malarial drug (Curd et al., 1945) and targets the parasite folic acid metabolism and acts, like many other antifolate derivatives, as a dihydrofolate reductase (DHFR) inhibitor. Thereby, this drug disrupts deoxythymidylate synthesis, which is part of the folic acid metabolism (Srivastava and Vaidya, 1999; Delves et al., 2012). Resistance to this drug combination spread globally (Korsinczky et al., 2000; Cottrell et al., 2014). It has been

shown that atovaquone resistant parasites show a mutation in the *cytochromeB* gene (Y268S). Notably, it is postulated that this mutation inhibits sporozoite formation in the mosquito. This can lead to reduced transmission rates through mosquitos due to a reduction in sporozoite formation. Atovaquone is therefore an important drug which can be used in combination therapies to advance malaria elimination programs (Goodman et al., 2017).

### 1.3.2.3 Artemisinin (ART) - the front-line drug against malaria

Artemisinin is extracted from the sweet wormwood *Artemisia annua* and has been part of the traditional Chinese medicine for more than 2000 years as the medical herb quinghaosu (now termed artemisinin). It was used for the treatment of parasitic diseases, diarrhea or as an antiseptic. In 1967, the chinese-vietnamese research collaboration "Project 523" was established to find potential drug candidates against malaria (White et al., 2015). Subsequently, the Chinese scientist Youyou Tu discovered artemisinin as an antimalarial drug and solved its chemical structure in 1979 (Tu et al., 1981; Tu, 2011), for which she received the Nobel Prize in Physiology and Medicine in 2015 (Nobelprize.org, 2015). ART is a sesquiterpene lactone that is active against chloroquine resistant *P. falciparum* parasites (WHO, 2001) and acts in asexual blood stages and in early sexual gametocytes. It may therefore also have some transmission blocking potential which has been noted as a desirable property of malaria drugs (WHO, 2001). ART is a fast-acting drug, leading to a 10 000-fold reduction of parasitemia within 48 hours (Tilley et al., 2016). Artemether, artesunate and arteether are the most common ART derivatives, which are transformed to the active metabolite dihydroartemisinin (DHA) (Krishna et al., 2008; Tse et al., 2019). Due to its short half-life (< 1 h), ART is used in a combination therapy with a slower acting and longer half-life drug in so called Artemisinin Combination Therapies (ACTs). For this, the highly efficient artemisinin derivatives artesunate, dihydroartemisinin (DHA) and artemether are combined with mefloquine, piperaquine or lumefantrine. Since 2001, the WHO recommends ACTs as first-line treatment against malaria to prevent resistance against ART (see 1.5.1) (WHO, 2001; White, 2004). Interestingly, artemisinin is also used for cancer treatment. Cancer cells exposed to ART demonstrate less cell proliferation, enhanced oxidative stress levels, increased apoptosis and angiogenesis inhibition (Krishna et al., 2008).

The mechanism of action of ART is still unclear (O'Neill et al., 2010; Tse et al., 2019). Artemisinins contain a unique endoperoxide bridge which needs to be activated by scission through heme-derived iron (Meshnick et al., 1991, Klonis et al., 2013). Cleavage of this bond leads to the release of highly reactive carbon-centered radicals, which inhibit and react with lipids, proteins and metabolites (Hartwig et al., 2009; Wang et al., 2015; Wang and Lin, 2016). It has been hypothesized that this leads to the damage of cellular structures and proteasomal degradation of proteins resulting in cell death (Tilley et al., 2016).

Hemoglobin degradation is initiated by a series of protease enzymes such as falcipains and plasmepsins and leads to the formation of peptides and amino acids. During this proteolytic degradation of

hemoglobin, hematin is formed by hydrogen bonding of heme monomers (Pagola et al., 2000), which occurred to be toxic for the parasite. Detoxification of the hemoglobin by-products is essential for parasite survival and is implemented by the conversion of free heme to hemozoin (see 1.2.1.2) (O'Neill et al., 2010). Hemoglobin uptake and digestion takes place primarily in trophozoite stages, consequently ART is most active in trophozoites (Klonis et al., 2013). Recently, it was demonstrated that host cell cytosol is already endocytosed in ring stages (Birnbbaum and Scharf et al., 2020) which explains ART activity in early parasite stages (Klonis et al., 2013; Xie et al., 2016).

## 1.4 The biology of *Plasmodium falciparum* parasites

### 1.4.1 Cellular biology and protein export of *P. falciparum* parasites

The cellular structure of *P. falciparum* parasites consists of typical eukaryotic organelles such as an endoplasmic reticulum (ER), a Golgi-apparatus (G), a nucleus, and mitochondria (Figure 8). For the highly specialized invasion process (see 1.2.1.2) the merozoites harbor apical secretory organelles: micronemes, rhoptries, exonemes and dense granula (Figure 8).

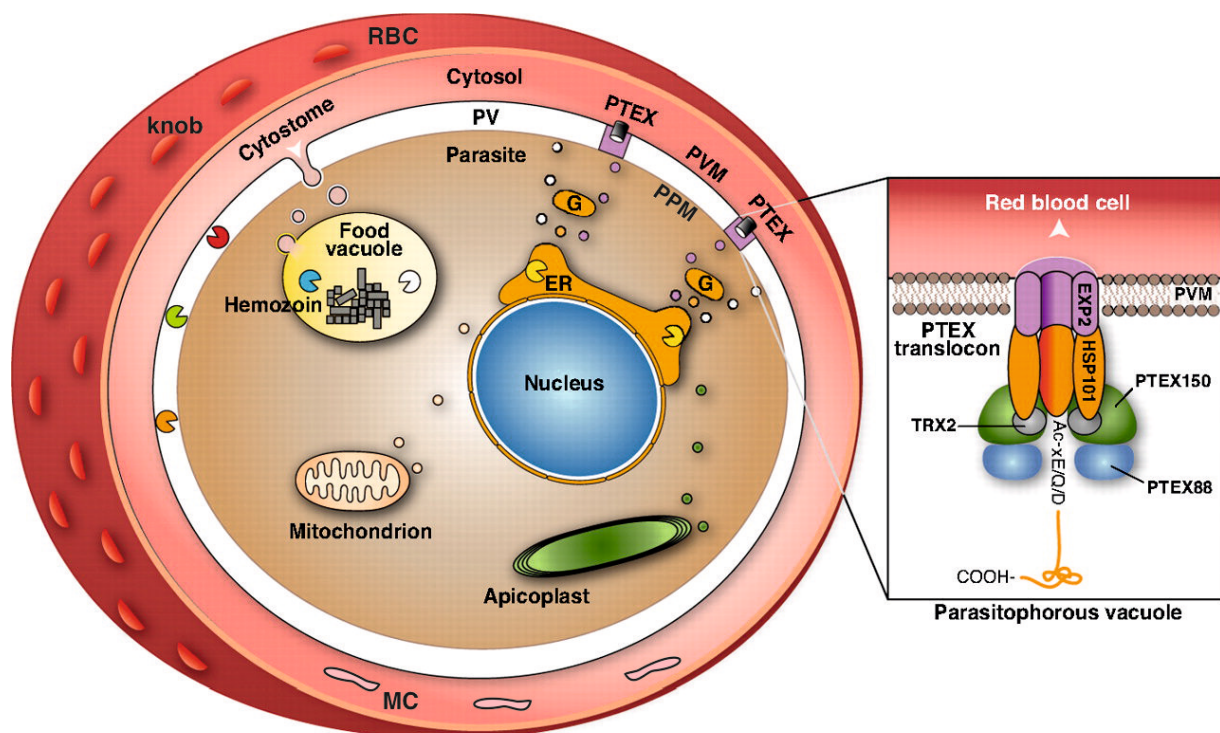


**Figure 8. Schematic illustration of *P. falciparum* organelles, membranes and host cell modifications.** Shown is the parasite in the red blood cell (RBC) and parasite organelles such as the nucleus, apicoplast, mitochondrion, ER, Golgi-apparatus (G) and the food vacuole. The parasite is surrounded by the parasite plasma membrane (PPM) and the parasitophorous vacuolar membrane (PVM) which define the parasitophorous vacuole (PV); Cytostome: invagination of the PVM that is assumed to be involved in host cell cytosol uptake; PTEX: Plasmodium translocon of exported proteins which is located at the PVM and consists of the indicated subunits; Maurer's clefts (MC) and knob: host cell modification (modified from Kappe et al., 2010).

In order to gain nutrition and space within the RBC the parasite takes up large amounts of hemoglobin and digests it in an acidic, lysosome-like compartment termed the DV (also termed food vacuole) where several different proteinases are present (Banerjee and Goldberg 2001) (Figure 8). The DV becomes

apparent in early trophozoites (Abu Baker et al., 2010). Cytostomes (Figure 8) are ring-shaped structures involved in host cell cytosol uptake (HCCU) (see 1.4.2), is present in *P. falciparum* parasites (Aikawa et al., 1966, Xie et al., 2020). In malaria parasites cytotomes are defined as invaginations of the PPM and PVM that are filled with hemoglobin and are believed to be part of the endocytosis process in *P. falciparum* (Abu Baker et al., 2010) although this has so far not formally been demonstrated (Spielmann et al., 2020). A particularly remarkable structure of malaria parasites is the apicoplast (Figure 8). The apicoplast is surrounded by four membranes and is a DNA containing plastid of Apicomplexa. It is of secondary endosymbiotic origin and likely originates from a green or a red alga (Lim and McFadden, 2010). During the asexual stage, the apicoplast has an elongated shape and was found in close proximity to the mitochondrion (Figure 8) (van Dooren et al., 2005). In the intra-erythrocytic stage (see 1.2.1.2), the parasite modifies its host cell via protein export. MCs are one prominent example for a structure in the RBC that is build up by the parasite. MCs were first described in 1902 (Maurer, 1902) and are sack-like, flattened circular discs (Figure 8) (Mundwiler-Pachlatko and Beck, 2010). MCs are formed already in early ring stages during which they are mobile in the host cell but become fix in position when parasites reach the trophozoite stage (Grüring et al., 2011) and contain many exported parasite proteins such as for instance the skeleton binding protein 1 (SPB1), ring exported protein 1 (REX1), and Maurer's clefts associated histidine rich protein (MAHRP1) (Blisnick et al., 2000; Hawthorne et al., 2004; Spycher 2003; Spielmann et al., 2006).

Furthermore, the most important virulence factor protein *PfEMP1* (*Plasmodium falciparum* erythrocyte membrane protein 1) is sorted by the MC and transported to the RBC surface (Su et al., 1995; Janes et al., 2011). *PfEMP1* is responsible for cytoadherence and binding to the endothelial receptors leading to sequestration of infected RBCs, for instance in the brain which can result in cerebral malaria in patients (see 1.1.3) (Lennartz et al., 2017). Exported proteins contain either a protein export motif termed the PEXEL (*Plasmodium* export element) (Marti et al., 2004; Hiller et al., 2004) or are PEXEL negative exported proteins (PNEPS) (Spielmann et al., 2006). The PEXEL consists of the amino acids RxLxE/Q/D and is located approximately 20 amino acids downstream of the signal peptide that mediates ER entry. PEXEL proteins are inserted into the ER by the ER translocon Sec61 (Marapana et al., 2018). The PEXEL motif is processed in the ER by plasmepsin V (Boddey et al., 2010; Russo et al., 2010), likely concomitant with ER entry (Boddey et al 2016). The first discovered PNEPs all contained a transmembrane domain which mediates entry into the ER and is also needed for further transport to the host cell (Spielmann et al., 2006; Haase et al., 2009; Saridaki et al., 2009). From the ER, exported proteins are transported in the secretory pathway through the Golgi to reach the parasite plasma membrane to reach the PV (Figure 8). To reach the host cell, the exported protein then has to cross the PVM which occurs through translocation via the *Plasmodium* translocon of exported proteins (PTEX). PTEX is a protein complex at the PVM that comprises an ATPase (heat shock protein 101, HSP101), EXP2 (exported protein 2) and PTEX150 (Figure 8). The proteins TRX2 (thioredoxin 2) and PTEX88 are also associated with the PTEX translocon and are suspected to have a regulatory function (de Koning-Ward et al., 2009). In addition, it was recently shown that EXP2 also has a second function as a nutrient transporting pore (Garten et al., 2018). A different PVM protein, EXP1, is required for the

EXP2-based nutrient-permeable channel activity at the PVM, indicating that there are two EXP2 containing complexes at the PVM, one for protein and one for nutrient transport (Mésen-Ramírez et al., 2019).

### 1.4.2 Endocytosis in *P. falciparum* and the endolysosomal pathway

Endocytosis is defined as the internalization of extracellular material by a vesicle-mediated process (Sorkin and Zastrow, 2009; Kumari et al., 2010; Spielmann et al., 2020). The external material is then transported in endocytic vesicles (EVs) in the endolysosomal pathway (Figure 9 A). In mammalian cells the endolysosomal pathway starts with the transport of the EVs to the early endosome (EE), followed by transport to the late endosome (LE) and further to the lysosome (Figure 9 A). The EE is characterized by the presence of Rab5 (Ras related protein in brain 5), the early endosome antigen 1 (EEA1) and PI(3)P (phosphoinositol-3-phosphate) on its membranes and functions as sorting station for the EVs (Gorvel et al., 1991; Christoforidis et al., 1999; Jovic et al., 2010; Eaton and Martin-Belmonte, 2014). During the late endosomal and lysosomal pathway Rab7, PI(3,5)P<sub>2</sub> (phosphoinositol-3,5-biphosphate) and PI(3,4)P<sub>2</sub> (phosphoinositol-3,4-biphosphate) are involved (Figure 9 A) (Huotari et al., 2011; Nagano et al., 2015). During transport of the EVs recycling processes via the trans-Golgi network the plasma membrane (PM) and the recycling endosome (RE) mediate the addition and removal of material from and to the EV (Figure 9 A) (Sabharanjak et al., 2012).

For malaria parasites, endocytosis is particularly prominent in intraerythrocytic stages. During its development in the RBC, the parasite ingests host cell cytosol (HCC) (see 1.2.1.2) (Francis et al., 1997). In this endocytic process, HCC is taken up in hemoglobin-containing structures which are invaginated at the parasite periphery, but HCCU is still not completely understood (Spielmann et al., 2020). Two major structures are discussed to be involved in the initiation of HCCU in *Plasmodium* parasites: the cytostome (Figure 9 B) and the phagotrophe (Aikawa et al., 1966; Abu et al., 2010; Liu et al., 2019; reviewed in Spielmann et al., 2020). The internalized HCC is transported through the endolysosomal pathway to the DV (Figure 9 A) where the degradation of hemoglobin takes place, resulting in the formation of free heme. During this process, plasmepsins, falcipains and other proteins catalyze hemoglobin cleavage (Goldberg, 2005). The resulting free heme is detoxified by conversion into hemozoin crystals. During the cleavage process peptides and amino acids are released which are needed for the parasite development (Sherman, 1997).

The proteins involved in *P. falciparum* HCCU are so far not well known, but recent studies reported the involvement of PfVPS45 and inhibitor studies implicated motor proteins (actin myosin and dynamin) and SNAREs (Lazarus et al., 2008; Smythe et al., 2008; Zhou et al., 2009; Milani et al., 2015; Jonscher et al., 2019) in this process. PfVPS45 (Figure 9 A) was the first protein identified to be involved in HCCU in *P. falciparum*. The conditional inactivation of PfVPS45 led to the accumulation of PI(3)P positive HCC-filled vesicles in the parasite cytosol. It is suggested that PfVPS45 is functions during the late endosomal steps in HCCU (Jonscher et al., 2019). Recently, it was shown that the ART resistance protein PfKelch13 defines a complex that is involved in endocytosis (Birnbaum and Scharf et al., 2020).

This study provided evidence that *Plasmodium* parasites display a unique, clathrin-independent endocytosis pathway and that Kelch13 as well as the Kelch13-complex proteins UBP1, KIC7, AP2 $_{\mu}$  and Eps15 are part of the initial steps of HCCU (Figure 9 A) (Birnbaum and Scharf et al., 2020, see 1.6).

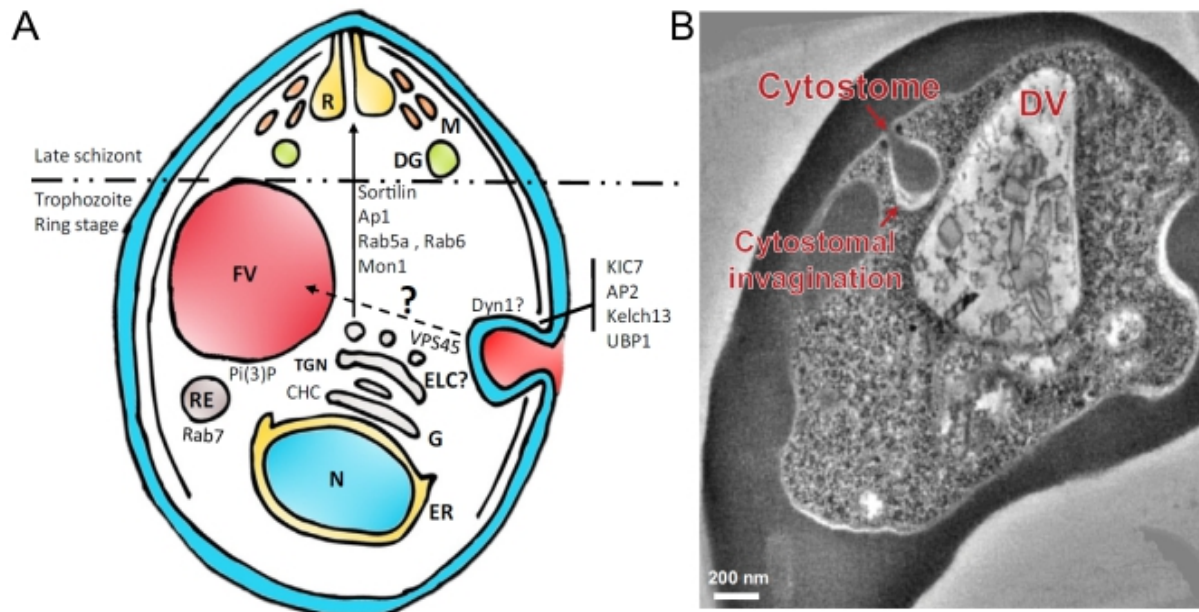


**Figure 9. Host cell cytosol uptake in *P. falciparum*.** (A) Schematic illustration of the current model of the endocytosis trafficking system (not to scale). Structures above the dotted line are only present in late schizont stages. The exact transport of host cell cytosol filled vesicles to the food vacuole is not fully understood yet (indicated by the question mark). Abbreviations: DG, dense granules; EE, early endosome; ELC, endosome-like compartment; ER, endoplasmic reticulum; FV, food vacuole; G, Golgi; L, lysosome; LE, late endosome; M, micronemes; N, nucleus; PR, pre-rhoptries; R, rhoptries; RE, recycling endosome; SV, secretory vesicles; TGN, trans-Golgi network; VAC, vacuolar-like compartment (modified from Spielmann et al., 2020). (B) Virtual section from an electron tomogram of a red blood cell showing a cytostome. Size bar: 200 nm. DV, digestive vacuole (Xie et al., 2020).

## 1.5 Artemisinin resistance

### 1.5.1 Emergence and distribution of ART resistance

Historically, the Greater Mekong Sub-region (GMS) in Southeast Asia has been the epicenter for the development of antimalarial drug resistance. The chloroquine resistance in Thailand, Cambodia, Laos, Myanmar and Vietnam demanded the widespread use of artemisinin since the 1990s. In 2008 first cases of ART resistant parasites were reported in Cambodia (Noedel et al., 2008). As a molecular marker for ART resistance, single point mutations in the *pfkelch13* gene (encoding for *PfKelch13* (K13)) were identified and were shown to explain resistance (see section 1.5.3) (Ariey et al., 2014). This was evident from a delayed parasite clearance in patients with uncomplicated malaria after an extended ART treatment period of 3 to 7 days (Noedel et al., 2008; Dondrop et al., 2009). Witkowski et al. developed an *in vitro* assay to measure this phenomenon, by exposing synchronized early ring stages parasites to a clinical concentration of dihydroartemisinin (DHA; 700 nM) for six hours and evaluating the parasite survival rate after a further 66 hours of culturing the parasites (Witkowski et al., 2013). This assay is

termed ring stage survival assay (RSA) and parasites were defined as ART resistant if the survival rate (SR) assessed by the RSA was above 1 % compared to not DHA treated parasites (Witkowski et al., 2013). ART resistance conferring mutations are correlate with a slow parasite clearance rate in clinical studies and with an elevated RSA survival rate *in vitro* (WHO, 2017). Kelch13 mutations can mediate ART resistance only in ring stages (Saralamba et al., 2011; Witkowski et al., 2013; Klonis et al., 2013). Today, ART resistance is widespread in the Southeast Asia (Figure 10), especially in Thailand, Vietnam, Myanmar and Laos (Dondrop et al., 2009; Phyo et al., 2012; Ashley et al., 2014). The treatment failure rates of ACTs among patients with *P. falciparum* malaria in Southeast Asia is up to 20 % (WHO, 2020). To date there is only limited evidence that clinical ART resistance is present in Africa. Since 2013, there were only two case reports from Africa that describe slow parasite clearance in *P. falciparum* infected travelers upon ACT treatment. From 2010 to 2019, 562 studies reported ACT treatment failure rates among patients infected with *P. falciparum* in African region (WHO, 2020; Diallo et al., 2020). Most of them (302 studies) documented treatment failures with artemether-lumefantrine (AL) combination therapies (WHO, 2020). Nevertheless, the total treatment failure rate of ACTs in Africa remains less than 5 % (WHO, 2020). Therefore, the overall treatment efficacy of ACTs in African countries for *P. falciparum* caused malaria still ranges between 98 % and 99.3 %. (WHO, 2019 b).

According to the Kelch13 Artemisinin Resistance Multicenter Assessment (KARMA) study in 2014, malaria patient samples harboring Kelch13 mutations were found in 70 % in Cambodia and in 3.8 % - 8% in African samples. The nonsynonymous Kelch13 mutations C580Y, R539T, Y493H, and I543T are most frequent in Cambodia, Vietnam and Laos, whereas F446I, N458Y, P574L are mostly present in Thailand, Myanmar and China (Figure 10) (Ménard et al., 2016).

To date, 5 Kelch13 mutations were documented, which are validated to correlate with increased RSA survival rates *in vitro* and delayed parasite clearance in patients: N458Y, Y493H, R539T, I543T and C580Y (Ariey et al., 2013; Amaratunga et al., 2014; Huang et al., 2015; Straimer et al., 2015; WWARN, 2019; Siddiqui et al., 2020). The mutation C580Y is the most prominent Kelch13 mutation in Southeast Asia (van der Pluijm et al., 2019). Additionally, *pfKelch13C580Y* alleles were also found in Guyana (Chenet et al., 2016) Cameroon (Amato et al., 2016) and Ghana (Aninagyei et al., 2020). Fifteen additional *pfkelch13* mutant alleles were found in a higher proportion in patients with slow parasite clearance upon ART treatment (including e.g., E252Q) (Phyo et al., 2016; WWARN, 2019). The resistance conferring mutations in Kelch13 are most prevalent in Southeast Asia and are considered to be absent outside of Southeast Asia (WWARN, 2019), but single reports from Papua New Guinea (C580Y) (Miotto et al., 2020) and Rwanda (P574L and A675V) came up documenting the prevalence of resistance conferring Kelch13 mutations (WHO, 2019 b; Uwimana et al., 2020). Additionally, the prevalence and the spread of the resistance conferring Kelch13 mutation R561H was recently documented in Rwanda (Uwimana et al., 2020, Stokes et al., 2021). The Kelch13R561H mutation was found in samples from an ACT efficacy trial in 19 of 257 patient samples in Rwanda and it was confirmed by gene editing that K13R561H mediates ART resistance *in vitro* (Uwimana et al., 2020).

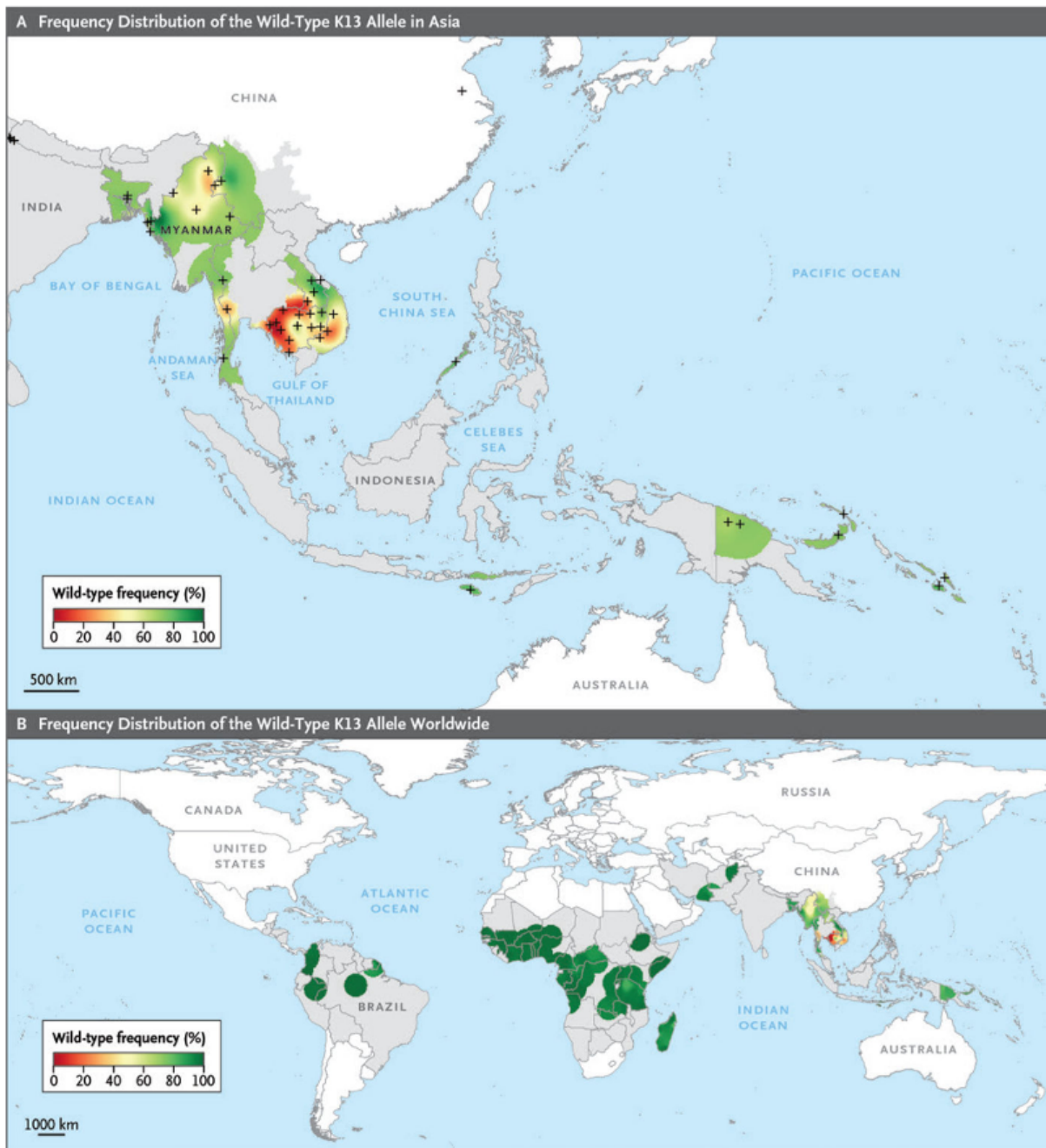


**Figure 10.** Frequency distribution of Kelch13 wild-type alleles in Asia (A) and worldwide (B). Sample collection sites in (A) are indicated with a cross. Grey coloured regions: malaria endemic countries. The color code indicates the frequency of the wild type allele in % (Ménard et al., 2016).

## 1.5.2 Proteins associated with ART resistance

Ariey et al. were the first investigating genome differences from ART resistant and ART sensitive parasites. For this, the group exposed F32 parasites from Tanzania with increasing ART concentrations over a 5-year time period and performed whole genome sequencing, which was compared to parasites cultured in the same conditions without ART treatment. They observed the mutation M476I in the *pfkelch13* gene, which first associated mutations in the Kelch13 protein with ART resistance. Next, they analyzed *P. falciparum* parasites derived from patients with slow parasite clearance upon ART treatment, and screened them for Kelch13 mutations (Ariey et al., 2014). Interestingly, the *in vitro*

discovered M476I mutation was not found in the patient samples, however the field isolates carried the resistance conferring Kelch13 mutations C580Y, R539T, I543T and Y493H (Ariey et al., 2014; Straimer et al., 2015).

Culture-adapted field isolate parasites from Senegal that were exposed to increasing DHA concentrations over 4 years obtained parasites, which were resistant to DHA in a standard RSA, and identified mutations in PfCoronin (encoded by *PF3D7\_1251200*) (Demas et al., 2018).

Additionally, it was shown that ART resistant *P. chabaudi* parasites, that were selected laboratory conditions under DHA drug pressure, carried a S160N mutation in the AP-2 $\mu$  protein (Henriques et al., 2013). Notable, AP-2 $\mu$  has also been linked to reduced sensitivity to other antimalarial drugs like chloroquine and lumefantrine (Henriques et al., 2015).

Furthermore, studies with culture-adapted *P. falciparum* field isolates from Thailand and Kenya, which showed decreased susceptibility to artemisinin treatment, observed polymorphisms in gene encoding Ubiquitin carboxyl-terminal hydrolase 1 (UBP1) (Borrmann et al., 2013; Henriques et al., 2014).

### 1.5.3 Kelch13 – the major ART resistance marker protein

Kelch13 is the major molecular marker protein associated with ART resistance (Ariey et al., 2014). *Pfkelch13* is located on chromosome 13 and encodes a 726 amino acid protein termed Kelch13 (Figure 11). The protein has a molecular weight of 84 kDa and consists of four major domains: A N-terminal *Plasmodium*-specific region (PSR), followed by a coiled-coil containing region (CC, amino acids 212 - 341) defined by two helices coiling together (Coppée et al., 2019), a BTB domain (Broad-complex, Tramtrack and Bric-à-Brac, also known as putative BTB/POZ (Poxvirus and Zinkfinger), amino acids 350 - 437) and six C-terminally located Kelch-repeat domains forming a six-bladed  $\beta$ -propeller (KREP, amino acids 443 - 726) (Figure 11).

The PSR is predicted to exhibit a random coil conformation (Coppée et al., 2019) with no significant similarities to other organisms (Tilley et al., 2016; Coppée et al., 2019).

The BTB motif is a protein-protein interaction motif which can mediate binding, homodimerization (Ito et al., 2009) and oligomerization (Pérez-Torrado et al., 2006) in other organisms. BTB domain-containing proteins are conserved across eukaryotes and are highly sequence divergent (Pérez-Torrado et al., 2006). Eukaryotic proteins containing a BTB domain were shown to be involved in numerous cellular functions such as regulating actin in cytoskeletal dynamics (Ziegelbauer et al., 2001) or cell-cycle control (Melnick et al., 2000) but many BTB domain proteins have in common that they are substrate-specific adaptors for E3 ubiquitin ligases (van der Heuvel, 2004).

The BACK (BTB and C-terminal Kelch) domain is conserved across BTB-Kelch proteins, but is absent in PfKelch13 (Tilley et al., 2016). The BACK domain is predicted to be involved in BTB-E3 complex formation and functions as a binding domain for the E3 ubiquitin ligase cullin 3 (Furukawa et al., 2003) and it was previously shown that mutations in this region can cause diseases in humans (Friedman et al., 2009).

The Kelch propeller can mediate protein-protein interactions and functions as a putative binding site for numerous proteins in other organisms (Adams et al., 2000; Tilley et al., 2016; Coppée, et al., 2019). Interestingly, ART resistance-conferring mutations are mainly located in the KREP region of Kelch13 (Tilley et al., 2016).

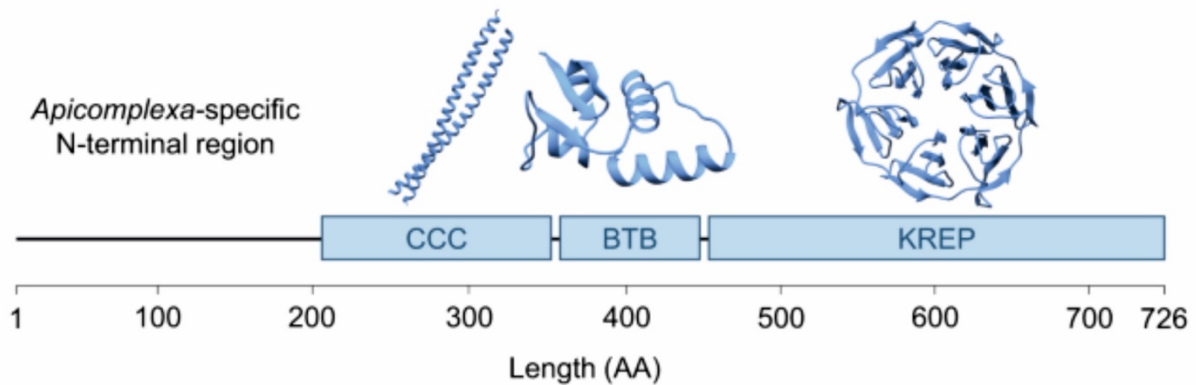


**Figure 11. Schematic illustration of Kelch13.** Kelch13 consist of a N-terminal Apicomplexa-specific region, a coiled coil containing (CCC) domain, a BTB domain and 6 C-terminal Kelch repeats forming a propeller (KREP), AA: amino acids (modified from Coppée et al., 2019).

### 1.5.4 The Kelch repeat superfamily

Kelch proteins include a large number of Kelch-repeat domain containing proteins that are highly diverse in their function and are part of the Kelch repeat superfamily (Adams et al., 2000; Gupta and Beggs, 2014). The gene members of the Kelch repeat superfamily are evolutionarily conserved across diverse organisms including eukaryotes (e.g., plants, fungi, mammals, parasites) and viruses (Prag and Adams, 2003) and are involved in cytoskeleton organization and actin regulation (Soltysik-Espanola et al., 1999), glucose metabolism (Murzin, 1992), G-protein control (Harashima and Heitman, 2002) or regulation of stress induced protein degradation (Tediosiet al., 1999). The Kelch repeat superfamily is defined by structural similarities among the members and can be categorized into three subfamilies: KLHL proteins (Kelch-like), KBTBD proteins (Kelch repeat and BTB domain-containing) and KLHDC proteins (Kelch-domain containing) (see section 1.5.3) (Adams et al., 2000). KLHDC subfamily members only contain kelch repeats, without a BTB/POZ domain (Gupta and Beggs, 2014). KBTBD proteins lack the BACK (BTB and C-terminal Kelch) domain (see section 1.5.3) and consist of one BTB/POZ domain and typically two to four Kelch repeats (Dhanao et al., 2013). KLHL protein members are widely distributed and highly conserved in eukaryotes (Dhanao et al., 2013). Forty-two KLHL proteins were identified in humans and they generally consist of a BTB/POZ domain, a BACK domain and five to six Kelch repeats (Dhanona et al., 2013).

### 1.5.5 Potential ART resistance mechanisms

Kelch13 shares 25 - 30 % sequence identity with the human KEAP1 (Kelch-like ECH-associated protein1) (Tilley et al., 2016), which is a negative regulator of Nrf2 transcription factor and regulates an

oxidative stress response (Zhang et al., 2004). It was hypothesized that Kelch13 has a similar function to that of KEAP1 in mammals and is involved in stress regulation (Ariey et al., 2014). Based on the structure of the protein and function of other Kelch repeat proteins, it was suggested that Kelch13 functions as a ubiquitin E3 ligase substrate adaptor which is involved in the unfolded protein response (UPR) and stress response regulation (Mok et al., 2015; Tilley et al., 2016). The BACK domain is sufficient in other Kelch repeat proteins to mediate binding of the BTB domain to the substrate E3 (see section 1.5.3). However, the BACK domain is lacking in PfKelch13 which makes the hypothesis that Kelch13 might function as an E3 ligase adaptor, unlikely (Tilley et al., 2016).

Moreover, there was evidence that artemisinins are potent inhibitors of *Plasmodium falciparum* phosphatidylinositol-3-kinase (PfPI3K). The lipid phosphatidylinositol-3-phosphate (PI3P) is associated with ART resistance and it was shown that parasites carrying the ART resistance conferring Kelch13 mutation C580Y have an altered Kelch13-PI3K interaction, which leads to decreased ubiquitination and consequently an increase of PI3K and PI3P levels. It was suggested that upregulated PI3P could mediate downstream amplification of unknown pathways which leads to ART resistance (Mbengue et al., 2015). Furthermore, PfKelch13 was found in close proximity to the ER which led to the hypothesis that Kelch13 could influence the ER stress response (Bhattacharjee et al., 2018; Siddiqui et al., 2020).

It was also postulated that, similar to mammalian cells, increased phosphorylation of the eukaryote translation initiation factor 2 $\alpha$  (eIF2 $\alpha$ ), might result in the upregulation of the translation of stress response proteins which might lead to altered stress response and parasite survival upon ART treatment (Zhang et al., 2017). However, the finding, that resistant parasites which are not exposed to ART already have an increased level of eIF2 $\alpha$  phosphorylation (Zhang et al., 2017) led to the hypothesis that elevated eIF2 $\alpha$  phosphorylation might not be the key factor for ART resistance (Yang et al., 2019).

## 1.6 Preliminary data on Kelch13 function and its role in ART resistance

Kelch13 is the molecular marker protein associated with ART resistance (Ariey et al., 2014) (see 1.5.3). However, the cellular function of Kelch13 was unclear (Birnbaum and Scharf et al., 2020; see 1.5.5). Preliminary and published data established the tools to study Kelch13 and provided the initial characterization of Kelch13 (Birnbaum et al., 2017; Birnbaum and Scharf et al., 2020). These findings are summarized in section 1.6.1 - 1.6.3. The preliminary data and parts of this thesis were published (Birnbaum and Scharf et al., 2020, including the preliminary data that formed the basis for this thesis (derived from Birnbaum, 2017 and Jonscher, 2018) but also data generated in this thesis).

### 1.6.1 Studying Kelch13 function and role in resistance

For functional analysis and localization studies, *pfkelch13* was tagged N-terminally via the SLI system (GFP-2xFKBP-Kelch13, termed as K13WT<sup>endo</sup>) (Birnbaum et al., 2017). To investigate the molecular resistance mechanism of parasites carrying the Kelch13 resistance conferring mutation C580Y, a parasite cell line with the mutated Kelch13 was generated using the SLI system (GFP-2xFKBP-Kelch13 C580Y, termed as K13C580Y<sup>endo</sup>) (Birnbaum et al., 2017). Furthermore, two parasite cell lines were established to conditionally inactivate Kelch13 via knock sideways (KS). For Kelch13 partial inactivation (90 % mislocalization of Kelch13) K13WT<sup>endo</sup> parasites were co-transfected with a 3xNLS mislocalizer, for complete inactivation of Kelch13 (100 % mislocalization of Kelch13) K13WT<sup>endo</sup> parasites were co-transfected with a 1xNLS mislocalizer (Birnbaum et al., 2017). Additionally, K13WT<sup>endo</sup> parasites were co-transfected with pSLI\_DiCre for conditional excision of the wild type *kelch13* gene. Inactivation of Kelch13, either with KS or via the DiCre system, resulted in the arrest of the parasites in rings stages followed by death of these parasites (Birnbaum et al., 2017).

### 1.6.2 Kelch13 defines an unknown compartment containing multiple unknown proteins

K13WT<sup>endo</sup> was expressed in all intra-erythrocytic stages and was found in foci in close proximity to the food vacuole and PI(3)P positive structures but did not co-localize with subcellular marker proteins for the ER or the golgi-apparatus (Birnbaum et al., 2017; Birnbaum and Scharf et al., 2020). This gave first evidence that Kelch13 is located at an unknown compartment. To gain insight into the Kelch13 compartment, DIQ-BioID experiments were performed with K13WT<sup>endo</sup> parasites and proteins in close proximity to Kelch13 were identified (Figure 12).

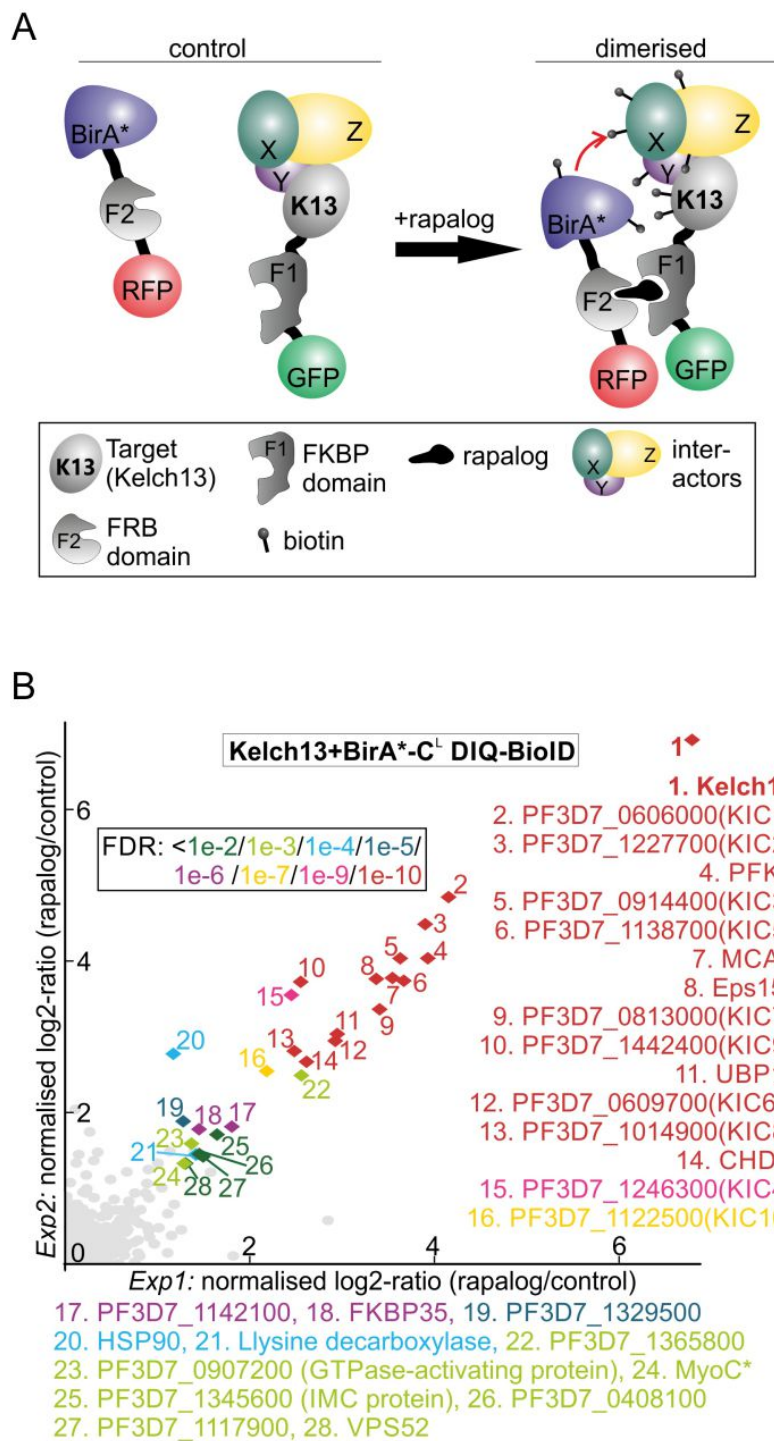


**Figure 12. DIQ-BioID experiment with endogenously tagged K13WT<sup>endo</sup> parasites. (A)** Schematic illustration of DIQ-BioID. Upon addition of rapalog, the biotin ligase BirA\* (biotinyliizer: BirA\* fused with FRB-mCherry) is conditionally recruited to Kelch13 (K13) and labelling of proteins in close proximity is initiated. **(B)** Top-right quadrant of scatter plot of K13WT<sup>endo</sup> DIQ-BioID showing enriched proteins identified by mass spectrometry (figure modified from Birnbaum and Scharf et al., 2020).

The top DIQ-BioID hits were tagged endogenously (via the SLI system) and the localization of the 13 candidates in the Kelch13 defined compartment was validated by co-localization with Kelch13, resulting in 11 co-localizing proteins (Table 1). These potential Kelch13 interacting candidates (KIC) were predominantly of unknown function and termed KIC1-KIC9, except for the proteins EPS15, UBP1, and MCA2 that had been named before (Figure 12, Table 1). KIC10, the only candidate that did not co-localize with Kelch13 was also retained and used as a control (Table 1). Of particular interest, the DIQ-

BioID analysis identified proteins that had already been associated with ART resistance in previous work: the ubiquitin carboxyl-terminal hydrolase 1 (UBP1), Eps15, MyosinC (MyoC) (not validated to co-localize with Kelch13 as not in the group of hits with the highest confidence) and KIC6. To functional analyze the Kelch13 compartment proteins and to assess whether the corresponding genes were essential for parasite survival, selected-linked integration gene disruption (SLI-TGD) was carried out if possible (Table 1). Only *pfkic7*, *pfubp1* and *pfeps15* could not be disrupted with this approach and therefore were likely essential for parasite survival (Birnbaum and Scharf et al., 2020).

**Table 1. Overview of analyzed K13WT<sup>endo</sup> DIQ-BioID hits.** 'K13 coloc' column: co-localization of the indicated proteins with episomally expressed Kelch13<sup>WT</sup>; green check mark: candidate co-localized with Kech13; red crosses: candidate did not co-localize with Kelch13; nd: not done (candidate couldn't be tagged via SLI). 'SLI-TGD' column: green check marks indicate successful disruption of the gene; red crosses attempt to disrupt using SLI-TGD were not successful, indicating essentiality of the corresponding genes (table from Birnbaum and Scharf et al., 2020).

	K13 coloc	SLI-TGD
KIC1	✓	✓
KIC2	✓	✓
PFK9	✗	nd
KIC3	✓	✓
KIC4	✓	✓
MCA2	nd	✓
Eps15	✓	✗
KIC5	✓	✓
KIC6	✓	✓
UBP1	✓	✗
KIC7	✓	✗
KIC8	✓	✓
KIC9	✓	✓
KIC10	✗	✓

### 1.6.3 The role of Kelch13 and Kelch13 compartment proteins in endocytosis

Based on the finding that Eps15 and also the known endocytosis marker AP2<sub>μ</sub> (as determined in Birnbaum and Scharf et al., 2020) was part of the Kelch13 defined compartment, it was investigated whether Kelch13 and its compartment proteins are involved in endocytosis. Correlative light and electron microscopy was performed and Eps15 was detected in close proximity to host cell cytosol - filled membranous structures (Birnbaum and Scharf et al., 2020; Flemming, 2015). Additionally, it was shown in a bloated food vacuole assay that inactivation of UBP1, Eps15, AP2<sub>μ</sub>, and KIC7 led to reduced hemoglobin uptake in trophozoites, whereas inactivation of Kelch13 itself did not influence hemoglobin uptake in this stage. Experiments with fluorescent dextran showed that endocytosis in *P. falciparum* already takes place in ring stages, the ART resistance relevant stage. Importantly, inactivation of Kelch13 in ring stages (0 - 6 hpi) reduced endocytic uptake of the fluorescent dextran (Figure 13 A). To test whether less endocytosis and consequently less hemoglobin degradation and ART activation could be the reason for ART resistance, hemoglobin uptake was measured in K13C580Y<sup>endo</sup> parasites. This demonstrated that resistant parasites endocytose less host cell material (Figure 13 C). To further confirm the relation between resistance and endocytosis, Kelch13 was conditionally inactivated and a standard ring stage survival assay (RSA, Witkowski et al., 2013) was performed. Interestingly, inactivation of

K13WT<sup>endo</sup> render the parasites resistant against ART (Figure 13 D) and also decreases host cell cytosol uptake in ring stages (Figure 13 A) (Birnbbaum and Scharf et al., 2020). Overall, these findings indicated that Kelch13 was needed for endocytosis in ring stages and that reducing this Kelch13 mediated function resulted in ART resistance.

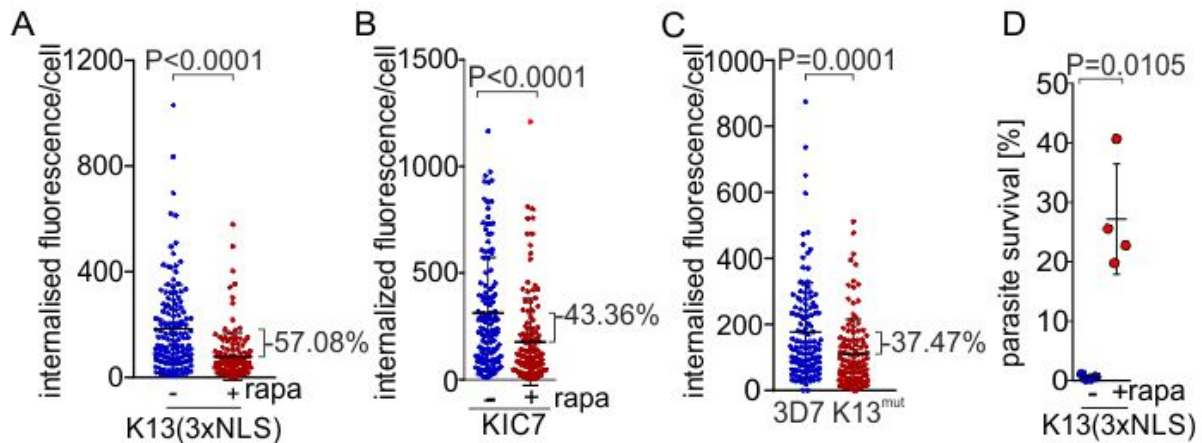


**Figure 13. Kelch13-defined complex is involved in endocytosis and resistance. (A - C)** Endocytic uptake was measured in a fluorescent dextran uptake assay and the internalized fluorescence per cell was determined upon K13 and KIC7 inactivation (+rapa) compared to the control (- rapa). Quantification of dextran uptake into 3 to-6-hour rings after inactivation (rapa) of Kelch13 by KS in the 3xNLS line (Birnbbaum et al., 2017) (A) or KIC7 (B) compared with control (no rapa) or in the K13mut parasites compared with wild type (3D7) (C). Each point shows the amount of fluorescence internalized into one cell (arbitrary fluorescence units). Data pooled from three independent experiments with a total of n = 138, 140, 132, 130, 122, and 114 cells for Kelch13 KS control, rapa, KIC7 control, KIC7 rapa, 3D7, and K13<sup>mut</sup>, respectively. Unpaired, two-tailed t test. P values and percent reduction of the mean are indicated. **(D)** RSAs after conditionally inactivation of Kelch13 (+rapa) compared with the control (- rapa) Unpaired, two-tailed t test with Welch's correction. Each point indicates an independent experiment (figure from Birnbbaum and Scharf et al., 2020).

To further investigate the role of the Kelch13 defined compartment in resistance, the Kelch13 compartment members UBP1, Eps15, AP2<sub>μ</sub>, and KIC7 were inactivated by knock sideways and ART susceptibility was determined by RSA. Inactivation of these candidates led to ART resistant parasites (Figure 14). This confirmed the involvement of the Kelch13 compartment in ART resistance. Moreover, it was also demonstrated that, comparable to the findings with Kelch13, inactivation of KIC7 led to less hemoglobin uptake in ring stages (Figure 13 B). These findings suggest a role of the Kelch13 compartment member proteins in resistance and endocytosis (Birnbbaum and Scharf et al., 2020).

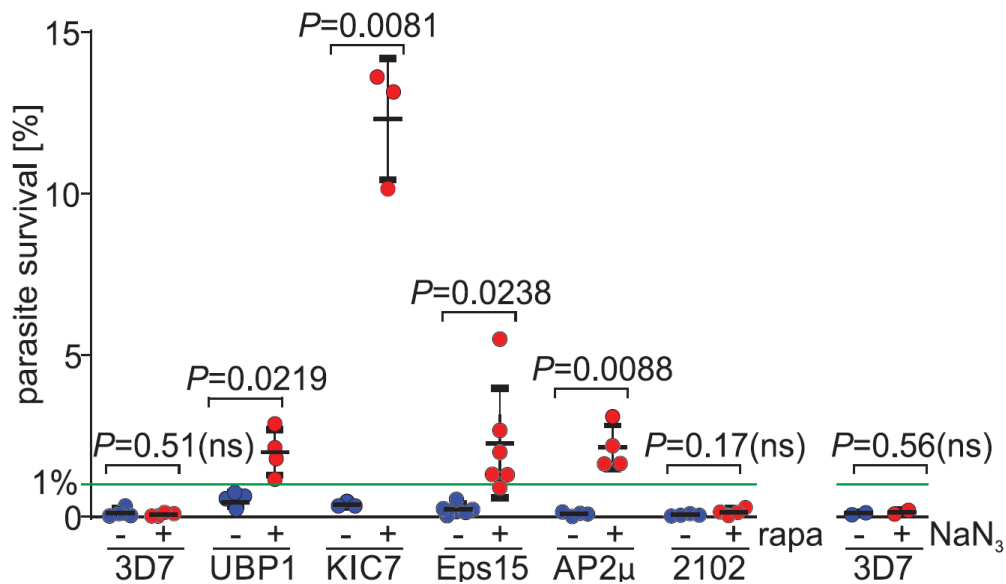


**Figure 14. The Kelch13 complex proteins are involved in ART resistance.** RSAs after inactivation of the indicated proteins via knock-sideways (+ rapa) compared to the control (- rapa or 3D7). Protein 2102 corresponds to PF3D7\_0210200 (Birnbaum et al., 2017) was used as an essential protein not part of the Kelch13 complex.  $\text{NaN}_3$  was used as a control to inhibit growth. Resistance in RSA defined as mean survival above 1 % (green line). Error bars show SD. ns: not significant. Unpaired, two-tailed t test with Welch's correction. Each point indicates an independent experiment (figure from Birnbaum and Scharf et al., 2020).

## 1.7 Aims of this thesis

The successes achieved in the fight against malaria in the last decades are threatened by increasing drug resistances, particularly by the resistance to the first line drug artemisinin and its derivatives. It is therefore critical to understand the molecular mechanism of artemisinin resistance. The previous and preliminary data indicate that Kelch13 mediates ART resistance by reducing hemoglobin endocytosis in ring stage parasites. However, it is not known how mutations in Kelch13 influence this process and how the different domains of Kelch13 contribute to the function of this protein. This work therefore has the aim to determine how Kelch13 mediates resistance, to examine the contribution of the different domains of Kelch13 to function and resistance and finally, to investigate the role of Kelch13 compartment proteins in ART resistance.

## 2 Material and Methods

### 2.1 Material

#### 2.1.1 Bacterial and *Plasmodium* strains

*Escherichia coli* XL-10 Gold *Tet<sup>r</sup> Δ(mcrA)183 Δ(mcrCB-hsdSMRmrr) 173 endA1 supE44 thi-1 recA1 gyrA96 relA1 lac Hte [F<sup>'</sup>proAB lacI<sup>q</sup> Z ΔM15 Tn10 (Tet<sup>r</sup>) Amy Cam<sup>r</sup>]*

*Plasmodium falciparum* 3D7 Clone of NF54 isolate (MRA-1000) from a malaria patient near the Amsterdam airport (Walliker et al., 1987)

#### 2.1.2 Chemicals

---

Acetic acid	Roth, Karlsruhe
Acrylamide/Bisacrylamide solution (40 %)	Roth, Karlsruhe
Agar LB (Lennox)	Roth, Karlsruhe
Agarose	Invitrogen
AlbumaxII	Gibco, Life Technologies, USA
Albumin bovine Fraction V (BSA)	Biomol, Hamburg
Ammonium persulfate (APS)	Applichem, Darmstadt
Ampicillin	Roche, Mannheim
Bacto™ yeast extract	BD, USA
Bacto™ Pepton	BD, USA
Biotin	Sigma, Steinheim
Blasticidin S (BSD)	Invitrogen, Karlsruhe
Bromophenol blue	Merck, Darmstadt
Calcium chloride (CaCl <sub>2</sub> )	Sigma, Steinheim
Desoxynucleotides (dNTPs)	Thermo Scientific
4',6-diamidino-2-phenylindole (DAPI)	Roche, Mannheim
Dihydroartemisinin (DHA)	Adipogen, Switzerland
Dihydroethidium (DHE)	Cayman, Ann Arbor, USA
Dimethyl sulfoxide (DMSO)	Sigma-Aldrich, Steinheim

---

---

Dipotassium phosphate	Roth, Karlsruhe
Disodium phosphate	Roth, Karlsruhe
1,4,-dithiothreitol (DTT)	Roche, Mannheim
DSM1	BEI resources
Dulbecco's Phosphate Buffered Saline (DPBS)	Pan Biotech, Aidenbach
Ethanol	Merck, Darmstadt
Ethidium bromide	Sigma Aldrich, Steinheim
Ethylenediaminetetraacetic acid (EDTA)	Biomol, Hamburg
Ethylene glycol tetraacetic acid (EGTA)	Biomol, Hamburg
G418 disulfate salt	Sigma Aldrich, Steinheim
Gentamycin	Ratiopharm, Ulm
Giemsa's azure, eosin, methylene blue solution	Merck, Darmstadt
D-Glucose	Merck, Darmstadt
Glutardialdehyd (25 %)	Roth, Karlsruhe
Glycerol	Merck, Darmstadt
Glycine	Biomol, Hamburg
Hoechst33342	Cheomdex, Switzerland
(4-(2-Hydroxyethyl)-1-piperazineethanesulfonic acid) (HEPES)	Roche, Mannheim
Hydrochloric acid (HCl)	Merck, Darmstadt
Hypoxanthin	Biomol, Hamburg
Isopropanol	Roth, Karlsruhe
Magnesium chloride (MgCl <sub>2</sub> )	Merck, Darmstadt
Manganese(II) chloride (MnCl <sub>2</sub> )	Merck, Darmstadt
β-Mercaptoethanol	Merck, Darmstadt
Methanol	Roth, Karlsruhe
3-(N-morpholino)propansulfonic acid (MOPS)	Sigma Aldrich, Steinheim
Milk powder	Roth, Karlsruhe
Percoll	GE Healthcare, Sweden
Phenylmethylsulfonylfluorid (PMSF)	Sigma Aldrich, Steinheim
Potassium chloride	Merck, Darmstadt
Protease inhibitor cocktail ("Complete Mini")	Roche, Mannheim
Rapalog (A/C Heterodimerizer AP21967)	Clontech, Mountain View, USA
Rubidium chloride	Sigma Aldrich, Steinheim
RPMI (Roswell Park Memorial Institute)-Medium	Applichem, Darmstadt
Saponin	Sigma-Aldrich, Steinheim
Sodium acetate	Merck, Darmstadt

---

Sodium chloride	Gerbu, Gaiberg
Sodium bicarbonate	Sigma Aldrich, Steinheim
Sodium dodecyl sulfate (SDS)	Applichem, Darmstadt
Sodium dihydrogen phosphate	Roth, Karlsruhe
Sodium hydroxide	Merck, Darmstadt
Sorbitol	Sigma Aldrich, Steinheim
N, N, N, N-Tetramethylethylenediamin (TEMED)	Merck, Darmstadt
Tris base	Roth, Karlsruhe
Tris-EDTA (TE)	Invitrogen, Karlsruhe
Triton X-100	Biomol, Hamburg
Water (Ampuwa)	Fresenius Kabi, Bad Homburg
WR99210	Jacobus Pharmaceuticals, Washington, USA

### 2.1.3 DNA- and protein-ladders

GeneRuler™ 1 kbp ladder	Thermo Scientific, Schwerte
PageRuler™ prestained protein ladder	

### 2.1.4 Kits

QIAamp DNA Mini Kit	Qiagen, Hilden
QIAGEN Plasmid Midi Kit	
Western Blot ECL-Clarity Detection Kit	Bio-Rad, USA
Western Blot ECL-SuperSignal West Pico	Thermo Scientific, Schwerte
NucleoSpin. Plasmid	Macherey-Nagel, Düren
NucleoSpin. Extract II	

### 2.1.5 Antibodies

Primary antibodies	anti-GFP (mouse)	1:1000 for Western Blots	Roche, Mannheim
	anti-GFP (rabbit)	1:2000 for Western Blots	Thermo Scientific, Waltham MA (USA)
	anti-RFP (rat)	1:1000 for Western Blots	Chromotek, Munich
	anti-BIP (rabbit)	1:2000 for Western Blots	Struck

	anti-Aldolase (rabbit)	1:2000 for Western Blots	Secondary antibodies
	anti-Kelch13_E3	1:200 for IFA	David Fidock
Secondary antibodies	anti-mouse-HRP	1:3000 for Western Blots	Dianova, Hamburg
	anti-rabbit-HRP	1:2500 for Western Blots	Dianova, Hamburg
	anti-rat-HRP	1:3000 for Western Blots	Dianova, Hamburg
	Streptavidin-HRP	1:1000 for Western Blots	Thermo Scientific, Waltham MA (USA)
Antibody coupled beads	Streptavidin-Sepharose	for protein pulldown	GE Healthcare life science

### 2.1.6 Fluorescence dyes

Hoechst 33342	Chemodex
Dihydroethidium	Cayman
DAPI	Roche

### 2.1.7 Enzymes and polymerases

Enzymes	Restriction Enzymes	NEB, Ipswich, USA.
	T4 DNA-Ligase [3 U/ $\mu$ l]	NEB, Ipswich, USA.
Polymerases	FirePol DNA Polymerase [5 U/ $\mu$ l]	Solis Biodyne, Taipei, Taiwan
	Phusion. High-Fidelity DNA Polymerase [2 U/ $\mu$ l]	NEB, Ipswich, USA
	Taq DNA Polymerase [5 U/ $\mu$ l]	NEB, Ipswich, USA

### 2.1.8 Oligonucleotides

All oligonucleotides were synthesized by Sigma-Aldrich, Steinheim and are shown in Appendix 7.

### 2.1.9 Plasmids

Plasmid	Source
pSLI-TGD (pARL1-GFP-T2A-Neo <sup>R</sup> )	(Birnbaum et al., 2017)

pSkipFlox	(Birnbaum et al., 2017)
pSLI_N_GFP-2xFKBP-Kelch13C580Y (DSM1 <sup>R</sup> )	(Birnbaum et al., 2017)
nmd3 5'UTR_mCherry-Kelch13 (BSD <sup>R</sup> )	(Birnbaum et al., 2017)
nmd3 5'UTR_BirA*-2xGGGGS-FRB-mCherry (BSD <sup>R</sup> ) (BirA-N <sup>L</sup> )	cloned by Kruse (Jonscher et al., 2019)
nmd3 5'UTR_-mCherry- FRB-2xGGGGS-BirA* (BSD <sup>R</sup> ) (BirA-C <sup>L</sup> )	cloned by Kruse (Jonscher et al., 2019)
crt SidM546-647-linker-GFP	cloned by Sven Flemming

### 2.1.10 Labware and disposables

Labware and disposables	Specifications	Manufacturer
Conical falcon tubes	15 ml, 50 ml	Sarstedt, Nümbrecht
Cryotubes	1.6 ml	Sarstedt, Nümbrecht
Culture bottles	50 ml	Sarstedt, Nümbrecht
Disposable pipette tips	1-10 / 20-200 / 100-1000 µl	Sarstedt, Nümbrecht
Eppendorf reaction tubes	1.5 / 2 ml	Sarstedt, Nümbrecht; Eppendorf, Hamburg
Filter tips	1-10 / 20-200 / 100-1000 µl	Sarstedt, Nümbrecht
Flow cytometry tubes	55.1579	Sarstedt, Nümbrecht
Glass cover slips	24 x 65 mm thickness 0.13-0.16 mm	R. Langenbrinck, Emmerdingen
Glass slides		Engelbrecht, Edermünde
Gloves, latex		Kimtech Science EcoShield
Leukosilk tape		BSN medical
Multiply-µStrip Pro 8-Strip		Sarstedt, Nümbrecht
PCR-reaction tube		Sarstedt, Nümbrecht
Nitrocellulose blotting membrane Protean	Amersham 0.45 µm	GE Healthcare
One-way canulas		Braun, Melsungen
One-way syringe		Braun, Melsungen
Parafilm		Bemis, USA
Pasteur pipettes		Brand, Wertheim
Petri dishes	15 x 60mm / 14x90 mm	Sarstedt, Nümbrecht
Plastic pipettes	5 / 10 / 25 ml	Sarstedt, Nümbrecht
Scalpel		Braun, Melsungen
Sterile filter	0.22 µm	Sarstedt, Nümbrecht
Transfection cuvettes	0.2 cm	Bio Rad, München

### 2.1.11 Software and bioinformatics tools

A plasmid Editor (ApE)	Open Source ( <a href="http://biologylabs.utah.edu/jorgensen/wayned/ape/">http://biologylabs.utah.edu/jorgensen/wayned/ape/</a> )
Axio Vision 40 v4.7.0.0	Zeiss, Jena
Corel Draw 2018	Corel Corporation, Ottawa
Corel Photo Paint 2018	Corel Corporation, Ottawa
Xcellence rt v5.2.0.3554	Olympus, Hamburg
GraphPad Prism 6.0d	GraphPad Software, La Jolla, USA
ImageJ 64 1.43u	Open Source ( <a href="http://rsbweb.nih.gov/ij/">http://rsbweb.nih.gov/ij/</a> )
Microsoft Office 2021 v.16.47	Microsoft Corporations, Redmond, USA
HHpred	<a href="https://toolkit.tuebingen.mpg.de/#/tools/hhpred">https://toolkit.tuebingen.mpg.de/#/tools/hhpred</a>
MotifScan	<a href="http://myhits.isb-sib.ch/cgi-bin/motif_scan">http://myhits.isb-sib.ch/cgi-bin/motif_scan</a>
PlasmoDB	Plasmodb.org
UbPred	<a href="http://www.ubpred.org/cgi-bin/ubpred/ubpred.cgi">http://www.ubpred.org/cgi-bin/ubpred/ubpred.cgi</a>
ProtParam tool – Expasy	<a href="http://web.expasy.org/protparam/">web.expasy.org/protparam/</a>
NCBI databases	<a href="https://www.ncbi.nlm.nih.gov/">https://www.ncbi.nlm.nih.gov/</a>
ClustalOmega	<a href="https://www.ebi.ac.uk/Tools/msa/clustalo/">https://www.ebi.ac.uk/Tools/msa/clustalo/</a>
BLAST	<a href="http://blast.ncbi.nlm.nih.gov/Blast.cgi">http://blast.ncbi.nlm.nih.gov/Blast.cgi</a>
the Image Lab software (v 5.2.1)	Bio Rad

### 2.1.12 Technical devices

Device	Specifications	Company
Agarose gel chamber	Sub Cell GT basic	Bio-Rad, München
Analytical Balance	870	Kern
Autoclave	V120	Systec, Wettenberg
Bacterial incubator	Thermo function line	Heraeus, Hannover
Centrifuge	J2-HS	Beckmann Coulter, Krefeld
Centrifuge	Avanti J-26S XP	Beckmann Coulter, Krefeld
Centrifuge	Megafuge 1.0R	Heraeus, Hannover
Centrifuge	5415 C	Eppendorf, Hamburg
Confocal microscope	Olympus FV1000	Olympus, Hamburg
Electro blotter	Phase	Bio-Rad, Munich
Electroporator	Gene Pulser X- Cel	Bio-Rad, Munich
Electroporator	Nucleofector II AAD-1001N	Amaxa Biosystems, Germany
Flow cytometer	LSR II	BD Instruments, USA
Fluorescence microscope	Axioscope 1	Zeiss, Jena
Gel imager	ChemiDoc XRS+	Bio-Rad, Munich
Ice machine	EF 156 easy fit	Scotsmann, Venon Hills, USA
Laboratory scale	Acculab Atilon-ATL	Acculab Sartorius, Göttingen
Light microscope	Axio Lab A1	Zeiss, Jena

Microscope digital camera	Orca C4742-95	Hamamatsu Phototonics, K.K.
Microwave	Micro 750W	Whirlpool, China
<i>P. falciparum</i> cell culture incubator	Heratherm IGS400	Thermo Scientific, Langenselbold
PCR mastercycler	Eppgradient	Eppendorf, Hamburg
pH-meter	SevenEasy	Mettler-Toledo, Gießen
Photometer	Bio Photometer plus	Eppendorf, Hamburg
Photometer	Nano Drop	Eppendorf, Hamburg
Pipettes	1-10/200/1000 µl	Gilson, Middleton, USA
Pipettor	Matrix Cellmate II	Thermo Scientific, Schwerte
Pipettor	Pipetboy acu	IBS, USA
Power supply	Power PAC 300	VWR, Taiwan
Roller mixer	STR6	Bio-Rad, München
Shaking Incubator	Max Q4000	Barnstead, Iowa, USA
Sterile laminar flow bench	Sterile Gard III Advance	Baker, Stanford, USA
Sterile laminar flow bench	Safe 2020	Thermo Scientific, Pinneberg
Thermoblock	Thermomixer compact	Eppendorf, Hamburg
Ultrapure water purification	Milli Q	Merck, Darmstadt
UV transluminator	PHEROLum 289	Biotec Fischer, Reiskirchen
Vacuum pump	BVC Contorl	Vacuubrand, Wertheim
Vortexer	Genie 2	Scientific Industries, USA
Waterbath	1083	GFL, Burgwedel

### 2.1.13 Solutions and buffers for biochemical experiments

#### SDS-PAGE and Western Blot

10 x Running buffer	250 mM Tris-Base 1.92 M Glycine 1 % (w/v) SDS in dH <sub>2</sub> O
Separating gel buffer	1.5 M Tris-Base 0.4 % SDS pH 8.8 in dH <sub>2</sub> O
Stacking gel buffer	0.5 M Tris-Base 0.4 % SDS pH 6.8 in dH <sub>2</sub> O
Separating gel (10 %)	2 ml dH <sub>2</sub> O 1.35 ml separating gel buffer 3.3 ml Acrylamide (30 %) 100 µl APS (10 %) 6 µl TEMED

Stacking gel	2.95 ml stacking gel buffer 2.17 ml dH <sub>2</sub> O 830 µl Acrylamide (30 %) 50 µl APS (10 %) 7 µl TEMED
Ammonium persulfate (APS)	10% (w/v) in dH <sub>2</sub> O
6 x SDS sample buffer	375 mM tris HCl pH 6.8 12 % (w/v) SDS 60 % (v/v) Glycerol 0.6 M DTT 0.06 % (w/v) Bromophenol blue
10x Western Blot transfer buffer	250 mM Tris-Base 1.92 M glycerol 0.1 % (w/v) SDS in dH <sub>2</sub> O
1x Western Blot transfer buffer	10 % 10 x Western transfer buffer 20 % Methanol in dH <sub>2</sub> O

### 2.1.14 Solutions and buffers for microbiological culture

10x LB stock solution	10 % NaCl 5 % peptone 10 % yeast extract in dH <sub>2</sub> O, autoclaved
LB working solution	1 % (w/v) NaCl 0.5 % (w/v) peptone 1 % (w/v) yeast extract in dH <sub>2</sub> O
LB Agar plate solution	1.5 % Agar-Agar 1x LB medium

Ampicillin stock solution	100 mg/ml in 70 % ethanol
Glycerol freezing solution	50 % (v/v) glycerol in 1x LB medium
TFBI buffer	30 mM acetic acid 50 nM MnCl <sub>2</sub> 100 mM RbCl 10 mM CaCl <sub>2</sub> 15 % (v/v) glycerol pH 5.8 (with 0.2 N Acetic acid) ad 500 ml H <sub>2</sub> O
TFBII buffer	10 mM MOPS 75 mM CaCl <sub>2</sub> 10 mM RbCl 15 % (v/v) glycerol pH 7.0 (with NaOH) ad 500 ml H <sub>2</sub> O

## 2.1.15 Solutions and buffers for molecular biological experiments

### Gibson assembly buffers

5x isothermal reaction buffer (6 ml)	3 ml 1 M Tris-HCl pH 7.5 150 µl 2 M MgCl <sub>2</sub> 60 µl each of 100 mM dGTP/dATP/dTTP/dCTP 300 µl 1 M DTT 1.5 g PEG-8000 300 µl 100 nM NAD ad 6 ml dH <sub>2</sub> O
Assembly master mixture (1.2 ml)	320 µl 5x isothermal reaction buffer 0.64 µl 10 U / µl T5 exonuclease 20 µl 2 U / µl Phusion DNA polymerase 160 µl 40 U / µl Taq DNA ligase ad 1.2 ml dH <sub>2</sub> O

### DNA gel electrophoresis

50x TAE	2 M Tris base
---------	---------------

	1 M Pure acetic acid 0.05 M EDTA pH 8.5
6x Loading buffer	40 % Glycerol (v/v) 2.5 % (w/v) Xylene cyanol 2.5 % (w/v) Bromophenol blue in dH <sub>2</sub> O

**DNA precipitation**

Sodium acetate	3 M NaAc, pH 5.2
Tris-EDTA (TE) buffer	10 mM Tris-HCl pH 8.0 1 mM EDTA pH 8.0

**2.1.16 Solutions and buffers for cell biological experiments*****P. falciparum* in vitro culture**

RPMI complete medium	1.587 % (w/v) RMPI 1640 12 mM NaHCO <sub>3</sub> 6 mM D-Glucose 0.5 % (v/v) Albumax II 0.2 mM Hypoxanthine 0.4 mM Gentamycin pH 7.2 in dH <sub>2</sub> O sterile filtered
Synchronization solution	5 % (w/v) D-Sorbitol in dH <sub>2</sub> O sterile filtered
Parasite freezing solution (PFS)	4,2 % (w/v) D-Sorbitol 0,9 % (w/v) NaCl 28 % (v/v) Glycerol in dH <sub>2</sub> O sterile filtered

Parasite thawing solution (PTS)	3,5 % (w/v) NaCl in dH <sub>2</sub> O sterile filtered
Transfection buffer (Cytomix)	120 mM KCl 150 μM CaCl <sub>2</sub> 2 mM EGTA 5 mM MgCl <sub>2</sub> 10 mM K <sub>2</sub> HPO <sub>4</sub> / KH <sub>2</sub> PO <sub>4</sub> 25 mM Hepes pH 7.6 in dH <sub>2</sub> O sterile filtered
Amaxa transfection buffer	90 mM NaPO <sub>4</sub> 5 mM KCl 0.15 mM CaCl <sub>2</sub> 50 mM HEPES pH 7.3 in dH <sub>2</sub> O sterile filtered
WR99210 stock solution	20 mM WR99210 in DMSO
WR99210 working solution	1:1000 dilution of stock solution in RPMI complete medium sterile filtered
Blasticidin S (BSD) working solution	5 mg/ml BSD in RPMI complete medium sterile filtered
G418 working solution	50 mg/ml in RPMI complete medium sterile filtered
DSM1 stock solution (50x)	187.5 mM DSM1 in DMSO
DSM1 working solution	100 μl DSM1 stock solution add 5 ml in 95 % DMSO / 5 % 1xPBS solution
Human red blood cells	Bloodgroup 0+, sterile concentrate, Blood bank Universitätsklinikum Eppendorf (UKE), Hamburg

Percoll stock solution	90 % (v/v) Percoll 10 % (v/v) 10x PBS
60 % Percoll solution	6.7 ml Percoll stock solution 3.3 ml RPMI complete medium 0.8 g Sorbitol sterile filtered
Parasite lysis buffer	4 % SDS 0.5 % Triton 0.5x PBS in dH <sub>2</sub> O
DHE stock solution (10x)	5 mg DHE in 1 ml DMSO
DHE working solution (1x)	0.5 mg DHE in 1 ml DMSO
Ho33342 stock solution (10x)	4.5 mg Ho33342 in 1 ml DMSO
Ho33342 working solution (1x)	0.45 mg Ho33342 in 1 ml DMSO
FACS stop solution	0.5 µl Glutaraldehyde (25%) in 40 ml RPMI complete medium
Rapalog (AP21967) stock solution	500 mM in ethanol
Rapalog working solution	1:20 dilution of stock solution in RPMI complete medium
DHA stock solution	0.001g DHA in 11 ml DMSO
DHA working solution	100 µl DHA stock solution in 200 µl DMSO / 1x PBS (1:10)

## 2.2 Methods

### 2.2.1 Microbiological Methods

#### 2.2.1.1 Sterilization of solutions and devices

Working solutions and objects used in the following experiments were sterilized at 121 °C and 1.5 bar steam pressure. In order to be able to sterilize heat-sensitive liquids, they were sterile filtered using disposable filters with a pore size of 0.2 µm.

#### 2.2.1.2 Production of competent *E. coli*

(Hanahan, 1983)

In order to be able to propagate plasmids in molecular biology, they are usually introduced and propagated in non-pathogenic strains of the intestinal bacterium *Escherichia coli*. In order to ensure efficient uptake of the plasmid in the bacteria, the bacterial cell walls and plasma membranes must first be chemically destabilized using calcium chloride. The cells are then referred to as "competent cells". For this purpose, a 200 ml LB medium glass flask is first inoculated with 4 ml of an *E. coli* XL gold strain overnight culture and incubated at 37 °C in a shaker for about 2 hours. The bacterial culture should achieve an OD600 of 0.5 - 0.55. The liquid bacterial culture is then centrifuged in pre-cooled 50 ml Falcon tubes at 2600 g for 20 min at 4 °C. The pelleted bacteria are then carefully resuspended in 15 ml of ice-cold TFBI solution and incubated on ice for 10 minutes and then pelleted again at 2400 g for 20 minutes at 4 °C. The pellet is again resuspended in a calcium chloride-containing solution (TFBII solution) and aliquoted in 100 µl units. The competent bacterial cells are then stored at - 80 °C until they are used.

#### 2.2.1.3 Transformation of chemo-competent *E. coli*

To transform plasmid DNA into *E. coli* bacteria, one unit of 100 µl competent bacteria was thawed for 10 min on ice. 0.3 µl of an amplified (via mini preparation) and sequenced plasmid (final concentration 0.5 - 1 µg DNA) was added and incubated in presence of the competent cells on ice for 20-30 min. The mixture was heat shocked for 30 sec at 42 °C and afterwards immediately cooled down on ice again. The complete suspension was plated on pre-warmed (37 °C) LB agar plates containing ampicillin as a selection marker. To ensure growth of plasmid positive bacteria the plate was incubated for 15-20 h at 37 °C.

#### 2.2.1.4 Cultivation and storage of *E. coli*

After plasmid DNA has been successfully transformed into *E. coli* bacteria, the bacteria are cultivated in LB liquid medium or LB agar plates, which contain the antibiotic ampicillin (final concentration of 100 µg / ml). This enables successfully transformed bacteria to be selected which are resistant to ampicillin due to the plasmid taken up. Insert-positive single colonies are then taken up in LB<sub>AMP</sub>- liquid

medium and incubated overnight at 37 °C on a shaker at 1000 rpm. The genetically modified *E. coli* bacteria can then be treated with 50 % glycerol for permanent storage and stored at -80 °C.

## 2.2.2 Molecular biological Methods

### 2.2.2.1 Polymerase chain reaction

The polymerase chain reaction (PCR) is based on *in vitro* amplifying of specific DNA fragments and was used to detect DNA fragments and to quantitatively assess its DNA content. The thermostable DNA polymerase elongates, and consequently amplifies, single stranded nucleotides. Specific forward and reverse primer, which flank the DNA target sequence, were designed and the polymerase can amplify the defined DNA fragment resulting in an exponential increase with every cycle reaction. The reaction steps are defined as denaturation, annealing and extension. During the denaturation, the template DNA is heated up to 95 °C leading to the conversion of double to single stranded DNA. In the second step the temperature decreases leading to the annealing of the oligonucleotides to the complement sequence of the template DNA (annealing step). The annealing temperature depends on the melting temperature of the primer. In the last step, called elongation, the temperature is slightly increased again in order to achieve maximum efficiency of the DNA polymerase. The polymerase attaches deoxyribonucleotide triphosphates (dNTPs) to the 3'- end of the nucleotides and thus extends the oligonucleotides, creating a complementary DNA strand to the template DNA. Elongation times depend on the expected size of the PCR product (usually 1 min per 1000 bp). For amplification of a PCR product with subsequent cloning a Phusion – high fidelity polymerase (NEB) was used. It has an additional 3' - 5' - exonuclease activity, which means that the incorporation of incorrect nucleotides can be corrected. For analytical PCRs, like colony screens for the identification of insert positive clones after the transformation of a plasmid or integration check, FirePol DNA polymerase (Solis Biodyne) was used.

**Table 2. PCR mix for FirePol DNA polymerase (10 µl batch).**

Reagent	Volume [µl]
Ampuwa® H <sub>2</sub> O	6.4
MgCl <sub>2</sub> (25 mM)	0.6
dNTPs (2 mM)	1
Forward Primer (10 mM)	0.4
Reverse Primer (10 mM)	0.4
10x FirePol Buffer	1
FirePol DNA Polymerase	0.1
DNA template	0.1

**Table 3. Conditions for analytic PCRs.**

Cycle number	Denaturation	Annealing	Elongation
1	2 min, 95 °C		
2–30	30 s, 95 °C	30 s, 45-68 °C	1 min/kb, 68-72 °C
31			10 min, 72 °C

**Table 4. PCR mix for Phusion DNA Polymerase (50 µl batch).**

Reagent	Volume [µl]
Ampuwa <sup>®</sup> H <sub>2</sub> O	30.4
dNTPs (2 mM)	5
Forward Primer (10 mM)	2
Reverse Primer (10 mM)	2
5x Phusion Buffer	10
Phusion DNA Polymerase (2 U/µl)	0.3
DNA template	0.3

**Table 5. PCR conditions for preparative purpose.**

Cycle number	Denaturation	Annealing	Elongation
1	2 min, 95 °C		
2–30	30 s, 95 °C	30 s, 45-72 °C	0.5 min/kb, 72 °C
31			5 min, 72 °C

### 2.2.2.2 Agarose gel electrophoresis

(Garoff and Ansoerge, 1981)

To separate molecules according to their molecular weight, agarose gel electrophoresis was used. A size-specific separation of the amplified double-stranded DNA takes place, which is induced by an electric field. Due to the negative charge of DNA, which is caused by phosphate groups, the DNA migrates in the electric field towards the anode. Gels with 1 % agarose were used for Agarose is extracted from seaweed and has a melting temperature of approx. 95 °C. Based on this, the suspension was heated in a microwave for approx. 1 min until the powder has dissolved and at the same time homogenized with the buffer. The liquid suspension was cooled down to a moderate temperature, ethidium bromide (1 µg / ml) was added and the solution was given in a plastic carrier. After 30 min the polymers formed a solid gel structure. The gel was placed in a gel chamber filled with TAE buffer and 6 µl of the PCR sample treated with 6 x loading buffer were applied to the pockets. In addition, a DNA size standard was applied as. The DNA fragments were separated for 30 min at 150 V. DNA molecules only have a primary and secondary structure and their charge and length correlate, so the size of the fragment from the distance traveled by the samples can be deduced proportionally. The ethidium bromide contained in the gel intercalates into the DNA structure during this process, so that the fragments can later be made visible by means of UV radiation. The gel was analyzed using the ChemiDoc™ XRS (Biorad) imager and the ImageLab software.

### 2.2.2.3 PCR-product and plasmid purification

In order to be able to remove reagents such as oligonucleotides, salt-containing buffers or restriction enzymes from a PCR product or to purify a plasmid after digestion steps, the Nucleo Spin Gel and PCR

Clean-up kit was used as instructed in the manual. The process is based on the binding of the negatively charged DNA to a silica membrane, which is initiated by adding a binding buffer. Afterwards, salts and polymerases can be separated from the bound DNA by using a buffer containing ethanol. Next the purified PCR product or plasmid can be dissolved in 20 – 50 µl elution buffer.

### 2.2.2.4 Restriction digest

For cloning procedures restriction approaches were conducted with restriction enzymes (NEB) for DNA, PCR products and vector products. Approximately 50 µl of eluted PCR product was mixed with 0.5 µl (1.5 U Enzyme/ µg DNA) and 5 µl buffer. During restriction digestion of the DNA sequence, after amplification of the insert on a plasmid, the generated insert was digested with the enzyme *DpnI*. *DpnI* cuts specifically methylated DNA sequences in vectors which have already been expressed in *E. coli*. For the preparative digestion of a vector, ~ 1 µg of vector was added to the digestion mixture. The digestion mix was incubated in both cases at 37 °C for 3 h.

Reagent	PCR product digestion (µl)	Plasmid digestion (µl)
CutSmart® buffer (10x)	5	2
PCR product / Plasmid DNA	20	1
Enzym 1	1	0,5
Enzym 2	-	0,5
Ampuwa® H <sub>2</sub> O	24	16

### 2.2.2.5 Gibson assembly

(Gibson et al., 2009)

Gibson assembly enables the ligation of one up to six inserts into a linearized vector. For the Gibson ligation, a DNA sequence was amplified with specially designed Gibson primers. The oligonucleotides that were used had a longer overlap area in the complementary DNA strands, which led to sticky ends of the same length in the resulting PCR products. The restricted PCR product was inserted into a target vector. For this, the vector and the insert were brought into solution with an isothermal reaction buffer, a T5 exonuclease, a DNA polymerase and a DNA ligase (Gibson Assembly Master Mix) in the following proportion:

Reagent	Volume (µl)
Gibson Assembly Master Mix	8
Vector	1
Insert	0,5

The reaction mixture was incubated for 1 h at 50 °C and then transformed into competent *E. coli* bacteria by heat shock (30 sec, 42 °C).

### 2.2.2.6 Plasmid isolation

To isolate plasmid DNA from transformed *E. coli* cells, these were first incubated in a 2 ml batch (mini preparation) or 200 ml batch (midi preparation) overnight at 37 °C while shaking. The suspension was pelleted for 2 min at 6000 × g (mini preparation) or for 15 minutes at 6000 × g at 4 °C (midi preparation). The plasmid DNA isolation was then carried out according to the manufacturer's instructions using commercially available kits (Nucleo Spin Plasmid, Macherey-Nagel for mini preparations or QIAfilter Plasmid Midi Kit, QIAGEN for Midi preparations). In the last step, the plasmid DNA was eluted with 20 µl in the mini standard or 200 µl in the midi standard with elution buffer and could then be examined photometrically for concentration determinations.

### 2.2.2.7 Sequencing of plasmid DNA

In order to examine DNA sequences for possible mutations, the respective DNA fragments were sequenced. In addition, this procedure was used to confirm the correct insertion of DNA sequences in vectors. The sample including 200 – 800 ng plasmid DNA and 3 µl of 10 mM sequencing primer was diluted in 15 µl Ampuwa® H<sub>2</sub>O and was sent to Seqlab (Sequence Laboratories, Göttingen). The sequencing results were downloaded the following day from the company's website.

### 2.2.2.8 DNA precipitation

To precipitate DNA, 20 – 100 µg plasmid DNA was dissolved in sodium acetate (3 M) in a ratio 10:1 and 2.5 volumes of absolute ethanol. The suspension was mixed gently and centrifuged for 15 min at 1800 x g. The precipitated DNA pellet was treated with 100 µl of 70 % ethanol for disinfection, centrifuged again for 2 in 1800 x g and taken up in 10 – 20 µl TE buffer for further use. The DNA was stored at 4 °C.

### 2.2.2.9 Nucleic Acid quantification

For an exact determination of nucleic acid concentration and the assessment of its purity, photometric analysis was used. This was important for following ligation as well as transfection steps. DNA concentration determination was carried out using a Nano Drop 2000c spectrometer (Thermo Scientific). Because of its bases, DNA absorbs a certain wavelength, the absorption maximum being 260 nm (A260), with maximum absorption values of 280 nm (A280) being determined for proteins. For photometric quantification, the quotient of A260 to A280 was determined in 1 µl of dissolved DNA and calculated against a previously determined zero value. Values from 1.8 to approx. 2.0 provided information about an acceptable purity of the sample.

### 2.2.2.10 Genomic DNA isolation

To confirm the correct integration of a plasmid into the genomic locus of the target gen, genomic DNA (gDNA) from transgenic parasite cell lines was isolated using the QIAfilter Plasmid Midi Kit according to the manufacturer's protocol. The gDNA was used as a template for integration check PCR, 3D7 wild

type gDNA fungated thereby as a negative control. For gDNA isolation, transgenic parasite cells were harvested with at least 1 % parasitemia.

## 2.2.3 Cell biological Methods

### 2.2.3.1 Continuous culture of *P. falciparum*

(Trager and Jensen, 1976)

The *P. falciparum* parasite was cultivated for proliferation in human erythrocytes. For this purpose, 5 ml of the culture medium RPMI was mixed with erythrocytes of blood group 0 + (transfusion blood, Universitätsklinikum Hamburg-Eppendorf) in a 5 ml petri dish in order to set a hematocrit value of 5 %. To imitate the natural conditions of the human body as best as possible, the culture dishes were stored in boxes and incubated at 37 ° C. The boxes were previously gassed with a gas mixture (5 % CO<sub>2</sub>, 5 % O<sub>2</sub>, and 90 % N<sub>2</sub>) for about 30 seconds. Transgenic parasites were selected by adding WR99210 (4 nM), Blasticidin S (2 µg / ml) and DSM1 (0.9 µM). The selection for knock-in integrants was enabled by the addition of G418 (Neomycin, 400 µg / ml) to the parasite culture.

To obtain the percentage of infected blood cells (= parasitemia), Giemsa smears were prepared and checked by microscopy. The parasitemia was kept at approximately 3 % during the cultivation to suit experimental requirements. For this purpose, the cell culture was diluted by a factor of 1:10 with preheated RPMI every 48 hours, depending on the growth rate of the parasites. In addition, the full medium was changed every second day at the latest to ensure a constant supply of the parasites with sufficient nutrients.

### 2.2.3.2 Cryo-stabilates of *P. falciparum*

*P. falciparum* parasite culture can be stored for time periods of several years either at -80 °C or in liquid nitrogen. In order to produce cryo-stabilates from a parasite culture, the cells were adjusted to 5 % parasitaemia in the early ring stage, since later stages do not survive the treatment with cryo-stabilate solution. The culture was centrifuged at 1800 x g for 3 min and the supernatant was discarded. The pelleted cells were then taken up in 1 ml Malaria Freezing Solution (MFS), transferred to a labeled cryogenic vessel and stored at - 80 °C or in a liquid nitrogen tank at - 196 °C.

### 2.2.3.3 Thawing procedure of *P. falciparum* cryo-stabilates

For thawing of *P. falciparum* parasites, the cryo-tube was heated in a water bath at 37 °C for about 1 min. The cell suspension was transferred to a culture tube and was centrifuged (1800 x g for 3 min) at room temperature. The supernatant was discarded and the cell pellet was resuspended in 1 ml Malaria Thawing Solution (MTS). This was followed by another centrifugation step at 1800 × g for 3 min, the supernatant was removed again and the cells were washed in pre-warmed RPMI complete medium. The washed cells were transferred to a petri dish for cultivation at 37 °C.

### 2.2.3.4 Blood smears and Giemsa staining

Preparation and staining of thin blood smears of *P. falciparum* infected red blood cells were done for following purposes: to determine the parasitemia, to analyze parasite's development or to assess the condition of the cell cultures. For blood smears 0.5 – 1 µl infected erythrocytes were transferred to a glass slide. The drop was smeared using a second glass slide in a 45 ° angle to obtain a single cell layer. After drying, the smear was fixed in methanol (99 %) for 10-30 sec and transferred in a staining bath containing Giemsa's azur eosin methylene blue solution (Merck, Darmstadt, Germany) and stained for 10 min. After washing off the staining solution, the slide was dried and analyzed by using an optical light microscope (Carl Zeiss, Oberkochen, Germany).

### 2.2.3.5 Transfection of *P. falciparum*

Transfection is defined by the introduction of foreign DNA into eukaryotic cells. Electroporation is used for the transfection of *P. falciparum*. This method ensures the smuggling of the foreign DNA via the erythrocyte plasma membrane, the parasitophorous vacuole membrane (PV), the parasite plasma membrane (PPM) and the nuclear cell membrane of the parasite. Permeable pores are formed in the respective membranes in order to absorb the transgenic DNA.

For *P. falciparum* transfection, the two following electroporation methods were used.

#### Segmenter transfection

For the transfection, late schizonts from a synchronized 10 ml parasite culture were isolated using Percoll (see 2.2.3.8) and taken up in 90 µl of pre-warmed TB-BSF buffer. At the same time, 50 to 100 µg of the plasmid DNA was precipitated with a tenth volume of 3 M sodium acetate and 3 times the volume of 100 % ethanol and then washed in 70 % ethanol. The DNA was then dissolved in 10 µl of TE buffer and dried at room temperature. The parasite solution containing schizont stages was then added to the DNA and the reaction mixture was transferred to an electroporation cuvette and placed in the Amaxa Biosystems Nucleofector II (Lonza) device. The foreign DNA was introduced into the *P. falciparum* parasites using the UO33 program. The cells were then taken up in 200 µl of pre-warmed RPMI medium and 300 µl of erythrocytes and incubated for 30 min at 37 ° C on a thermal shaker. The batch was then taken up and transferred in a petri dish containing RPMI complete medium and 5 % hematocrit. The culture medium was changed daily for the following 7 days to ensure nutrient supply. In addition, transgenic parasites were selected with the respective selection drug.

#### Ring stage transfection

To transfect ring stage *P. falciparum* parasites, the BioRad transfection system was used. 10 ml parasite culture of ring stage parasites with a parasitemia of 5 – 10 % was spun down for 3 min at 2800 x g. Meanwhile, plasmid DNA was precipitated (see segmenter transfection) and 100 µg of DNA was solved in 20 µl TE buffer. 380 µl Cytomix was added to the solved DNA, mixed with 200 µl of the pelleted infected erythrocytes, and transferred to an electroporation cuvette (2 mm, Biorad). The electroporation was performed using a Gene Pulser Xcell (Biorad; conditions: 310 V, 950 µF, ∞ Ω). The batch was then taken up and transferred in a petri dish containing RPMI complete medium and 5 % hematocrit. The culture medium was changed daily for the following 7 days to ensure nutrient supply. In addition, transgenic parasites were selected with the respective selection drug.

### 2.2.3.6 Selection for transgenic parasite cell lines using SLI

To select for integrants carrying the episomal plasmid, the SLI system was used (Birnbaum et al., 2017). Therefore, the selective drug WR99210 was applied, followed by adding G418 to a final concentration of 400 µg / ml to the parasite culture with 4 – 10 % parasitemia in 10 ml RPMI complete medium. Parasites, carrying a plasmid with yDHODH as SLI resistance marker, 1.5 µM DSM1 was added instead of G418. After supplying the selective drug, the culture medium was changed daily for a time period of 7 days. Afterwards the medium was changed every second day until parasites were obtained. The cultures were maintained for a maximum of 100 days, if no parasites appeared the culture was discarded. To monitor parasite appearance during the selective process, Giemsa smears were made every second day, but the latest every third day. In the case of parasite growth, genomic DNA was isolated with the QIAamp DNA Mini Kit to check for correct integration of the plasmid in the genomic locus of the target gene using integration check PCR. If original wild type locus was detected, WR99210 was supplied for two more weeks before the correct integration was checked again.

### 2.2.3.7 Sorbitol synchronization of *P. falciparum*

In order to synchronize infected blood cells with *P. falciparum* in the ring stage, the parasite culture was treated with D-sorbitol. With this method, the resulting osmotic pressure selects the parasites at ring stages of up to 18 hpi.

For this, the infected erythrocytes were centrifuged at 1800 × g for 3 min and the resulting pellet was resuspended in a five-fold volume of a sterile and pre-warmed (37 °C) 5% D-sorbitol solution. The cell suspension was then incubated for 10 min at 37 °C and centrifuged again at 1800 × g for 3 min for sedimentation. The cell pellet, which now contained uninfected erythrocytes as well as erythrocytes infected with ring stages, was then washed once with RPMI medium and taken up again in culture medium incubated at 37 °C for further cultivation.

### 2.2.3.8 Percoll gradient of *P. falciparum* infected erythrocytes

In order to be able to transfect wild-type 3D7 cells with DNA in segmenter stages and carry out stage-specific investigations in *P. falciparum*, the parasite culture was synchronized using a Percoll solution. Furthermore, parasites were selected for the schizont stage in order to be able to carry out controlled invasion of young ring stage parasites in erythrocytes.

For this, 5 or 10 ml of an asynchronized culture were added to 4 ml of 60 % Percoll, so that the Percoll solution was slowly covered and a clear separating layer emerged between the two solutions. This was followed by a centrifugation step at 2800 x g for 6 min, so that a gradient between the Percoll solution and the overlying culture medium emerged. The enriched schizonts are clearly recognizable as a dark ring structure between the two solutions. Uninfected erythrocytes and earlier stages of the parasite could be recognized as a pellet on the bottom of the falcon tube. In order to be able to isolate the schizonts from the suspension, the medium stored above was removed and the parasite ring was taken up with a pipette and washed with 10 ml of RPMI. The synchronous schizonts could then be recultivated or used for further experiments.

### 2.2.3.9 Saponin lysis of *P. falciparum* infected erythrocytes

(Umlas and Fallon, 1971)

The isolation of the parasite from the RBC has to be performed to analyze parasite's proteins. Saponin is a detergent that lyses the membrane of the erythrocyte as well as the parasitophorous vacuole membrane (PVM) but keeps the integrity of the parasite plasma membrane (PPM). 10 ml of parasite culture with a parasitemia of 5 – 10 % was harvested and centrifuged for 5 min 11.000 x g. The supernatant was discarded and the cells were washed once with 10 ml 1 x PBS to remove medium left overs. After centrifugation, the supernatant was removed and the pellet was mixed carefully. Next, 10 pellet volumes of ice-cold and fresh prepared 0.03 % saponin in PBS was added, gently mixed with the cells and incubate on ice for 10 min. The suspension was centrifuged for 5 min at 11.000 x g at 4 °C and the supernatant was removed. From now on the procedure was continued on ice and if necessary, in cooled centrifuges. The lysed cells were transferred into a 2 ml tube and centrifuged for 3 min at 1800 x g followed by washing steps with ice cooled 1 x PBS until no hemoglobin is visible in the supernatant anymore. Next, depending on the size of the pellet 1 - 5 µl of 25 x protease inhibitor cocktail and 1 mM PMSF was added and mixed with the pellet. The suspension was resuspended in 50 - 150 µl SDS - lysis buffer (depending on the size of the pellet) for 5 min to lyse the PVM. After centrifugation for 3 min at 1800 x g the proteins remained in the supernatant, which is transferred gently into a new tube without disrupting the pellet at the bottom of the reaction tube. The mixture can be stored at -20 °C for further use. To avoid protein degradation, the lysate was immediately mixed with 90 °C heated 4 x blue dye (15 µl 4 x blue dye per 50 µl supernatant) and was used for SDS-PAGE (see 2.2.4.1) for further analysis. After adding the blue dye, the samples can't be stored on ice anymore.

### 2.2.3.10 Biotin labeling of proteins using DIQ-BioID

To perform dimerization induced quantitative BioID (DIQ-BioID, Birnbaum and Scharf et al., 2020) experiment proximate proteins of the target proteins needed to be biotinylated. For this purpose, the biotin ligase BirA\* tagged with FRB-FRB-mCherry C- as well as N-terminally (Birnbaum and Scharf et al., 2020) was expressed on a genomic parasite background modified with SLI (Birnbaum et al., 2017). It was necessary to provide a huge amount of cell material for mass spectrometry analysis for which reason the biotin labelling was performed twice with 150 ml parasite culture with approximately 5 % parasitemia (3 x 50 ml culture bottles per condition).

Asynchrony parasite culture was splitted into 6 x 50 ml culture bottles. 3 bottles were treated with 250 nM rapalog to induce dimerization, the other 3 bottles fungated as a control with no dimerization. Simultaneously, 50 µM biotin was added to all culture bottles for 24 h. The cultures were fed every 8 h to ensure nutrient supply.

After 24 h incubation the culture was centrifuged (6000 x g, 20 min) and the supernatant discarded. The parasites were lysed with saponin as already described (see 2.2.3.9). During the saponin lysis TBS was used instead of PBS. The samples were transferred to a 2 ml reaction tube and washed two times with DPBS Next, the cells were lysed in 2 ml lysis buffer for mass spectrometry analysis. The reaction tubes were sealed with parafilm and two times frozen (at -80 °C) and thawed (on ice) to increase cell lysis. The cell leftovers were centrifuged at 16000 x g for 10 min and the supernatant was transferred to a 15 ml falcon and diluted 1:2 with TrisHCl (50 mM, pH 7.5), 2 x protease inhibitor cocktail and 1 mM PMSF. Next, 50 µl of Streptavidin-Sepharose was equilibrated with TrisHCL (50 mM, pH 7.5), added

to the samples and incubated overnight rotating head over head at 4 °C. The beads were sedimented by centrifugation at 1600 x g for 1 min, transferred in a 1.5 ml reaction tube and washed twice with 500 µl lysis buffer, once in 500 µl ice cooled dH<sub>2</sub>O (Ampuwa®), two times in 500 µl ice cooled TrisHCl (50 mM, pH 7.5) and three times in 500 µl cold TEAB (100 mM). During each washing step the samples were incubated rolling and centrifuged at 1600 x g for 2 min afterwards.

The sepharose was then re-suspended in 50 µl TEAB (100 mM) and the samples were sent on ice for mass-spectrometry analysis to our collaboration partner (Bartfai lab, Radboud Institute, Nijmegen, Netherlands) where stable-isotope dimethyl labelling was used for quantification.

### 2.2.3.11 Flow cytometry growth assay

(Boersema et al., 2009)

To determine parasite's growth rate and parasitemia over a defined time window, Flow cytometry analysis was performed using the LSRII flow cytometer (Malleret et al., 2011). Growth assays were performed with asynchron parasite cultures using a defined start parasitemia that was observed for either 5 or 7 following days. To avoid overgrowing of the culture, the start parasitemia was adjusted between 0.05 – 0.3 % and the parasites were fed every day with RPMI complete medium. For staining of the cells, 20 µl cell suspension was transferred in a FACS tube and mixed with a 80 µl of RPMI medium containing Hoechst 33342 (4.5 µl / ml) and dihydroethidium (DHE, 0.5 µg/ml) for 20 min at room temperature in a dark box. Next, 400 µl FACS staining stop solution (0,003 % glutaraldehyde) was added to stop the staining reaction. 100.000 events were counted per sample and analyzed with FACSDiva.

### 2.2.3.12 Stage specific experiments upon knock sideways induction

Knock sideways (KS) experiments were performed to observe stage specific impact of target protein inactivation due to mislocalisation on the parasite development.

#### KS induction in rings

For KS induction in rings, 10 ml parasite culture with 4 – 6 % mature schizonts was purified with 60 % percoll (see 2.2.3.8). The cells were washed once with RPMI medium and transferred in a 1.5 ml tube containing 100 µl fresh erythrocytes and 50 µl RPMI, followed by rupturing of the mature stages and controlled invasion of ring stages parasites in RBCs (30 min, 37 °C, 800 rpm). The cells were recultivated for 8 hours using standard culture conditions and were then synchronized with 1 ml pre-warmed 5 % sorbitol at 37 °C for 10 min to obtain 0 – 8 hour old rings. The young rings were washed three times with RPMI, resuspended in RPMI and splitted into two culture dishes. 250 nM rapalog was added to one dish to induce the KS in ring stages, the other culture dish served as a control. The culture medium was changed every day and new rapalog (250 nM) was added each time to the cells cultivated in the presence of rapalog. Giemsa smears were made every 8 hours. If the parasitemia was too high the culture was diluted to avoid overgrowing.

#### KS induction in trophozoites

For KS induction in trophozoite stages, the parasites were synchronized as describes above for rings stage induction. 0 – 8 h Ring stage parasites were grown at 37 °C for 16 more hours before inducing KS

by adding rapalog to one of the culture dishes. The following procedure was the same as described for ring stage induction.

Furthermore, KS with the 3xNLS-FRB-mCherry mislocalizer was performed to observe ring stage development in Kelch13 deficient parasites. The induction of the KS was performed 12 hours before purifying 10 ml asynchron parasite culture, containing 4 – 6 % mature schizonts, using 60 % percoll (see 2.2.3.8). The cells were washed once with RPMI medium and transferred in a 1.5 ml tube containing 100 µl fresh erythrocytes and 50 µl RPMI, followed by rupturing of the mature stages and controlled invasion of ring stages parasites in RBCs (30 min, 37 °C, 800 rpm). The cells were recultivated for 2.5 hours in a petri dish and synchronized with 1 ml pre-warmed 5 % sorbitol at 37 °C for 10 min to obtain 0 – 3 hour old rings. The young rings were washed three times with RPMI and transferred into 5 culture dishes reflecting the different sample probes for each time point. This setup allows continuous culturing of each sample without disturbing the culture process for making smears. Simultaneously as a negative control, a proportion of the same cells which were cultivated without rapalog were treated and cultivated the in the same setup.

### 2.2.3.13 In-vitro ring stage survival assay<sup>0-3 h</sup> (RSA)

(Witkowski et al., 2013)

In order to determine the survival rate of *P. falciparum* parasites after a dihydroartemisinin (DHA) pulse, 10 ml asynchron parasite culture, containing 4 – 6 % mature schizonts, was purified using 60 % percoll (see 2.2.3.8). The cells were washed once with RPMI medium and transferred in a 1.5 ml tube containing 100 µl fresh erythrocytes and 50 µl RPMI, followed by rupturing of the mature stages and controlled invasion of ring stages parasites in RBCs (30 min, 37 °C, 800 rpm). The cells were recultivated for 2.5 hours in a petri dish and synchronized with 1 ml pre-warmed 5 % sorbitol at 37 °C for 10 min to obtain 0 – 3 hour old rings. The young rings were washed three times with RPMI, resuspended in 4 ml RPMI and splitted into two 2 ml culture dishes. Next, 11.2 µl freshly prepared DHA (final concentration 700 nM) was added to one of the dishes, the cells in the second petri dish were not challenged with DHA, and both samples were incubated at 37 °C for 6 h. After 6 hours DHA was removed, the cells were transferred in a 1.5 ml tube and washed three times with RPMI. The parasites were then grown for 66 hours at 37 °C and fed after 48 hours. To assess the parasite survival rate Giemsa smears were made and analyzed with microscopy via counting survived parasites after DHA treatment compared to the parasitemia of the control without DHA treatment.

### 2.2.3.14 Immunofluorescence assay (IFA) of transgenic parasites

#### Wet acetone IFA

The immunofluorescence analysis is based on the antigen - antibody binding and is used for the visualization and analysis of target proteins. In contrast to fluorescence microscopy (see 2.2.5.1), the cells were fixed using acetone.

300 µl of parasite culture was transferred into a 1.5 ml reaction tube and centrifuged for 30 sec at 9000 x g. The supernatant was discarded and the cells were washed once with 1 x PBS. An eight-well glass slide was coated with ConcanavalinA in  $d_4H_2O$  (ConA, 0.5 mg / ml, 20 µl per well) in a humid chamber

for 30 min at 37 °C (Spielmann et al., 2003). ConA was washed off three times with 1 x PBS and 50 – 100 µl cells were applied to each well. The immobilized cells were washed three times with 1 x PBS to remove unbound cells, the liquid layer was removed and the cells were fixed on the glass slide for 30 min in 100 % acetone. The slide was dried at room temperature for 1 min and re-hydrated and washed with 1 x PBS. The fixed cells were incubated with 20 µl primary antibody in 3 % BSA in 1 x PBS for 1 h at room temperature. For co-localization experiments, two primary antibodies produced in different animals were mixed. The primary antibody was removed and the cells were washed two times with 1 x PBS, followed by incubation of the cells in the presence of 20 µl secondary antibody in 3 % BSA in 1 x PBS, containing 1 µg / ml DAPI, for 1 h at room temperature in a dark chamber. 5 Washing steps with 1 x PBS were following and 4 drops of DAKO fluorescent mounting medium were added and carefully covered with a cover slip to avoid air bulbs. To fixate the cover slip, nail polish was used at the outer area of the slide and dried at room temperature. The IFA was analyzed using fluorescence microscopy.

### **2.2.3.15 Knock sideways induction**

For functional analysis of essential proteins, the target gene was tagged endogenously with GFP and FKBP domains using the SLI system (see 2.2.3.6) and the integrant cell line was transfected with an episomal plasmid expressing a mislocalizer fused to FRB domains and mCherry under a *nmd3* promoter (Birnbaum and Scharf et al., 2020) was used. The episomal plasmid was selected with 2 µg/ml blasticidin S (Invitrogen). To induce the dimerization based mislocalization, the parasite culture was split into two identical cultures. One culture served as a negative control and the other one was treated with 250 nm rapalog (AP21967, Clontech). The knock sideways was inspected with fluorescence microscopy.

### **2.2.3.16 DiCre induction**

For rapalog induced gene excision, the plasmid pSLI-N-GFP-2xFKBP-loxP (Birnbaum et al., 2017) was used for genomic integration whereby the target gene was flanked with loxP. A second plasmid pSkipFlox was transfected carrying separated Cre recombinase fragments. Upon addition of 250 nm rapalog (AP21967, Clontech), the Cre dimerization was induced which led to the excision of the loxP flanked region. The inducible knockout was analyzed using fluorescence microscopy and FACS analysis.

## **2.2.4 Biochemical Methods**

### **2.2.4.1 Western Blot analysis**

#### **2.2.4.1.1 Sodium dodecyl sulfate polyacrylamide gel electrophoresis (SDS PAGE)**

(Laemmli, 1970)

SDS PAGE was used to separate proteins according to their molecular weight. For this purpose, *P. falciparum* infected erythrocytes were treated with saponin as described in 2.2.3.9 and were applied to a Sodium dodecyl sulfate polyacrylamide gel consisting of two parts. The upper third of the gel consists

of a large-pored stacking gel in which the proteins are first concentrated before they then run through an applied electric field into the fine-meshed separating gel, where they are separated according to their molecular weight.

Depending on the expected size of the analyzed fusion protein, the separation gel was used with different concentrations.

The mixture was pipetted into a gel chamber to polymerize and covered gently with 200  $\mu$ l isopropanol to form a straight. After incubation for 30 minutes at room temperature, the gel has polymerized, isopropanol was removed, and the separation gel was covered with the liquid stacking gel.

In addition, a plastic comb was positioned in the liquid layer so that the samples could later be applied separately.

As described in 2.2.3.9, the isolated proteins were denatured and linearized and mixed with SDS loading buffer before being applied to the SDS-PAGE. Dithiothreitol (DTT) in the SDS loading buffer led to the cleavage of disulfide bridges by a reduction reaction and the cleavage of secondary and tertiary structures of proteins.

5 - 15  $\mu$ l of the protein pellet were loaded onto the polyacrylamide gel, which was clamped together with a running buffer in an electrophoresis chamber. An electric field of 80 V was then applied for 10 min and was then increased to 150 V for 1 h, as a result of which the negatively charged molecules migrated towards the anode and the samples were separated according to molecular weight. In addition to the sample, a size standard (PageRuler Prestained Protein Ladder) was also applied to the gel in order to determine the exact size of the target proteins.

#### **2.2.4.1.2 Western Blot**

(Kyhse-Andersen, 1984)

The separated proteins were transferred to a nitrocellulose membrane using the Western blot method. For this purpose, the acrylamide gel was clamped from both sides with Whatman papers (three-ply) and plastic sponges soaked in transfer buffer in a holder cassette. This was positioned in a tank blotter for protein transfer. In addition, a nitrocellulose membrane was placed on one side between the gel and Whatman papers. The holder cassette was aligned in the blot system in such a way that the proteins migrate towards the anode when an electrical field is applied and are thereby transferred to the membrane. The protein transfer is based on hydrophobic interactions, which lead to the binding of the proteins in the gel to the nitrocellulose membrane and took place at 299 V and 390 mA for 1 h 30 min. The Western blot transfer chamber was filled with ice cooled transfer buffer and kept cold with a cooling system at 4 °C during the process in order to avoid overheating.

#### **2.2.4.1.3 Detection of proteins**

To ensure that subsequent treatment with antibodies does not lead to unspecific bindings with free epitopes of the proteins, the membrane was then incubated for 1 h at room temperature with 5% milk powder in PBS. A primary antibody, specific to the protein's fluorochrome tag, was diluted in the appropriate dilution in 2 % milk and incubated with the membrane rolling at 4 °C overnight. After incubation with the primary antibody, the cellulose membrane was washed 3 times with PBS and then treated for 1 h with a secondary antibody in the appropriate dilution at room temperature. The secondary antibody was linked to the enzyme horseradish peroxidase (HRP), that the antibody-protein binding could be visualized after adding a substrate due to the enzymatic activity of the HRP. This reaction is based on the conversion of luminol into an oxidized form, which can be observed and documented in

the form of chemiluminescence using a gel documentation device. After adding the second antibody, the membrane was washed again 3 times with PBS-Tween (0.1 % Tween), 3 times with and once with  $dH_2O$  (5 min per washing step at RT). The two solutions of the SuperSignal West Pico chemiluminescence kit were then applied to the membrane in a ratio of 1: 1 and incubated in the dark for 1 min. The signal of the enzymatic activity of the HRP was then detected and recorded with a ChemiDoc XRS + system from Biorad.

#### 2.2.4.1.4 Quantitative Western Blot analysis

For quantification of wild type and mutated Kelch13 relative protein levels, serial dilutions of protein extracts derived from parasites expressing either K13WT<sup>endo</sup> or K13C580Y<sup>endo</sup> with an identical N-terminal GFP fusion from the endogenous locus (Birnbbaum et al., 2017) were compared on the same immunoblot. The same blots were re-probed for aldolase. The average GFP signal of wild type Kelch13 and Kelch13C580Y was normalized to the average aldolase signal of the respective samples of the blot and used to determine the relative levels of wild type Kelch13 and Kelch13C580Y by measuring the signal intensity using the Image Lab software v 5.2.1 (Bio Rad) with lane background subtraction (disc size 10). Three independent biological replicas were done.

Protein extracts from episomal expressed constructs (complementation constructs overexpressed on K13C580Y<sup>endo</sup> parasites) were analyzed with an anti-RFP antibody using Western Blot analysis. The same immunoblot was re-probed with an anti-BIP antibody as a loading control. The intensity of the appropriate protein bands was determined using the Image Lab software (v 5.2.1, Bio Rad). The mean RFP intensity signal (corresponding to K13WT<sup>epi</sup> and the construct to be investigated, respectively) was normalized to the corresponding mean BIP signal intensity and the intensity ratios were calculated. The intensity ratios for the investigated episomal construct were divided by the ratios of K13WT<sup>epi</sup> to obtain the abundance of the investigated episomal construct relative to K13WT<sup>epi</sup> and the signal intensity was measured using the Image Lab software v 5.2.1 (Bio Rad) with lane background subtraction (disc size 10).

## 2.2.5 Microscopy

### 2.2.5.1 Live cell and fluorescence microscopy

To analyze proteins of *P. falciparum* the target genes were genetically modified and tagged with different fluorochromes such as GFP (green fluorescent protein) or mCherry. This enabled the detection after expression in the cell and the proteins were visualized by fluorescence microscopy.

For this purpose, 500  $\mu$ l of the parasite culture were initially stained for 3 min with 1  $\mu$ g / ml DAPI (4',6-diamidino-2-phenylindole) in order to recognize the parasitic nucleoli. The cells were centrifuged for 1 min at 1800 x g and the pellet was resuspended in one third of the supernatant. For examination by fluorescence microscopy, 2.5  $\mu$ l of the suspension was placed on a slide and covered with a cover slip, on which 1 drop of immersion oil was placed. The living intracellular parasites were examined with a 100x oil objective for detailed images and with a 64x oil objective for overview images. To avoid movement of the cells during microscopy, it was also possible to smear 1  $\mu$ l of the cells on a glass slide and detect them without covering with a cover slip. In this case the immersion oil was placed directly on the smeared cells.

GFP-labeled proteins have an absorption maximum at a wavelength of 395 / 475 nm, with a wavelength of 509 / 540 nm being emitted. The fluorochrome mCherry, has an absorption / emission spectrum at 587 and 610 nm. By stimulating the transgenic cells with the respective wavelengths, the labeled proteins can be assigned temporally and locally to an expression in different stages of development of the *P. falciparum*. The DAPI staining can contribute to the visualization of the cell nuclei when excited with UV light.

For co-localization studies, parasites were smeared and dried on a glass slide and GFP and mCherry fluorescence was immediately imaged.

To measure fluorescence intensity of foci in living parasites (trophozoites and ring stages) parasites were selected based on the DIC channel and images were taken with identical acquisition settings for the GFP channel. ImageJ was used to measure the mean fluorescence intensity of Kelch13 foci after background fluorescence subtraction.

Images were edited with Corel Photo Paint x10, brightness and intensity were adjusted.

## 3 Results

### 3.1 Functional analysis of Kelch13 compartment proteins

#### 3.1.1 Ring stage survival assays with KIC-TGDs

To further analyze the proteins of the Kelch13 compartment, it was assessed whether Kelch13 interaction candidates (KICs, Birnbaum and Scharf et al., 2020) play a role in resistance. For this, cell lines with nonessential disrupted KICs (KIC-TGD) were tested in a ring stage survival assay (RSA, Witkowski et al., 2013, Figure 15 A). RSAs were carried out with synchronized ring stages (0 – 3 h) in 3 to 5 independent experiments. The cells were treated with a Dihydroartemisinin (DHA) pulse (700 nM) for 6 hours and then cultured for 66 more hours to determine the parasite survival rate (SR) after DHA treatment. Resistance to DHA was previously defined as an RSA survival rate above 1 % (Witkowski et al., 2013, Arey et al., 2014). One of the KICs (KIC10) did not co-localize with Kelch13 and was used as an extra control beside 3D7 wild type parasites.

Tested in a standard RSA parasites with a KIC1-TGD showed a mean survival rate of 0.3 % (SD = 0.1%, n = 4), KIC2-TGD parasites showed a mean survival of 0.4 % (SD = 0.4 %, n = 3), KIC3-TGD parasites showed a mean survival of 0.03 % (SD = 0.1 %, n = 3), KIC6-TGD parasites showed a mean survival of 0.0 % (SD = 0.0 %, n = 3), KIC8-TGD parasites showed a mean survival of 0.3 %, (SD = 0.4 %, n = 3), KIC9-TGD parasites showed a mean survival of 0.1 % (SD = 0.2 %, n = 3) and parasites with a KIC10-TGD showed a mean survival of 0.0 % (SD = 0.0 % n = 3) (Figure 15 A), indicating that the disruption of any of these genes did not lead to a decreased susceptibility to ART. MCA2-TGD parasites showed a mean SR of 5.4 % (SD = 2.5 %, n = 4), KIC4-TGD parasites of 1.4 % (SD = 0.4 %, n = 3) and KIC5-TGD parasites of 12.0 % (SD = 7.3 %, n = 5), which indicates that the disruption of these genes decreased the susceptibility to DHA (Figure 15 A). As a positive control ART resistant K13C580Y<sup>endo</sup> knock-in parasites (GFP-2xFKBP-Kelch13<sup>C580Y</sup>, Birnbaum et al., 2017) and as a negative control 3D7 wild type parasite were tested under the same conditions as KIC-TGD parasites. As expected, the negative control showed a mean SR below 1 % (SR = 0.16 %, SD = 0.4 %, n = 6, Figure 15 A) and resistant K13C580Y<sup>endo</sup> parasites show a mean SR of 24.5 % (SD = 11.1 %, n = 7, Figure 15 B). Taken together, it can be concluded that the disruption of a subset of Kelch13 compartment proteins (KIC4-TGD, KIC5-TGD and MCA2-TGD) led to a reduced susceptibility to DHA.

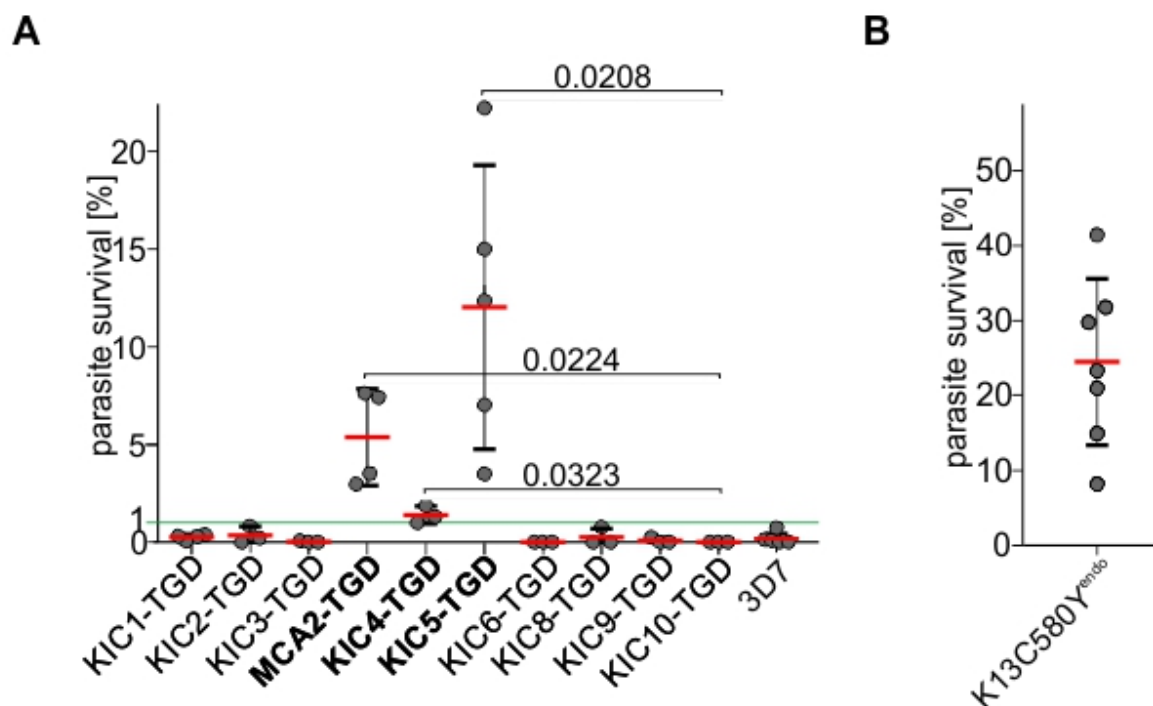


**Figure 15. Ring stage survival Assay with KIC-TGD parasites. (A)** RSA survival rate (% DHA-treated to untreated parasites; RSA: Witkowski et al., 2013) for the parasite cell lines with targeted gene disruptions (TGDs) of the proteins indicated. Each point corresponds to an independent RSA. 3D7: negative control (fully susceptible parasites),  $n=3$ ; TGD: targeted gene disruption (TGD) of potential Kelch13 interacting candidates (KICs) and metacaspase2 (MCA2),  $n = 3 - 5$ . **(B)** RSA with K13C580Y<sup>endo</sup> knock in parasites (GFP-2xFKBP-Kelch13<sup>C580Y</sup>, Birnbaum et al., 2017) was used as positive control. Each point corresponds to an independent RSA,  $n = 7$ . The green line marks 1 % survival. Error bars show SD. P values are indicated (unpaired, two tailed t test with Welch's correction).

### 3.1.2 Impact of KIC-TGDs on parasite growth

In order to assess if the RSA results (see 3.1.1) were influenced by potential growth defects and to test if any of the gene disruptions affected parasite growth, the SLI-TGD cells lines were analyzed in a FACS based growth assay over 2 development cycles (Figure 16) (Malleret et al., 2011; Birnbaum et al., 2017). For this, the KIC-TGD parasite cultures were adjusted to 0.05 % start parasitemia and the growth of these cell lines was then compared to that of 3D7 wild type parasites which were analyzed in the same manner. KIC10-TGD, which is not associated with the Kelch13 compartment, was used as an extra control beside 3D7 wild type parasites.

The growth rate of the MCA2-TGD and KIC5-TGD parasites was significantly reduced compared to the 3D7 control (Figure 16). The targeted disruption of KIC1, KIC2, KIC3, KIC8, and KIC10 resulted in a milder but still significant growth defect. No significant reduction in growth compared to 3D7 was observed with the KIC4-TGD and KIC6-TGD parasites. The growth defect of MCA2-TGD and KIC5-TGD parasites indicate that these candidates are important for parasite growth. As MCA2-TGD and KIC5-TGD parasites showed reduced susceptibility to ART (Figure 15 A), this might indicate that there is a correlation between reduced susceptibility to ART and a defect in growth in the MCA2-TGD and KIC5-TGD parasites (Figure 16). There was only a slight evidence for a correlation between resistance and growth for the other KIC-TGDs, with exception for KIC10-TGD. The disruption of KIC10 did not

lead to reduced susceptibility to ART but resulted in significant growth defect compared to 3D7 parasites. This excludes the possibility that resistance is dependent on the growth rate of the KIC-TGDs.

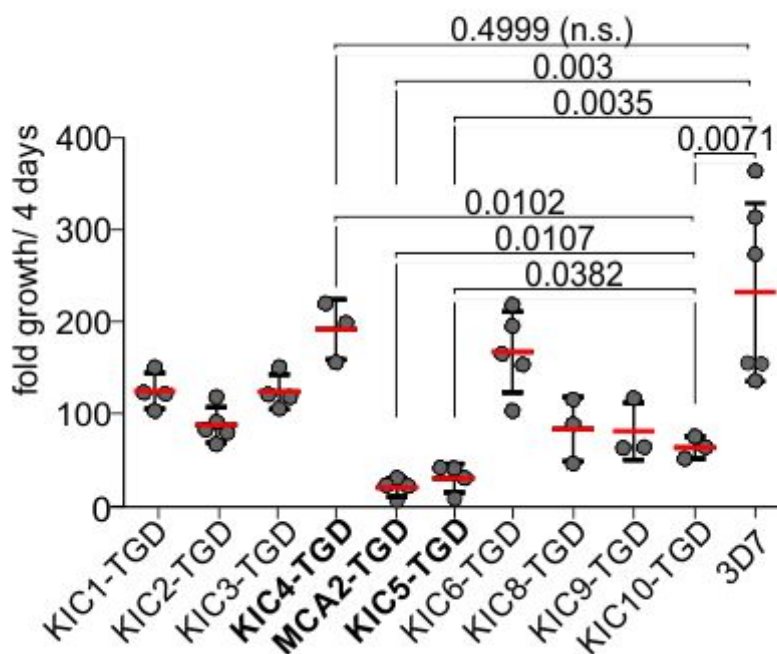


**Figure 16. FACS based growth analysis with KIC-TGD parasites.** Data points indicate growth rate for the indicated TGD lines in three to six independent experiments (TGD: targeted gene disruption; KIC: Kelch13 interacting candidate; MCA2: metacaspase2). 3D7 wild type parasites were used as a control. Error bars show SD. P values (determined using an unpaired, two tailed t test with Welch's correction) are indicated, n.s. = not significant.

### 3.1.3 Stage-specific phenotype after Kelch13, UBP1 and KIC7 inactivation

To determine detailed stage-specific phenotypes after inactivation of Kelch13, UBP1 and KIC7, 250 nM rapalog was added to synchronized knock in parasites (GFP-2xFKBP-Kelch13, UBP1-2xFKBP-GFP-2xFKBP, KIC7-2xFKBP-GFP-2xFKBP; Birnbaum et al., 2017; Birnbaum and Scharf et al., 2020) episomally expressing a mislocalizer (1xNLS or 3xNLS) in ring (0 – 8 hpi) or in trophozoite (16 – 24 hpi) stages to initiate the knock sideways of Kelch13, UBP1 or KIC7. The parasites were monitored for 56 hours after the induction of the knock sideways by generating Giemsa smears every 8 hours and the development stages of the parasites were determined. The stages distribution was then compared to the same parasites grown without rapalog (control). Kelch13, UBP1 and KIC7 were grown in parallel to increase comparability and in order to gain more information about the similarities of the function of these proteins in the development stages. The growth experiments of UBP1 and KIC7 (up to the preparation of Giemsa smears) was kindly performed by Jakob Birnbaum.

#### 3.1.3.1 Stage-specific impact on parasites development upon inactivation of KIC7

Inactivation of KIC7 in rings (Figure 17 A) led to an arrest of the parasites in ring stages after 16 – 24 hours, a time point when a small proportion of control parasites already developed to young trophozoites. This effect was observed even more clearly 24 – 32 hours post induction (hpi). Only a

minor proportion of parasites of the KIC7 knock sideways parasites developed to young trophozoites, and the majority of the parasites arrested in rings (Figure 17 A). The arrest in ring stages was also observed during the following three time points (32 – 40, 40 – 48 and 48 – 56 hpi), with limited progression of the parasites to the trophozoite stage (Figure 17 A). Furthermore, pycnotic parasites were observed in increasing numbers over time. Interestingly, the parasites which developed to trophozoites showed less hemozoin crystal formation compared to the control (Figure 17 B). The control parasites, harboring an active KIC7 protein, developed normally from rings, to trophozoites and schizonts followed by reinvasion (Figure 17 A).

Inactivation of KIC7 in early trophozoites (Figure 17 C) allowed further progression to late trophozoites but prevented the development of the parasites into schizont stages. Thirty-two hours post inactivation of KIC7 in trophozoites, first pycnotic or dead parasites were observed in Giemsa smears (Figure 17 C). The control developed as expected. These results suggest an essential function of KIC7 in ring as well as in trophozoite stages.

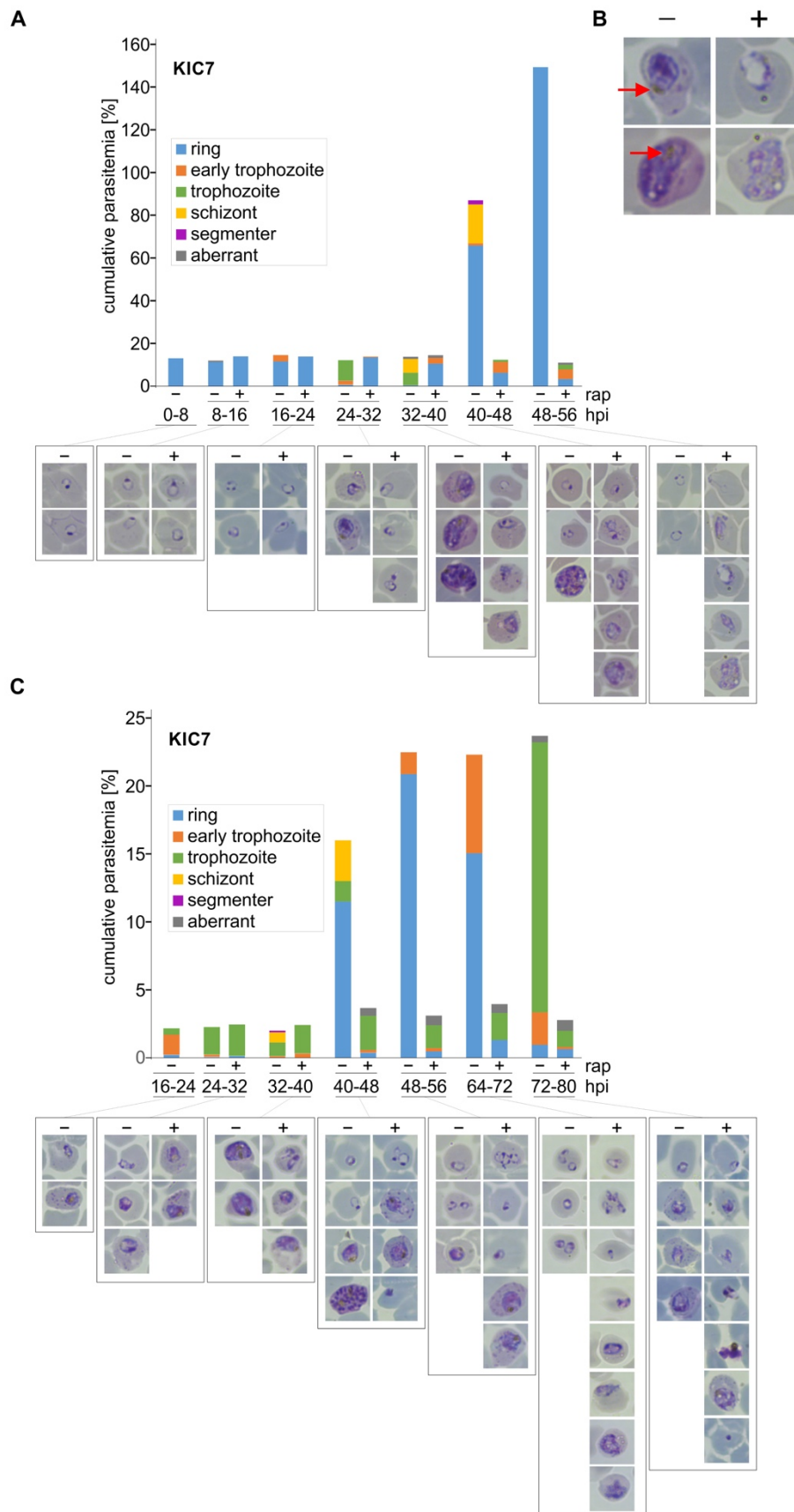


**Figure 17. Stage-specific phenotypes after inactivation of KIC7.** Knock sideways with KIC7 knock in parasites (KIC7-2xFKBP-GFP-2xFKBP, Birnbaum and Scharf et al., 2020) expressing an episomal mislocalizer (1xNLS) upon the addition of rapalog (+rap) in rings (**A**) or in trophozoites (**C**). Giemsa smears were made at the indicated time points. –rap: control; hpi: hours post invasion; aberrant: dead or non-typical parasites. One of two representative independent biological replicas are shown. Replicas are shown in Appendix 1. (**B**) Representative Giemsa smears of an early (upper row) and a late trophozoite (lower row). -: control; +: rapalog treated; Red arrows show hemozoin crystals.

### 3.1.3.2 Stage-specific impact on parasites development upon inactivation of UBP1

Inactivation of UBP1 in rings led to an arrest of the parasites in ring stages after 16 – 24 h, whereas control parasites developed to young trophozoites (Figure 18 A). This was also observed 24 – 32 hours post knock sideways induction and during the following three time points (32 – 40, 40 – 48 and 48 – 56 hpi) (Figure 18 A). Only some parasites developed to trophozoites after UBP1 inactivation. Pycnotic and dead parasites were observed 32 hours after inactivation of UBP1. Control parasites developed normally, as expected (Figure 18 A).

Inactivation of UBP1 in trophozoites (Figure 18 B) resulted in a delay in trophozoite stages, followed by parasite death. Already 8 hours after rapalog was added (and also in the following time points), aberrant cells were detected, whereas the control parasites developed normally and completed the cycle in the red blood cells (Figure 18 B). These results indicated a function of UBP1 in ring as well as in trophozoite stages. The observed phenotype is comparable with the phenotype that was observed after the inactivation of KIC7 (Figure 17). This supports a similar function of UBP1 and KIC7 in parasite development.

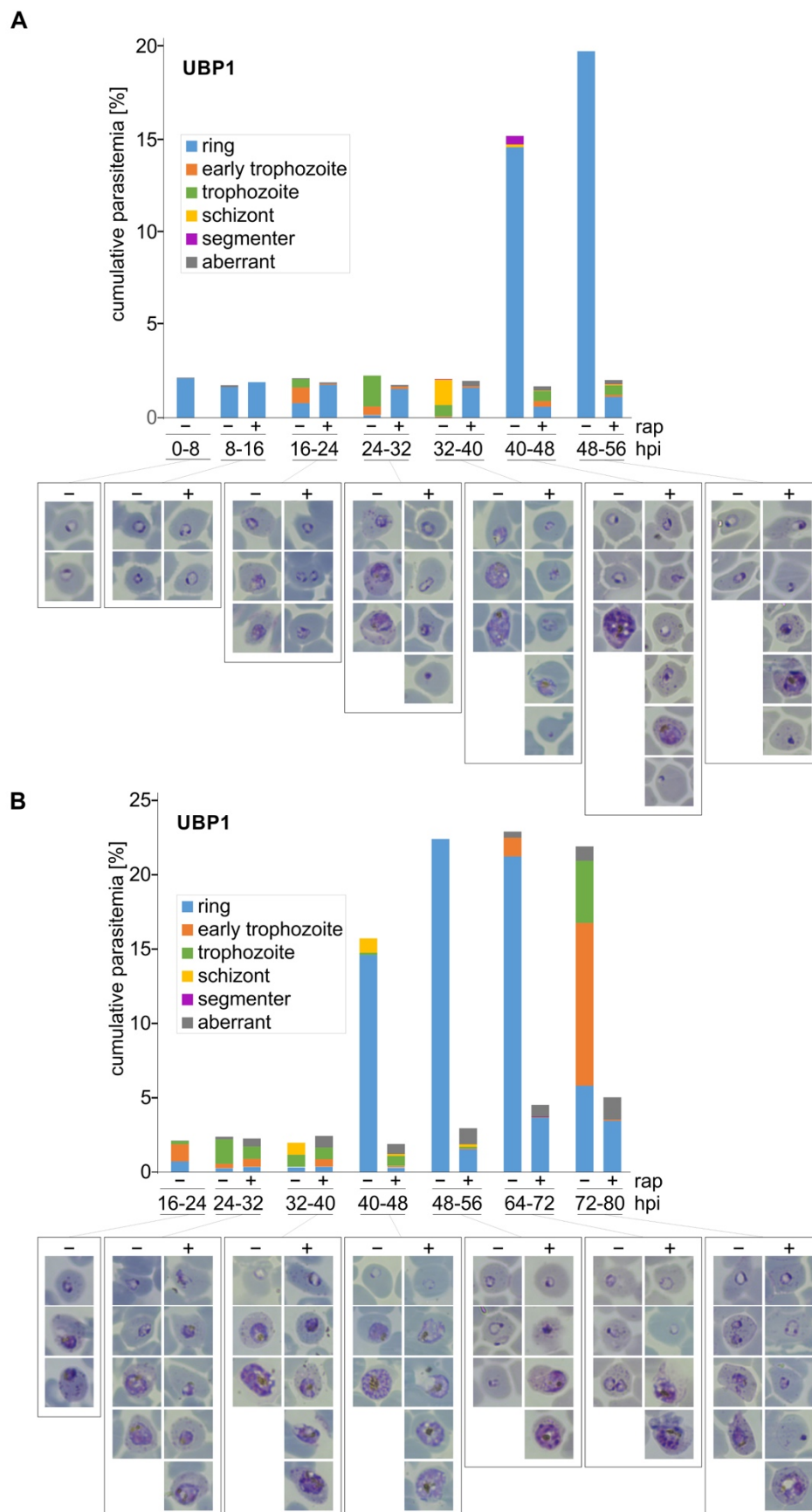


**Figure 18. Stage-specific phenotypes after inactivation of UB1.** Knock sideways with UB1 knock in parasites (UBP1-2xFKBP-GFP-2xFKBP, Birnbaum and Scharf et al., 2020) expressing an episomal mislocalizer (1xNLS) upon the addition of rapalog (+rap) in rings (**A**) or in trophozoites (**B**). Giemsa smears were made at the indicated time points. –rap: control; hpi: hours post invasion; aberrant: dead or non-typical parasites. One representative of two independent biological replicas is shown. Replicas are shown in Appendix 1.

### 3.1.3.3 Stage-specific impact on parasites development upon inactivation of Kelch13

To gain more insight into stage specific essentiality of Kelch13, rapalog was added to endogenously tagged Kelch13 (GFP-2xFKBP-Kelch13) parasites episomally expressing the 1xNLS mislocalizer (Birnbaum et al., 2017) in ring (Figure 19 A, 0 – 8 hpi) as well as in trophozoite stages (Figure 19 B, 16 – 24 hpi) to induce the knock sideways of Kelch13. 16 hours after the addition of rapalog in rings (Figure 19 A, time point 16 – 24 hpi) the parasites showed a delay in ring stages (as apparent by failure to progress to trophozoites), followed by a permanent arrest of the parasites in the ring stage. Only few parasites progressed to the trophozoite stage. This was also observed in the following time points (Figure 19 A, time points 24 – 32, 32 – 40, 40 – 48 and 48 – 56 hpi).

In contrast to the phenotype that was observed upon inactivation of KIC7 and UBP1 in trophozoites, there was no phenotype observed in trophozoite stages when Kelch13 was inactivated (Figure 19 B). The parasites progressed normally to late trophozoites (time point 32 – 40 hpi) and completed the intra-erythrocytic cycle, comparable to the controls. Forty hours after full mislocalization of Kelch13 in trophozoites (time point 64 – 72 and 72 – 80 hpi), an arrest in the subsequent ring stages was observed (Figure 19 B). Control parasites without an inactivation of Kelch13 progressed as expected and completed the asexual cycle (Figure 19 A and B, –rap). This suggests that Kelch13 is dispensable in trophozoites and highlights the essential role of Kelch13 in ring stages.

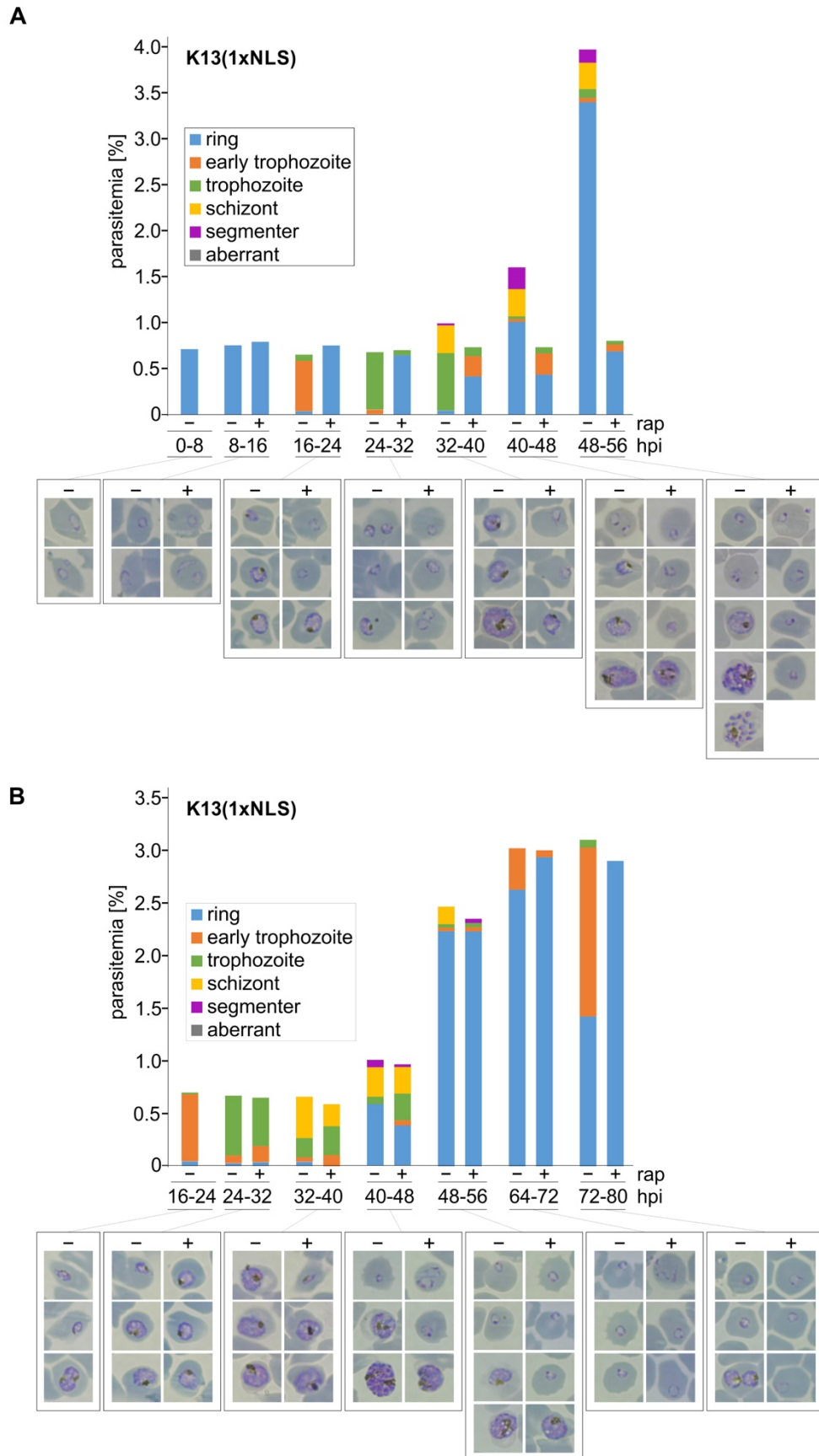


**Figure 19. Stage-specific phenotypes after full inactivation of Kelch13 (1xNLS).** Knock sideways with Kelch13 knock in parasites (GFP-2xFKBP-Kelch13, Birnbaum et al., 2017) expressing an episomal mislocalizer (1xNLS) upon the addition of rapalog (+rap) in rings (**A**) or in trophozoites (**B**). Giemsa smears were made at the indicated time points. –rap: control; hpi: hours post invasion; aberrant: dead or non-typical parasites. One representative of two independent biological replicas is shown. Replicas are shown in Appendix 1.

Partial inactivation of Kelch13 using an episomally expressed 3xNLS mislocalizer (Birnbaum et al., 2017) in rings (0 – 8 hpi) led to a comparable, but much milder, phenotype than that observed upon full inactivation of Kelch13 (Figure 20 A). 16 hours after knock sideways induction, a delay in the development of ring stages was observed. In the following time points the parasites developed further into trophozoite stages and were able to complete the cycle (40 – 48 hpi), comparable to the control (Figure 20 A).

Partial inactivation of Kelch13 in trophozoites (Figure 20 B) had no noticeable effect in the corresponding stage but led to a mild delay in the following ring stages (Figure 20 B, time point 72 – 80 hpi). Nevertheless, the parasites were able to complete the intra-erythrocytic cycle. Hence, compared with the phenotype that was observed after full inactivation of Kelch13 (1xNLS) (Figure 19), partial inactivation with the 3xNLS mislocalizer had a comparable but much milder effect, resulting in a delay in rings rather than a growth defect (Figure 20).

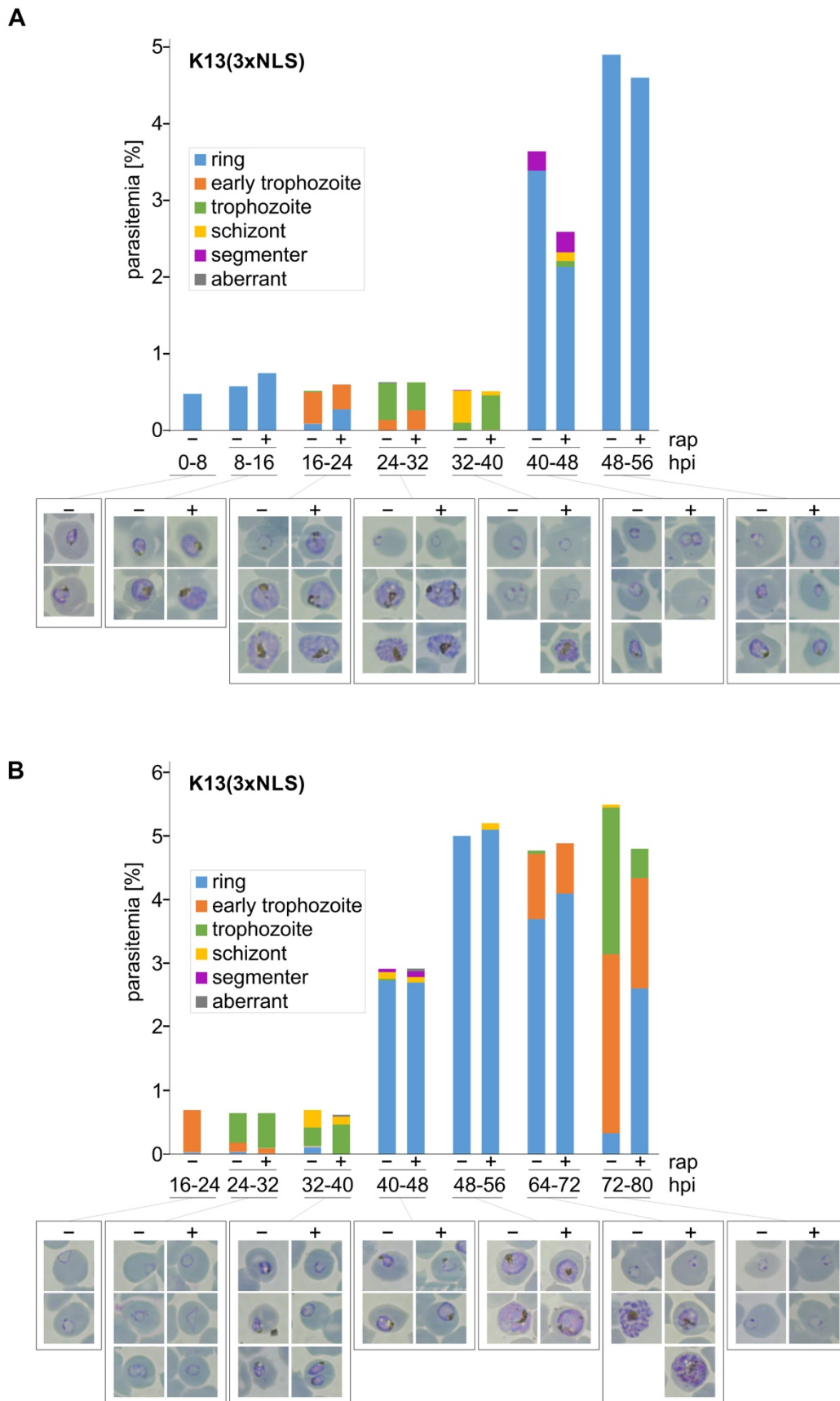


**Figure 20. Stage-specific phenotypes after partial inactivation of Kelch13 (3xNLS).** Knock sideways with Kelch13 knock in parasites (GFP-2xFKBP-Kelch13, Birnbaum et al., 2017) expressing an episomal mislocalizer (3xNLS) upon the addition of rapalog (+rap) in rings (**A**) or in trophozoites (**B**). Giemsa smears were made at the indicated time points. –rap: control; hpi: hours post invasion; aberrant: dead or non-typical parasites. One representative of two independent biological replicas is shown. Replicas are shown in Appendix 1.

### 3.1.4 KIC7 inactivation leads to increased numbers of PI4P positive circular structures

To further analyze the function of KIC7, KIC7 was inactivated using knock sideways and the effect on membranous structures in the parasite was analyzed. For this purpose, the P4M domain of SidM (Balla et al., 2013; Hammond et al., 2014) was used. This domain detects membrane associated Phosphatidylinositol-4-phosphate (PI4P) and in mammalian cells marks the plasma membrane, the golgi and late endosomal and lysosomal structures (Hammond et al., 2014). KIC7 knock in parasites (KIC7-2xFKBP-GFP-2xFKBP, Birnbaum and Scharf et al., 2020) were co-transfected with an episomally expressed 1xNLS-L-FRB-2xmyc-T2A-SidM-L-mCherry plasmid (the plasmid to PCR amplify the region encoding amino acid 546 – 647 of SidM was a kind gift of Tamas Balla; SidM was initially cloned by Sven Flemming).

In contrast to the mislocalizer used for other knock sideways experiments (see 3.1.3), this plasmid version did not contain a fluorescent tag on the mislocalizer. This made it possible to specifically detect the mCherry tagged SidM. KIC7 inactivation was initiated (using 250 nM rapalog) in young trophozoite stages. To determine the time after initiation of the knock sideways when KIC7 was efficiently mislocalized, this was examined by fluorescence microscopy in preliminary experiments at 2, 4 and 6 hours after the addition of rapalog (Figure 21 A). As KIC7 translocation to the nucleus was complete in 94 % of the examined cells after 6 hours incubation in the presence of rapalog (Figure 21 A) this time point was used in the following experiments. In control parasites, fluorescence microscopy showed that SidM was detected in circular accumulations (in the following defined as SidM positive foci, Figure 21 B, yellow arrows, control) that located at the PM, in the cytosol or close to likely vesicular structures (based on the DIC image) (Figure 21 B, control). As expected, SidM was also found at the PM but this was not obvious in all cells (Figure 21 B, pink arrows, control). In some cells, small rings of SidM signal were observed (white arrow, defined as circular structures (CS), Figure 21 B, control). In the cells which were grown in the presence of rapalog for 6 h, SidM showed a similar phenotype (Figure 21 B, +rapa). However, in DIC larger vesicular structures (Figure 21 B, orange arrows, +rapa) were apparent (see below).

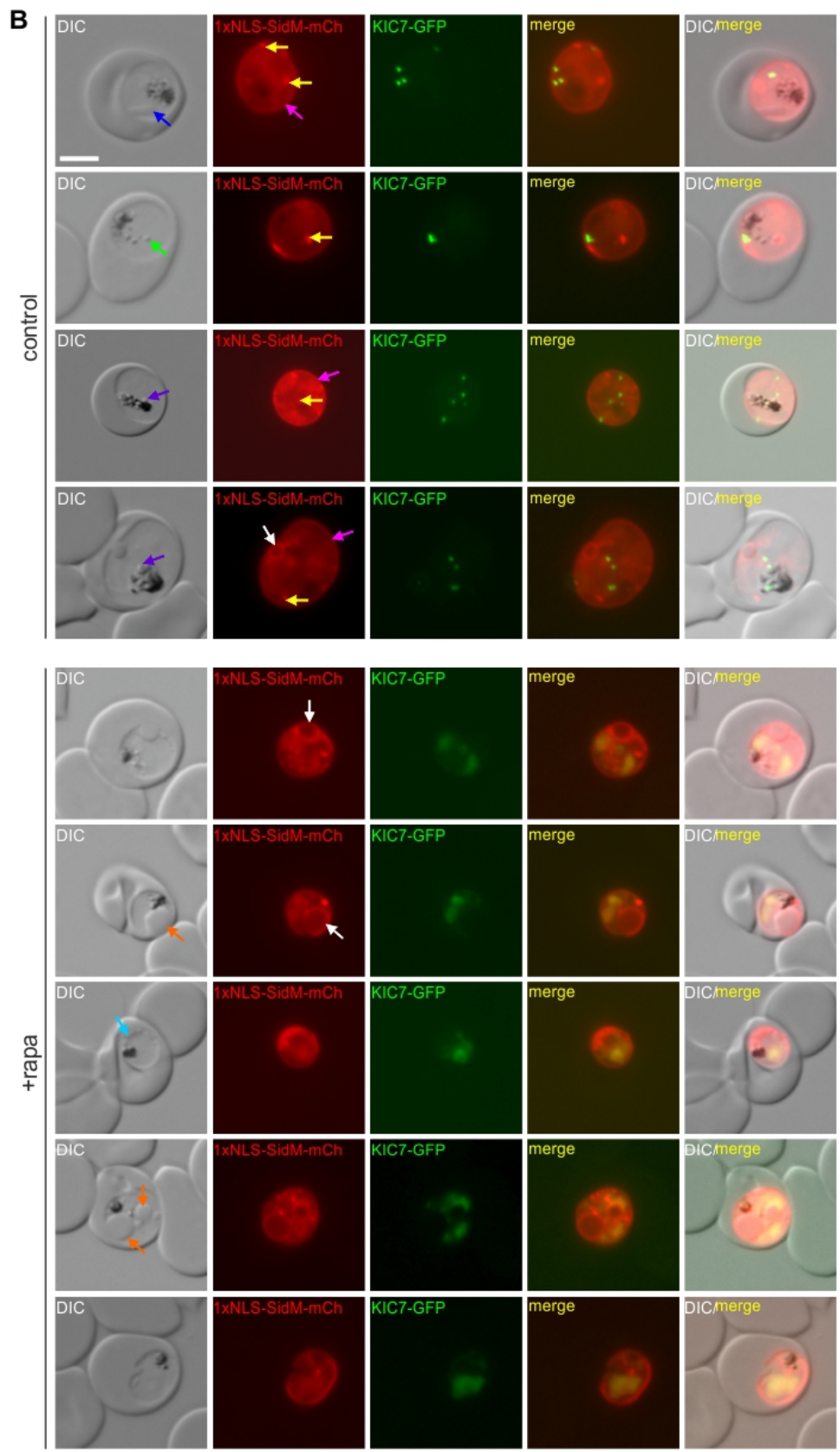
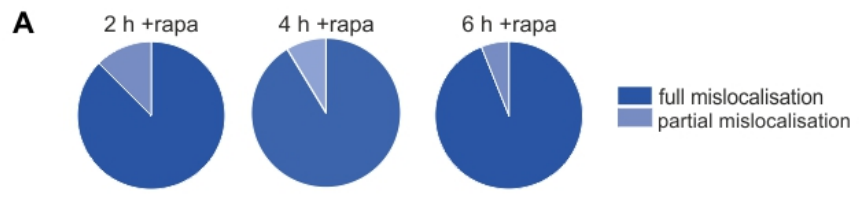


**Figure 21. Localisation of SidM positive structures upon KIC7 knock sideways.** (A) Quantification (based on fluorescence microscopy) of KIC7 mislocalisation at 2, 4 and 6 hours after the addition of rapalog to KIC7-2xFKBP-GFP-2xFKBP (Birnbaum and Scharf et al., 2020) parasites episomally expressing 1xNLS-L-FRB-2xmyc-T2A-SidM-L-mCherry (2h: n total scored cells = 26, n cells with complete KIC7 translocation = 21, n cells with partial KIC7 translocation = 5; 4h: n total scored cells = 26, n cells with complete KIC7 translocation = 21, n cells with partial KIC7 translocation = 2; 6h: n total scored cells = 33, n cells with complete KIC7 translocation = 31, n cells with partial KIC7 translocation = 2). (B) Representative fluorescence live cell images of the cell line indicated in (A). Parasites were grown in the presence (+rapa) or absence (control) of rapalog for 6 hours. Colored arrows show examples of focal structures quantified in figure 22. Scale bar 5  $\mu$ m, DIC: differential interference contrast; GFP: green fluorescent protein; mCh: mCherry red fluorescent protein; merge: GFP and mCherry channels merged.

As no immediate difference in the SidM signal was observed after KIC7 inactivation, the phenotype was more carefully quantified. To assess whether the inactivation of KIC7 increased the number of SidM positive foci (Figure 21 B, yellow arrows) in the cell, the number of SidM positive foci was determined 6 h after addition of rapalog (+rapa) und compared to the control (control) (Figure 22 A). The number of SidM foci per cell upon KIC7 inactivation (mean = 3.2, SD = 1.6) was similar to the control (mean = 2.9, SD = 1.6) (Figure 22 A). In contrast, the number of SidM positive circular structures (CS) in the cytosol of the parasite (Figure 21 B, white arrows) increased upon KIC7 inactivation (mean = 0.7, SD = 0.2) compared to the control (mean = 0.2, SD = 0.08), although this was not statistically significant (Figure 22 B). This shows that inactivation of KIC7 leads to a slight increase of unknown PI4P positive membranous structures in the cytosol of the parasite.

It was also investigated whether vesicle-like structures, independent of the SidM signal, differ to the control when KIC7 was inactivated. For this, vesicle-like structures visible in the DIC images (Figure 21 B) were classified into: vesicles that were detected in the parasite cytosol (Figure 21 B, green arrow), vesicles that were at the PM (Figure 21 B, light blue arrow), large vesicles that were either in the parasite cytosol or attached to the PM (Figure 21 B, orange arrows), vesicles that had a tube-like shape (Figure 21 B, dark blue arrow) and vesicles detected in close proximity to the food vacuole (Figure 21 B, purple arrows). Interestingly, 6 hours after the addition of rapalog the number of all of these vesicular structures increased slightly, although only the number of tubes and large vesicles increased significantly compared to the control (Figure 22 C–F) (vesicles in cytosol: control: mean = 0.13, SD = 0.06, +rapa: mean = 0.54, SD = 0.36; vesicles at PM: control: mean = 0.53, SD = 0.34, +rapa: mean = 1.89, SD = 1.79; large vesicles: control: mean = 0.01, SD = 0.02, +rapa: mean = 0.34, SD = 0.08; tubes: control: mean = 0.03, SD = 0.03, +rapa: mean = 0.12, SD = 0.02) with exception of vesicles close to the food vacuole, which decreased slightly, although this was not statistically significant (Figure 22 G) (vesicles at FV: control: mean = 1.48, SD = 0.86, +rapa: mean = 0.96, SD = 0.32).

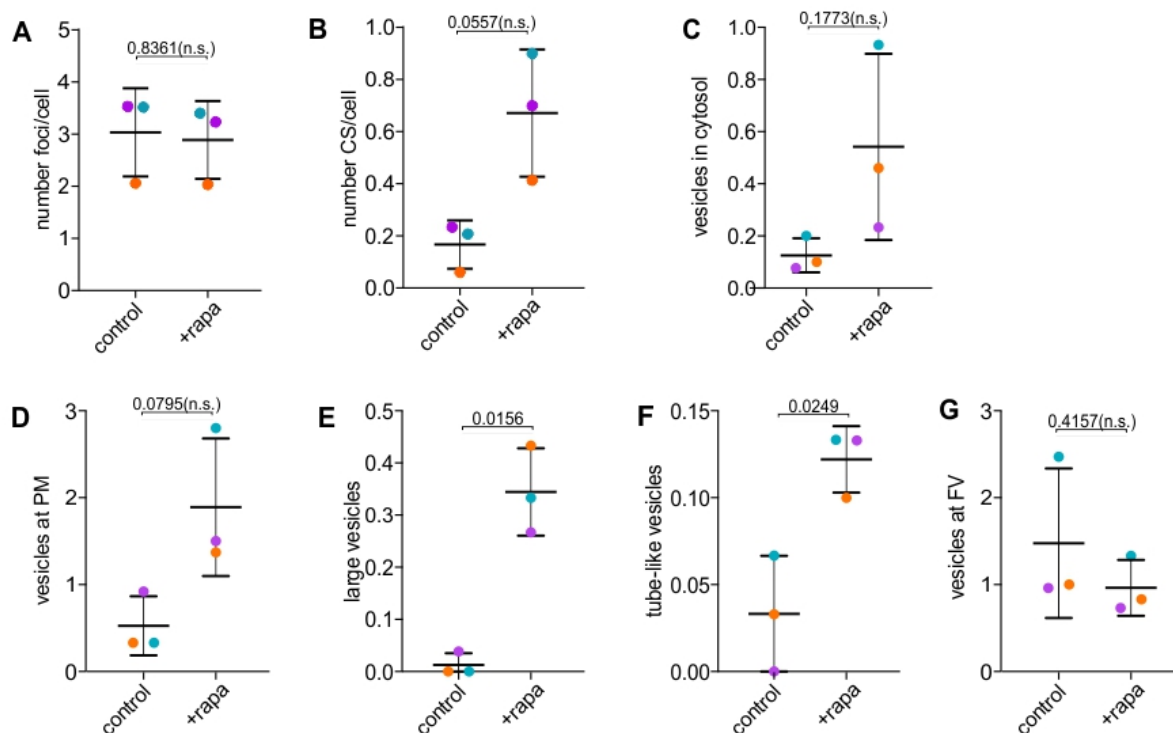


**Figure 22. Consequences on PI4P-positive membranes and vesicular structures after inactivation of KIC7.** KIC7-2xFKBP-GFP-2xFKBP (Birnbbaum and Scharf et al., 2020) parasites episomally expressing 1xNLS-L-FRB-2xmyc-T2A-SidM-L-mCherry were grown in the presence (+rapa) or absence (control) of rapalog for 6 hours. **(A)** Number of SidM positive foci per cell. **(B)** Number of SidM positive circular structures (CS) per cell. **(C)** Number vesicle-like structures in the cytosol per cell as determined by inspection of the DIC images. **(D)** Number of vesicles at the plasma membrane (PM) per cell. **(E)** Number of large vesicles per cell. **(F)** Number of tube-like vesicles per cell. **(G)** Number of vesicles close to the food vacuole (FV) per cell. **(A)** and **(B)** Control: n analyzed cells = 89; +rapa: n analyzed cells = 91. **(C) – (G)** Control: n analyzed cells = 71; +rapa: n analyzed cells = 75. Data points of the same color are from the same experiment. Each data point represents the average of the total number of each type of structure per cell. n=3. Error bars show SD. P values (determined using an unpaired, two tailed t test with Welch's correction) are indicated, n.s. = not significant.

## 3.2 Investigation of the resistance causing mechanism

### 3.2.1 DIQ-BioID with ART resistant K13C580Y<sup>endo</sup> parasites

To further investigate the resistance causing mechanism and to assess how mutations in the Kelch13 protein influence ART resistance, it was determined whether a changed interaction profile of mutated Kelch13 parasites could lead to resistance. To test this, dimerization induced quantitative BioID (DIQ-BioID, Birnbbaum and Scharf et al., 2020) experiments were performed using K13C580Y<sup>endo</sup> knock in parasites (GFP-2xFKBP-Kelch13<sup>C580Y</sup>, Birnbbaum et al., 2017). The DIQ- BioID approach is based on inducible heterodimerization which relies on the FKBP-FRB system to recruit the promiscuous biotin ligase BirA\* to a target of interest so that it will biotinylate proteins in close proximity (Birnbbaum, 2018; Jonscher, 2017, Birnbbaum and Scharf et al., 2020). The biotinylated proteins can be purified by streptavidin beads and analyzed by mass spectrometry as done for conventional BioID (Roux et al., 2012; Kim et al., 2016; Blancke-Soares, 2016; Kosh-Naucke, 2018).

To carry out DIQ-BioID with the K13C580Y<sup>endo</sup> parasites, they were co-transfected with an episomally expressed mCherry-FRB-BirA\* plasmid (BirA\*<sup>NL</sup>, Birnbbaum and Scharf et al., 2020). Fluorescence

microscopy confirmed the expression of mCherry-FRB-BirA\* in the cytosol of the parasite (Figure 23, control). To induce dimerization of FKBP and FRB, rapalog was added to the cells which resulted in the recruitment of mCherry-FRB-BirA\* to K13C580Y<sup>endo</sup> (Figure 23, +rapa).

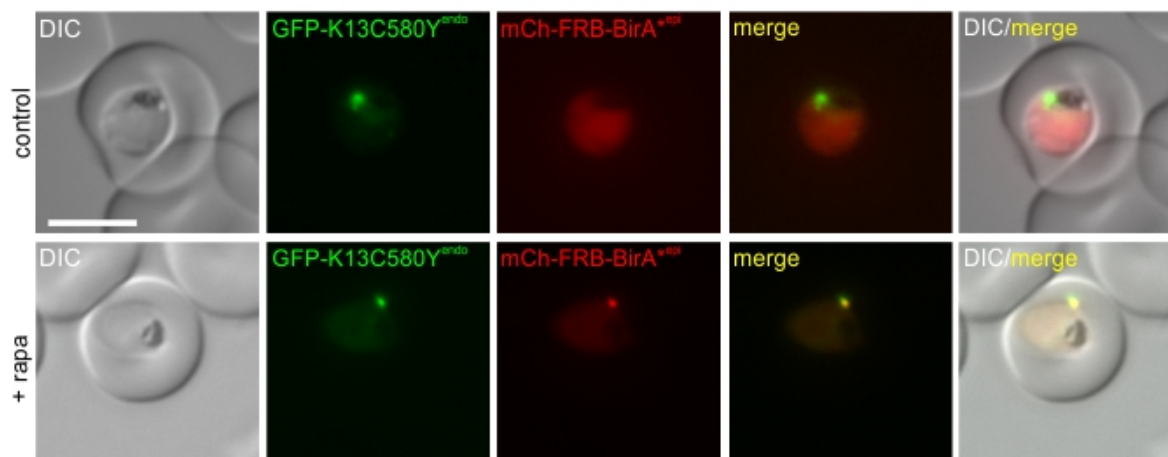


**Figure 23. Inducible dimerization of K13C580Y<sup>endo</sup> with mCherry-FRB-BirA\*.** Representative live cell images ( $n \geq 3$  fluorescence microscopy sessions, with at least 20 inspected cells per session) of knock-in cell line of GFP 2xFKBP-Kelch13<sup>C580Y</sup> (Birnbaum et al., 2017) with mCh-FRB-BirA\* with (+rapa) or without (control) rapalog. Scale bar 5  $\mu$ m, DIC: differential interference contrast; GFP: green fluorescent protein; mCh: mCherry red fluorescent protein; merge: GFP and mCherry channels merged.

The DIQ-BioID experiment was carried out as described in 2.2.3.10 and was performed in two biological replicas. The samples were analyzed by mass spectrometry by Christa Toenhake (Bartfai lab, Radboud University, Netherlands). To analyze the enrichment of proteins, the false discovery rate (FDR) was determined and the analysis of the enrichment of the dimerization induced sample (+rapa) compared to the control was displayed in scatter plot (Figure 24). The color code of the plotted hits correlates with the significance (according to FDR) of the enrichment (Figure 24, red: highly significant). The results are plotted as log<sub>2</sub>-normalized ratio on the x (experiment 1) and y (experiment 2) axis (Figure 24) and only proteins, in total 22 proteins, enriched with FDR < 1 % are shown as labelled dots, all the other hits are shown as grey dots (Figure 24). Successful dimerization and hence recruitment of the BirA\* ligase to the K13C580Y<sup>endo</sup> target was confirmed as Kelch13 itself is the most significantly enriched protein identified in this experiment (FDR < 1e-10) (Figure 24). The high confidence hits included KICs and other proteins identified to be found at the Kelch13 compartment before using DiQ-BioIDs with wild type Kelch13 and Eps15. Besides Kelch13, 11 other hits were highly enriched (FDR < 1e-10), one protein was identified with an FDR < 1e-9, one with an FDR < 1e-6 and one with an FDR < 1e-5 (KIC4). The identified candidates with the numbers 16 – 22 had an FDR < 1e-3 or FDR < 1e-2 (Figure 24).

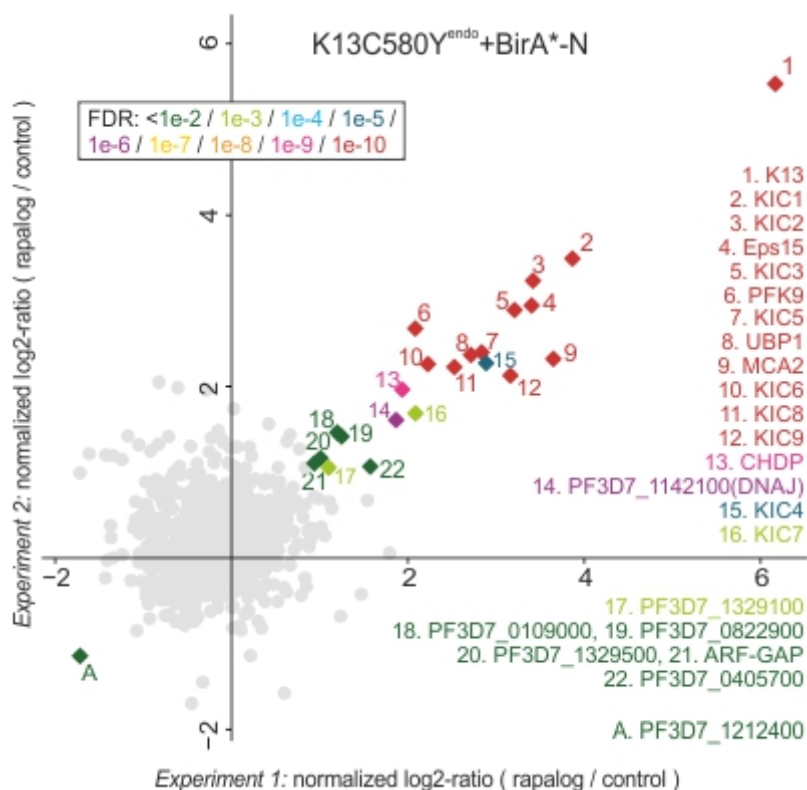


**Figure 24. Scatter plot of K13C580Y<sup>endo</sup> DIQ-BioID.** Plotted are the log<sub>2</sub>-ratios from two independent experiments (x and y axis). The experiments were conducted with GFP-2xFKBP-Kelch13<sup>C580Y</sup> parasites (Birnbaum et al., 2017) episomally expressing BirA\*-N. The color code indicates the false discovery rate (FDR) which defines the significance of the hits as defined in the legend on the top. The upper right quarter of the scatter plot shows the enriched hits with numbers and their corresponding ID at the right (all data are shown in Appendix 2).

### 3.2.2 Interactome comparison of K13WT<sup>endo</sup> and K13C580Y<sup>endo</sup>

To assess whether resistance of K13C580Y<sup>endo</sup> parasites could be influenced or based on a different interactome profile compared to of K13WT<sup>endo</sup> parasites, the hits identified by the DIQ-BioID experiments of the wild type (Birnbaum and Scharf et al., 2020) and the mutant Kelch13 (see 3.2.1) were compared and the enrichment of the top hits of both experiments was clustered (using K-means clustering) and displayed in a heat map (analysis kindly carried out by Christa Toenhake, Barfai lab, Radboud University, Netherlands) (Figure 25). Interestingly, 20 of the 22 identified top hits using K13C580Y<sup>endo</sup> as the target were also significantly enriched in DIQ-BioID experiments using K13WT<sup>endo</sup> as the target protein (Birnbaum, 2017; Birnbaum and Scharf et al., 2020). None of the highly enriched proteins was found to be exclusively enriched in K13WT<sup>endo</sup> and not in K13C580Y<sup>endo</sup>, except for KIC10, a protein not co-localizing with Kelch13 (Birnbaum and Scharf et al., 2020) which was highly enriched in K13WT<sup>endo</sup> but only significantly enriched in K13C580Y<sup>endo</sup> in one of the two experiments (Figure 25). Taken together, the interaction profile of K13C580Y<sup>endo</sup> and K13WT<sup>endo</sup> show no notable differences which indicates that mutating Kelch13 does not change a specific interaction of the protein.

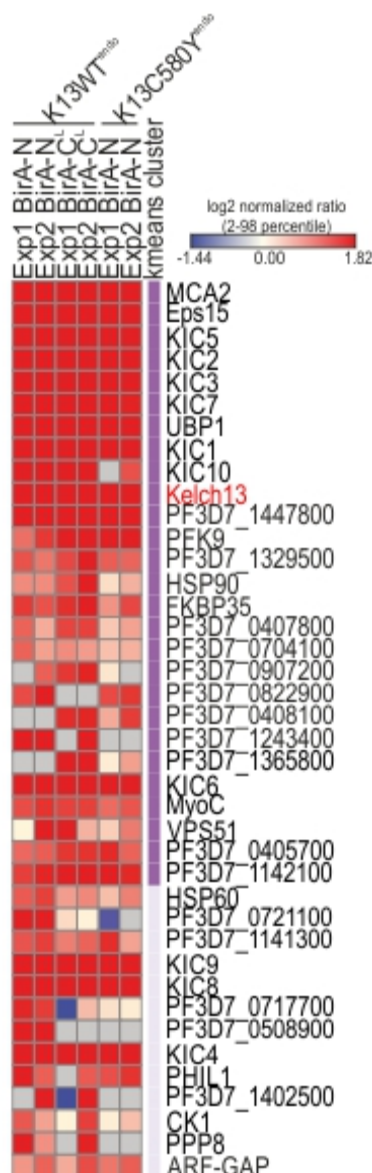


**Figure 25. Interactome comparison of K13WT<sup>endo</sup> and K13C580Y<sup>endo</sup>.** Heatmap of K13WT<sup>endo</sup> and K13C580Y<sup>endo</sup> DIQ-BioID experiment hits. K-means clustering into two clusters highlights overlap of K13WT<sup>endo</sup> and K13C580Y<sup>endo</sup>. Hits were chosen based on a significance of FDR < 1 % in 2 or more out of 4 (K13WT<sup>endo</sup>) or 2 (K13C580Y<sup>endo</sup>) experiments or filtered for a significance of FDR < 1 % in at least 1 experiment. Color intensities range from the 2<sup>nd</sup> - 98th percentile of log2 rapalog / control normalized ratios of all hits in this analysis. Grey blocks indicate not identified or no ratio due to missing label. Red font marks protein used as target for DIQ-BioID.

### 3.2.3 Kelch13 abundance in K13C580Y<sup>endo</sup> parasites is reduced compared to K13WT<sup>endo</sup> parasites

As the interactome study of K13C580Y<sup>endo</sup> parasites showed no clear difference to K13WT<sup>endo</sup> parasites (see 3.2.2), it was hypothesized that a reduced protein level of the mutant could lead to resistance. To investigate if this could be the resistance causing mechanism, it was tested whether mutant parasites harbor less Kelch13 protein than wild type parasites. To test this hypothesis, quantitative Western Blot analysis was performed using K13WT<sup>endo</sup> and K13C580Y<sup>endo</sup> knock in parasites (Birnbau et al., 2017). For this, the parasite cell lines expressing K13WT<sup>endo</sup> and K13C580Y<sup>endo</sup> were grown under the same conditions and were harvested at a parasitemia of approximately 3 – 5 %. For quantification the resulting

parasite protein extracts were diluted in serial dilutions and quantitative immunoblot analysis was conducted (see 2.2.4.1.4). The amount of K13WT<sup>endo</sup> and K13C580Y<sup>endo</sup> was analyzed with an anti-GFP antibody with the protein extracts of the respective cell lines on the same immunoblot. The same immunoblot was re-probed with an anti-aldolase antibody as a loading control and the mean GFP intensity of the K13WT<sup>endo</sup> and K13C580Y<sup>endo</sup> signal was normalized to the corresponding mean aldolase signal to calculate the intensity ratios (Figure 26). The experiment was repeated in three independent biological replicas and band intensity analysis was conducted using the Image Lab software (v 5.2.1, Bio Rad). This demonstrated that the ratio of the GFP intensity to the aldolase intensity is higher in K13WT<sup>endo</sup> parasites than in K13C580Y<sup>endo</sup> parasites (Figure 26 A), indicating that mutant Kelch13 parasites harbor less Kelch13 protein compared to wild type parasites: K13C580Y<sup>endo</sup> parasites were found to contain 41.6 %, 54.8 % and 68.5 % (mean = 54.0 %, SD = 13.5%, n = 3) of the amount of Kelch13 protein found in K13WT<sup>endo</sup> parasites (Figure 26 B). These findings indicated that the resistance conferring mutation led to a reduced level of Kelch13 in the cell (Figure 26 B).

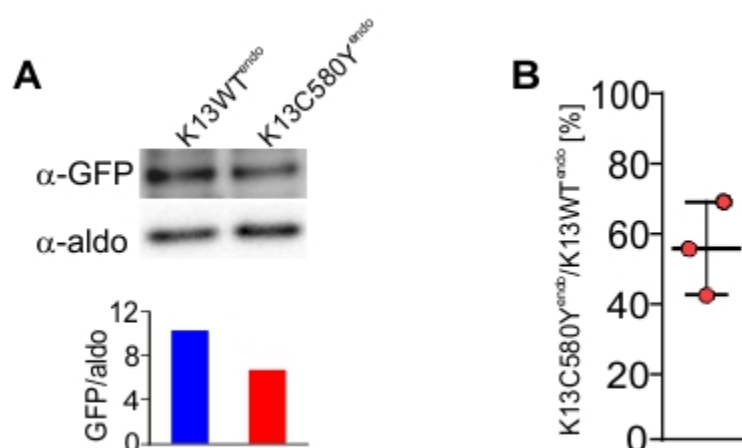


**Figure 26. Quantitative Western Blot analysis of K13WT<sup>endo</sup> and K13C580Y<sup>endo</sup>.** (A) Amounts of Kelch13 protein in K13WT<sup>endo</sup> and K13C580Y<sup>endo</sup> (GFP-2xFKBP-Kelch13<sup>WT</sup> and GFP-2xFKBP-Kelch13<sup>C580Y</sup>, Birnbaum et al., 2017) expressing parasite cell lines. A representative band pair of the Kelch13 signals and aldolase signals (top) from three independent experiments is shown (immunoblots used for quantification are shown in Appendix 3). Bottom, graphical representation of the band intensities of this example. Blue bar: GFP/aldo ratio of K13WT<sup>endo</sup> parasites, red bar: GFP/aldo ratio of K13C580Y<sup>endo</sup> parasites. (B) Graph showing quantification of Western Blot from serial dilutions (of which one band pair is shown in A). Each point defines the average of serial dilution of the protein extracts calculated as GFP/aldo ratio of K13C580Y<sup>endo</sup> divided by the ratio of K13WT<sup>endo</sup> (n=3). Bars show SD, mean is indicated.

To detect, whether the change of the protein levels can also be observed in intact and living parasites, the intensity of Kelch foci was analyzed in K13WT<sup>endo</sup> and K13C580Y<sup>endo</sup> parasites. Images of the two parasite cell lines were taken in living cells and the fluorescence intensities of the GFP signal of the Kelch13 foci were measured in trophozoite (Figure 27 A) and in ring stages (Figure 27 B). The images were taken with identical settings (see 2.2.5.1) in three independent experiments. The mean fluorescence intensity per focus of K13C580Y<sup>endo</sup> trophozoites and ring stages (mean = 7387.1, SD = 2423.6 and mean = 3386.5, SD = 1136.2, respectively) was significantly lower compared to parasites expressing K13WT<sup>endo</sup> trophozoite and ring stages (mean = 10529.6, SD = 4669.1 and mean = 5299, SD = 1349.7, respectively). This demonstrates that K13C580Y<sup>endo</sup> parasites harbor 29.73 % less Kelch13<sup>endo</sup> protein than K13WT<sup>endo</sup> parasites in trophozoite stages and 36.77 % less in ring stages (Figure 27) in good agreement with the Western Blot results.

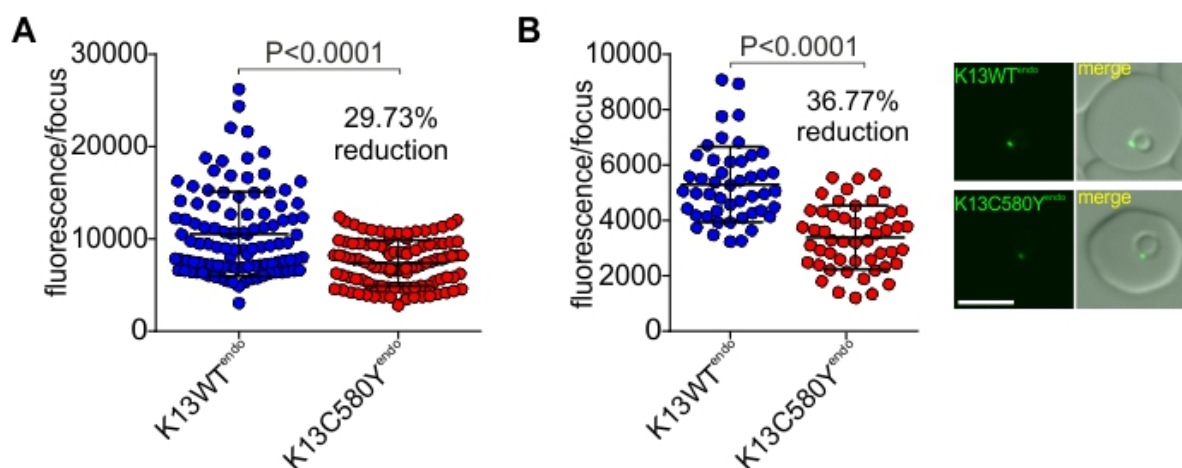


**Figure 27. Fluorescence intensity quantification of K13WT<sup>endo</sup> and K13C580Y<sup>endo</sup> foci.** Plot showing fluorescence per focus of K13WT<sup>endo</sup> and K13C580Y<sup>endo</sup> (GFP-2xFKBP-Kelch13<sup>WT</sup> and GFP-2xFKBP-Kelch13<sup>C580Y</sup>, Birnbaum et al., 2017). Parasites expressing the indicated constructs were imaged under the same conditions in trophozoite (**A**) and in ring (**B**) stages. Each point shows fluorescence intensity of a focus from three independent experiments (K13C580Y<sup>endo</sup>: trophozoites: n analyzed cells = 102; rings: n analyzed cells = 51; K13WT<sup>endo</sup>: trophozoites: n analyzed cells = 105; rings: n analyzed cells = 47). Images in (**B**) show a representative examples of fluorescence images in ring stages. Mean reduction in % is indicated. Scale bar 5 µm. Bars show SD, mean is indicated. Unpaired, two-tailed t test with Welch's correction. P values are indicated.

### 3.3 Functional analysis of Kelch13

#### 3.3.1 Kelch13 protein level influences resistance

To test whether less Kelch13 protein levels in resistant parasites (see 3.2.3) directly influence resistance, it was determined if increasing Kelch13 abundance in resistant parasites changes the level of resistance. In order to test this, the ART resistant K13C580Y<sup>endo</sup> knock in parasites (GFP-2xFKBP Kelch13<sup>C580Y</sup>, Birnbaum et al., 2017) were co-transfected with a plasmid overexpressing mCherry-L-K13WT (K13WT<sup>epi</sup>) (Figure 28 A). Fluorescence microscopy was used to investigate the localization of K13C580Y<sup>endo</sup> and K13WT<sup>epi</sup>. This showed that the overexpressed construct was found in the same foci as endogenously expressed K13C580Y in ring, trophozoite and schizont stages (Figure 28 B, live). To confirm that small differences in the location of the two signals was due to parasite movement (in rings) or movement of foci (as previously documented, Jonscher, 2018) during live cell microscopy rather than a true difference in location, the parasites were also imaged after smearing and drying on a glass slide (see 2.2.5.1). This enables an exact localization of target proteins without the confounder that the Kelch13-defined foci might have moved between the times the different image channels were recorded. This analysis confirmed that K13C580Y<sup>endo</sup> and K13WT<sup>epi</sup> co-localize (Figure 28 B, dried), which was already observed in previous studies (Birnbaum, 2017). To evaluate the integrity of the mCherry-L-K13WT<sup>epi</sup> - fusion protein, Western Blot analysis (see 2.2.4.1) was conducted using an anti-RFP antibody. The construct was detected in two bands with a migration consistent with the expected molecular weight of 101 kDa. The same immunoblot was re-probed with an anti-BIP antibody as a loading control (Figure 28 C). The doublet of mCherry-L-K13WT<sup>epi</sup> bands consistently detected in eight independent experiments. To test whether the increased expression of Kelch13 protein could influence the resistance level of the mutant K13 background, the K13C580Y<sup>endo</sup> parasites overexpressing K13WT<sup>epi</sup> were challenged in four independent experiments with 700 nM DHA for 6 hours in a standard

ring stage survival assay (RSA, Witkowski et al., 2013) (Figure 28 D, see 2.2.3.13). Surprisingly, expression of K13WT<sup>epi</sup> on the resistant background rendered the resistant parasites fully sensitive to DHA (mean = 0.1 % SR, SD = 0.1 %, n = 4) while the parent K13C580Y<sup>endo</sup> knock in parasites without an episomally expressed Kelch13 were resistant to DHA (mean = 12.7 % SR, SD = 3.4 %, n = 16). These data indicated that the expression of K13WT<sup>epi</sup> on the resistant background was sufficient to revert resistance and provides evidence that Kelch13 protein levels alone influences resistance.

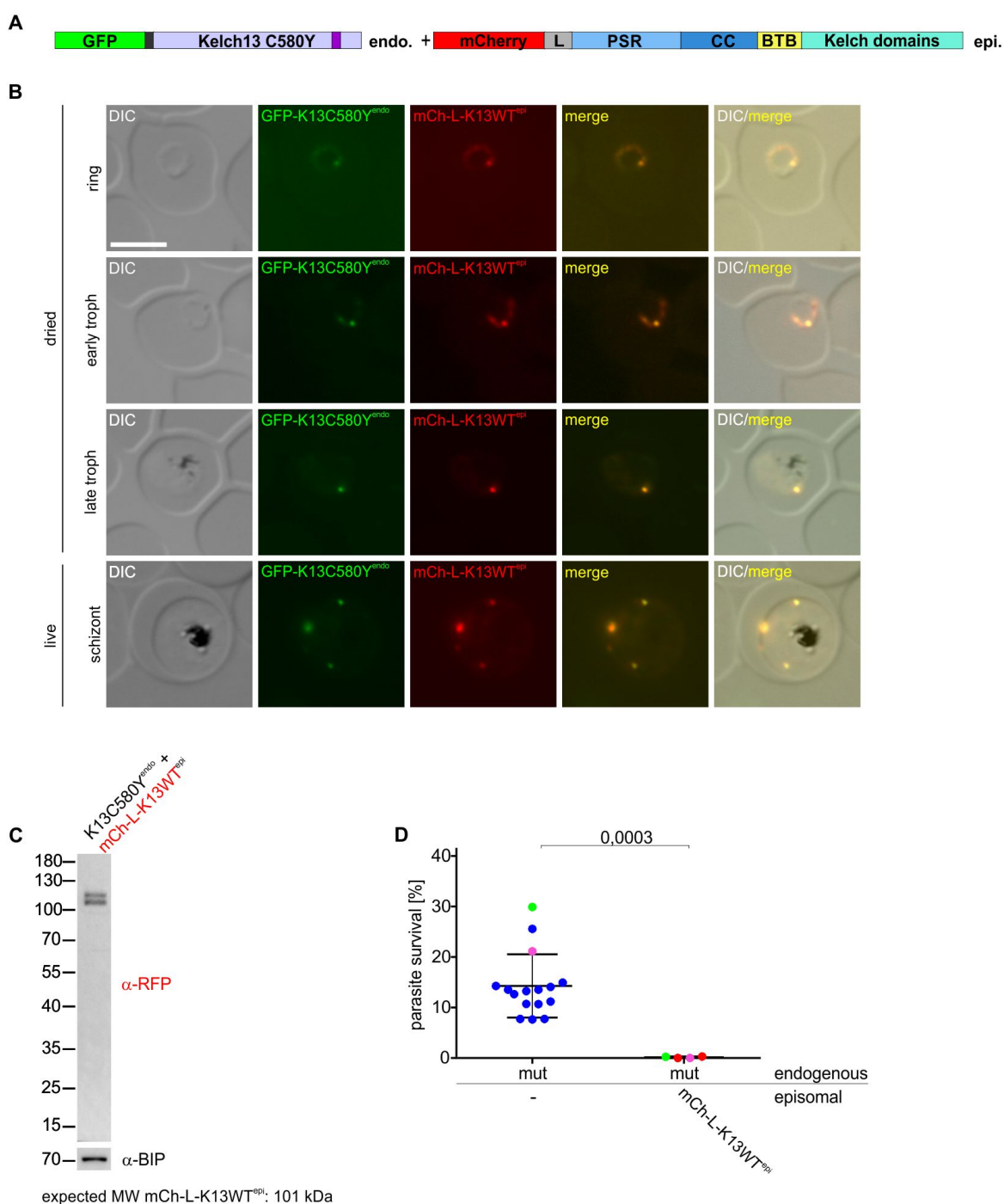


**Figure 28. Functional analysis of endogenous K13C580Y<sup>endo</sup> parasites episomally expressing K13WT<sup>epi</sup>.** (A) Schematic illustration (not to scale) of the modifications of the used parasite line: endogenous (endo) K13C580Y<sup>endo</sup> (GFP-2xFKBP-Kelch13<sup>C580Y</sup>, Birnbaum et al., 2017) and episomally expressed mCherry-L-K13WT<sup>epi</sup> (PSR: *Plasmodium* specific region; CC: coiled coil region; BTB: BTB/POZ domain; Kelch domains: Kelch propeller domain consisting of six Kelch motif repeats; mCh: mCherry red fluorescent protein; L: linker). (B) Fluorescence microscopy images of parasites indicated in (A). Parasites were imaged using fluorescence microscopy in the indicated development stages on at least three independent occasions. Ring, early trophozoites (early troph) and late trophozoites (late troph) were imaged after smearing on a glass slide

(dried); schizont stage show live cells (live). Scale bar 5  $\mu\text{m}$ , DIC: differential interference contrast; GFP: green fluorescent protein; mCh: mCherry red fluorescent protein; merge: GFP and mCherry channels merged. **(C)** Immunoblot with protein extracts of the cell line expressing the constructs indicated in (A) probed with anti-RFP and anti-BIP antibodies. MW: molecular weight. **(D)** RSAs with the respective cell lines expressing the constructs indicated (four independent experiments, each data point represents one experiment). Equally colored data points represent data required in the same round of experiments. K13C580Y<sup>endo</sup>: mut (n = 16). Bars show SD, mean is indicated. Unpaired, two-tailed t test with Welch's correction. P values are indicated.

To further investigate the correlation between Kelch13 protein level and resistance, it was analyzed, whether the loss of resistance due to the episomal expression of K13WT<sup>epi</sup> on the resistant background, could be attributed due to an additional property of Kelch13 wild type parasites that are lacking in Kelch13 mutant parasites. To test this, resistant K13C580Y<sup>endo</sup> parasites were co-transfected with an episomally expressed plasmid carrying the resistance-conferring C580Y mutation (mCherry-L-K13C580Y<sup>epi</sup> (K13C580Y<sup>epi</sup>), Figure 29 A). For the episomal construct a different codon usage was used for K13C580Y (termed codon usage 2) than that of the codon adjusted K13C580Y sequence of the K13C580Y inserted into the genome (defined as codon usage 1 in this study, Birnbaum et al., 2017). The sequence was re-codonized (Geneskript) to avoid unintentional integration of the episomal plasmid into the modified genomic K13C580Y<sup>endo</sup> locus. Fluorescence microscopy confirmed the identical localization of K13C580Y<sup>endo</sup> and K13C580Y<sup>epi</sup> (Figure 29 B). Using smeared and dried parasites again confirmed that small differences in the location of the two signals was due to movement of foci or parasites during live cell microscopy (Figure 29 B). The K13C580Y<sup>endo</sup> knock in parasites overexpressing the mCherry-L-K13C580Y<sup>epi</sup> construct were challenged in three independent experiments with 700 nM DHA for 6 hours in a standard ring stage survival assay (RSA, Witkowski et al., 2013) (Figure 29 C, see 2.2.3.13). Interestingly, parasites overexpressing K13C580Y<sup>epi</sup> on the resistant K13C580Y<sup>endo</sup> background were sensitive to DHA (mean = 0.3 % SR, SD = 0.0 %, n = 3) while the parental K13C580Y<sup>endo</sup> knock in control parasites without an episomally expressed Kelch13 construct were resistant to DHA (mean = 12.7 % SR, SD = 3.4 %, n = 16) (Figure 29 C). This confirmed the assumption that Kelch13 protein levels influences resistance.



foci in ring, trophozoite and schizont stages (Figure 30 B). Using smeared and dried parasites again confirmed that small differences in the location of the two signals was due to movement of foci or parasites during live cell microscopy (Figure 30 B). To evaluate the integrity of the mCherry-L-K13R539T<sup>epi</sup> – fusion protein, Western Blot analysis (see 2.2.4.1) was conducted using an anti-RFP antibody. The construct was detected at a molecular weight corresponding well with the predicted molecular weight of 101 kDa. The construct was detected in two bands with a migration consistent with the expected molecular weight of 101 kDa. The same immunoblot was re-probed with an anti-BIP antibody as a loading control (Figure 30 C). The K13C580Y<sup>endo</sup> parasites overexpressing the mCherry-L-K13R539T<sup>epi</sup> construct were challenged in three independent ring stage survival assays (RSAs, Witkowski et al., 2013) (Figure 30 D, see 2.2.3.13). Parasites expressing K13R539T<sup>epi</sup> on the resistant K13C580Y<sup>endo</sup> background were sensitive to DHA (mean = 0.7 % SR, SD = 0.5 %, n = 3), while the K13C580Y<sup>endo</sup> knock in control parasites without an overexpressed Kelch13 construct were resistant to DHA (mean = 12.7 % SR, SD = 3.4 %, n = 16). Hence, also the overexpression of a Kelch13 with a different resistance-conferring mutation than that in the parasite background resulted in a loss of resistance to DHA.

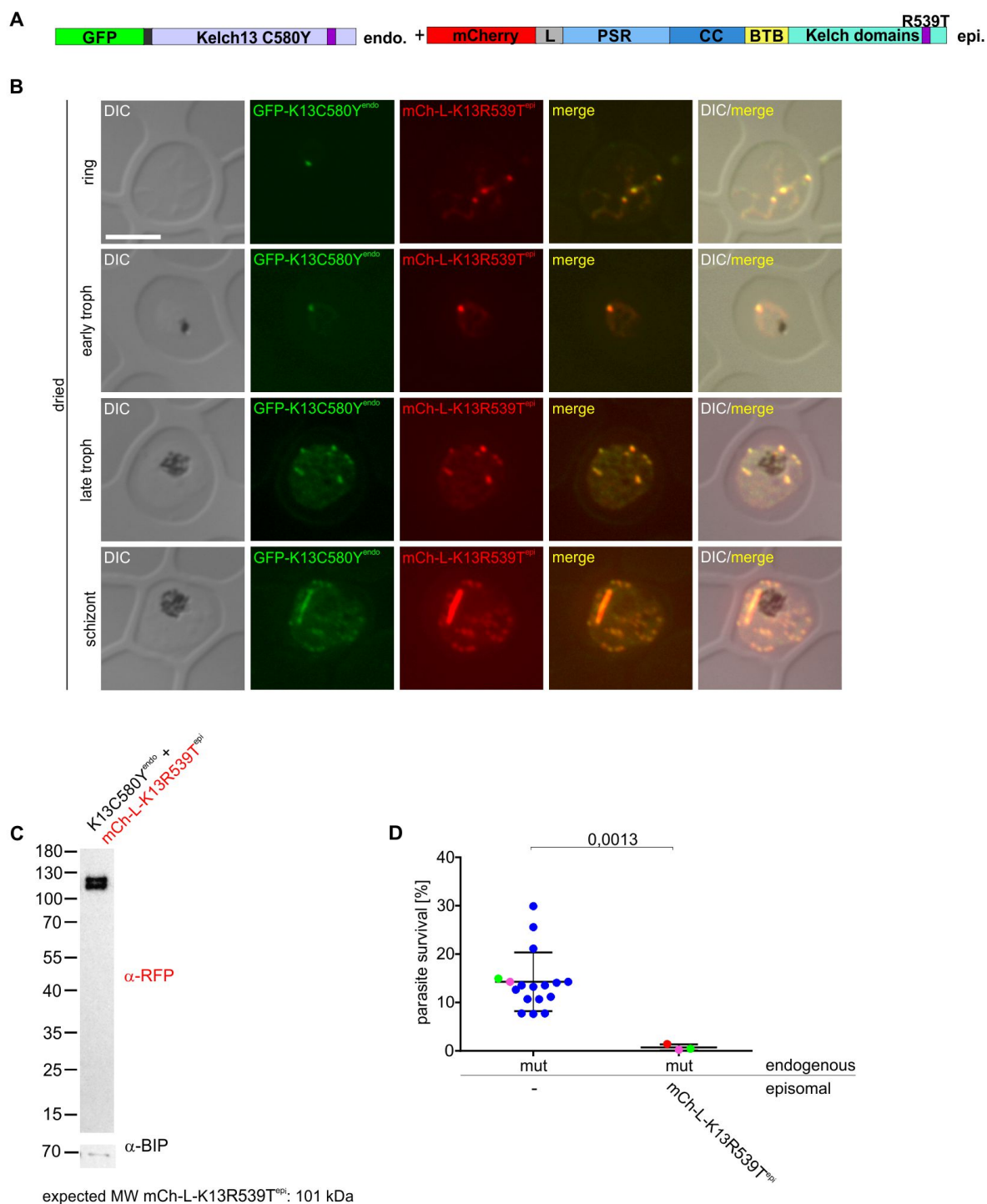


**Figure 30. Functional analysis of endogenous K13C580Y<sup>endo</sup> parasites episomally expressing K13R539T<sup>epi</sup>.** (A) Schematic illustration (not to scale) of the modifications of the used parasite line: endogenous (endo) K13C580Y<sup>endo</sup> (GFP-2xFKBP-Kelch13<sup>C580Y</sup>, Birnbaum et al., 2017) and episomally expressed mCherry-L-K13R539T<sup>epi</sup> (PSR: *Plasmodium* specific region; CC: coiled coil region; BTB: BTB/POZ domain; Kelch domains: Kelch propeller domain consisting of six Kelch motif repeats; mCh: mCherry red fluorescent protein; L: linker). (B) Fluorescence microscopy images of parasites indicated in (A). Parasites were smeared on a glass slide and imaged using fluorescence microscopy in ring, early trophozoites (early troph), late trophozoites (late troph) and schizont stages on at least three independent occasions. Scale bar 5  $\mu$ m, DIC: differential interference contrast; GFP: green fluorescent protein; mCh: mCherry red fluorescent protein; merge: GFP and mCherry channels merged. (C) Immunoblot with protein extracts of the cell line expressing the constructs indicated in (A) probed with anti-RFP and anti-BIP antibodies. MW: molecular weight. (D) RSAs with the respective cell lines expressing the constructs indicated (three independent experiments, each data point represents one experiment). Equally colored data points represent data required in the same round of experiments. K13C580Y<sup>endo</sup>: mut (n = 16). Bars show SD, mean is indicated. Unpaired, two-tailed t test with Welch's correction. P values are indicated.

Furthermore, resistant GFP-2xFKBP-Kelch13<sup>C580Y</sup> (K13C580Y<sup>endo</sup>, Birnbaum et al., 2017) parasites were co-transfected with a plasmid mediating the expression of Kelch13 with the resistance conferring K13E252Q mutation (mCherry-L-K13E252Q<sup>epi</sup>) (Figure 31 A). Analysis by fluorescence microscopy confirmed that K13C580Y<sup>endo</sup> and K13E252Q<sup>epi</sup> co-localize in foci in ring, trophozoite and schizont stages (Figure 31 B). Using smeared and dried parasites again confirmed that small differences in the location of the two signals was due to movement of foci or parasites during live cell microscopy (Figure 31 B). To evaluate the size of the mCherry-L-K13E252Q<sup>epi</sup> - fusion protein, Western Blot analysis (see 2.2.4.1) was conducted using an anti-RFP antibody. The construct was detected at a molecular weight corresponding well with the predicted molecular weight of 101 kDa. The construct was detected in two bands with a migration consistent with the expected molecular weight of 101 kDa. The same immunoblot was re-probed with an anti-BIP antibody as a loading control (Figure 31 C). The K13C580Y<sup>endo</sup> parasites overexpressing the mCherry-L-K13E252Q<sup>epi</sup> construct were challenged in three independent ring stage survival assays (RSAs, Witkowski et al., 2013) (Figure 31 D, see 2.2.3.13). Parasites expressing K13E252Q<sup>epi</sup> on the resistant K13C580Y<sup>endo</sup> background were sensitive to ART (mean = 0.2 % SR, SD = 0.1 %, n = 3), while the K13C580Y<sup>endo</sup> knock in control parasites without an overexpressed Kelch13 construct were resistant to DHA (mean = 12.7 % SR, SD = 3.4 %, n = 16). This indicated that the extra expression of also this resistance conferring Kelch13 protein (K13E252Q<sup>epi</sup>) was sufficient to revert resistance.

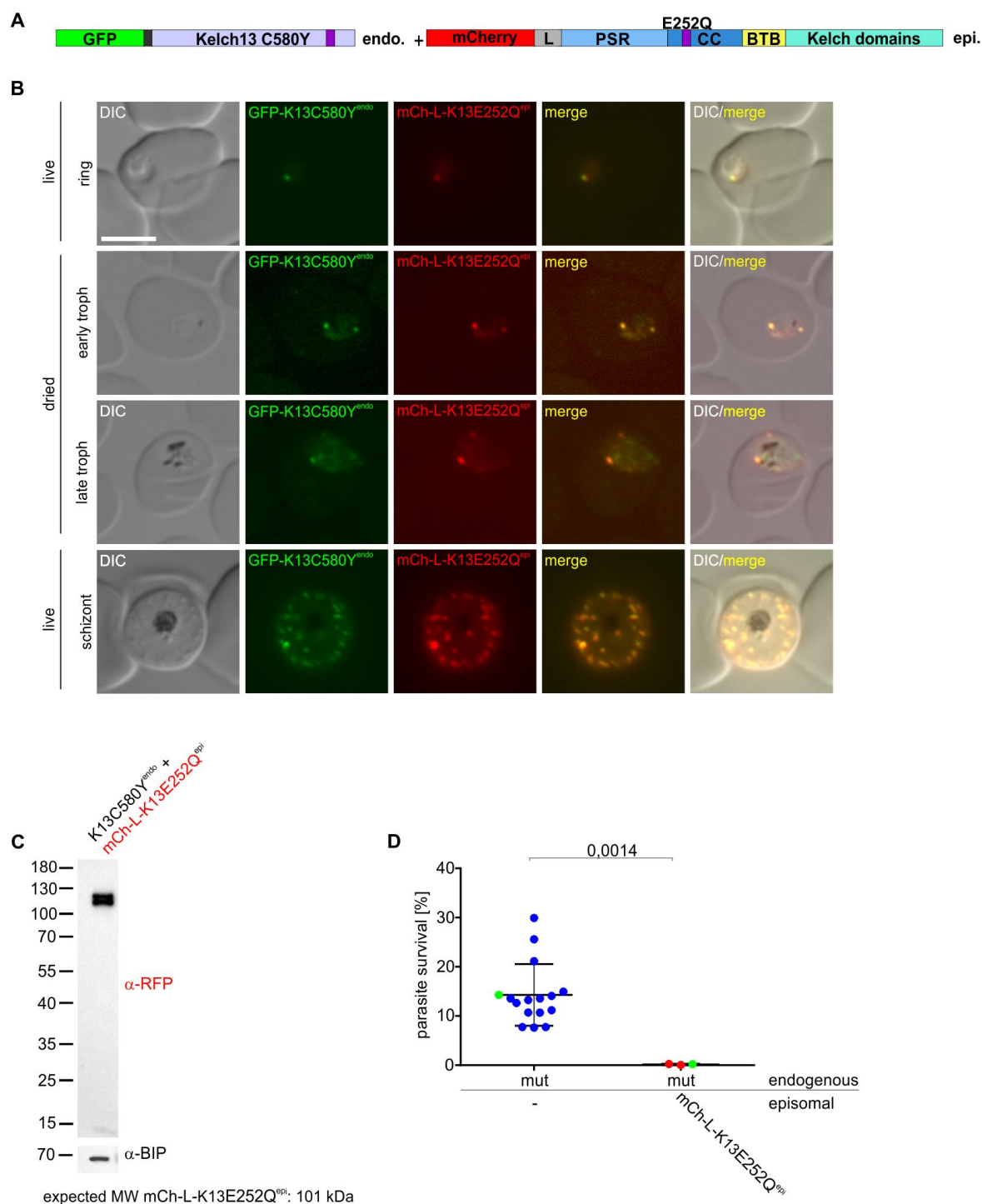


**Figure 31. Functional analysis of endogenous K13C580Y<sup>endo</sup> parasites episomally expressing K13E252Q<sup>epi</sup>.** (A) Schematic illustration (not to scale) of the modifications of the used parasite line: endogenous (endo) K13C580Y<sup>endo</sup> (GFP-2xFKBP-Kelch13<sup>C580Y</sup>, Birnbaum et al., 2017) and episomally expressed mCherry-L-K13E252Q<sup>epi</sup> (PSR: *Plasmodium* specific region; CC: coiled coil region; BTB: BTB/POZ domain; Kelch domains: Kelch propeller domain consisting of six Kelch motif repeats; mCh: mCherry red fluorescent protein; L: linker). (B) Fluorescence microscopy images of parasites expressing the constructs indicated in (A). Parasites were imaged using fluorescence microscopy in the indicated development stages on at least three independent occasions. Early trophozoite (early troph) and late trophozoite (late troph) stages were imaged after smearing on a glass slide; ring and schizont stage show live cells. Scale bar 5  $\mu$ m, DIC: differential interference contrast; GFP: green fluorescent protein; mCh: mCherry red fluorescent protein; merge: GFP and mCherry channels merged. (C) Immunoblot with protein extracts of the cell line expressing the constructs indicated in (A) probed with anti-RFP and anti-BIP antibodies. MW: molecular weight. (D) RSAs with the respective cell lines expressing the constructs indicated (three independent experiments, each data point represents one experiment). Equally colored data points represent data acquired in the same round of experiments. K13C580Y<sup>endo</sup>: mut (n = 16). Bars show SD, mean is indicated. Unpaired, two-tailed t test with Welch's correction. P values are indicated.

Taken together, episomal expression of K13C580Y<sup>epi</sup>, K13R539T<sup>epi</sup> and K13E252Q<sup>epi</sup> on resistant K13C580Y<sup>endo</sup> parasites demonstrated, that the observed sensitivity to DHA of resistant parasites episomally expressing K13WT<sup>epi</sup> (Figure 28 D) is not based on an additional property of Kelch13 wild type parasites that is lacking in resistant parasites and that rather Kelch13 abundance might influences resistance.

### 3.3.2 Functional analysis of the Kelch13 domains

To analyze the function of individual domains of Kelch13 and to investigate which domain of Kelch13 promotes resistance, different Kelch13 domain combinations were expressed on the resistant background. The importance of the domains for the function of the protein was then dissected by determining ART sensitivity with ring stage survival assays (RSAs, Witkowski et al., 2013, see 2.2.3.13). As it was already shown that sensitivity to ART is restored when a functional Kelch13 copy is expressed on a resistant background (see 3.3.1), it was expected that this analysis provides insight into the mechanistic function of the Kelch13 domains. The Kelch13 protein consists of an N-terminal *Plasmodium* specific region (PSR) followed by a coiled coil region (CC), a BTB domain and 6 Kelch motif repeats (Kelch propeller domain, from now on described as Kelch domains, KD, Figure 32).

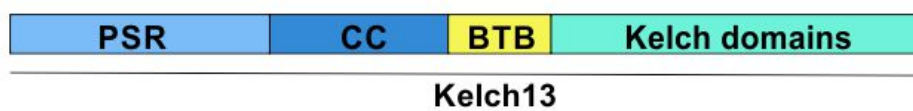


**Figure 32. Schematic illustration (not to scale) of the domains of Kelch13.** PSR: *Plasmodium* specific region; CC: coiled coil region; BTB: BTB/POZ domain; Kelch domains: Kelch propeller domain consisting of six Kelch motif repeats.

To assess the function of the C-terminus of Kelch13, an episomal construct expressing only the BTB and Kelch domains (mCherry-L-BTB-KD<sup>epi</sup>: BTB-KD<sup>epi</sup>) was co-transfected on GFP-2xFKBP-Kelch13<sup>C580Y</sup> (K13C580Y<sup>endo</sup>, Birnbaum et al., 2017) parasites (Figure 33 A). Fluorescence microscopy was used to assess the localization of BTB-KD<sup>epi</sup> in ring, trophozoite and schizont stages (Figure 33 B). Using smeared and dried parasites confirmed that small differences in the location of the two signals was due to movement of foci or parasites during live cell microscopy (Figure 33 B). This analysis showed, that BTB-KD<sup>epi</sup> is located in the cytosol of the parasite and was not found at the typical Kelch13 foci. This indicates that the N-terminus of Kelch13 is needed for the correct localization of the protein. To confirm the integrity of the mCherry-L-BTB-KD<sup>epi</sup> -fusion protein, Western Blot analysis (see 2.2.4.1) was conducted using an anti-RFP antibody. The construct was detected at approximately 60 kDa, below the expected molecular weight of 71 kDa. The same immunoblot was re-probed with an anti-BIP antibody as a loading control (Figure 33 C). To dissect the importance of BTB-KD<sup>epi</sup> to maintain the function of the protein, the parasites were challenged with DHA using RSAs (Figure 33 D, see 2.2.3.13). Episomal expression of BTB-KD<sup>epi</sup> did not change the overall resistance level of the parasites (mean = 14.7 % SR, SD = 3.4 %, n = 3), while K13C580Y<sup>endo</sup> knock in control parasites without an overexpressed Kelch13 construct were resistant to DHA (mean = 12.7 % SR, SD = 3.4 %, n = 16).

This indicates that that the C-terminal part consisting of BTB and KD is not sufficient to maintain the function of Kelch13.

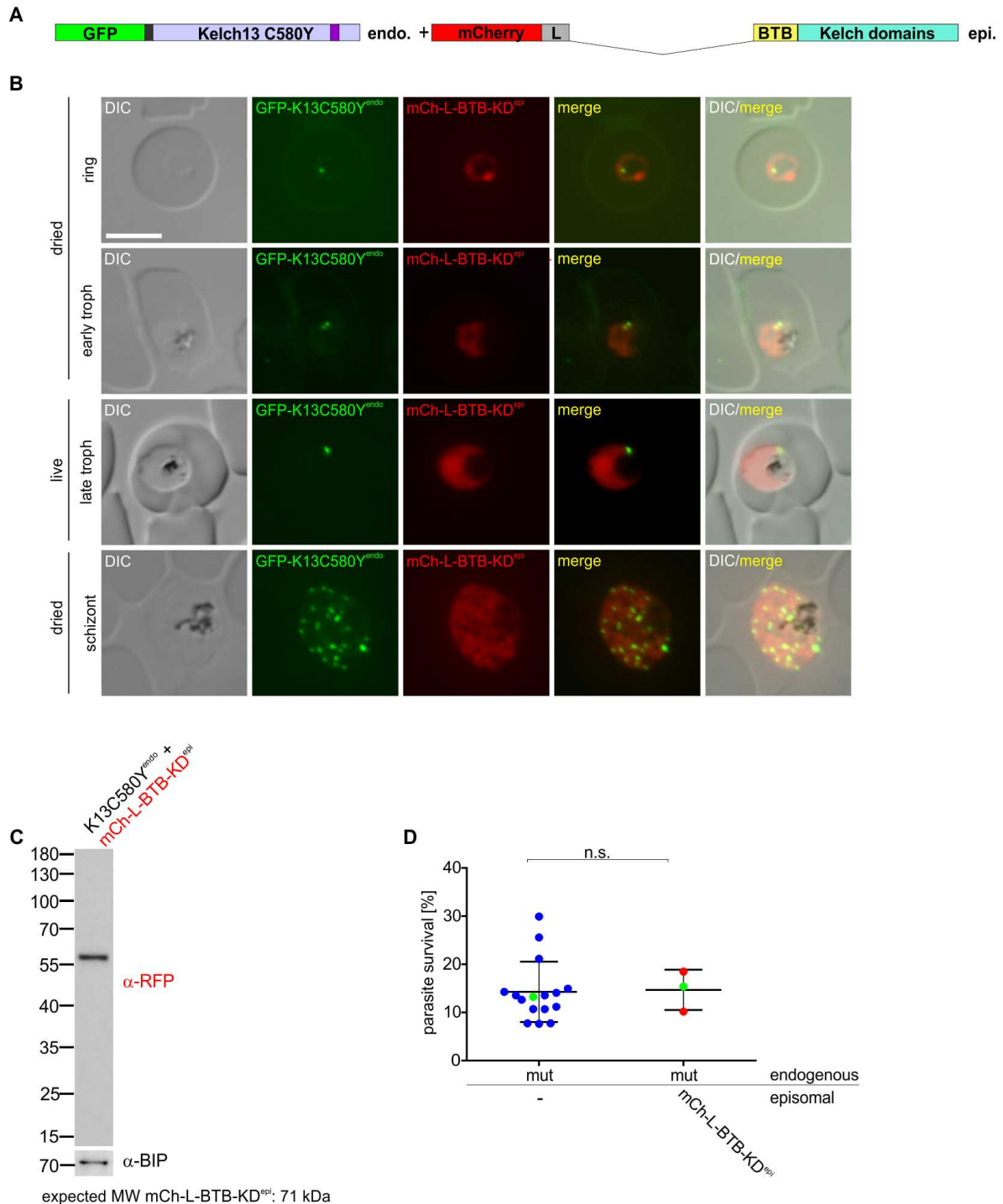


**Figure 33. Functional analysis of endogenous K13C580Y<sup>endo</sup> parasites episomally expressing mCherry-L-BTB-KD<sup>epi</sup>.** (A) Schematic illustration (not to scale) of the modifications of the used parasite line: endogenous (endo) K13C580Y<sup>endo</sup> (GFP-2xFKBP-Kelch13<sup>C580Y</sup>, Birnbaum et al., 2017) and episomally expressed mCherry-L-BTB-KD<sup>epi</sup> (BTB: BTB/POZ domain; Kelch domains: Kelch propeller domain consisting of six Kelch motif repeats; mCh: mCherry red fluorescent protein; L: linker). (B) Fluorescence microscopy images of parasites expressing the constructs indicated in (A). Parasites were imaged using fluorescence microscopy in the indicated development stages on at least three independent occasions. Ring, early trophozoite (early troph) and schizont stages were imaged after smearing on a glass slide; late trophozoite (late troph) stage shows a living cell. Scale bar 5  $\mu$ m, DIC: differential interference contrast; GFP: green fluorescent protein; mCh: mCherry red fluorescent protein; merge: GFP and mCherry channels merged. (C) Immunoblot with protein extracts of the cell line

expressing the constructs indicated in (A) probed with anti-RFP and anti-BIP antibodies. MW: molecular weight. **(D)** RSAs with the respective cell lines expressing the constructs indicated (three independent experiments, each data point represents one experiment). Equally colored data points represent data acquired in the same round of experiments. K13C580Y<sup>endo</sup>: mut (n = 16). Bars show SD, mean is indicated. Unpaired, two-tailed t test with Welch's correction. P values are indicated.

Next, resistant GFP-2xFKBP-Kelch13<sup>C580Y</sup> (K13C580Y<sup>endo</sup>, Birnbaum et al., 2017) parasites were co-transfected with a plasmid overexpressing mCherry-L-Linker-BTB-KD<sup>epi</sup> (Linker-BTB-KD<sup>epi</sup>, Figure 34 A). The flexible linker region (7xGGGGS, Birnbaum et al., 2017) was used as a placeholder before the BTB domain to add distance between the mCherry tag and the BTB domain, which is usually provided by the presence of the PSR in the Kelch13 protein. Fluorescence microscopy was used to investigate the localization of Linker-BTB-KD<sup>epi</sup> in ring, trophozoite and schizont stages (Figure 34 B). This analysis showed, that Linker-BTB-KD<sup>epi</sup> is located in the cytosol of the parasite but not at the Kelch13 foci (Figure 34 B). To evaluate the integrity of the mCherry-L-Linker-BTB-KD<sup>epi</sup> -fusion protein, Western Blot analysis (see 2.2.4.1) was conducted using an anti-RFP antibody. The construct was detected at approximately 60 kDa, below the expected molecular weight of 73 kDa. The same immunoblot was re-probed with an anti-BIP antibody as a loading control (Figure 34 C). The K13C580Y<sup>endo</sup> parasites overexpressing the mCherry-L-Linker-BTB-KD<sup>epi</sup> construct were challenged with DHA using standard RSAs (Figure 34 D, see 2.2.3.13). These experiments showed that parasites expressing mCherry-L-Linker-BTB-KD<sup>epi</sup> on the resistant background were still resistant to ART (mean = 13.4 % SR, SD = 1.6 %, n = 3), while K13C580Y<sup>endo</sup> knock in control parasites without an overexpressed Kelch13 construct were resistant to DHA (mean = 12.7 % SR, SD = 3.4 %, n = 16). This shows that the additional linker before the BTB-KD did not restore the mechanistic function of Kelch13 and that the mCherry-L-Linker-BTB-KD construct was non-functional in respect to resistance-conferring activities.

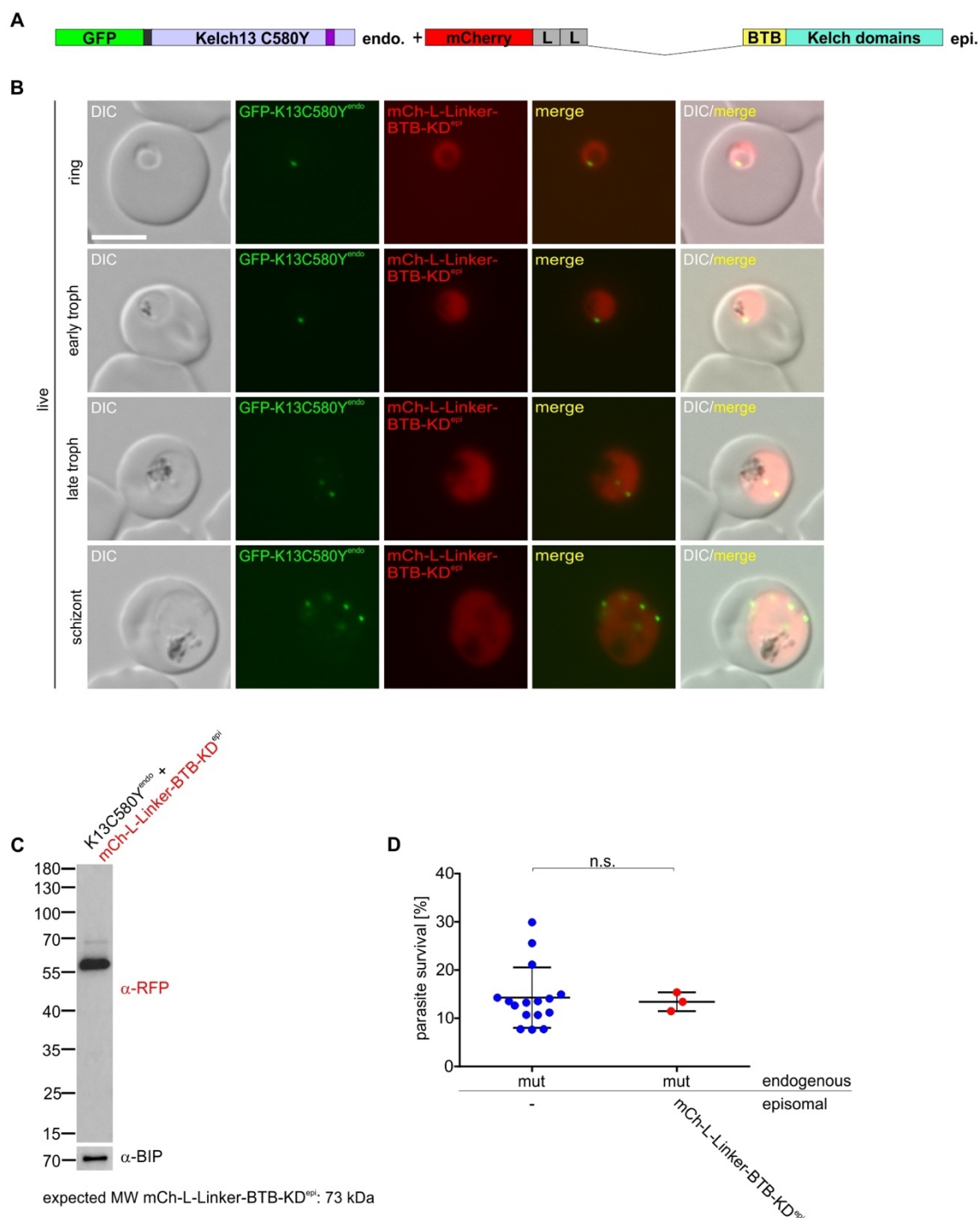


**Figure 34. Functional analysis of endogenous K13C580Y<sup>endo</sup> parasites episomally expressing mCherry-L-Linker-BTB-KD<sup>epi</sup>.** (A) Schematic illustration (not to scale) of the modifications of the used parasite line: endogenous (endo) K13C580Y<sup>endo</sup> (GFP-2xFKBP-Kelch13<sup>C580Y</sup>, Birnbaum et al., 2017) and episomally expressed mCherry-L-Linker-BTB-KD<sup>epi</sup> (BTB: BTB/POZ domain; Kelch domains: Kelch propeller domain consisting of six Kelch motif repeats; mCh: mCherry red fluorescent protein; L: linker). (B) Fluorescence microscopy images of parasites expressing the constructs indicated in (A). Living parasites were imaged using fluorescence microscopy in ring, early trophozoite (early troph), late trophozoite (late troph) and schizont stages on at least three independent occasions. Scale bar 5  $\mu$ m, DIC: differential interference contrast; GFP: green fluorescent protein; mCh: mCherry red fluorescent protein; merge: GFP and mCherry channels merged. (C) Immunoblot with protein extracts of the cell line expressing the constructs indicated in (A) probed with anti-RFP and anti-BIP antibodies. MW: molecular weight. (D) RSAs with the respective cell lines expressing the constructs indicated (three independent experiments, each data point represents one experiment). K13C580Y<sup>endo</sup>: mut (n = 16). Bars show SD, mean is indicated. Unpaired, two-tailed t test with Welch's correction. P values are indicated.

To investigate, whether the BTB domain alone is sufficient to provide the function of Kelch13, resistant GFP-2xFKBP Kelch13<sup>C580Y</sup> (K13C580Y<sup>endo</sup>, Birnbaum et al., 2017) parasites were co-transfected with a plasmid overexpressing mCherry-L-BTB<sup>epi</sup> (BTB<sup>epi</sup>, Figure 35 A). Fluorescence microscopy was used to investigate the localization of mCherry-L-BTB<sup>epi</sup> in ring, trophozoite and schizont stages (Figure 35 B). This analysis showed, that BTB<sup>epi</sup> is located in the cytosol of the parasite and was not found at the typical Kelch13 foci. This indicates that the BTB domain of Kelch13 is not sufficient to maintain the correct localization of the protein. To evaluate the integrity of the mCherry-L-BTB<sup>epi</sup> – fusion protein, Western Blot analysis (see 2.2.4.1) was conducted using an anti-RFP antibody. The construct was detected in three bands, a faint band consistent with the expected molecular weight of 39 kDa (Figure 35 C, arrow) and two strong bands at approximately 28 kDa and 34 kDa (Figure 35 C, asterisks). The same immunoblot was re-probed with an anti-BIP antibody as a loading control (Figure 35 C). These findings indicated that BTB<sup>epi</sup> was processed or degraded. The K13C580Y<sup>endo</sup> parasites overexpressing the mCherry-L-K13BTB<sup>epi</sup> construct were challenged in three independent ring stage survival assays (RSAs, Witkowski et al., 2013) (Figure 35 D, see 2.2.3.13). Episomal expression of the BTB<sup>epi</sup> domain has a slight but no significant impact on the resistance level of Kelch13 mutant parasites (mean = 9.6 % SR, SD = 4.3 %, n = 3), while the K13C580Y<sup>endo</sup> knock in control parasites without an overexpressed Kelch13 construct were resistant to DHA (mean = 12.7 % SR, SD = 3.4 %, n = 16). Overall, these findings indicate that the mCherry-L-BTB<sup>epi</sup> construct was instable or proteolytically processed, which might also implicate that the fluorescence signal detected in the parasite originated from degraded protein and complicates the interpretation of the data. However, it can be concluded that at least the small amount of full length BTB domain construct alone was not sufficient to maintain the function of Kelch13.

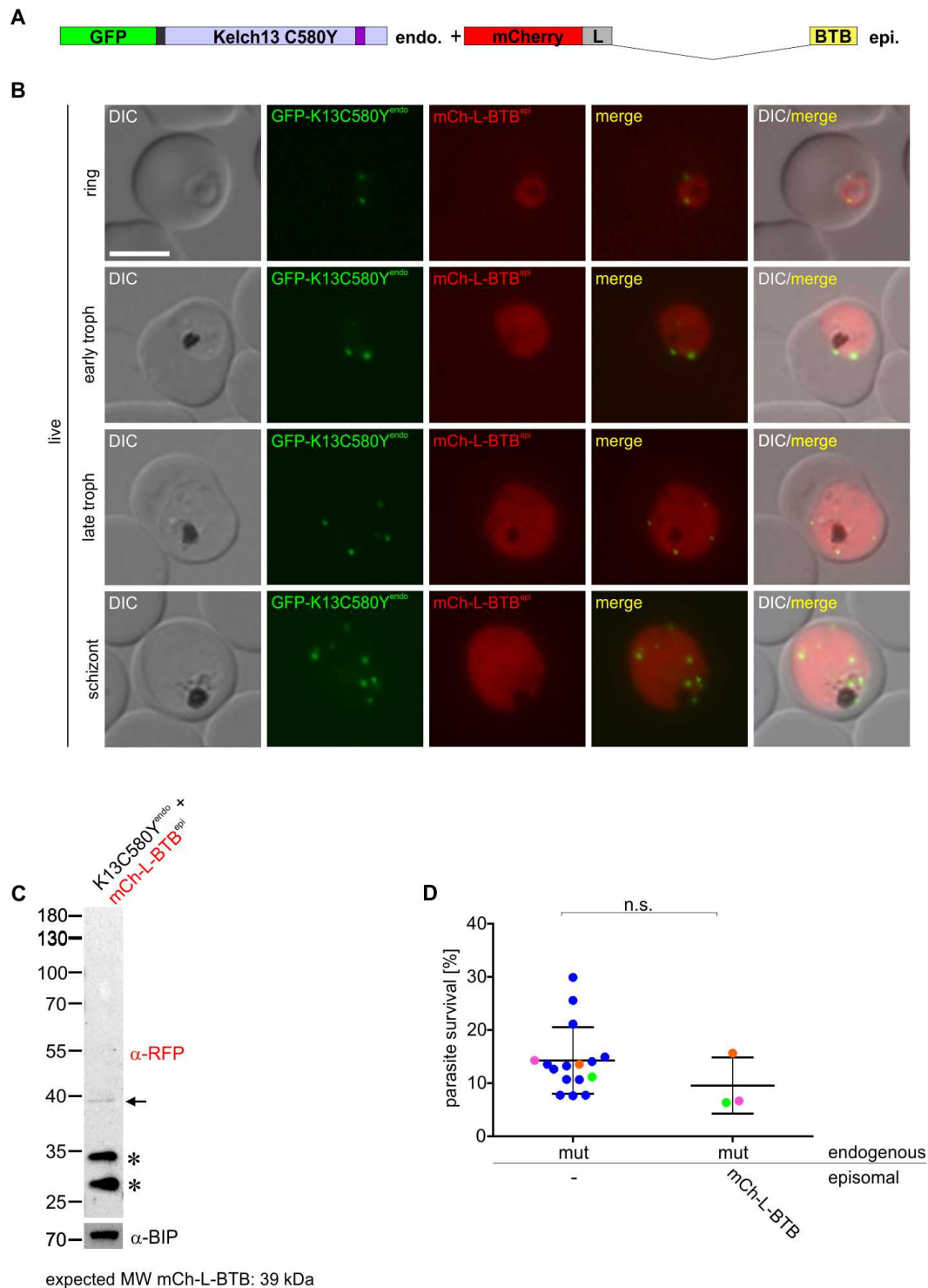


**Figure 35. Functional analysis of endogenous K13C580Y<sup>endo</sup> parasites episomally expressing mCherry-L-BTB<sup>epi</sup>.** (A) Schematic illustration (not to scale) of the modifications of the used parasite line: endogenous (endo) K13C580Y<sup>endo</sup> (GFP-2xFKBP-Kelch13<sup>C580Y</sup>, Birnbaum et al., 2017) and episomally expressed mCherry-L-BTB<sup>epi</sup> (BTB: BTB/POZ domain; mCh: mCherry red fluorescent protein; L: linker). (B) Fluorescence microscopy images of living parasites expressing the constructs indicated in (A). Parasites were imaged using fluorescence microscopy in the indicated development stages on at least three independent occasions. Ring, early trophozoite (early troph), late trophozoite (late troph) and schizont stage show living cells (live). Scale bar 5  $\mu$ m, DIC: differential interference contrast; GFP: green fluorescent protein; mCh: mCherry red fluorescent protein; merge: GFP and mCherry channels merged. (C) Immunoblot with protein extracts of the cell line expressing the constructs indicated in (A) probed with anti-RFP and anti-BIP antibodies. MW: molecular weight. Arrow shows band at the expected MW of the fusion protein indicated in (A). Asterisks show lower bands not consistent with the expected MW of the indicated fusion protein (D) RSAs with the respective cell lines expressing the constructs indicated (three independent experiments, each data point represents one experiment). Equally colored data points represent data acquired in the same round of experiments. K13C580Y<sup>endo</sup>: mut (n = 16). Bars show SD, mean is indicated. Unpaired, two-tailed t test with Welch's correction. P values are indicated.

For further analysis resistant GFP-2xFKBP-Kelch13<sup>C580Y</sup> (K13C580Y<sup>endo</sup>, Birnbaum et al., 2017) parasites were co-transfected with a plasmid overexpressing mCherry-L-CC-BTB-KD<sup>epi</sup> (CC-BTB-KD<sup>epi</sup>, Figure 36 A). Fluorescence microscopy was used to investigate the localization of CC-BTB-KD<sup>epi</sup> (Figure 36 B, live). Using smeared and dried parasites again confirmed that small differences in the location of the two signals was due to movement of foci or parasites during live cell microscopy (Figure 36 B, dried). This indicated that the CC domain of Kelch13 is important for bringing the C-terminus of the protein to the correct location in the cell. To evaluate the integrity of the mCherry-L-CC-BTB-KD<sup>epi</sup> – fusion protein, Western Blot analysis (see 2.2.4.1) was conducted using an anti-RFP antibody. The construct was detected at approximately 70 kDa, below the expected molecular weight of 89 kDa. The same immunoblot was re-probed with an anti-BIP antibody as a loading control (Figure 36 C). The K13C580Y<sup>endo</sup> parasites overexpressing the mCherry-L-CC-BTB-KD<sup>epi</sup> construct were challenged in three independent ring stage survival assays (RSAs, Witkowski et al., 2013) (Figure 36 D, see 2.2.3.13). Parasites expressing CC-BTB-KD<sup>epi</sup> on the resistant K13C580Y<sup>endo</sup> background were sensitive to ART (mean = 12.7 % SR, SD = 3.4 %, n = 16), while the K13C580Y<sup>endo</sup> knock in control parasites without an overexpressed Kelch13 construct were resistant to DHA (mean = 12.7 % SR, SD = 3.4 %, n = 16). This demonstrates that CC-BTB-KD<sup>epi</sup> led to the correct localization of the construct in Kelch13 foci and restored the function of the protein.

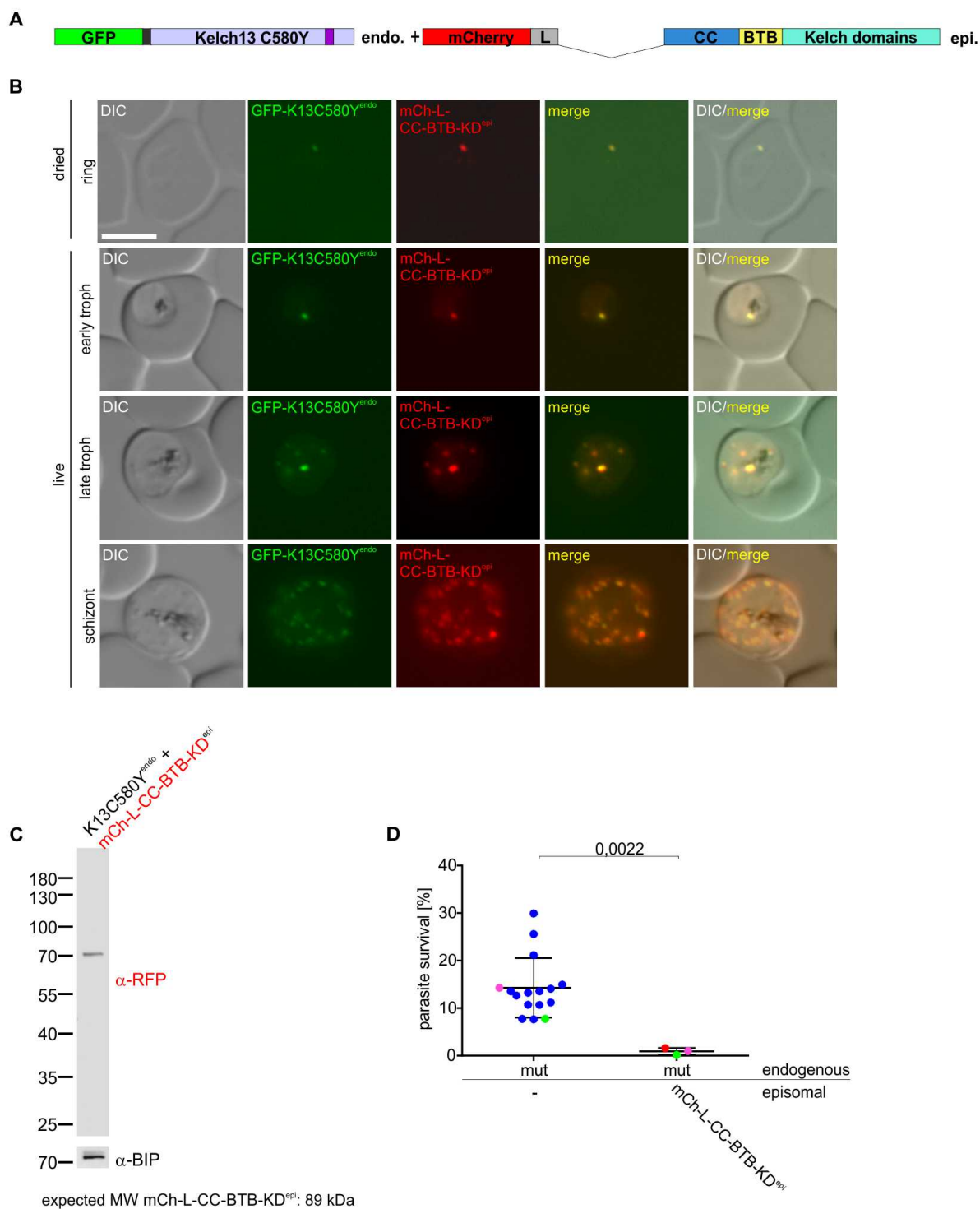


**Figure 36. Functional analysis of endogenous K13C580Y<sup>endo</sup> parasites episomally expressing mCherry-L-CC-BTB-KD<sup>epi</sup>.** (A) Schematic illustration (not to scale) of the modifications of the used parasite line: endogenous (endo) K13C580Y<sup>endo</sup> (GFP-2xFKBP-Kelch13<sup>C580Y</sup>, Birnbaum et al., 2017) and episomally expressed mCherry-L-CC-BTB-KD<sup>epi</sup> (CC: coiled coil region; BTB: BTB/POZ domain; Kelch domains: Kelch propeller domain consisting of six Kelch motif repeats; mCh: mCherry red fluorescent protein; L: linker). (B) Fluorescence microscopy images of parasites expressing the constructs indicated in (A). Parasites were imaged using fluorescence microscopy in the indicated development stages on at least three independent occasions. Ring stages were imaged after smearing on a glass slide (dried); early trophozoite (early troph), late trophozoite (late troph) and schizont stage show living cells. Scale bar 5  $\mu$ m, DIC: differential interference contrast; GFP: green fluorescent protein; mCh: mCherry red fluorescent protein; merge: GFP and mCherry channels merged. (C) Immunoblot with protein extracts of the cell line expressing the constructs indicated in (A) probed with anti-RFP and anti-BIP antibodies. MW: molecular weight. (D) RSAs with the respective cell lines expressing the constructs indicated (three independent experiments, each data point represents one experiment). Equally colored data points represent data acquired in the same round of experiments. K13C580Y<sup>endo</sup>: mut (n = 16). Bars show SD, mean is indicated. Unpaired, two-tailed t test with Welch's correction. P values are indicated.

Next, it was analyzed if the coiled coil region combined with the BTB domain was sufficient to maintain the function of Kelch13. To test this, resistant GFP-2xFKBP-Kelch13<sup>C580Y</sup> (K13C580Y<sup>endo</sup>, Birnbaum et al., 2017) parasites were co-transfected with a plasmid overexpressing mCherry-L-CC-BTB<sup>epi</sup> (CC-BTB<sup>epi</sup>, Figure 37 A). Fluorescence microscopy was used to investigate the localization of CC-BTB<sup>epi</sup> (Figure 37 B, live). Using smeared and dried parasites again confirmed that small differences in the location of the two signals was due to movement of foci or parasites during live cell microscopy (Figure 37 B, dried). This analysis showed, that CC-BTB<sup>epi</sup> was not sufficient for the correct localization of the protein. To evaluate the integrity of the mCherry-L-CC-BTB<sup>epi</sup> – fusion protein, Western Blot analysis (see 2.2.4.1) was conducted using an anti-RFP antibody. The construct was detected at approximately 50 kDa, below the expected molecular weight of 57 kDa. The same immunoblot was re-probed with an anti-BIP antibody as a loading control (Figure 37 C). The K13C580Y<sup>endo</sup> parasites overexpressing the mCherry-L-CC-BTB<sup>epi</sup> construct were challenged in three independent ring stage survival assays (RSAs, Witkowski et al., 2013) (Figure 37 D, see 2.2.3.13). Interestingly, episomal expression of CC-BTB<sup>epi</sup> reduced the resistance level of the K13C580Y<sup>endo</sup> parasites but was not sufficient to revert the resistant parasites back to full sensitivity (mean = 3.0 % SR, SD = 1.2 %, n = 3), while the K13C580Y<sup>endo</sup> knock in control parasites without an overexpressed Kelch13 construct were resistant to DHA (mean = 12.7 % SR, SD = 3.4 %, n = 16). This indicated that CC-BTB<sup>epi</sup> at least partially sustains the function of Kelch13. This finding was unexpected, because this construct did not appear to correctly localize. To investigate the hypothesis whether CC-BTB<sup>epi</sup> might localize in Kelch13 foci that are not visible due to the dominant cytosolic distribution of the construct in the cell, the cells were fixed with formaldehyde in order to lyse the PPM to release the cytosolic pool of CC-BTB<sup>epi</sup>. The cells were then stained with DAPI and analyzed by fluorescence microscopy (Figure 37 E). Interestingly, fixing the cells with 0.1 % or 0.5 % formaldehyde revealed a partial co-localization of endogenously tagged K13C580Y<sup>endo</sup> with the episomal construct CC-BTB<sup>epi</sup> (Figure 37 E). This suggests that at least a small population of CC-BTB<sup>epi</sup> is found at the localization typical for Kelch13.

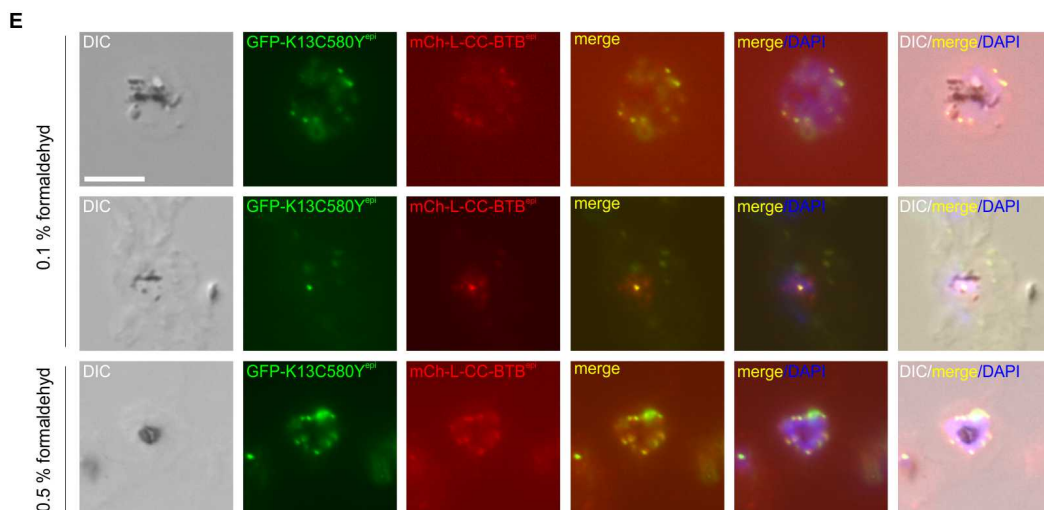
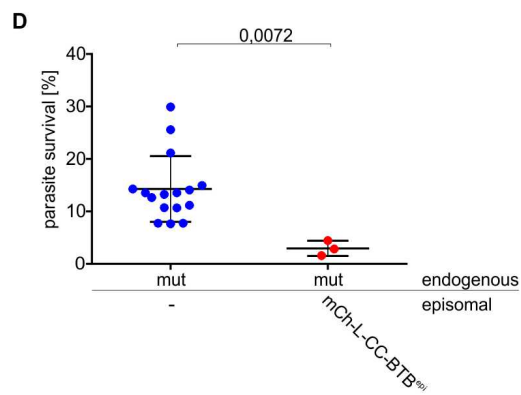
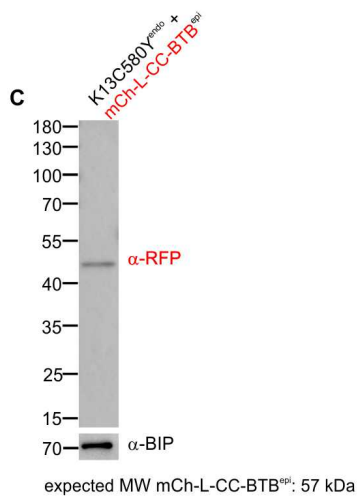
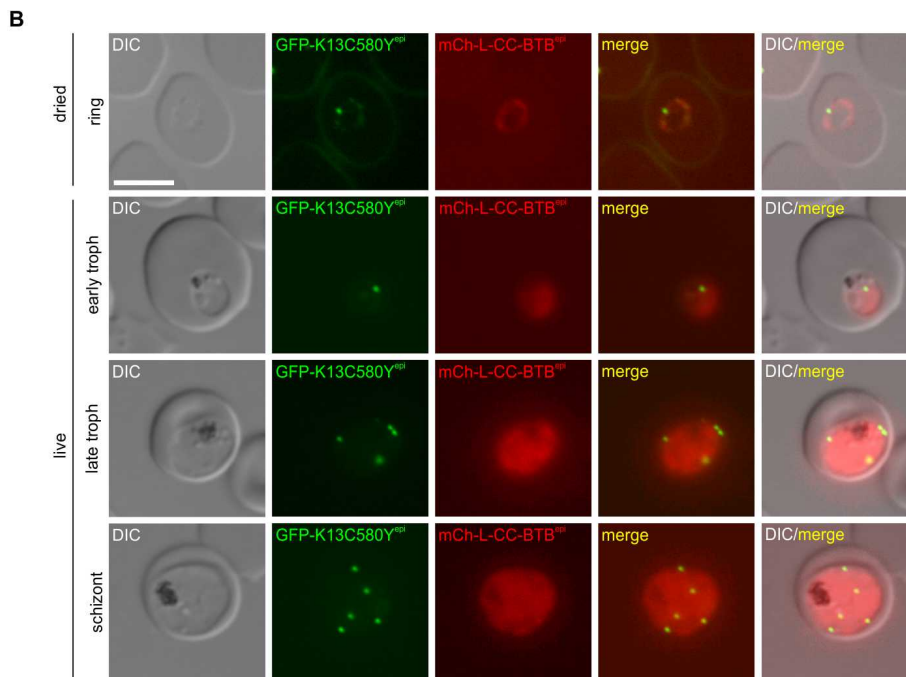


**Figure 37. Functional analysis of endogenous K13C580Y<sup>endo</sup> parasites episomally expressing mCherry-L-CC-BTB<sup>epi</sup>.** (A) Schematic illustration (not to scale) of the modifications of the used parasite line: endogenous (endo) K13C580Y<sup>endo</sup> (GFP-2xFKBP-Kelch13<sup>C580Y</sup>, Birnbaum et al., 2017) and episomally expressed mCherry-L-CC-BTB<sup>epi</sup> (CC: coiled coil region; BTB: BTB/POZ domain; mCh: mCherry red fluorescent protein; L: linker). (B) Fluorescence microscopy images of parasites expressing the constructs indicated in (A). Parasites were imaged using fluorescence microscopy in the indicated development stages on at least three independent occasions. Ring stages were imaged after smearing on a glass slide (dried); early trophozoite (early troph), late trophozoite (late troph) and schizont stage show living cells (live). (C) Immunoblot with protein extracts of the cell line expressing the constructs indicated in (A) probed with anti-RFP and anti-BIP antibodies. MW: molecular weight. (D) RSAs with the respective cell lines expressing the constructs indicated (three independent experiments, each data point represents one experiment). K13C580Y<sup>endo</sup>: mut (n = 16). Bars show SD, mean is indicated. Unpaired, two-tailed t test with Welch's correction. P values are indicated. (E) Fluorescence microscopy with formaldehyde fixed parasites indicated in (A). Scale bar 5  $\mu$ m, DIC: differential interference contrast; GFP: green fluorescent protein; mCh: mCherry red fluorescent protein; merge: green and red channels merged; DAPI: nuclei.

To further investigate the function of the Kelch13 domains, resistant GFP-2xFKBP-Kelch13<sup>C580Y</sup> (K13C580Y<sup>endo</sup>, Birnbaum et al., 2017) parasites were co-transfected with a plasmid overexpressing mCherry-L-PSR-CC-BTB<sup>epi</sup> (PSR-CC-BTB<sup>epi</sup>, Figure 38 A). Fluorescence microscopy was used to investigate the localization of PSR-CC-BTB<sup>epi</sup> in ring, trophozoite and schizont stages. This analysis showed a cytosolic distribution of PSR-CC-BTB<sup>epi</sup> with an additional partial co-localization of PSR-CC-BTB<sup>epi</sup> and K13C580Y<sup>endo</sup> (Figure 38 B). To evaluate the integrity of the mCherry-L-PSR-CC-BTB<sup>epi</sup> – fusion protein, Western Blot analysis (see 2.2.4.1) was conducted using an anti-RFP antibody. The construct was detected at a molecular weight corresponding well with the predicted molecular weight of 81 kDa. The same immunoblot was re-probed with an anti-BIP antibody as a loading control (Figure 38 C). The K13C580Y<sup>endo</sup> parasites overexpressing the mCherry-L-PSR-CC-BTB<sup>epi</sup> construct were challenged in three independent ring stage survival assays (RSAs, Witkowski et al., 2013) (Figure 38 D, see 2.2.3.13). Episomal expression of PSR-CC-BTB<sup>epi</sup> did not render the resistant parasites sensitive to DHA (mean = 27.7 % SR, SD = 9.3 %, n = 3), but unexpectedly increased the resistance level significantly compared to K13C580Y<sup>endo</sup> knock in control parasites without an episomally expressed Kelch13 construct (mean = 12.7 % SR, SD = 3.4 %, n = 16). This indicates that PSR-CC-BTB<sup>epi</sup> is not sufficient to maintain the function of Kelch13. The relevance of the increased resistance in this cell line is unclear, as there is often considerable variation in the resistance levels measured in the K13C580Y<sup>endo</sup> knock in control parasites and this finding would therefore need to be confirmed with more replicas.

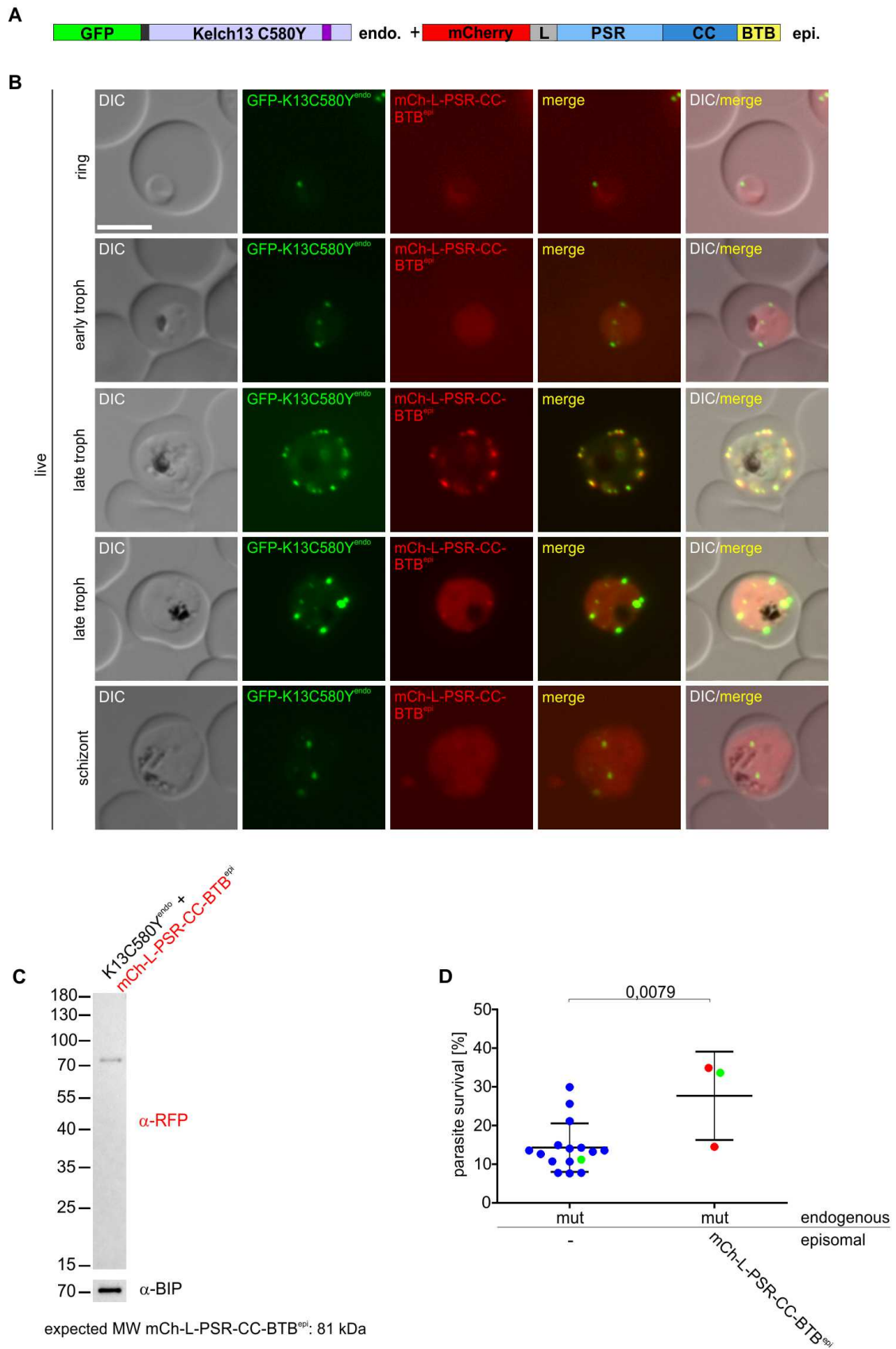


**Figure 38. Functional analysis of endogenous K13C580Y<sup>endo</sup> parasites episomally expressing mCherry-L-PSR-CC-BTB<sup>epi</sup>.** (A) Schematic illustration (not to scale) of the modifications of the used parasite line: endogenous (endo) K13C580Y<sup>endo</sup> (GFP-2xFKBP-Kelch13<sup>C580Y</sup>, Birnbaum et al., 2017) and episomally expressed mCherry-L-PSR-CC-BTB<sup>epi</sup> (PSR: *Plasmodium* specific region; CC: coiled coil region; mCh: mCherry red fluorescent protein; L: linker). (B) Fluorescence microscopy images of parasites expressing the constructs indicated in (A). Parasites were imaged using fluorescence microscopy in the indicated development stages on at least three independent occasions. Ring, early trophozoite (early troph), late trophozoite (late

troph) and schizont stage show living cells (live). Scale bar 5  $\mu\text{m}$ , DIC: differential interference contrast; GFP: green fluorescent protein; mCh: mCherry red fluorescent protein; merge: GFP and mCherry channels merged. **(C)** Immunoblot with protein extracts of the cell line expressing the constructs indicated in (A) probed with anti-RFP and anti-BIP antibodies. MW: molecular weight. **(D)** RSAs with the respective cell lines expressing the constructs indicated (three independent experiments, each data point represents one experiment). Equally colored data points represent data acquired in the same round of experiments. K13C580Y<sup>endo</sup>: mut (n = 16). Bars show SD, mean is indicated. Unpaired, two-tailed t test with Welch's correction. P values are indicated.

Next, the function of the PSR was further dissected by fusing only the second half of it with CC and BTB. For this, resistant GFP-2xFKBP-Kelch13<sup>C580Y</sup> (K13C580Y<sup>endo</sup>, Birnbaum et al., 2017) parasites were co-transfected with a plasmid overexpressing the last 107 amino acids (aa) of the PSR fused to the CC and BTB (mCherry-L-PSR107aa-CC-BTB<sup>epi</sup>: PSR107aa-CC-BTB<sup>epi</sup>) (Figure 39 A). Fluorescence microscopy was used to investigate the localization of PSR107aa-CC-BTB<sup>epi</sup> and using smeared and dried parasites again confirmed that small differences in the location of the two signals was due to movement of foci or parasites during live cell microscopy (Figure 39 B). This analysis showed that PSR107aa-CC-BTB<sup>epi</sup> is located in the cytosol of the parasites. To evaluate the integrity of the mCherry-L-PSR107aa-CC-BTB<sup>epi</sup> – fusion protein, Western Blot analysis (see 2.2.4.1) was conducted using an anti-RFP antibody. The construct was detected at approximately 85 kDa, above the expected molecular weight of 68 kDa. The same immunoblot was re-probed with an anti-BIP antibody as a loading control (Figure 39 C). The K13C580Y<sup>endo</sup> parasites overexpressing the mCherry-L-PSR107aa-CC-BTB<sup>epi</sup> construct were challenged in three independent ring stage survival assays (RSAs, Witkowski et al., 2013) (Figure 39 D, see 2.2.3.13). Episomal expression of PSR107aa-CC-BTB<sup>epi</sup> did not change the overall resistance level of the parasites (mean = 12.0 % SR, SD = 4.2 %, n = 3), while the K13C580Y<sup>endo</sup> knock in control parasites without an overexpressed Kelch13 construct were resistant to DHA (mean = 12.7 % SR, SD = 3.4 %, n = 16) (Figure 39 D). This indicates that PSR107aa-CC-BTB<sup>epi</sup> cannot fulfil the function of the intact Kelch13. In conclusion, the analysis of the episomally expressed PSR-CC-BTB<sup>epi</sup> and PSR107aa-CC-BTB<sup>epi</sup> constructs indicate, that the combination of these three domains without the KD is not sufficient to complement the resistant K13C580Y<sup>endo</sup> background and consequently to carry out the function of Kelch13.

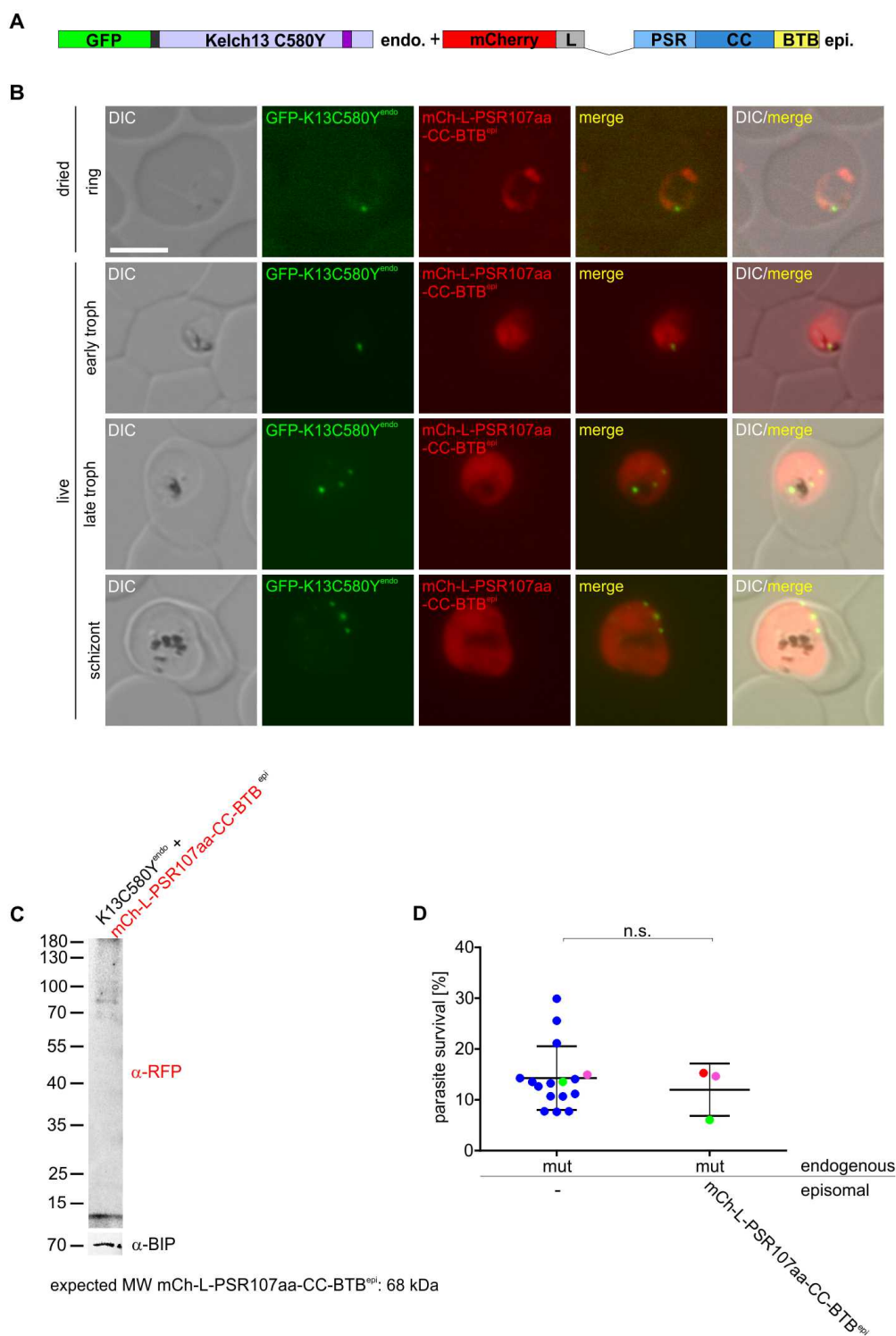


**Figure 39. Functional analysis of endogenous K13C580Y<sup>endo</sup> parasites episomally expressing mCherry-L-PSR107aa-CC-BTB<sup>epi</sup>.** (A) Schematic illustration (not to scale) of the modifications of the used parasite line: endogenous (endo) K13C580Y<sup>endo</sup> (GFP-2xFKBP-Kelch13<sup>C580Y</sup>, Birnbaum et al., 2017) and episomally expressed mCherry-L-PSR107aa-CC-BTB<sup>epi</sup> (PSR: *Plasmodium* specific region; CC: coiled coil region; BTB: BTB/POZ domain; aa: amino acids; mCh: mCherry red fluorescent protein; L: linker). (B) Fluorescence microscopy images of parasites expressing the constructs indicated in (A). Parasites were imaged using fluorescence microscopy in the indicated development stages on at least three independent occasions. Ring stages were imaged after smearing on a glass slide (dried). Early trophozoite (early troph), late trophozoite (late troph) and schizont stage show living cells (live). Scale bar 5  $\mu$ m, DIC: differential interference contrast; GFP: green fluorescent protein; mCh: mCherry red fluorescent protein; merge: GFP and mCherry channels merged. (C) Immunoblot with protein extracts of the cell line expressing the constructs indicated in (A) probed with anti-RFP and anti-BIP antibodies. MW: molecular weight. (D) RSAs with the respective cell lines expressing the constructs indicated (three independent experiments, each data point represents one experiment). Equally colored data points represent data acquired in the same round of experiments. K13C580Y<sup>endo</sup>: mut (n = 16). Bars show SD, mean is indicated. Unpaired, two-tailed t test with Welch's correction. P values are indicated.

To further investigate the function of the N-terminus of Kelch13, resistant GFP-2xFKBP-Kelch13<sup>C580Y</sup> (K13C580Y<sup>endo</sup>, Birnbaum et al., 2017) parasites were co-transfected with a plasmid overexpressing mCherry-L-PSR-CC<sup>epi</sup> (PSR-CC<sup>epi</sup>, Figure 40 A). Fluorescence microscopy was used to investigate the localization of PSR-CC<sup>epi</sup>. Using smeared and dried parasites again confirmed that small differences in the location of the two signals was due to movement of foci or parasites during live cell microscopy (Figure 40 B). The construct consisting of the PSR-CC<sup>epi</sup> was partially located in the cytosol of the parasites and partially in foci that co-localized with K13C580Y<sup>endo</sup>. This indicated that the PSR-CC<sup>epi</sup> is at least partially promotes the correct localization of the construct to the site Kelch13 is typically found. To evaluate the integrity of the mCherry-L-PSR-CC<sup>epi</sup> – fusion protein, Western Blot analysis (see 2.2.4.1) was conducted using an anti-RFP antibody. The construct was detected at a molecular weight of approximately 65 kDa, below the expected molecular weight of 70 kDa. The same immunoblot was re-probed with an anti-BIP antibody as a loading control (Figure 40 C). The K13C580Y<sup>endo</sup> parasites overexpressing PSR-CC<sup>epi</sup> were challenged in three independent ring stage survival assays (RSAs, Witkowski et al., 2013) (Figure 40 D, see 2.2.3.13). Interestingly, episomal expression of PSR-CC<sup>epi</sup> on the resistant background was partially sufficient to reduce the resistance level to DHA (mean = 3.6 % SR, SD = 2.1 %, n = 3). As expected, K13C580Y<sup>endo</sup> control parasites were resistant to DHA (mean = 12.7 % SR, SD = 3.4 %, n = 16). Hence, these results suggest that the N-terminus of Kelch13, consisting of the PSR and CC alone, is at least partial functional. It therefore appears that PSR-CC<sup>epi</sup> can partially maintain the function of Kelch13.

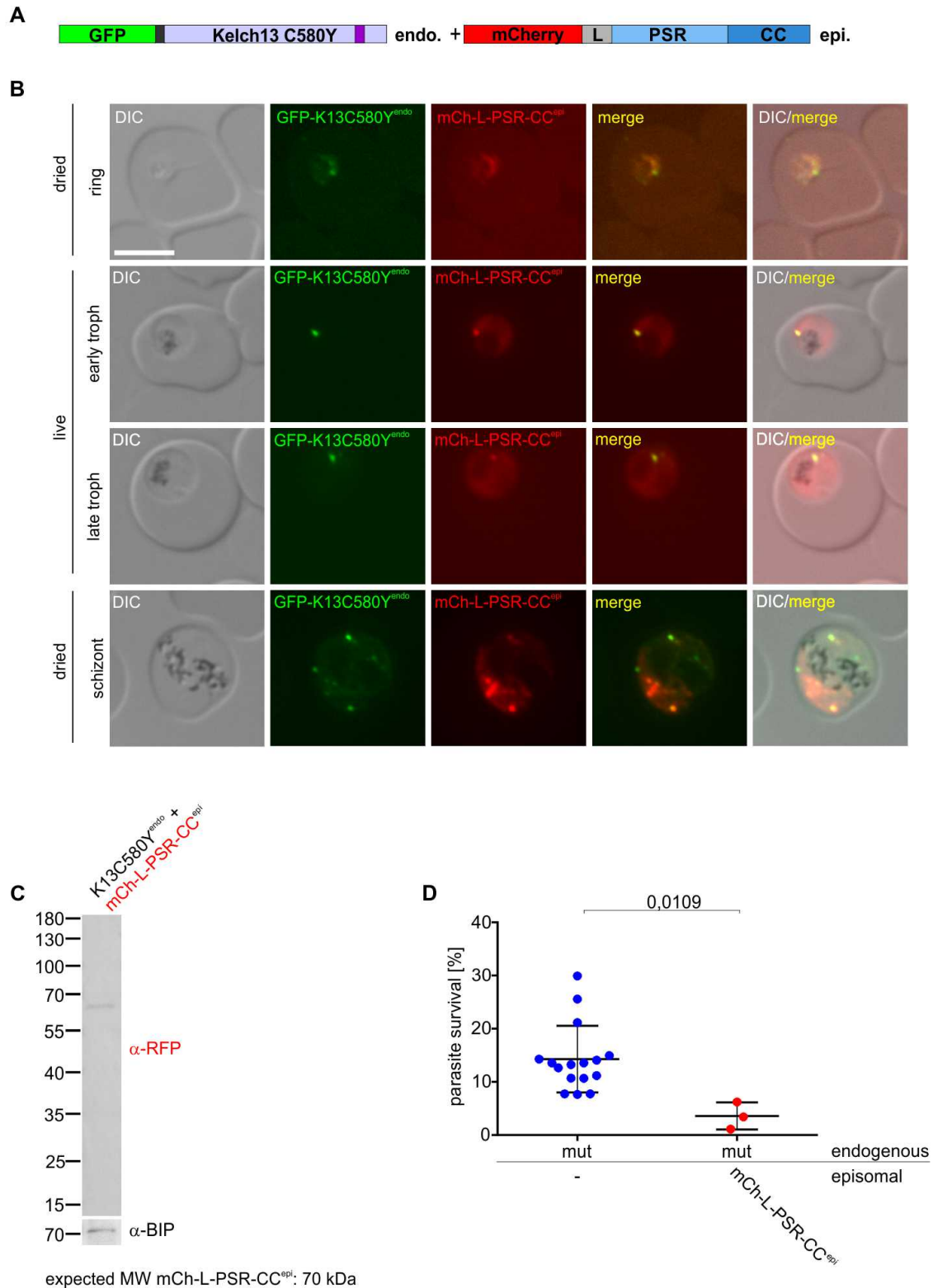


**Figure 40. Functional analysis of endogenous K13C580Y<sup>endo</sup> parasites episomally expressing mCherry-L-PSR-CC<sup>epi</sup>.** (A) Schematic illustration (not to scale) of the modifications of the used parasite line: endogenous (endo) K13C580Y<sup>endo</sup> (GFP-2xFKBP-Kelch13<sup>C580Y</sup>, Birnbaum et al., 2017) and episomally expressed mCherry-L-PSR-CC<sup>epi</sup> (PSR: *Plasmodium* specific region; CC: coiled coil region; mCh: mCherry red fluorescent protein; L: linker). (B) Fluorescence microscopy images of parasites expressing the constructs indicated in (A). Parasites were imaged using fluorescence microscopy in the indicated development stages on at least three independent occasions. Ring and schizont stages were imaged after smearing on a glass slide (dried); early trophozoite (early troph) and late trophozoite (late troph) stage show living cells (live). Scale bar 5  $\mu$ m, DIC: differential interference contrast; GFP: green fluorescent protein; mCh: mCherry red fluorescent protein; merge: GFP and mCherry channels merged. (C) Immunoblot with protein extracts of the cell line expressing the constructs indicated in (A) probed with anti-RFP and anti-BIP antibodies. MW: molecular weight. (D) RSAs with the respective cell lines expressing the constructs indicated (three independent experiments, each data point represents one experiment). K13C580Y<sup>endo</sup>: mut (n = 16). Bars show SD, mean is indicated. Unpaired, two-tailed t test with Welch's correction. P values are indicated.

Next, a construct mediating the expression of a Kelch13 version that lacked the BTB domain (mCherry-L-PSR-CC-L-KD<sup>epi</sup>: PSR-CC-L-KD<sup>epi</sup>) was transfected into resistant GFP-2xFKBP-Kelch13<sup>C580Y</sup> (K13C580Y<sup>endo</sup>, Birnbaum et al., 2017) parasites (Figure 41 A). K13C580Y<sup>endo</sup> parasites overexpressing PSR-CC-L-KD<sup>epi</sup> were smeared on a glass slide (see 2.2.5.1) and dried parasites were used to determine the localization of the indicated constructs in ring, trophozoite and schizont stages by fluorescence microscopy (Figure 41 B, dried). This showed, that PSR-CC-L-KD<sup>epi</sup> and K13C580Y<sup>endo</sup> co-localized, indicating that PSR-CC-L-KD<sup>epi</sup> can promote the localization of the protein to the Kelch13 compartment. To evaluate the integrity of the mCherry-L-PSR-CC-L-KD<sup>epi</sup> – fusion protein, Western Blot analysis (see 2.2.4.1) was conducted using an anti-RFP antibody. The construct was detected in three bands at a molecular weight between 100 and 120 kDa, above the expected molecular weight of 93 kDa. The same immunoblot was re-probed with an anti-BIP antibody as a loading control (Figure 41 C). The K13C580Y<sup>endo</sup> parasites overexpressing the mCherry-L-PSR-CC-L-KD<sup>epi</sup> construct were challenged in three independent ring stage survival assays (RSAs, Witkowski et al., 2013) (Figure 41 D, see 2.2.3.13). Interestingly, episomal expression of PSR-CC-L-KD<sup>epi</sup> on the resistant background partially reduced the resistance level to DHA (mean = 2.3 % SR, SD = 1.0 %, n = 3), while the K13C580Y<sup>endo</sup> knock in control parasites without an overexpressed Kelch13 construct were resistant to DHA (mean = 12.7 % SR, SD = 3.4 %, n = 16) (Figure 41 D). This demonstrates that PSR-CC-L-KD<sup>epi</sup> is at least partial sufficient to restore the function of Kelch13.

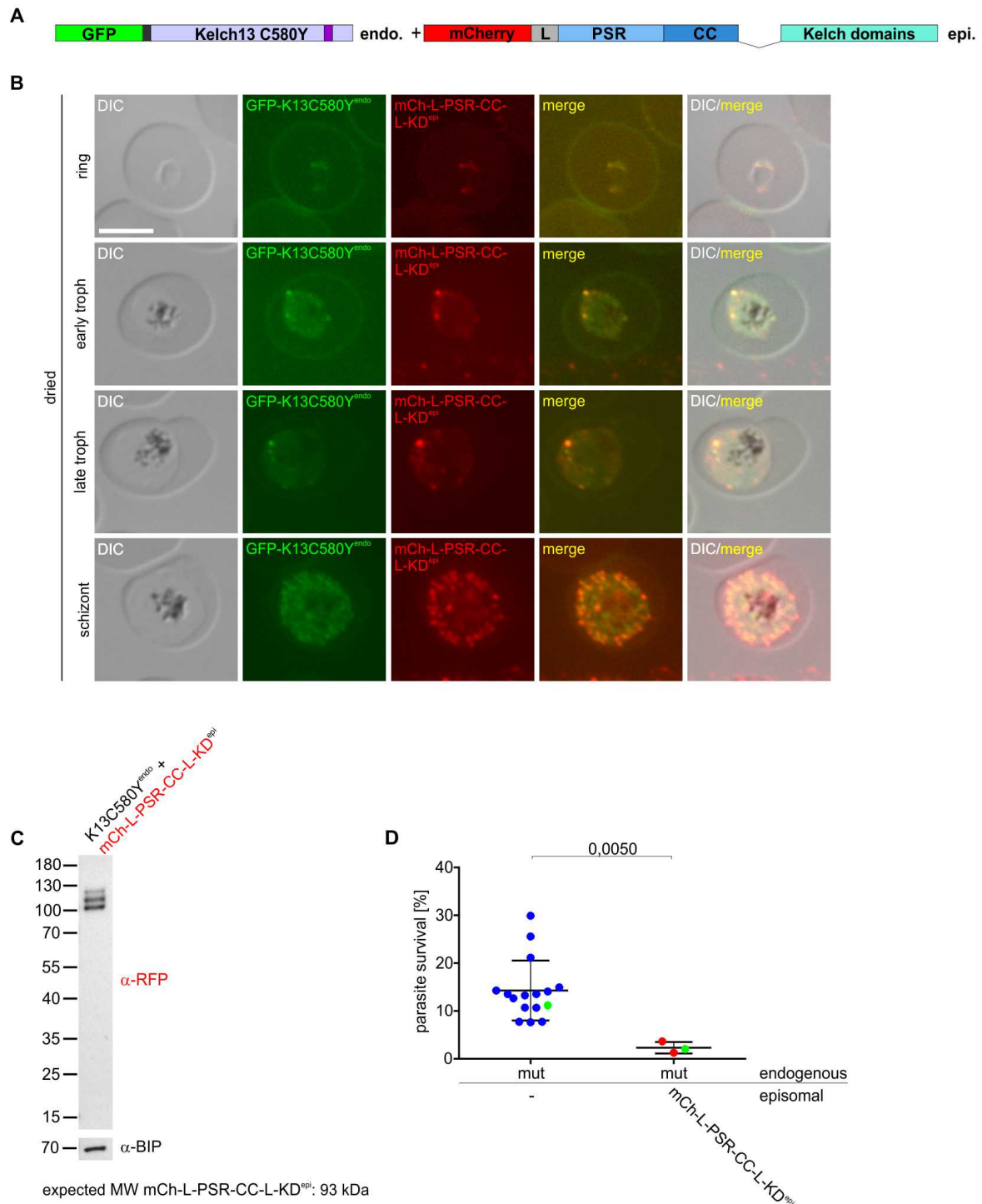


**Figure 41. Functional analysis of endogenous K13C580Y<sup>endo</sup> parasites episomally expressing mCherry-L-PSR-CC-L-KD<sup>epi</sup>.** (A) Schematic illustration (not to scale) of the modifications of the used parasite line: endogenous (endo) K13C580Y<sup>endo</sup> (GFP-2xFKBP-Kelch13<sup>C580Y</sup>, Birnbaum et al., 2017) and episomally expressed mCherry-L-PSR-CC-L-KD<sup>epi</sup> (PSR: *Plasmodium* specific region; CC: coiled coil region; Kelch domains: Kelch propeller domain consisting of six Kelch motif repeats; mCh: mCherry red fluorescent protein; L: linker). (B) Fluorescence microscopy images of parasites indicated in (A). Parasites were imaged using fluorescence microscopy on the indicated development stages on at least three independent occasions. Ring, early trophozoites (early troph), late trophozoites (late troph) and schizont stages were imaged after smearing on a glass slide (dried). Scale bar 5  $\mu$ m, DIC: differential interference contrast; GFP: green fluorescent protein; mCh: mCherry red fluorescent protein; merge: GFP and mCherry channels merged. (C) Immunoblot with protein extracts of the cell line expressing the constructs indicated in (A) probed with anti-RFP and anti-BIP antibodies. MW: molecular weight. (D) RSAs with the respective cell lines expressing the constructs indicated (three independent experiments, each data point represents one experiment). Equally colored data points represent data required in the same round of experiments. K13C580Y<sup>endo</sup>: mut (n = 16). Bars show SD, mean is indicated. Unpaired, two-tailed t test with Welch's correction. P values are indicated.

Next it was investigated whether after N-terminal integration of the SLI plasmid that was used for homologous recombination in the genomic locus of Kelch13 to obtain K13C580Y<sup>endo</sup> parasites (Birnbauer et al., 2017) the homology region is sufficient to fulfill the function of Kelch13 in combination with the disrupted protein. This was tested as the construct mCherry-L-PSR-CC<sup>epi</sup> (see Figure 40) appeared to be functional and reverted resistance of the K13C580Y<sup>epi</sup> background, but this contradicted the fact that the K13C580Y<sup>epi</sup> integrant alone was resistant. To test for the possibility that after N-terminal integration, the disrupted Kelch13 fused to a 2xmyc tag as well as loxP and a skip peptide (T2A) would be functional it was here tested by expressing it episomally in the resistant K13C580Y<sup>endo</sup> parasites. The corresponding construct, mCherry-L-PSR-CC-2aaBTB-2xmyc-loxP-T2A<sup>epi</sup>, was identical to the N-terminal truncated fragment except for the fact that it was N-terminally tagged with mCherry (Figure 42 A). To assess the localization of mCherry-L-PSR-CC-2aaBTB-2xmyc-loxP-T2A<sup>epi</sup>, the cells were smeared and dried on a glass slide (see 2.2.5.1) and fluorescence microscopy was performed in ring, trophozoite and schizont stages (Figure 42 B). The construct consisting of mCherry-L-PSR-CC-2aaBTB-2xmyc-loxP-T2A<sup>epi</sup> was located in the cytosol with a small proportion co-localizing with endogenous K13C580Y<sup>endo</sup> in the foci typical for Kelch13 compartment proteins. To evaluate the integrity of the mCherry-L-PSR-CC-2aaBTB-2xmyc-loxP-T2A<sup>epi</sup> – fusion protein, Western Blot analysis (see 2.2.4.1) was conducted using an anti-RFP antibody. The construct was detected at approximately 68 kDa, below the expected molecular weight of 76 kDa. The same immunoblot was re-probed with an anti-BIP antibody as a loading control (Figure 42 C). The K13C580Y<sup>endo</sup> parasites overexpressing the mCherry-L-PSR-CC-2aaBTB-2xmyc-loxP-T2A<sup>epi</sup> construct were challenged in three independent ring stage survival assays (RSAs, Witkowski et al., 2013) (Figure 42 D, see 2.2.3.13). Episomal expression of mCherry-L-PSR-CC-2aaBTB-2xmyc-loxP-T2A<sup>epi</sup> did not change the overall resistance level of the parasites (mean = 14.7 % SR, SD = 3.4 %, n = 3), while the K13C580Y<sup>endo</sup> knock in control parasites without an overexpressed Kelch13 construct were resistant to DHA (mean = 12.7 % SR, SD = 3.4 %, n = 16) (Figure 42 D). This indicated that mCherry-L-PSR-CC-2aaBTB-2xmyc-loxP-T2A<sup>epi</sup> is not sufficient to maintain the function of Kelch13. Consequently, it is unlikely that the disrupted Kelch13 is functional after the integration of pSLI\_GFP-2xFKBP-Kelch13<sup>C580Y</sup> in the genomic locus. Nevertheless, these data show that a small proportion of the mCherry-L-PSR-CC-2aaBTB-2xmyc-loxP-T2A<sup>epi</sup> molecules were found at the Kelch13 compartment, indicating that this construct partially maintains the correct localization.

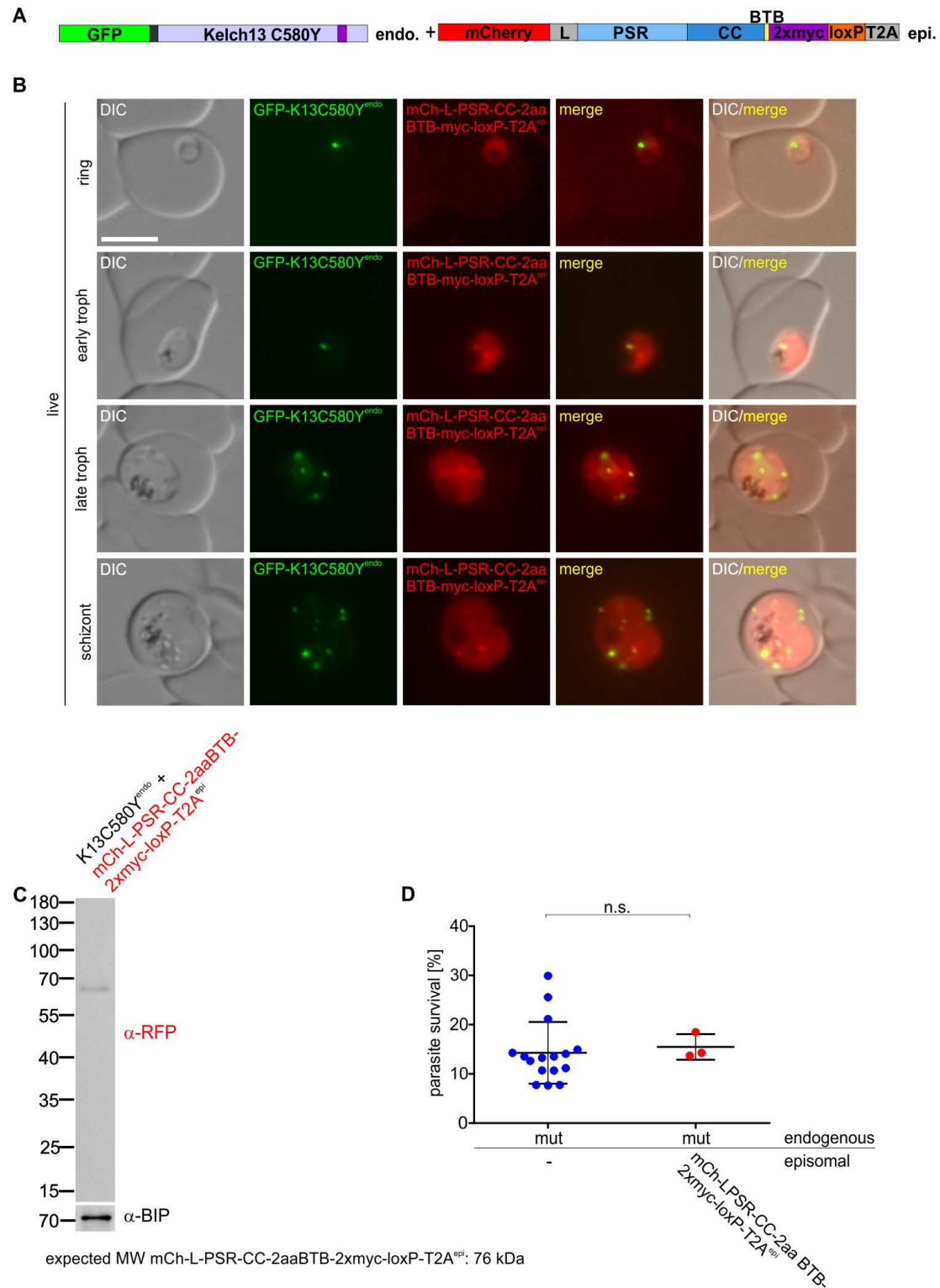


**Figure 42. Functional analysis of endogenous K13C580Y<sup>endo</sup> parasites episomally expressing mCh-L-PSR-CC-2aaBTB-2xmyc-loxP-T2A<sup>epi</sup>.** (A) Schematic illustration (not to scale) of the modifications of the used parasite line: endogenous (endo) K13C580Y<sup>endo</sup> (GFP-2xFKBP-Kelch13<sup>C580Y</sup>, Birnbaum et al., 2017) and episomally expressed mCh-L-PSR-CC-2aaBTB-2xmyc-loxP-T2A<sup>epi</sup> (PSR: *Plasmodium* specific region; CC: coiled coil region; BTB: BTB/POZ domain; aa: amino acids; mCh: mCherry red fluorescent protein; L: linker; T2A: skip peptide). (B) Fluorescence microscopy images of parasites expressing the constructs indicated in (A). Living parasites were imaged using fluorescence microscopy (live) in ring, early trophozoite (early troph), late trophozoite (late troph) and schizont stages on at least three independent occasions. Scale bar 5  $\mu$ m, DIC: differential interference contrast; GFP: green fluorescent protein; mCh: mCherry red fluorescent protein; merge: GFP and mCherry channels merged. (C) Immunoblot with protein extracts of the cell line expressing the constructs indicated in (A) probed with anti-RFP and anti-BIP antibodies. MW: molecular weight. (D) RSAs with the respective cell lines expressing the constructs indicated (three independent experiments, each data point represents one experiment). Equally colored data points represent data acquired in the same round of experiments. K13C580Y<sup>endo</sup>: mut (n = 16). Bars show SD, mean is indicated. Unpaired, two-tailed t test with Welch's correction. P values are indicated.

In conclusion these data show that increased expression of Kelch13 in resistant parasites can lead to the reduction or loss of resistance (as evident from expression of K13WT<sup>epi</sup>, K13C580Y<sup>epi</sup>, K13R539T<sup>epi</sup> and K13E252Q<sup>epi</sup> on the resistant background). Furthermore, the results indicate that the mechanistic function of Kelch13 is dependent on Kelch13 domain combinations (a side-by-side comparison of the RSA results of all complementation cell lines are shown in Figure 43). Interestingly, episomally expressed constructs containing the CC with only either C- or N-terminal fusion to another Kelch13 domain can at least partially maintain the function of Kelch13 (CC-BTB-KD<sup>epi</sup>, CC-BTB<sup>epi</sup>, PSR-CC<sup>epi</sup> and PSR-CC-L-KD<sup>epi</sup>). The other tested constructs (BTB-KD<sup>epi</sup>, L-BTB-KD<sup>epi</sup>, BTB<sup>epi</sup>, PSR107aa-CC-BTB<sup>epi</sup>, PSR-CC-BTB<sup>epi</sup>, PSR-CC-2aaBTB-2xmyc-loxP-T2A<sup>epi</sup>) seem not to be sufficient to render resistant parasites sensitive to DHA (Figure 43).

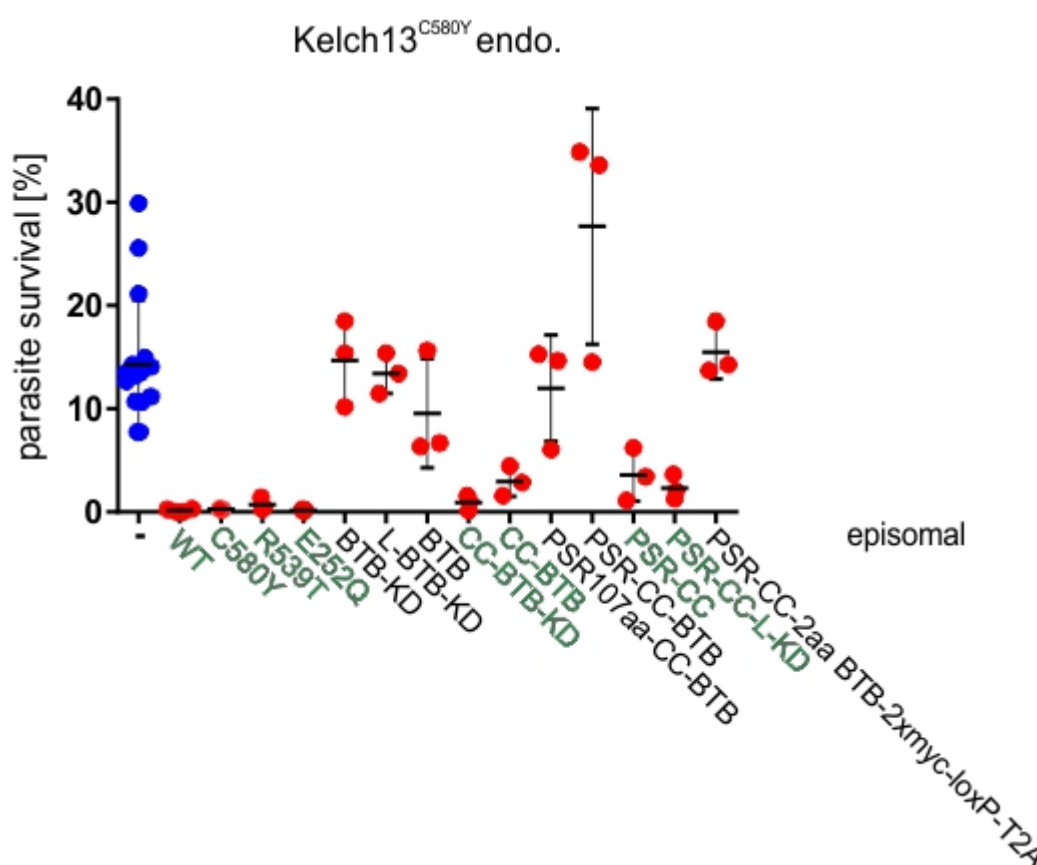


**Figure 43. Side-by-side comparison of RSA results of endogenous K13C580Y<sup>endo</sup> parasites episomally expressing different K13 domain constructs.** The RSA data from Figures 28-31 and 33-42 were plotted in the same graph. Endogenous (endo) K13C580Y<sup>endo</sup> (GFP-2xFKBP-Kelch13<sup>C580Y</sup>, Birnbaum et al., 2017) episomally expressing the indicated constructs. Control parasites (parent endogenous K13C580Y<sup>endo</sup> without an episomal plasmid, indicated by the dash) were tested in n = 16 RSAs. Green marked constructs rendered the resistant parasites fully or partially sensitive to DHA. PSR: *Plasmodium* specific region; CC: coiled coil region; BTB: BTB/POZ domain; Kelch domains: Kelch propeller domain consisting of six Kelch motif repeats; L: linker. WT: Kelch13WT<sup>epi</sup>. Each data point represents one experiment. Bars show SD, mean is indicated.

### 3.3.3 Influence of individual domains of Kelch13 for its abundance in the cell

As previous data showed that endocytosis and resistance is regulated by Kelch13 abundance (see 3.3.1, Birnbaum and Scharf et al., 2020), it was hypothesized that this might be due to a change in protein

stability that is regulated by individual domains of Kelch13. To investigate the impact of different Kelch13 domains on the abundance of the Kelch13 construct they are part of different K13 domain combinations were episomally expressed in resistant K13C580Y<sup>endo</sup> parasites (GFP-2xFKBP-Kelch13<sup>C580Y</sup>, Birnbaum et al., 2017) and the abundance of the episomal constructs was measured and quantified using immunoblot analysis. To determine the influence of K13 lacking the BTB and the Kelch domain region (i.e., a construct consisting only of the PSR and CC), K13C580Y<sup>endo</sup> parasites were co-transfected with mCherry-L-PSR-CC<sup>epi</sup> (PSR-CC<sup>epi</sup>). As a control, K13C580Y<sup>endo</sup> parasites were co-transfected with mCherry-L-K13WT<sup>epi</sup> (hereafter referred to as K13WT<sup>epi</sup>). Protein extracts from K13WT<sup>epi</sup> and PSR-CC<sup>epi</sup> parasites were analyzed with an anti-RFP antibody using Western Blot analysis (see 2.2.4.1). The same immunoblot was re-probed with an anti-BIP antibody as a loading control. The intensity of the appropriate protein bands was determined using the Image Lab software (v 5.2.1, Bio Rad). The mean RFP intensity signal (corresponding to K13WT<sup>epi</sup> and PSR-CC<sup>epi</sup>, respectively) was normalized to the corresponding mean BIP signal intensity and the intensity ratios were calculated (Figure 44 B). The intensity ratios for PSR-CC<sup>epi</sup> were divided by the ratios of K13WT<sup>epi</sup> to obtain the abundance of PSR-CC<sup>epi</sup> relative to K13WT<sup>epi</sup>. This analysis indicated that the levels of PSR-CC<sup>epi</sup> were 6.7 % (SD = 2.3 %, n = 2) of K13WT<sup>epi</sup>. The same experiment was carried out for mCherry-L-CC-BTB<sup>epi</sup> (CC-BTB<sup>epi</sup>) which showed 5.3 % (n = 1) of the abundance of K13WT<sup>epi</sup> and for mCherry-L-PSR-CC-BTB<sup>epi</sup> (PSR-CC-BTB<sup>epi</sup>) which showed 6.9 % (SD = 1.8 %, n = 3) of the abundance of K13WT<sup>epi</sup> (Figure 44 B). In contrast to these constructs that all lacked the Kelch propeller domain, mCherry-L-PSR-CC-L-KD<sup>epi</sup> (PSR-CC-L-KD<sup>epi</sup>) showed a more than 5-fold higher mean abundance (mean = 624.2 %, SD = 329.4 %, n = 2) compared to K13WT<sup>epi</sup>. PSR-CC-BTB<sup>epi</sup> showed 33.4 % (SD = 12.7 %, n = 2) of the abundance of K13WT<sup>epi</sup> (Figure 44 B). It therefore appears, that the constructs lacking the Kelch propeller domain (KD) (PSR-CC<sup>epi</sup>, CC-BTB<sup>epi</sup> and PSR-CC-BTB<sup>epi</sup>) show a strongly reduced abundance in the cell compared to constructs containing the KD or K13WT<sup>epi</sup>. This indicated that K13 protein levels are influenced by the presence or absence of the KD.

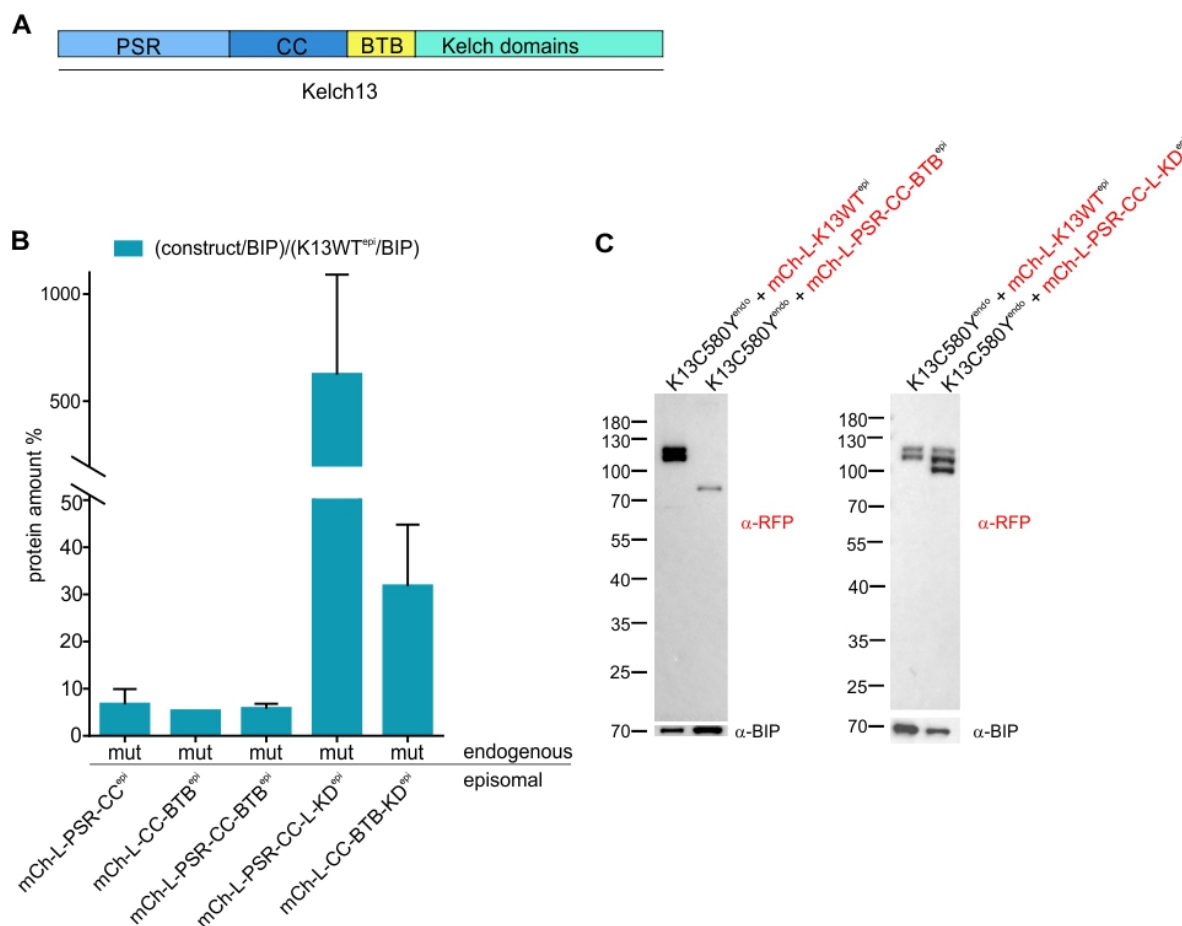


**Figure 44. Western Blot based quantification of the abundance of different Kelch13 domain constructs. (A)** Schematic illustration (not to scale) of Kelch13 (PSR: *Plasmodium* specific region; CC: coiled coil region; BTB: BTB/POZ domain; Kelch domains: Kelch propeller domain consisting of six Kelch motif repeats). **(B)** Graph showing protein abundance of the indicated constructs episomally expressed in GFP-2xFKBP-Kelch13<sup>C580Y</sup> knock in parasites (Birnbaum et al., 2017). Protein abundance was measured using quantitative immunoblot analysis: The protein extracts for quantification were run on the same SDS gel. Bars show SD for n = 2 or n = 3, mean is indicated. **(C)** Representative Western Blots of the indicated episomal constructs and BIP (all immunoblots that were used for quantification are shown in Appendix 4). mCh: mCherry. mut: K13C580Y<sup>endo</sup>.

As these data indicated that the C-terminal Kelch domain region of Kelch13 regulate the stability of the N-terminal Kelch13 part, the Kelch domain region of Kelch13 was replaced with an mDHFR domain to enable the regulation of Kelch13 abundance by taking advantage of the property of this domain to result in a strongly folded structure if a ligand such as WR99210 (WR) is present (Eilers and Schatz, 1986; Gehde et al., 2009; Grüning et al., 2012; Mésen-Ramírez et al., 2016). In its folded form (i.e., in presence of WR), the mDHFR domain can be assumed to be more stable (Eilers and Schatz, 1986; Gehde et al., 2009), permitting the regulation of protein abundance depending on the presence of WR. To detect, whether the fusion of PSR-CC-BTB with mDHFR could already influence the levels of Kelch13 in the absence of the ligand WR, fluorescence microscopy was performed with K13C580Y<sup>endo</sup> knock in parasites (Birnbaum et al., 2017) episomally expressing either mCherry tagged PSR-CC-BTB (mCherry-L-PSR-CC-BTB<sup>epi</sup>) or mCherry tagged PSR-CC-BTB-mDHFR (mCherry-L-PSR-CC-BTB-mDHFR<sup>epi</sup>) (Figure 45 A). Images of the two parasite cell lines were taken in living cells and fluorescence intensities of the mCherry signal of the Kelch13 foci were measured in ring stages (Figure 45 B). The images were taken with identical settings (see 2.2.5.1) in three independent experiments. The mean fluorescence intensity per focus of PSR-CC-BTB-mDHFR<sup>epi</sup> (mean = 1702.3, SD = 220.4) was

significantly higher compared to parasites expressing PSR-CC-BTB<sup>epi</sup> (mean = 968.4, SD = 328.0). This indicated that C-terminal tagging of PSR-CC-BTB with mDHFR already stabilizes the Kelch13 - fusion protein and this might be due to taking over the stabilizing function of the Kelch domain region.

To further investigate these findings, quantitative Western Blot analysis was performed with parasites expressing PSR-CC-BTB<sup>epi</sup> and PSR-CC-BTB-mDHFR<sup>epi</sup> (Figure 45 B). For this, the parasite cell line expressing PSR-CC-BTB-mDHFR<sup>epi</sup> was split into two culture dishes of which one served as control (-WR) and to the other WR99210 was added (4 nM) for 24 hours (+WR) to stabilize the mDHFR fusion part. As a control, K13C580Y<sup>endo</sup> parasites episomally expressing K13WT<sup>epi</sup> were used. Protein extracts from K13WT<sup>epi</sup>, PSR-CC-BTB<sup>epi</sup>, PSR-CC-BTB-mDHFR<sup>epi</sup> -WR and PSR-CC-BTB-mDHFR<sup>epi</sup> +WR parasites were analyzed with an anti-RFP antibody using Western Blot analysis (see 2.2.4.1). The same immunoblot was re-probed with an anti-BIP antibody as a loading control. The intensity of the appropriate protein bands was determined using the Image Lab software (v 5.2.1, Bio Rad). The mean RFP intensity of the Kelch13WT<sup>epi</sup>, PSR-CC-BTB<sup>epi</sup>, PSR-CC-BTB-mDHFR<sup>epi</sup> -WR and PSR-CC-BTB-mDHFR<sup>epi</sup> +WR signal was normalized to the corresponding mean BIP signal to calculate the intensity ratios (Figure 45 B). The intensity ratios relative to BIP for PSR-CC-BTB<sup>epi</sup>, PSR-CC-BTB-mDHFR<sup>epi</sup> -WR and PSR-CC-BTB-mDHFR<sup>epi</sup> +WR were divided by the ratios of K13WT<sup>epi</sup> to BIP. PSR-CC-BTB<sup>epi</sup> showed 6.9 % (SD = 1.8 %, n = 3) of K13WT<sup>epi</sup>, PSR-CC-BTB-mDHFR<sup>epi</sup> -WR 253.1 % (SD = 105.8 %, n = 3) and PSR-CC-BTB-mDHFR<sup>epi</sup> +WR 255.8 % (SD = 72.6 %, n = 3) of the abundance of K13WT<sup>epi</sup>. Consistent with the finding reported in 3.3.1, K13WT<sup>epi</sup> was detected as two bands between 110 and 130 kDa (expected molecular weight of the fusion protein: 101 kDa). The mCherry-L-PSR-CC-BTB - fusion protein migrated at a height congruent with the expected molecular weight of 81 kDa, the mCherry-L-PSR-CC-BTB-mDHFR - fusion protein with and without WR at the approximately 110 kDa, above the expected molecular weight of 96 kDa (Figure 45 D). While these data confirm the finding observed with fluorescence microscopy that the mDHFR domain fused to PSR-CC-BTB led to an increase of Kelch13 protein levels, this was independent of the presence or absence of WR and the difference was much more profound than measured in the imaging based assay. This suggests, that the mDHFR domain alone already provides stability to PSR-CC-BTB<sup>epi</sup> which results in a higher K13 protein level and that mCherry-L-PSR-CC-BTB-mDHFR<sup>epi</sup> is much more stable in protein extracts compared to mCherry-L-PSR-CC-BTB<sup>epi</sup>.

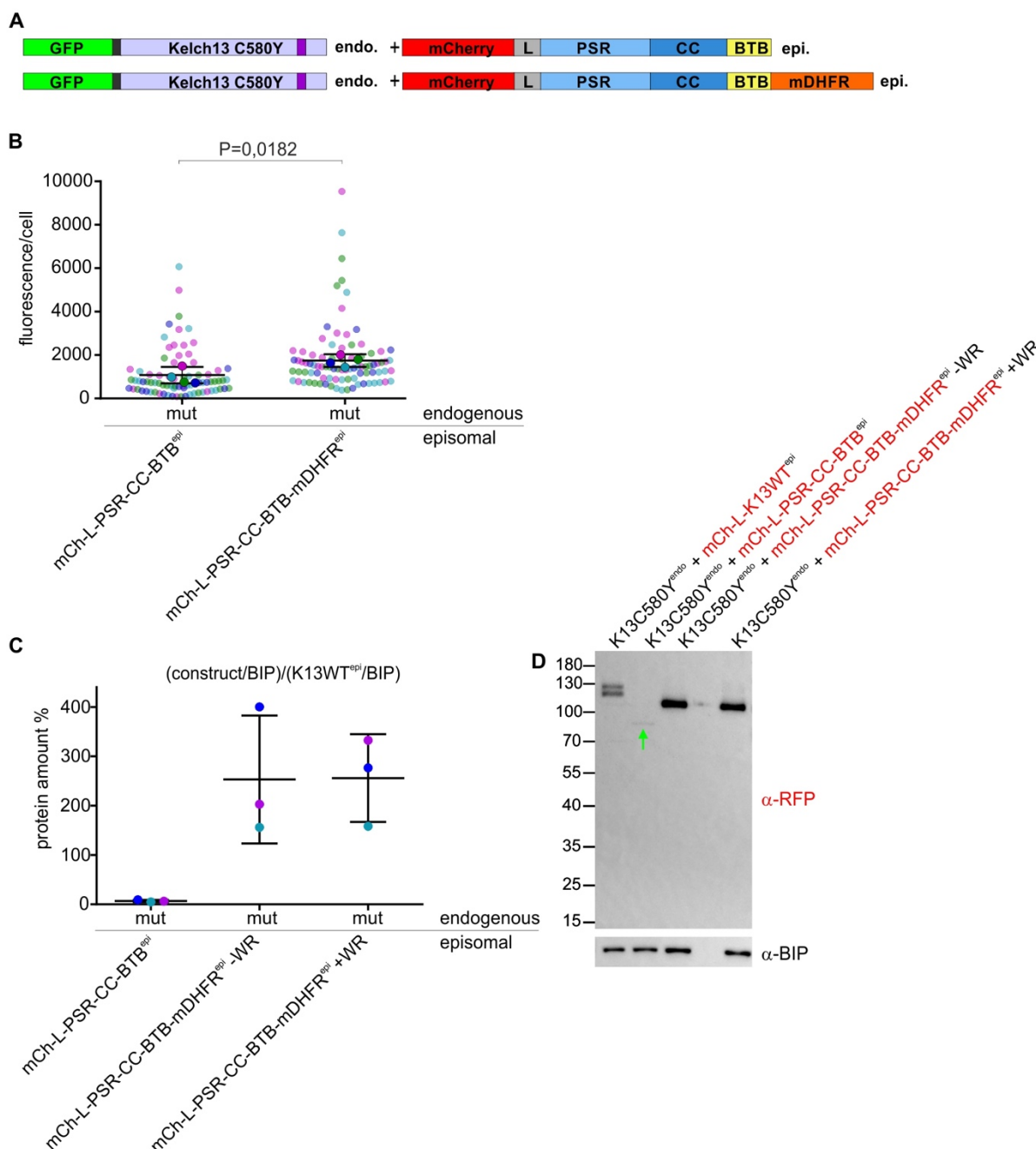


**Figure 45. Effect of mDHFR domain on relative cellular abundance of episomal Kelch13 constructs lacking the Kelch domain.** **(A)** Schematic illustration (not to scale) of the modifications of the used parasite line: endogenous (endo) K13C580Y<sup>endo</sup> (GFP-2xFKBP-Kelch13<sup>C580Y</sup>, Birnbaum et al., 2017) with episomally (epi) expressed mCherry-L-PSR-CC-BTB<sup>epi</sup> or mCherry-L-PSR-CC-BTB-mDHFR<sup>epi</sup> (PSR: *Plasmodium* specific region; BTB: BTB/POZ domain; mCh: mCherry red fluorescent protein; L: linker). **(B)** Superplot (Lord et al., 2020) showing fluorescence intensity quantification of parasites expressing the constructs indicated in (A). Parasites were imaged under the same conditions in ring stages in four different experiments. Each point shows fluorescence intensity of a focus. Points of the same color derive from foci imaged in the same experiment and the larger and darker point represents the mean of these measurements. The wider central bar shows the mean derived from the mean of the 3 experiments, bars represent SD. Total number of quantified foci: mCherry-L-PSR-CC-BTB-mDHFR<sup>epi</sup>: n = 88; mCherry-L-PSR-CC-BTB<sup>epi</sup>: n = 80 **(C)** Protein amount of the indicated episomally expressed constructs. The ratio of the RFP to the BIP signal was calculated (construct/BIP) and divided by K13WT<sup>epi</sup>/BIP. The protein extracts of K13 wild type and mutant parasites were run on the same SDS gel. n=3. Bars show SD, mean is indicated. Points of the same color derive from the same experiment. **(D)** Representative example of the immunoblot analysis with the samples indicated in (C) (all blots used for quantification are shown in Appendix 5). The marker was cut out and overlaid onto the blot. The arrow shows the faint band of mCherry-L-PSR-CC-BTB<sup>epi</sup>. mut: K13C580Y<sup>endo</sup>.

### 3.4 Functional analysis of a new K13C580Y<sup>endo</sup> integration cell line with a shortend homology region

In this study, an established parasite cell line with endogenously tagged K13C580Y<sup>endo</sup> (GFP-2xFKBP-Kelch13<sup>C580Y</sup>, Birnbaum et al., 2017) was used for many experiments. K13C580Y was N-terminally tagged via the SLI system. The length of the Kelch13 homology region (HR) that was used for homologous recombination into the genomic locus of Kelch13, was chosen so that the restored gene fragment downstream of the integration site would not contain a large part of the region encoding the N-terminus of Kelch13 (Birnbaum et al., 2017). Based on all the SLI lines established since, this precaution is not necessary, as so far there was no evidence of expression of this promoterless downstream gene-fragment and the current strategy is to place homology regions further upstream but block them with a stop codon in the reading frame.

In the previously established K13C580Y<sup>endo</sup> cell line, integration of the plasmid in the genomic locus of Kelch13 results in two expressed protein products: truncated Kelch13 fused with myc-loxP-T2A and the codon changed functional copy of Kelch13 N-terminally tagged with GFP-L-2xFKBP-L (Figure 46 A). The length of the disrupted copy of Kelch13 is defined by the length of the homology region of Kelch13 (base pair: bp 515 – 1058) with addition of the N-terminal region of Kelch13 that is located in front of the chosen HR (base pair: bp 1 – 515). As the data shown in 3.3.1 indicate that the N-terminal part of Kelch13 (PSR-CC) alone might already be sufficient to maintain the function of Kelch13, it was investigated, whether the truncated Kelch13 - fusion protein might be functional in K13C580Y<sup>endo</sup> knock in parasites. While these experiments (see 3.3.1) indicated that this concern was unfounded, the new cell line with a shorter truncated fragment was already being generated and would also enable to confirm that there is no influence of the disrupted Kelch13 on the phenotypes associated with K13C580Y<sup>endo</sup>. Consequently, this second K13C580Y<sup>endo</sup> knock in cell line was generated using SLI with a shorter and more N-terminal homology region was generated (GFP-L-2xFKBP-L-Kelch13<sup>C580Y</sup>\_HR260; in the following named as K13C580Y\_HR260<sup>endo</sup>, Figure 46 B). The new homology region for homologous recombination into the genomic locus of Kelch13 consisted of the sequence encoding 260 base pairs of the PSR (bp 53 – 313).

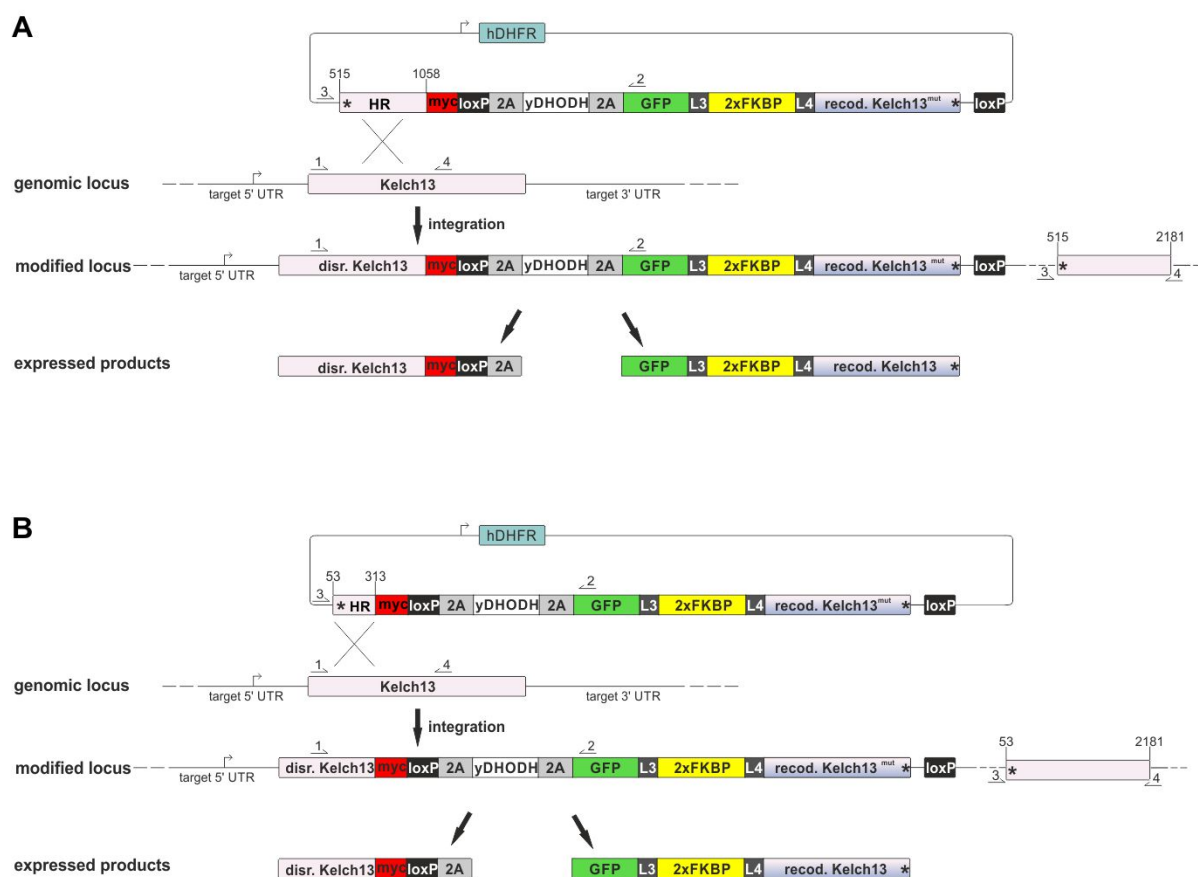


**Figure 46. Integration strategy for N-terminal tagging of K13C580Y<sup>endo</sup>.** (A), (B) Schematic illustration (not to scale) shows the episomal plasmids for integration which integrate via single crossover homologous recombination (black crossed lines) of a homologous region (HR) into the genome (SLI, Birnbaum et al., 2017). (A) HR: encoding bp 515 – 1058 and (B) HR: encoding base pair (bp) 53 – 313. The target gene is disrupted (disr. Kelch13) and a codon optimized N-terminally tagged Kelch13 copy (recod. Kelch13) is provided. The transgenic parasites can then be selected via the yDHODH resistance marker. L3 and L4: linkers (Varnai et al., 2006); 2A: T2A skip peptide; Asterisk: stop codon; yDHODH: yeast dihydroorotate dehydrogenase gene; arrows: promoters; human dehydrofolate reductase (hDHFR): episomal resistance marker; GFP: green fluorescence protein. Figure modified from Birnbaum et al., 2017.

The correct integration of pSLI\_GFP-L-2xFKBP-L-Kelch13<sup>C580Y</sup>\_HR260 into the genomic locus of Kelch13 was confirmed by PCR (Figure 47 A). To evaluate the integrity of the GFP-L-2xFKBP-L-Kelch13<sup>C580Y</sup>\_HR260 – fusion protein, Western Blot analysis (see 2.2.4.1) was conducted using an anti-RFP antibody. The construct was detected at a molecular weight corresponding well with the predicted molecular weight of 138 kDa. The same immunoblot was re-probed with an anti-BIP antibody as a loading control (Figure 47 B). Analysis by fluorescence microscopy showed that K13C580Y\_HR260<sup>endo</sup> localized in foci in a pattern typical for Kelch13 compartment proteins (Figure 47 C). The K13C580Y\_HR260<sup>endo</sup> parasites were challenged in three independent ring stage survival assays (RSAs, Witkowski et al., 2013) (Figure 47 D, see 2.2.3.13). Interestingly, K13C580Y\_HR260<sup>endo</sup> parasites were sensitive to DHA (mean = 0.6 % SR, SD = 0.2 %, n = 4) while K13C580Y<sup>endo</sup> knock in control parasites were resistant to DHA (mean = 12.7 % SR, SD = 3.4 %, n = 16).

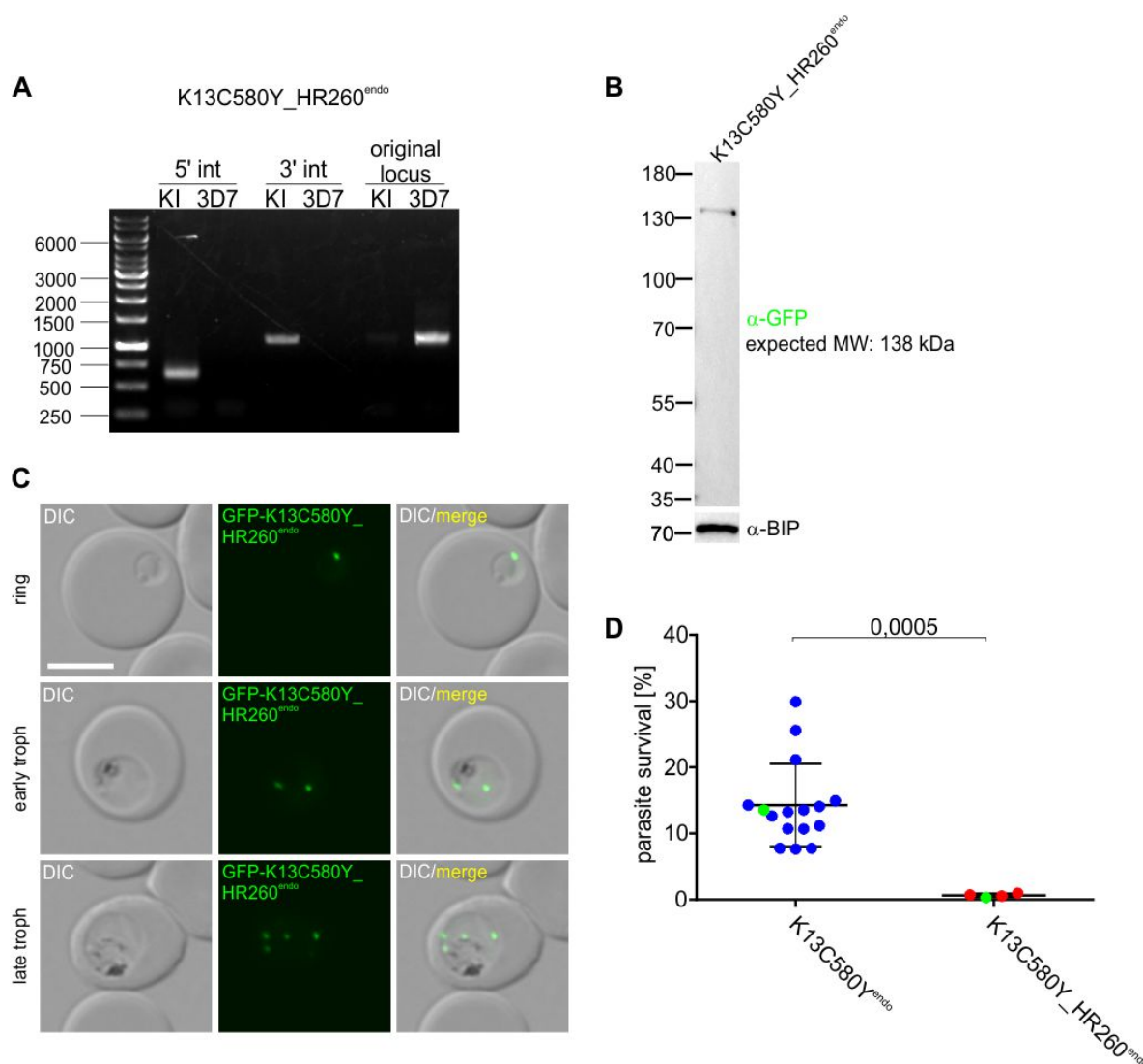


**Figure 47. Functional analysis of endogenously tagged K13C580Y\_HR260<sup>endo</sup> parasites.** (A) Agarose gel showing PCR products of diagnostic PCR to confirm the correct integration of the GFP-L-2xFKBP-L-K13<sup>C580Y</sup>\_HR260<sup>endo</sup> plasmid into the *kelch13* locus. PCR was performed using the genomic DNA (gDNA) of the transgenic parasites or the parent (3D7) as a template and PCR products were applied on an agarose gel. The primers that were used are indicated in figure 46. 5': primer combination 1+2, 3': primer combination 3+4. Original locus: primer combination 1+4 was used to show that original *Kelch13* locus was only found in 3D7 wild type gDNA and not in the knock in parasites (KI). The sizes of the marker bands are indicated. (B) Immunoblot with protein extracts of the cell line expressing the constructs indicated in (A) probed with anti-GFP antibody. MW: molecular weight. (C) Fluorescence microscopy images of parasites indicated in (A). Parasites were imaged using fluorescence microscopy in the indicated development stages on at least three independent occasions. Scale bar 5  $\mu$ m, DIC: differential interference contrast; GFP: green fluorescent protein; merge: GFP and DIC channels merged. (D) RSAs with the respective cell lines expressing the constructs indicated (four independent experiments, each data point represents one experiment). Equally colored data points represent data acquired in the same round of experiments. K13C580Y<sup>endo</sup>: control (n = 16). Bars show SD, mean is indicated. Unpaired, two-tailed t test with Welch's correction. P values are indicated.

Next, it was investigated whether the sensitivity to ART could be explained by a localization of *Kelch13C580Y* in the K13C580Y\_HR260<sup>endo</sup> parasites that is different to that in K13C580Y<sup>endo</sup> parasites. To test this, K13C580Y\_HR260<sup>endo</sup> parasites were co-transfected with a plasmid mediating the episomal expression of mCherry-L-K13WT<sup>epi</sup> (K13WT<sup>epi</sup>). Analysis by fluorescence microscopy confirmed that K13C580Y\_HR260<sup>endo</sup> and K13WT<sup>epi</sup> co-localized in foci in ring, trophozoite and schizont stages (Figure 48 A). Next, K13C580Y\_HR260<sup>endo</sup> knock in parasites were fixed with acetone and immunofluorescence assays (IFA, see 2.2.3.14) were performed using anti-GFP antibodies and previously investigated monoclonal antibodies raised against *Kelch13* (kindly provided by David

Fidock, Figure 48 B). This confirmed the correct localization of K13C580Y\_HR260<sup>endo</sup>, leading to the suggestion that the DHA sensitivity of K13C580Y\_HR260<sup>endo</sup> knock in parasites is not influenced by a different localization in the cell.

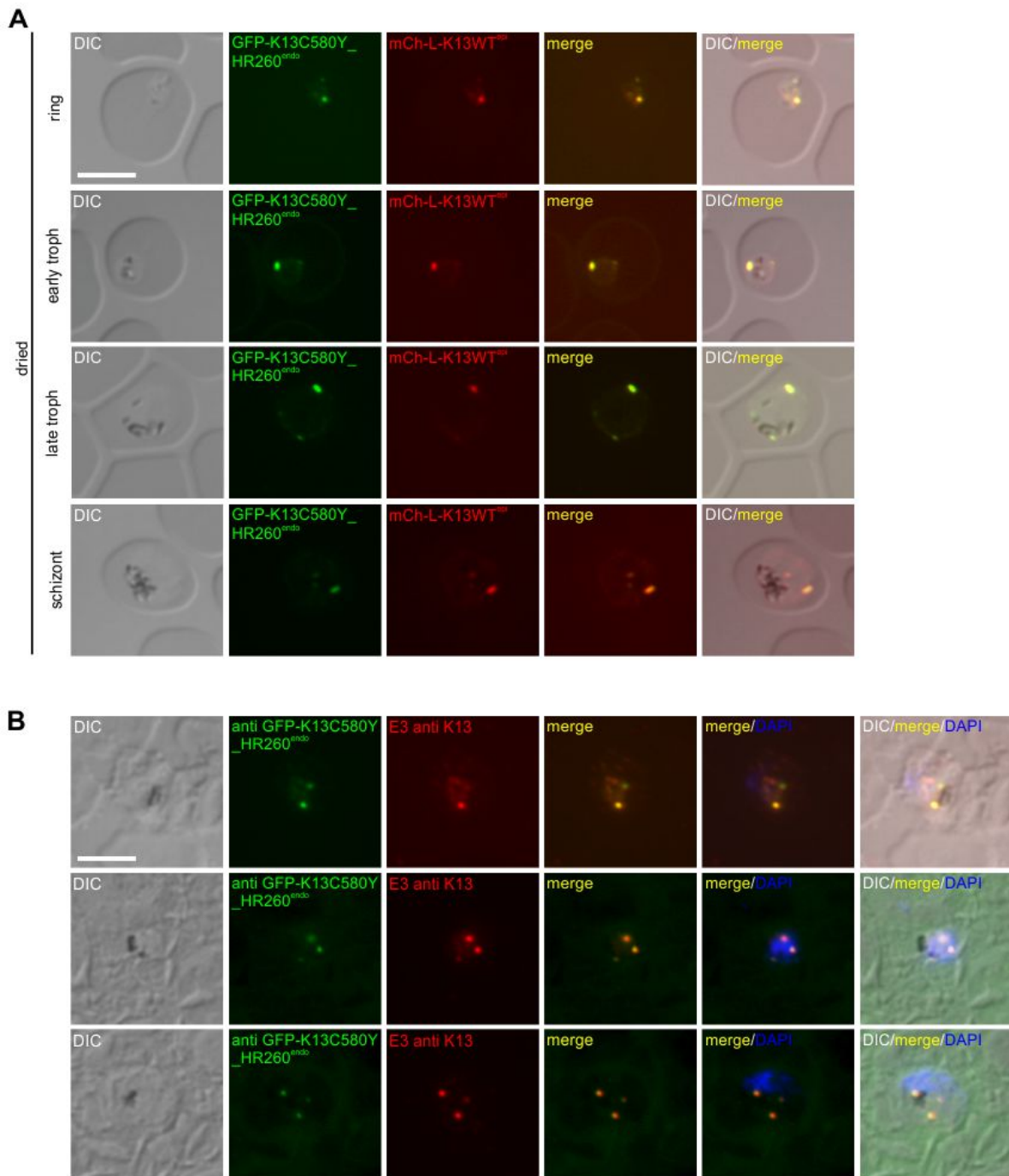


**Figure 48. Localization of endogenously tagged K13C580Y\_HR260<sup>endo</sup>.** (A) Fluorescence images of smeared and dried GFP-L-2xFKBP-L-Kelch13<sup>C580Y</sup>\_HR260<sup>endo</sup> (K13C580Y\_HR260<sup>endo</sup>) parasites episomally expressing mCherry-L-K13WT<sup>epi</sup>. Parasites were smeared on a glass slide for microscopy (dried) and images were taken at the indicated development stages; troph: trophozoite. (B) IFA with acetone fixed GFP-L-2xFKBP-L-Kelch13<sup>C580Y</sup>\_HR260<sup>endo</sup> parasites using anti-GFP mouse antibodies and monoclonal antibodies raised against Kelch13 (E3). Scale bar 5  $\mu$ m, DIC: differential interference contrast; GFP: green fluorescent protein; mCh: mCherry red fluorescent protein; merge: GFP and mCherry channels merged; DAPI (nuclei).

For functional analysis, K13C580Y\_HR260<sup>endo</sup> knock in parasites were co-transfected with pSkipFlox (Birnbbaum et al., 2017) and the excision of the mutated *kelch13* gene was induced by the addition of

rapalog (Figure 49 A). Thereafter parasite growth was observed using FACS based (Figure 49 B) determination of parasitemia (see 2.2.3.11) for the following five days and Giemsa smears were made to investigate the development of the parasites (Figure 49 C). As a control, the same parasites were cultured without rapalog (control). The excision of *kelch13* led to reduced growth of the parasites compared to the control which was manifested by an accumulation of ring stages (suggesting an arrest in this stage) and the formation of aberrant and pyknotic parasites. In contrast, the control parasites developed as expected (Figure 49 C). The delayed response of the phenotype in the conditional knock out in the K13C580Y\_HR260<sup>endo</sup> parasites was comparable to that previously observed in Kelch13<sup>endo</sup> conditional knock out parasites using the diCre system and likely was due to the time it took for the Kelch13 protein levels to drop under the threshold supporting growth (which was here not analyzed but observed before, Birnbaum et al., 2017). In conclusion, K13C580Y\_HR260<sup>endo</sup> knock in parasites resembled K13C580Y<sup>endo</sup> parasites in respect to the localization of K13C580Y\_HR260<sup>endo</sup> K13C580Y<sup>endo</sup> and in respect to the phenotype after removal of the gene (Birnbaum et al., 2017) but differed in respect to resistance because these parasites remained DHA sensitive.

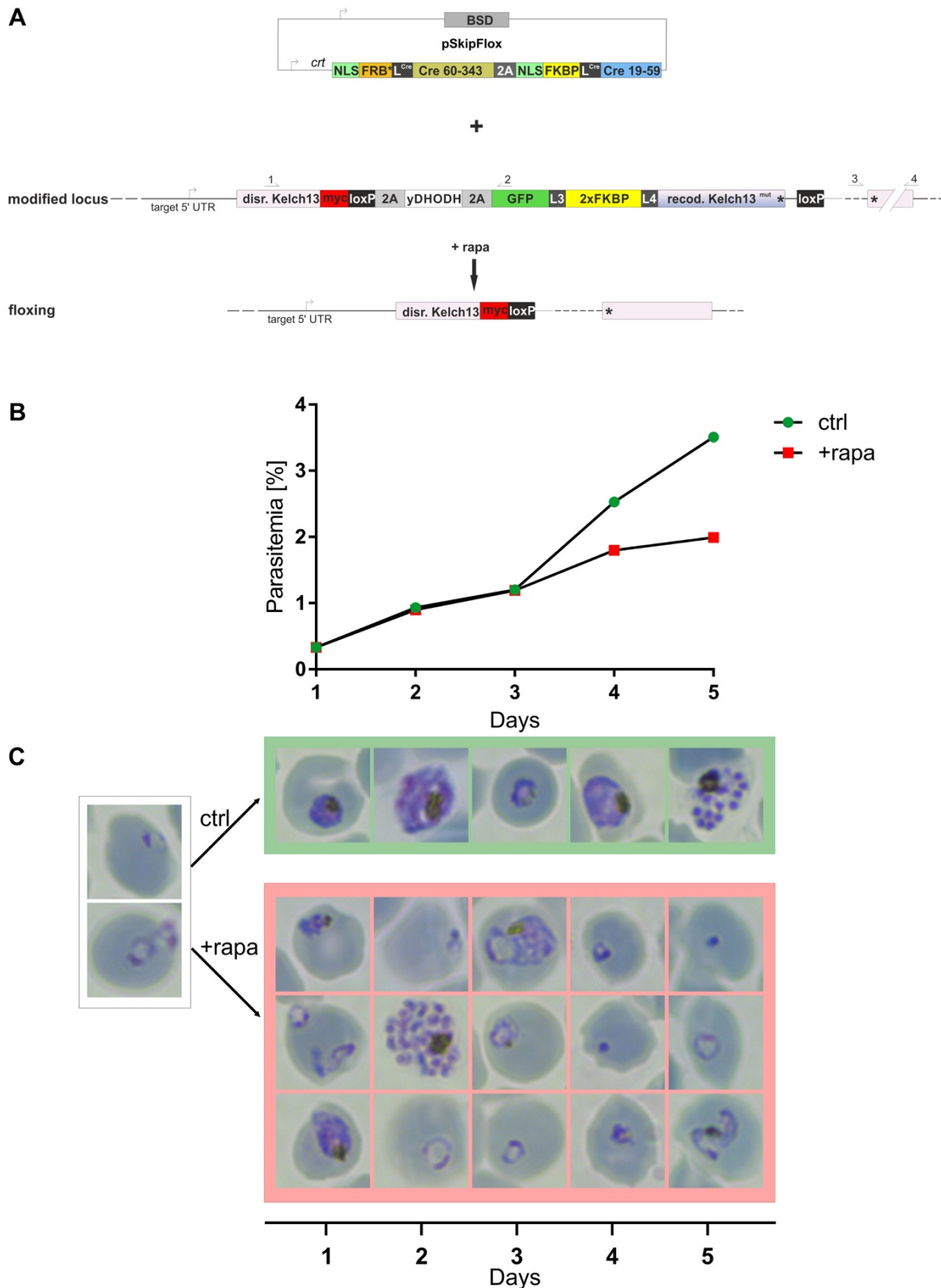


**Figure 49. Functional analysis of K13C580Y\_HR260<sup>endo</sup> parasites.** (A) Schematic illustration (not to scale) of pSkipFloX (top) and of the conditional excision of the mutated *kelch13* gene in K13C580Y\_HR260<sup>endo</sup> parasites using the diCre system (bottom). The target gene is disrupted (*disr. Kelch13*) and a codon optimized N-terminal K13C580Y copy (*recod. Kelch13*) is provided. The transgenic parasites can then be selected via the *yDHODH* resistance marker; *BSD*: Basticidin resistance marker to select for parasites carrying the episomal plasmid; arrows: promoters; *NLS* nuclear localisation signal; *Cre 60-343* and *Cre 19-59*: two diCre fragments. *L3* and *L4*: linkers (Varnai et al., 2006); *2A*: T2A skip peptide; Asterisk: stop codon; *yDHODH*: yeast dihydroorotate dehydrogenase gene; asterisks: stop codon; *GFP*: green fluorescence protein; *myc*: myc tag (modified from Birnbaum et al., 2017). (B) Shown is parasite growth as determined by flow cytometry of the K13C580Y\_HR260<sup>endo</sup> parasites grown in the presence (+rapa) and absence (ctrl) of rapalog. One representative of two independent experiments is shown (replica is shown in Appendix 6). (C) Representative Giemsa smears of the parasite cell lines indicated in (B) at the indicated time points (days after the addition of rapalog).

To investigate whether DHA sensitivity of K13C580Y\_HR260<sup>endo</sup> knock in parasites might correlate with increased Kelch13 protein levels compared to the K13C580Y<sup>endo</sup> parasite line, fluorescence microscopy was performed with K13C580Y\_HR260<sup>endo</sup> and K13WT<sup>endo</sup> and K13C580Y<sup>endo</sup> knock in parasites. As it was observed that K13C580Y<sup>endo</sup> parasites that were cultured for extended periods of time showed an increased RSA survival rate, K13C580Y<sup>endo</sup> parasites were differentiated to parasites that had been cultured continuously for approximately 4 years (K13C580Y<sup>endo</sup>\_long-term-cultured) and parasites that were cultured for approximately three months (K13C580Y<sup>endo</sup>\_short-term-cultured). Images of living parasites from these cell lines were taken and fluorescence intensities of the GFP signal of the Kelch13 foci were measured in ring stages (Figure 50). The images were taken with identically settings (see 2.2.5.1) in three independent experiments. K13C580Y\_HR260<sup>endo</sup> parasites showed a mean fluorescence intensity of 4016.8 (SD = 4880.6, n = 3), K13WT<sup>endo</sup> of 4092.6 (SD = 4919.1, n = 3), K13C580Y<sup>endo</sup>\_long-term-cultured of 2904.6 (SD = 3514.3, n = 3) and K13C580Y<sup>endo</sup>\_short-term-cultured of 3045.4 (SD = 3788.6, n = 3). This demonstrated, that K13C580Y\_HR260<sup>endo</sup> parasites had significantly higher Kelch13 protein levels compared to K13C580Y<sup>endo</sup>, and similar Kelch13 protein levels to K13WT<sup>endo</sup> (Figure 50). Fluorescence intensity of the Kelch13 foci in K13C580Y<sup>endo</sup>\_long-term-cultured and K13C580Y<sup>endo</sup>\_short-term-cultured parasites did not differ noticeable. This indicated that the higher resistance level of Kelch13<sup>C580Y</sup> long-term-cultured parasites (unpublished, data are not shown in this thesis) is not due to an increased Kelch13 protein abundance although there is a trend for lower amounts in the long-term-cultured cells (Figure 50). It is therefore possible that smaller changes that can't be measured with 3 replicas are the reason for the increased resistance after long-term culture. Moreover, these results show that the DHA sensitivity of K13C580Y\_HR260<sup>endo</sup> knock in parasites likely is due to a failure of the Kelch13 mutation in these parasites to decrease Kelch13 abundance, which was similar to that in K13WT<sup>endo</sup> parasites. The reason for this remains unclear but must be due to the shorter N-terminal truncated fragment, as this is the only known difference between the two parasite lines.

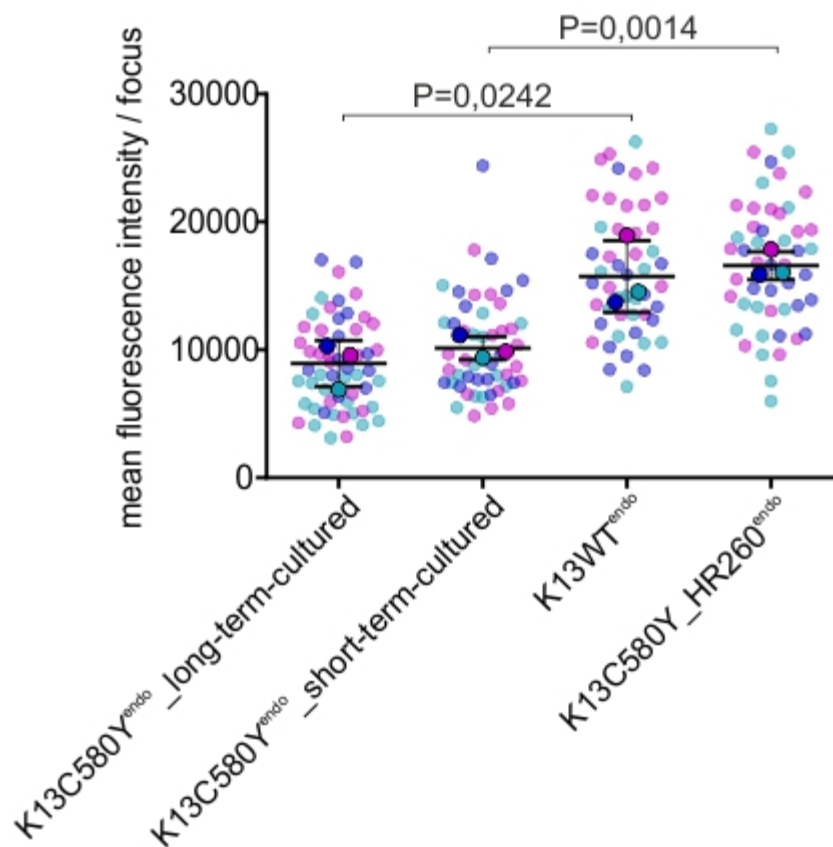


**Figure 50. Fluorescence intensity quantification of Kelch13 foci of different cell lines with endogenously tagged Kelch13.** Superplot (Lord et al., 2020) showing fluorescence intensity quantification of parasites expressing K13C580Y<sub>endo</sub>\_long-termed-cultured, K13C580Y<sub>endo</sub>\_short-termed-cultured, K13WT<sub>endo</sub> and K13C580Y\_HR260<sub>endo</sub>. Parasites were imaged under the same conditions in ring stages in three different experiments. Each point shows fluorescence intensity of a focus. Points of the same color derive from foci imaged in the same experiment and the larger and darker point represents the mean of these measurements. The wider central bar shows the mean derived from the mean of the 3 experiments, bars represent SD. Total number (n) of quantified foci: K13C580Y<sub>endo</sub>\_long-termed-cultured: n = 56; K13C580Y<sub>endo</sub>\_short-termed-cultured: n = 50; K13WT<sub>endo</sub>: n = 49; K13C580Y<sub>endo</sub>: n = 49.

## 4 Discussion

### 4.1 Kelch13 complex proteins are involved in resistance and endocytosis

Single point mutations in the Kelch13 protein confer ART resistance in *P. falciparum* parasites. Recent experiments have shown the involvement of Kelch13 and its compartment neighbors in endocytosis but the function of Kelch13 itself as well as its involvement in this process is poorly understood. It was described in Birnbaum and Scharf et al. that Kelch13 defines a novel compartment (Figure 52) that contains the typical endocytosis marker proteins of other organisms AP-2 $\mu$  (Kadlecova et al., 2017; Kaksonen and Roux et al., 2018) and Eps15 (Tebar et al., 1996; McMahon et al., 2011; Birnbaum and Scharf et al., 2020) but also UBP1, a protein that had previously been suspected in ART resistance (Hunt et al., 2007; Hunt et al., 2010; Borrmann et al., 2013; Henriques et al., 2014; Cerqueira et al., 2017). To better understand the involvement of the Kelch13-defined complex in ART resistance it was first assessed if other Kelch13 interacting candidates (KICs) were also involved in resistance which would substantiate their involvement in the Kelch13 pathway. This is particularly important for those proteins that were previously found not to be essential, as their function in endocytosis was unclear. The disruption of KIC4, KIC5 and MCA-2 led to reduced susceptibility to ART (see 3.1.1). Together with the findings that inactivation of UBP1, Eps15 and KIC7 resulted in decreased susceptibility of the parasites to DHA in a standard RSA (Birnbaum and Scharf et al., 2020) it can be concluded that the Kelch13 compartment is involved in ART resistance and that inactivation of these proteins or disrupting of the corresponding genes renders the parasite resistant to DHA. It was also observed that inactivation of KIC7 leads to less hemozoin crystals in the DV (see 3.1.3.1), which indicates that less hemoglobin reached the DV congruent with an endocytosis defect. This indicates an involvement of KIC7 in endocytosis. This result fits with previous findings that conditional inactivation of KIC7 decreases host cell cytosol uptake (Birnbaum and Scharf et al., 2020). Additionally, inactivation of KIC7 resulted in a similar phenotype to that of UBP1 inactivation when stage-specific parasite development was monitored using Giemsa smears, in support of a similar function of these proteins in parasite development. Interestingly, it was shown that, different to Kelch13, KIC7 and UBP1 are also essential for parasite survival in trophozoite stages (see 3.1.3). In accordance with this idea, Gimesa smear-based monitoring of parasite development after inactivation of Kelch13 in trophozoites did not show a phenotype in these stages. Control parasites and parasites with inactivated Kelch13 in trophozoites showed comparable development in whereas the development in the following cycle again showed the expected arrest towards the end of the ring stage (see 3.1.3.3). These experiments highlighted the already described essentiality of Kelch13 in the ART resistance relevant ring stage (Birnbaum et al., 2017). These data might give evidence that different Kelch13 complex proteins are involved in different parasite development steps (Birnbaum and Scharf et al., 2020).

Besides Kelch13, AP-2 $\mu$ , Eps15 and UBP1 only VPS45 was so far found to be directly involved in endocytosis (Figure 51) (Jonscher et al., 2019). The late endolysosomal transport (Figure 51, Late) in *P.*

*falciparum* seems to be partially conserved compared to eukaryotic cells, but the initiation of endocytosis (Figure 51, Early) seems to be unique in *P. falciparum* (Spielmann et al., 2020). For the understanding of the parasite-specific part of hemoglobin endocytosis, it is necessary to identify the proteins that are involved during the early step of formation of the endocytic vesicle and how this leads to endolysosomal transport to the DV.

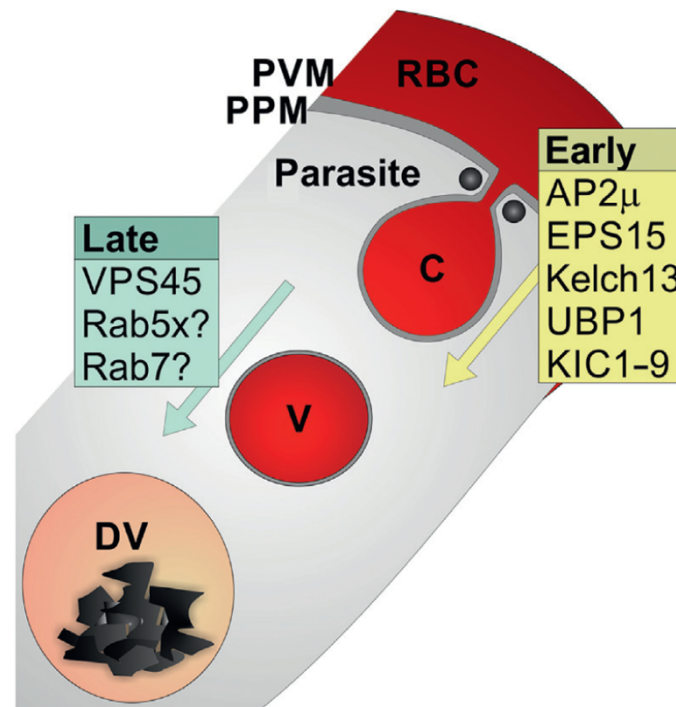


**Figure 51. Host Cell Cytosol Uptake (HCCU) in *P. falciparum*.** Shown are structures involved in endolysosomal transport and proteins that are known or suspected (indicated by the question mark) to be involved in this process. Of the indicated KICs, only KIC7 has been demonstrated to be directly involved in HCCU. Early: early endocytosis. Late: late endocytosis. Rab5x: Rab5b or Rab5c. PPM: parasite plasma membrane; PVM: parasitophorous vacuolar membrane; C: cytosome; V: HCC-containing vesicle; DV: digestive vacuole (modified from Spielmann et al., 2020)

As KIC7 co-localizes with Kelch13 (Birnbbaum and Scharf et al., 2020) and because KIC7 likely is part of the early endolysosomal pathway in *P. falciparum* (Figure 51), functional analysis of this candidate might give insights into the initial step of endocytosis in *P. falciparum*. In contrast to Kelch13, KIC7 is not only essential for parasite development in ring stages, but also in trophozoite stages (see 3.1.3.1) which makes it easier to functional analyze KIC7 than Kelch13. KIC7 therefore seems to be a good candidate to study early endocytic processes in *P. falciparum*. For functional analysis, the knock-sideways system was chosen to effectively and conditionally mislocalize KIC7 from its site of action. To investigate endolysosomal processes upon KIC inactivation, KIC7 was co-localized with the PI4P marker SidM (Balla et al., 2013) upon rapalog induced inactivation of KIC7 to observe membrane derived structures upon KIC7 inactivation. The number of SidM positive circular structures slightly increased after KIC7 was inactivated (see 3.1.4). It is likely that these circular structures are due to the impairment of host cell cytosol endocytosis and may even represent hemoglobin-filled vesicles disturbed in further transport to the digestive vacuole, although this was not specifically tested. This

interpretation is supported by the finding that KIC7 inactivation leads to slight (but not significant) increased vesicle formation or accumulation in the parasite and at the plasma membrane but not at the digestive vacuole. Overall, this is congruent with the hypothesis that endolysosomal transport of vesicles to the digestive vacuole is impaired after KIC7 inactivation. Taken together, these findings provide further evidence that endocytic processes are negatively influenced by KIC7 inactivation. However, it is still unclear how the observed PI4P positive structures connect to later endolysosomal transport. Based on immunofluorescence studies using Kelch13-specific monoclonal antibodies (E3) it was recently claimed that Kelch13 is found in proximity with the late endosome marker Rab7 in Cam3.II cell lines (Gnädig et al., 2020). However, it needs to be noticed that this association was assumed based on the calculation of a Pearson Correlation Coefficient (PCC) of 0.6, which does not confirm direct co-localization. Similar co-localization levels for Kelch13 were also observed to other Rabs, such as Rab5a, Rab5b and Rab5c (Gnädig et al., 2020). Assuming that these Rabs are found in different compartments, this might indicate that Kelch13 and the different Rab proteins do not co-localize but label different proximal compartments with similar small spatial separation. This could indicate that Kelch13 and the Rabs are involved in different endocytic steps (Figure 51). However, at least for Rab5a it was shown that it is not involved in endocytosis (Birnbaum et al., 2017). Hence, there is a need to better define the function and location of these compartment markers and for further investigations of the interaction and spatial arrangement of Kelch13 complex proteins (which are associated with the initiation of endocytosis) and those of later endocytosis steps such as VPS45 (Figure 51).

Endocytosis in *P. falciparum* seems to be unusual when compared to endocytosis in model organisms (Aikawa et al., 1966; Francis et al., 1997; Abu Baker et al., 2010; Henrici et al., 2019; Spielmann et al., 2020). It is clathrin-independent, but includes other proteins typically involved in clathrin-dependent endocytosis in other organisms such as AP-2 $\mu$ . Eps15 is a further protein typical for functioning in endocytic processes in other organisms (Tebar et al., 1996; McMahon et al., 2011) but most of the other Kelch13 compartment proteins are *Plasmodium* specific (designated as KICs, Figure 52) (Birnbaum and Scharf et al., 2020). It remains unclear how these proteins mechanistically mediate endocytosis. It is also unclear how endocytosis is regulated in malaria parasites and moreover, it is unclear how Kelch13 is involved in this process. The AP-2 complex is also involved in clathrin-independent endocytosis in the *Aspergillus* (Martzoukou et al., 2007). Based on their homology to proteins in other organisms, Kelch13 and UBP1 might not be mechanistic endocytosis proteins and might therefore regulate endocytosis (Figure 52, Birnbaum and Scharf et al., 2020). In further experiments DIQ-BioID could be performed with other Kelch13 complex proteins which are potentially involved in endocytosis such as UBP1 or MCA2.

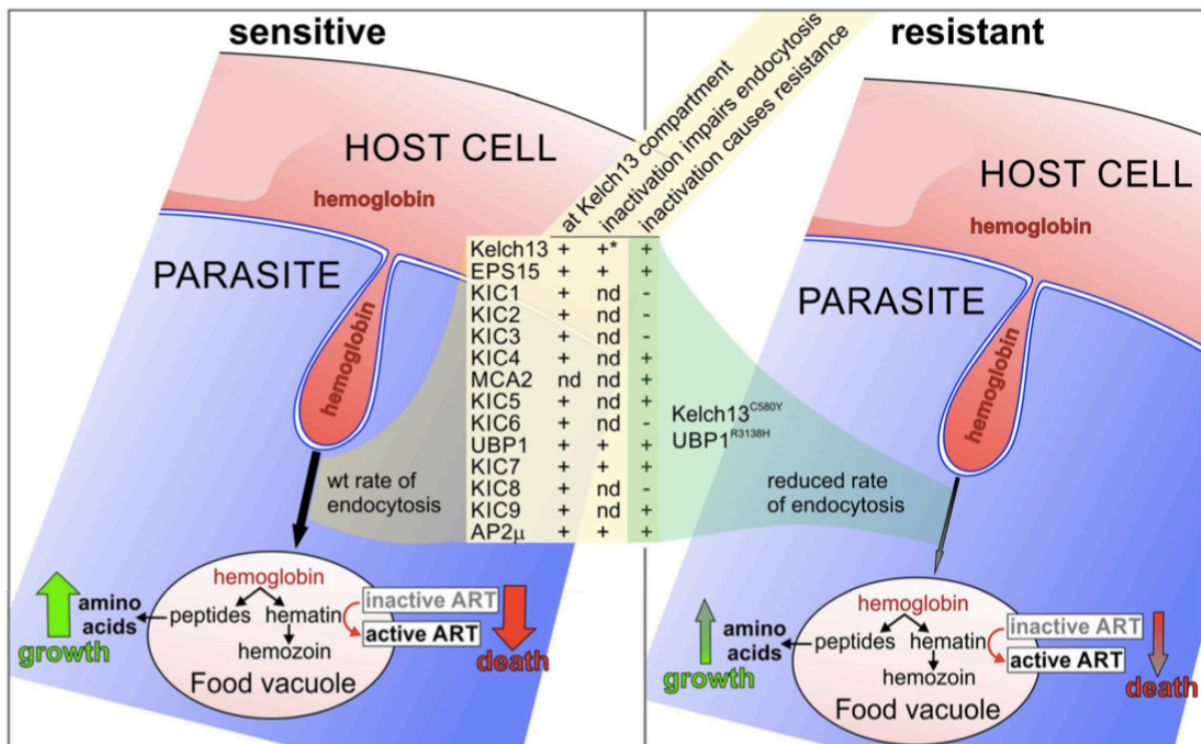


**Figure 52. Model of artemisinin resistance.** Asterisk: inactivation of Kelch13 impairs endocytosis exclusively in ring stages. nd: not determined (Birnbaum and Scharf et al., 2020).

## 4.2 Reduced Kelch13 protein level leads to resistance

It has been shown that K13C580Y<sup>endo</sup> is less abundant in the cell compared to K13WT<sup>endo</sup> (see 3.2.3). This might be due to diminished stability and resulted in less endocytosis, potentially indicating a regulatory role of Kelch13 (Figure 52). The finding that increased Kelch13 protein level in resistant parasites can lead to the loss of resistance (see 3.3.1) provided evidence that Kelch13 protein levels alone influence resistance. This seems to be independent of Kelch13 mutations as overexpression of K13C580Y<sup>epi</sup>, K13E252Q<sup>epi</sup> and K13R539T<sup>epi</sup> also renders resistant parasites to sensitive (see 3.3.1). This demonstrates that sensitivity to ART is not based on an additionally property exclusively held by Kelch13 wild type parasites.

The hypothesis that abundance rather than a qualitative change in mutated Kelch13 is the reason for resistance is also supported by the finding that parasites with mutated Kelch13 have the same interaction profile as parasites harboring K13WT<sup>endo</sup> (see 3.2.2). These findings indicate that mutated Kelch13 may simply reduce Kelch13 overall activity.

The finding that K13C580Y<sup>endo</sup> parasites harbor less Kelch13 protein than K13WT<sup>endo</sup> parasites (see 3.2.3) is consistent with previous studies (Siddiqui et al., 2017; Yang et al., 2019; Silva et al., 2019) from e.g., Siddiqui et al., showing an approximately 2-fold decrease in Kelch13 abundance in resistant field isolates (Cam3.II<sup>R539T</sup>) compared to isogenic wild type parasites in ring stages (Siddiqui et al., 2017). Less Kelch13 protein abundance in resistant parasites was recently also confirmed by Gnädig et al. in ring stage parasites, demonstrating 24 % and 34 % less Kelch13 protein level in Cambodian isolates

carrying the Kelch13 mutations C580Y and R539T (Cam3.II<sup>C580Y</sup> and Cam3.II<sup>R539T</sup>) compared to wild type parasites (Gnädig et al., 2020). A recent study reported no differences in Kelch13 protein levels in rings in Cam3.II<sup>C580Y</sup> parasites but in Cam3.II<sup>R539T</sup> parasites (Mok et al., 2021). There was also less Kelch13 abundance in trophozoites of Cam3.II<sup>C580Y</sup> and Cam3.II<sup>R539T</sup> parasites compared to Kelch13 wild type parasites (Mok et al., 2021). However, given the otherwise consistent reduction Kelch13 levels in Kelch13 mutant parasites (Siddiqui et al., 2017; Yang et al., 2019; Birnbaum and Scharf et al., 2020; Gnädig et al., 2020), it seems save to say that this mutation leads to a reduced cellular abundance of Kelch13.

In this work it was demonstrated using quantitative Western Blot analysis that resistant parasites show 30 - 50 % less Kelch13 protein abundance compared to wild type parasites (see 3.2.3). This was confirmed in living cells using fluorescence microscopy to exclude protein fluctuations due to saponin lysis of the cells and the sample preparation process for Western Blot analysis (see 3.2.3). There are many parameters that can influence the protein quantity determination by Western Blot analysis (see 4.3.1) (Pillai-Kastoori et al., 2020) which can be avoided by fluorescence intensity measurement of Kelch13 foci in living cells. On the other hand, microscope settings can also influence the fluorescence intensity measurement. It was therefore carefully ensured to find settings that do not result in oversaturation of the fluorescence image and that only samples were compared that were collected on the same occasion and with the identical acquisition settings. It was also taken care that the manual work, such as focusing, was performed quickly to avoid bleaching and therefore maintain comparability. K13C580Y<sup>endo</sup> and K13WT<sup>endo</sup> were tagged endogenously (Birnbaum et al., 2017) and expressed under the endogenous promoter from the endogenous locus which was essential to determine meaningful information about the expression levels of mutated and wild type Kelch13 in the cells.

### 4.3 Functional analysis of the Kelch13 domains

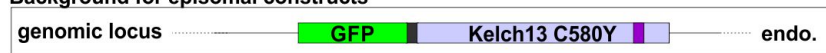
To better understand the molecular resistance mechanism of *P. falciparum* against artemisinin, it is essential to understand the cellular function of Kelch13. One approach to do this could be to dissect the functional domains of Kelch13 to understand contribution of the different parts to endocytosis and resistance. Based on homology similarities with other organisms, potential domain specific functions are predicted for the BTB and Kelch propeller domain (KD) but the N-terminal *Plasmodium* specific region (PSR) and the coiled coil region (CC) (see. 1.5.3) have no homologies to known domains and are not conserved in other organisms (Coppeé et al., 2019). It still remains unclear what are the functions of the single domains of Kelch13.

In order to investigate the Kelch13 domains in more detail, constructs consisting of different Kelch13 domain combinations were episomally expressed on the resistant K13C580Y<sup>endo</sup> background (see 3.3.2). The importance of the domains for the function of the protein was assessed by determining the resistance level by RSA as described (Witkowski et al., 2013) (Figure 53). Interestingly, overexpressing of the PSR-CC (i.e., the entire part specific for malaria parasites) alone was sufficient to revert the resistant

background sensitive to ART (Figure 53). This finding indicates that this part sustains the correct localization and function of the Kelch13 protein, assuming that resistance is due to an overall loss of Kelch13 function. In contrast to this, the BTB domain alone or in combination with the Kelch propeller domain (BTB-KD) (i.e., the conserved part of the protein) were not functional, as this construct did not revert the resistant parasites to sensitive (Figure 53). This indicates that the *Plasmodium* specific N-terminus of Kelch13 promotes function without BTB and the Kelch propeller domains and that the conserved C-terminus does not display a role in protein function but rather might function as a regulator of the stability (and hence abundance) in Kelch13. The finding that the CC-BTB-KD construct is fully functional and that the CC-BTB construct alone is at least partially sufficient to maintain Kelch13 protein function (Figure 53) would suggest that the coiled coil region is the key region to maintain Kelch13 functionality. Surprisingly, preliminary data (not shown in this thesis as analysis of this construct was not yet concluded before completing this thesis) gave evidence that the coiled coil region alone is not sufficient to promote the function of Kelch13 (i.e., it did not render the resistant parasites sensitive) and this might have been in part due to the observed failure of this construct to correctly localize.

By taking a closer look at those constructs that can maintain the function of Kelch13 (PSR-CC, CC-BTB-KD, CC-BTB and PSR-CC-L-KD), it becomes apparent that these constructs have in common that firstly, the coiled coil region is present and secondly, the coiled coil region is directly linked to only one other domain of Kelch13 at either the C- or the N-terminus (Figure 53). It is possible that in the absence of full length Kelch13, the coiled coil region is essential for the parasites to maintain Kelch13 functionality but that this functionality only works if another domain is also present.

## Background for episomal constructs



	RSA survival rate	localisation	abundance	bands on WB
+ no episomal construct	12.7 %	foci		
+ epi. 	0.1 %	foci		2
+ epi. 	0.3 %	foci		
+ epi. 	0.7 %	foci		2
+ epi. 	0.3 %	foci		2
+ epi. 	14.7 %	cytosolic		1
+ epi. 	13.4 %	cytosolic		1
+ epi. 	9.6 %	cytosolic		1
+ epi. 	0.9 %	foci	high	1
+ epi. 	3.0 %	partial	low	1
+ epi. 	12.0 %	cytosolic		1
+ epi. 	27.0 %	partial	low	1
+ epi. 	3.6 %	partial	low	1
+ epi. 	2.3 %	partial	high	3
+ epi. 	15.5 %	partial		1

**Figure 53. Overview of the functional analysis of endogenous K13C580Y<sup>endo</sup> parasites episomally expressing constructs consisting of different Kelch13 domain combinations.** Schematic illustration (not to scale) of the modifications of the used parasite lines: endogenous (endo) K13C580Y<sup>endo</sup> (GFP-2xFKBP-Kelch13<sup>C580Y</sup>, Birnbaum et al., 2017) episomally (epi) expressing the indicated constructs were tested in a RSA (RSA survival rate) (Witkowski et al., 2013), the localization was determined by fluorescence microscopy (localisation of the episomal construct in foci (foci), in the cytosol of the parasite (cytosolic) or partial in the cytosol and partial in foci (partial)) and protein abundance of the episomal construct (abundance) was measured by Western Blot analysis. Bands on WB: number of different bands that were detected by Western Blot analysis of the episomal constructs. GFP: green fluorescent protein; mCherry: red fluorescent protein; L: linker; PSR: *Plasmodium* specific region; CC: coiled coil region; BTB: BTB/POZ domain; Kelch domains: Kelch propeller domain consisting of six Kelch motif repeats; 2xmyc: myc tag; T2A: skip peptide; loxP: loxP site.

Due to the fact that these constructs are expressed episomally while the endogenous K13C580Y<sup>endo</sup> is simultaneously present in the cell, it also has to be taken into consideration that there might be an interaction between the episomal and the endogenous construct. It is possible that this interaction influences the localization of the episomal construct and this could have a direct impact on the functionality of the construct. Furthermore, it is also possible that the episomal and endogenous construct dimerize, which might influence the interaction of endogenous Kelch13 with other proteins or the modification of Kelch13 by other proteins. It is also possible that the binding of the episomal construct to endogenous Kelch13 permits the localization of the overexpressed construct in the Kelch13 foci and this might allow the interaction of the episomal construct to other proteins. It is also possible that endogenous Kelch13 is stabilized by binding of the episomal Kelch13 domains. This hypothesis would implicate increased protein abundance of endogen K13C580Y<sup>endo</sup>. To investigate this in more detail, fluorescence intensity of endogen expressed K13C580Y<sup>endo</sup> foci was compared to the same cell line co-expressing episomal PSR-CC (data are not shown in this thesis). No differences in fluorescence intensity were observed indicating that the overexpressed PSR-CC construct does not influence protein

abundance of the endogenous K13C580Y<sup>endo</sup>. However, such an effect can in principle not be excluded for the other constructs used.

As previous experiments showed that endocytosis and resistance is influenced by Kelch13 abundance (Birnbaum and Scharf et al, 2020), it was here investigated whether this might be due to protein stability which might be regulated by the Kelch propeller domain (see 3.3.3). Quantitative Western Blot analysis confirmed that episomal constructs containing the Kelch propeller domain have significantly higher Kelch13 protein levels than constructs lacking the Kelch propeller domain which supports the suggested function of the Kelch propeller domain as a regulator of protein abundance. Although the copy number of the episomal plasmids is unknown (further discussed in 4.3.1), it can be assumed to be similar between the different constructs, indicating that this difference is likely due to protein stability. This work therefore indicates that the Kelch propeller domain regulates Kelch13 protein levels. Interestingly, immunoblot analysis showed that the abundance of the episomally expressed PSR-CC-BTB is approximately 200-fold increased upon C-terminal fusion of an mDHFR domain. While the protein levels were not dependent on the folding status of mDHFR, this nevertheless suggests that any folded domain can stabilize the *Plasmodium* specific part and thereby increase abundance of the construct in the cell. This gives evidence that Kelch13 is stabilized by its C-terminus and supports the potential regulatory function of the Kelch propeller domain. However, it is at present unclear whether the C-terminal mDHFR domain only provides stability to PSR-CC-BTB (which is promoted by the Kelch propeller domain in wild type Kelch13) or can also functionally replace the Kelch propeller domain. It was shown that the Kelch propeller domain in combination with other Kelch13 domains (PSR-CC-L-KD, CC-BTB-KD; Figure 53) is sufficient to maintain the function of Kelch13, at least in part. It is possible that the Kelch propeller domain, in combination with the indicated domains, also provides function for the protein. To investigate whether the mDHFR domain might overtake a specific function of the Kelch propeller domains, RSAs could be performed with the K13C580Y<sup>endo</sup> parasites overexpressing PSR-CC-BTB-mDHFR<sup>epi</sup>. Complementation of the resistant background would then give evidence that the mDHFR domain might not only influence protein levels due to stability but also due to functional properties that might be executed by the Kelch propeller domain in wild type Kelch13. In the case that overexpressing PSR-CC-BTB-mDHFR<sup>epi</sup> in K13C580Y<sup>endo</sup> parasites could not complement the resistant background this then might indicate that the Kelch propeller domain has additional functions that can't be overtaken by the mDHFR domain.

The putative ubiquitin hydrolase UBP1, an enzyme that deubiquitinates proteins, is part of the Kelch13 complex (Birnbaum and Scharf et al., 2020). It is known that the Kelch13 interactor Eps15 and its function in endocytosis can in other organisms be regulated by ubiquitination (Van Bergen En Henegouwen, 2009), raising the possibility that ubiquitination might be involved in regulating endocytosis also in *P. falciparum* parasites. Interestingly, it was observed that episomal constructs expressing Kelch13 full length (irrespective of whether this was a wild type Kelch13 or mutated Kelch13) were detectable as two clearly defined bands by Western Blot analysis (see 3.3.1 and 3.3.2) (Figure 53). The differences in molecular weight of these two bands ranged between 6 - 7.2 kDa. The

construct PSR-CC-L-KD was detected in three bands at a molecular weight between 100 and 120 kDa (Figure 53). As mono-ubiquitination increases the molecular weight of its target by 8.6 kDa, it might be possible that the detection of multiple bands is due to ubiquitination. Mono-ubiquitination has been shown to regulate many intracellular processes such as translation, DNA repair or endocytic trafficking (Bridgford et al., 2018; Cho et al., 2020). The hypothesis that Kelch13 can be ubiquitinated and that this is involved in regulation of its abundance needs further investigations. It could be tested whether deubiquitinating enzymes (DUBs, e.g., UCH-L3, UCH-L54) (Artavanis-tsakonas et al., 2006; Frickel et al., 2007; Ponder and Bogyo, 2007) might influence the ubiquitination status of the episomal constructs. It is possible that the ubiquitination of the episomal constructs can then be visualized by immunoblot analysis based on the hypothesis that ubiquitinated proteins are detectable at a higher molecular weight compared to deubiquitinated proteins. Parasite extracts of the cell lines with the episomal constructs could be treated with DUBs and immunoblot analysis could be performed to investigate whether DUB treatment influences the molecular weight or the number of detected bands compared to DUB untreated parasite extracts of the same cell lines. Interestingly, only episomally expressed Kelch13 constructs (and not endogenous Kelch13) were detected in multiple bands by immunoblot analysis. It is possible that the copy number of the episomal plasmids resulted in an overabundance of the constructs in the cell (further discussed in 4.3.1) and that higher protein abundance of the episomal constructs enables the visualization of the different ubiquitination status of the corresponding proteins by immunoblot analysis while this is not detectable using endogenous Kelch13.

### 4.3.1 Technical considerations

A number of issues should be considered in regard to determining protein levels in the cell. As mentioned above (see 4.2), quantitative Western Blot analysis can be influenced by different parameters (Murphy and Lamb, 2013; Pillai-Kastoori et al., 2020). The sample preparation is already a critical step for quantitative immunoblotting. The conditions during cell lysis (e.g., temperature) or detergents that are used for cell lysis can influence the lysis process and protein degradation (James, 2015). For quantitative immunoblotting it is also important to note and reconsider the essential role of loading controls to normalize for cell numbers in the different samples (Murphy and Lamb, 2013; Marcus, 2014). Differences in protein abundance in different parasite stages can also influence the output of immunoblot analysis. Besides that, the transfer of the separated proteins from the SDS-PAGE to the membrane as well as the following visualization of the target protein by primary and secondary antibodies are also critical steps that may influence the comparability of the analysis between different samples (Pillai-Kastoori et al., 2020).

Nevertheless, quantitative immunoblot analysis is a powerful tool to examine protein abundance (Pillai-Kastoori et al., 2020). Protein expression in the cell is controlled on several levels by transcription, translation and post translational modifications. Expression of fusion proteins under the same endogenous promoter can be assumed to lead to comparable expression levels. In contrast, episomally expressed constructs are often controlled by a different promoter. While transcription levels might be

comparable if the same promoter is used to drive expression of the different constructs, the copy number of the plasmid is not. To quantify the abundance of episomally expressed proteins it is essential to calculate the ratio of the abundance of the protein to be examined to the abundance of a housekeeping protein in the same cells, which functions as a loading control and reference the amount of the loaded extract. In this study, to maintain comparability, all episomal complementation constructs were expressed under the same promoter which is active in all asexual blood stages and the parasite protein BIP was used as a loading control. This analysis allowed to assess how the phenotypes detected by investigating the episomally expressed Kelch13 domain constructs on the resistant background (see 3.3.1, 3.3.2 and 3.3.3) is influenced by overall amount of the episomal construct in the cell. Nevertheless, the calculated ratios didn't reflect differences in copy number of the plasmid which influences the protein abundance of the different Kelch13 domain constructs in the cells. For this it would be necessary to determine the copy number of the episomal construct. A surrogate for this could be another protein expressed from the plasmid. Parasites overexpressing the complementation constructs were selected by using a Blasticidin (BSD) resistance marker which is encoded on the plasmid. Hence, BSD could be used to normalize for plasmid copy number. However, in experiments with an anti-BSD antibody (data are not shown in this thesis) no signal could be detected in immunoblot analysis which might indicate that further analysis will be needed to improve BSD detecting by immunoblot analysis and hence to use BSD as a control for the copy numbers of the episomal constructs. In absence of copy number data, it can only be assumed that the copy number of the different plasmids was comparable. However, the quantity of episomal complementation constructs could be related to the absolute quantity of the episomal wild type Kelch13 construct which is expressed under the same promoter as the other episomal constructs used in this thesis. This facilitated the quantification of Kelch13 domain-specific differences in protein levels and ensured comparability between the different cell lines.

The main advantage of the expression of episomal Kelch13 complementation constructs is the ability to rapidly analyze the Kelch13 domains for essentiality in function and localization without long time periods that are needed to obtain endogenously tagged integrants. The results presented in this thesis provide first functional data of the single Kelch13 domains and represent a connecting point for subsequent analyses (see 4.3.2). Further experiments to investigate the function of the Kelch13 domains can either focus on key domains of Kelch13 that based on this work are likely important to maintain the function of Kelch13 (*Plasmodium* specific region and coiled coil region) or with focus on those which are suggested to have a regulatory function (Kelch repeat domains).

#### **4.3.2 Further experiments to investigate the function of the Kelch13 domains**

As summarized in 4.3.1, the data presented in this thesis indicate that the C-terminal Kelch propeller region of Kelch13 might function as a regulator for protein stability and abundance and that the *Plasmodium* specific N-terminus of Kelch13 (especially the coiled coil domain) might be essential to maintain the function of Kelch13. As these data are based on episomally expressed complementation constructs that are present together with endogenously expressed K13C580Y<sup>endo</sup> at the same time, this

needs further investigation. For this, a conditional complementation system could be used. The resistant K13C580Y<sup>endo</sup> background could be conditionally excised, resulting in parasites relying on an episomally expressed construct that is provided simultaneously. K13C580Y<sup>endo</sup> parasites are endogenously tagged with GFP using pSLI-N-loxP (Figure 54 A, Birnbaum et al., 2017). Episomal expression of pSkipFlox (Birnbaum et al., 2017) with an additional cassette, consisting of the Kelch13 domain combination of interest, can be expressed under the *nmd3* promoter, replacing the BSD cassette. Additionally, the BSD resistance marker would still need to be present which could be achieved by adding it to the *crt* controlled open reading frame using one skip peptides behind the BSD resistance marker (Figure 54 B). The basis for such constructs, albeit without the Kelch13 construct are now available in the lab (Stäcker, Scharf and Spielmann, unpublished). In the presence of rapalog, the recodonized *kelch13C580Y* is excised and parasite survival is dependent on the Kelch13 domain construct that is overexpressed. To evaluate the finding that PSR-CC is important to maintain the function of Kelch13, PSR-CC would be the first Kelch13 domain construct to be tested with this system. Parasite survival upon *kelch13C580Y* excision could confirm the essentiality of PSR-CC for the function of the Kelch13 protein.

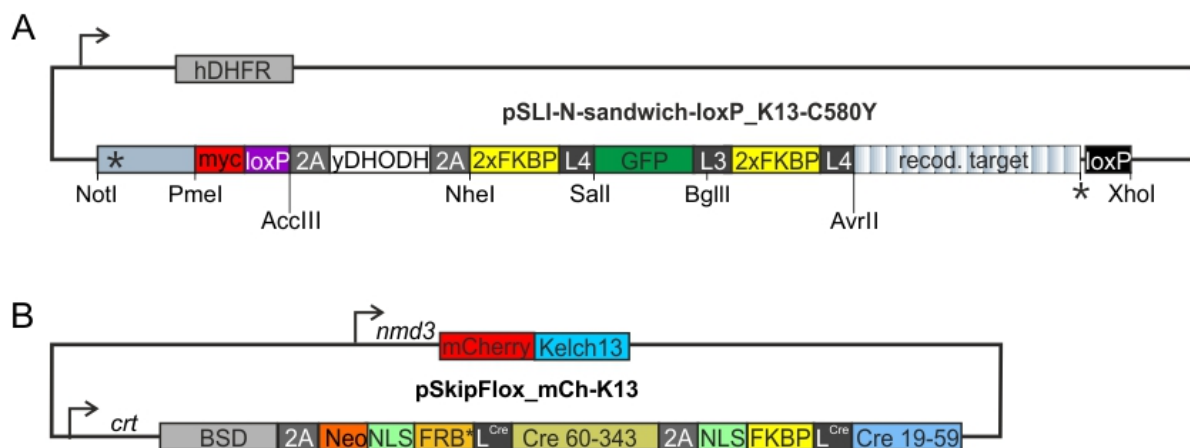


**Figure 54. Schematic illustrations (not to scale) of pSLI-N-sandwich-loxP\_K13C580Y and pSkipFlox\_mChK13. (A)** Shown is the plasmid that was used for integration to obtain K13C580Y<sup>endo</sup> parasites (GFP-2xFKBP-Kelch13<sup>C580Y</sup>, Birnbaum et al., 2017). **(B)** Episomal plasmid that can be transfected on K13C580Y<sup>endo</sup> parasites. recod. target: codon optimized Kelch13C580Y copy; L: linker; 2A: T2A skip peptide; Asterisk: stop codon; yDHODH: yeast dihydroorotate dehydrogenase gene; arrows: promoters; human dihydrofolate reductase (hDHFR): episomal resistance marker; GFP: green fluorescent protein; NLS: nuclear localisation signal; BSD: Blasticidine S resistance marker; Cre 60-343 and Cre 19-59: two diCre fragments; Neo: 7 amino acids of the neomycin resistance marker. (Top: Birnbaum et al., 2017).

Moreover, it is still not clear how and if Kelch13 interacts with the KICs. Although all candidates were shown to localize to the Kelch13-defined focal structure (Birnbaum and Scharf et al., 2020) that was proposed to correspond to the cytostome (Yang et al., 2019), so far only Eps15 was confirmed to be an interactor by co-immunoprecipitation (Birnbaum and Scharf et al., 2020). To further investigate the function of the different Kelch13 domains it would also be important to determine which domain of Kelch13 promotes binding and interaction to other Kelch13 complex proteins. For this, Kelch13 domain-specific DIQ-BioID could be performed using constructs consisting of the PSR-CC, BTB-KD

or CC-BTB (Figure 55). As it was shown that PSR-CC promotes localization of Kelch13, DIQ-BioID with these constructs might be particularly interesting.

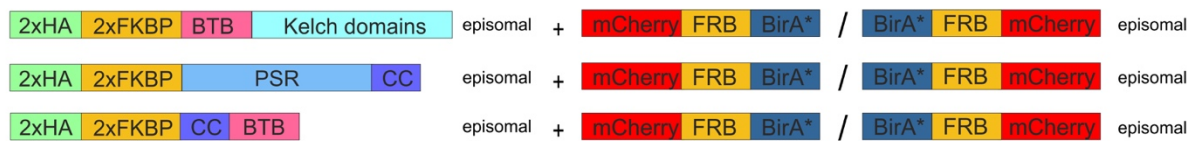


**Figure 55. Schematic illustration of episomally expressed constructs for Kelch13 domain-specific DIQ-BioID.** Kelch13 domain combination constructs and BirA\*-N<sup>L</sup> (BirA\*-FRB-mCherry) and BirA\*-C<sup>L</sup> (mCherry-FRB-BirA\*) (Birnbaum, 2017; Jonscher et al., 2019; Birnbaum and Scharf et al., 2020). PSR: *Plasmodium* specific region; BTB: BTB/POZ domain; CC: coiled coil region; Kelch domains: Kelch propeller domain consisting of six Kelch motif repeats.

#### 4.4 Prevalence of Kelch13C580Y, resistance and fitness cost

The C580Y point mutation in Kelch13 is associated with ART resistance (Ariey et al., 2014) and reduced endocytosis in ring stages (Birnbaum and Scharf et al., 2020). This is the most prominent and widespread resistance conferring Kelch13 mutation in Southeast Asia. In order to understand the molecular mechanism that underlies resistance, this thesis focused on the functional analysis of the Kelch13 protein and assessed the impact of some of its interactors on resistance. Reduced activity of Kelch13 (Birnbaum and Scharf et al., 2020) or disruption of several non-essential interactors (see 3.1.1) resulted in resistance. However, as this is mediated by reduced endocytosis (Birnbaum and Scharf et al., 2020), this can be expected to have negative consequences for the parasite. Reduced endocytosis, and hence reduced hemoglobin uptake and digestion, in resistant parasites may diminishes the parasite's amino acid supply which could result in a fitness cost.

For many microbial pathogens it is known that resistance is associated with a fitness cost (Rosenthal, 2013). Fitness can be measured in competitive growth experiments (Gordo et al., 2011) and it has been shown in bacteria that resistant pathogens can increase compensatory mechanism and mutations to improve fitness (Andersson and Hughes, 2010). In malaria parasites resistance to atovaquone and chloroquine was already found to be associated with a fitness cost (Peters et al., 2002; Hayward et al., 2005). Artemisinin resistance was also connected to a fitness cost of the parasites (Straimer et al., 2017; Nair et al., 2018; Siddiqui et al., 2020; Uwimana et al., 2020; Stokes et al., 2021). Growth competition assays in Cam3.II parasites demonstrated a high fitness cost in Kelch13R539T and Kelch13I543T parasites (Straimer et al., 2017). Data from recent studies gave evidence that the genetic background of parasite strains influence both, resistance and fitness of the parasite (Straimer et al., 2015; Cerqueira et al., 2017; Nair et al., 2018; Sharma et al., 2021; Stokes et al., 2021).

The results shown in 3.1.3.3 demonstrate that partial inactivation of Kelch13 leads to a delay in parasite development in rings stages indicating a fitness cost. As inactivation of Kelch13 leads to ART resistance (Birnbaum and Scharf et al., 2020) this underpins the predicted correlation between resistance and fitness cost. Additionally, it was shown that the disruption of three of the non-essential KICs (MCA2-TGD, KIC4-TGD and KIC5-TGD) leads to resistance to ART (see 3.1.1) and that two of these (MCA2-

TGD and 5-TGD) result in a growth defect (see 3.1.2) and hence decreased fitness levels. As the TGD system is not inducible, it cannot be determined whether the other KIC-TGDs might also have a growth defect that is not detectable with the growth assay as it is possible that growth defects or delays are masked in the following stage or that compensatory changes have already occurred due to the time period required to generate such parasite lines. This could be clarified in a stage experiment with the corresponding KIC cell lines with an inducible knock-out system. It is unpredictable whether functional data of the KIC-TGDs with the 3D7 laboratory strain background would be transferable to them in field isolates giving the need for further investigations.

## 4.5 A new *Kelch13C580Y* integration cell line with shortened homology region

The results in this work showed that a new *Kelch13C580Y* integration cell line (referred to as K13C580Y\_HR260<sup>endo</sup>, see 3.4) with shorten homology region (base pairs (bp) 53 - 313) was not resistant to ART when tested in a standard RSA. This was in contrast to the previously established K13C580Y<sup>endo</sup> cell line that has a homology region of 543 base pairs (bp 515 - 1058), 1058 bp of *Kelch13* that are still expressed in addition to the recodonized full length K13C580Y (see 3.4). In an attempt to explain this difference in ART resistance, it was demonstrated that K13C580Y\_HR260<sup>endo</sup> parasites harbor significantly more *Kelch13* protein than the K13C580Y<sup>endo</sup> parasites and show similar *Kelch13* protein levels as K13WT<sup>endo</sup> parasites. As resistance is dependent on *Kelch13* abundance (Birnbbaum and Scharf et al., 2020), increased *Kelch13* abundance in the K13C580Y\_HR260<sup>endo</sup> parasites (see 3.4) might explain ART sensitivity. However, the question remains why a shorten homology region, which is used for homologous recombination into the genomic locus of *kelch13* via SLI, could influence protein abundance of *Kelch13*. The data presented in 3.2.2 indicates that the N-terminal *Plasmodium* specific region together with the coiled coil domain (PSR-CC) might be sufficient to maintain the function of *Kelch13*, whereas PSR-CC-BTB is not functional. In K13C580Y<sup>endo</sup> cells after N-terminal integration, the disrupted *Kelch13* product included the *Plasmodium* specific region, the coiled coil region as well as two amino acids of the BTB domain. It was shown in 3.2.2 with an episomal complementation construct expressed on the resistant K13C580Y<sup>endo</sup> background that the corresponding expressed product (PSR-CC-2aaBTB-2xmyc-loxP-T2A) is not functional by its own. Additionally, preliminary experiments (not shown in this thesis) indicated that episomal expression of the truncated product, which is expressed in K13C580Y\_HR260<sup>endo</sup> parasites after integration (consisting only of the 312 N-terminal bp of the PSR fused to 2xmyc-loxP-T2A: 312bpPSR-2xmyc-loxP-T2A), can't render resistant parasites sensitive and this construct is not correctly localized to the *Kelch13* compartment (Scharf and Spielmann, unpublished). This gives evidence that the observed sensitivity of K13C580Y\_HR260<sup>endo</sup> knock in parasites is unlikely due to an extra *Kelch13* protein product that is complementing the resistant background. Rather, it might be possible that *Kelch13* protein abundance is influenced in this cell line by yet unknown molecular mechanisms. This might

include modifications or influences on the genetic level that might occur during integration in the genomic locus and needs to be further investigated.

## 4.6 Conclusion

This work shows that Kelch13 protein abundance is critical for resistance of *P. falciparum* parasites to artemisinin. It also shows that non-essential Kelch13 compartment proteins influence artemisinin resistance, strengthening the idea that Kelch13 and its compartment neighbors are involved in a common pathway influencing resistance. The domain complementation experiments indicate that Kelch13 is divided into different subdomains that may correspond to a mechanistic part (likely in endocytosis) that seems to reside in the N-terminal part of the protein and a regulatory part that influences the overall activity through a regulation of the stability of the protein. This latter part appears to be contained in the C-terminal, conserved part, of the protein. These results set the stage for further work to elucidate how Kelch13 functions in endocytosis and resistance.

## 5 References

- Abu Bakar, N., Klonis, N., Hanssen, E., Chan, C., & Tilley, L. (2010). Digestive-vacuole genesis and endocytic processes in the early intraerythrocytic stages of *Plasmodium falciparum*. *J Cell Sci*, *123*(Pt 3), 441-450. doi:10.1242/jcs.061499
- Achan, J., Talisuna, A. O., Erhart, A., Yeka, A., Tibenderana, J. K., Baliraine, F. N., . . . D'Alessandro, U. (2011). Quinine, an old anti-malarial drug in a modern world: role in the treatment of malaria. *Malar J*, *10*, 144. doi:10.1186/1475-2875-10-144
- Adams, J., Kelso, R., & Cooley, L. (2000). The kelch repeat superfamily of proteins: propellers of cell function. *Trends in Cell Biology*, *10*(1), 17-24. doi:10.1016/s0962-8924(99)01673-6
- Aikawa, M., Hepler, P. K., Huff, C. G., & Sprinz, H. (1966). The feeding mechanism of avian malarial parasites. *J Cell Biol*, *28*(2), 355-373. doi:10.1083/jcb.28.2.355
- Aly, A. S., Vaughan, A. M., & Kappe, S. H. (2009). Malaria parasite development in the mosquito and infection of the mammalian host. *Annu Rev Microbiol*, *63*, 195-221. doi:10.1146/annurev.micro.091208.073403
- Amaratunga, C., Witkowski, B., Khim, N., Menard, D., & Fairhurst, R. M. (2014). Artemisinin resistance in *Plasmodium falciparum*. *The Lancet Infectious Diseases*, *14*(6), 449-450. doi:10.1016/s1473-3099(14)70777-7
- Anderson, T. J., Haubold, B., Williams, J. T., Estrada-Franco, J. G., Richardson, L., Mollinedo, R., . . . Day, K. P. (2000). Microsatellite markers reveal a spectrum of population structures in the malaria parasite *Plasmodium falciparum*. *Mol Biol Evol*, *17*(10), 1467-1482. doi:10.1093/oxfordjournals.molbev.a026247
- Andersson, D. I., & Hughes, D. (2010). Antibiotic resistance and its cost: is it possible to reverse resistance? *Nat Rev Microbiol*, *8*(4), 260-271. doi:10.1038/nrmicro2319
- Aninagyei, E., Duedu, K. O., Rufai, T., Tetteh, C. D., Chandi, M. G., Ampomah, P., & Acheampong, D. O. (2020). Characterization of putative drug resistant biomarkers in *Plasmodium falciparum* isolated from Ghanaian blood donors. *BMC Infect Dis*, *20*(1), 533. doi:10.1186/s12879-020-05266-2
- Ariey, F., Witkowski, B., Amaratunga, C., Beghain, J., Langlois, A. C., Khim, N., . . . Menard, D. (2014). A molecular marker of artemisinin-resistant *Plasmodium falciparum* malaria. *Nature*, *505*(7481), 50-55. doi:10.1038/nature12876
- Artavanis-Tsakonas, K., Misaghi, S., Comeaux, C. A., Catic, A., Spooner, E., Duraisingh, M. T., & Ploegh, H. L. (2006). Identification by functional proteomics of a deubiquitinating/deNeddylating enzyme in *Plasmodium falciparum*. *Mol Microbiol*, *61*(5), 1187-1195. doi:10.1111/j.1365-2958.2006.05307.x
- Ashley, E. A., Dhorda, M., Fairhurst, R. M., Amaratunga, C., Lim, P., Suon, S., . . . Tracking Resistance to Artemisinin, C. (2014). Spread of artemisinin resistance in *Plasmodium falciparum* malaria. *N Engl J Med*, *371*(5), 411-423. doi:10.1056/NEJMoa1314981
- Ashley, E. A., Pyae Phyo, A., & Woodrow, C. J. (2018). Malaria. *Lancet*, *391*(10130), 1608-1621. doi:10.1016/S0140-6736(18)30324-6
- Atkinson, C. T., & Aikawa, M. (1990). Ultrastructure of malaria-infected erythrocytes. *Blood Cells*, *16*(2-3), 351-368. Retrieved from <https://www.ncbi.nlm.nih.gov/pubmed/2257318>
- Autino, B., Noris, A., Russo, R., & Castelli, F. (2012). Epidemiology of malaria in endemic areas. *Mediterr J Hematol Infect Dis*, *4*(1), e2012060. doi:10.4084/MJHID.2012.060
- Arrow KJ, Panosian C, Gelband H, editors. (2004). Institute of Medicine (US) Committee on the Economics of Antimalarial Drugs. Saving Lives, Buying Time: Economics of Malaria Drugs in an Age of Resistance. Washington (DC): National Academies Press (US). PMID: 25009879.
- Balla, T. (2013). Phosphoinositides: tiny lipids with giant impact on cell regulation. *Physiol Rev*, *93*(3), 1019-1137. doi:10.1152/physrev.00028.2012

- Banerjee, R., and D.E. Goldberg. (2000). The *Plasmodium* food vacuole. Antimalarial Chemotherapy: Mechanisms of Action, Resistance, and New Directions in Drug Discovery. P.J. Rosenthal, editor. Humana Press, Totowa, NJ. 43–63.
- Bargieri, D. Y., Andenmatten, N., Lagal, V., Thiberge, S., Whitelaw, J. A., Tardieux, I., . . . Menard, R. (2013). Apical membrane antigen 1 mediates apicomplexan parasite attachment but is dispensable for host cell invasion. *Nat Commun*, 4, 2552. doi:10.1038/ncomms3552
- Barr, P. J., Green, K. M., Gibson, H. L., Bathurst, I. C., Quakyi, I. A., & Kaslow, D. C. (1991). Recombinant Pfs25 protein of *Plasmodium falciparum* elicits malaria transmission-blocking immunity in experimental animals. *J Exp Med*, 174(5), 1203-1208. doi:10.1084/jem.174.5.1203
- Beck-Johnson, L. M., Nelson, W. A., Paaijmans, K. P., Read, A. F., Thomas, M. B., & Bjornstad, O. N. (2013). The effect of temperature on Anopheles mosquito population dynamics and the potential for malaria transmission. *PLoS One*, 8(11), e79276. doi:10.1371/journal.pone.0079276
- Besteiro, S., Michelin, A., Poncet, J., Dubremetz, J. F., & Lebrun, M. (2009). Export of a *Toxoplasma gondii* rhoptry neck protein complex at the host cell membrane to form the moving junction during invasion. *PLoS Pathog*, 5(2), e1000309. doi:10.1371/journal.ppat.1000309
- Bhattacharjee, S., Coppens, I., Mbengue, A., Suresh, N., Ghorbal, M., Slouka, Z., . . . Haldar, K. (2018). Remodeling of the malaria parasite and host human red cell by vesicle amplification that induces artemisinin resistance. *Blood*, 131(11), 1234-1247. doi:10.1182/blood-2017-11-814665
- Billker, O., Lindo, V., Panico, M., Etienne, A. E., Paxton, T., Dell, A., . . . Morris, H. R. (1998). Identification of xanthurenic acid as the putative inducer of malaria development in the mosquito. *Nature*, 392(6673), 289-292. doi:10.1038/32667
- Billker, O., Shaw, M. K., Margos, G., & Sinden, R. E. (1997). The roles of temperature, pH and mosquito factors as triggers of male and female gametogenesis of *Plasmodium berghei* in vitro. *Parasitology*, 115 (Pt 1), 1-7. doi:10.1017/s0031182097008895
- Birnbaum, J. (2017). A novel genetic system for the functional analysis of essential proteins of the human malaria parasite *Plasmodium falciparum*, Universität Hamburg.
- Birnbaum, J., Flemming, S., Reichard, N., Soares, A. B., Mesen-Ramirez, P., Jonscher, E., . . . Spielmann, T. (2017). A genetic system to study *Plasmodium falciparum* protein function. *Nat Methods*, 14(4), 450-456. doi:10.1038/nmeth.4223
- Birnbaum, J., Scharf, S., Schmidt, S., Jonscher, E., Hoeijmakers, W. A. M., Flemming, S., . . . Spielmann, T. (2020). A Kelch13-defined endocytosis pathway mediates artemisinin resistance in malaria parasites. *Science*, 367(6473), 51-59. doi:10.1126/science.aax4735
- Blancke-Soares, A. (2016). Identification of trafficking determinants in novel PNEPs of the human malaria parasite *Plasmodium falciparum*, Universität Hamburg.
- Blisnick, T., Morales Betoulle, M. E., Barale, J. C., Uzureau, P., Berry, L., Desroses, S., . . . Braun Breton, C. (2000). Pfsbp1, a Maurer's cleft *Plasmodium falciparum* protein, is associated with the erythrocyte skeleton. *Mol Biochem Parasitol*, 111(1), 107-121. doi:10.1016/s0166-6851(00)00301-7
- Boddey, J. A., Hodder, A. N., Gunther, S., Gilson, P. R., Patsiouras, H., Kapp, E. A., . . . Cowman, A. F. (2010). An aspartyl protease directs malaria effector proteins to the host cell. *Nature*, 463(7281), 627-631. doi:10.1038/nature08728
- Boddey, J. A., O'Neill, M. T., Lopaticki, S., Carvalho, T. G., Hodder, A. N., Nebl, T., . . . Cowman, A. F. (2016). Export of malaria proteins requires co-translational processing of the PEXEL motif independent of phosphatidylinositol-3-phosphate binding. *Nat Commun*, 7, 10470. doi:10.1038/ncomms10470
- Boersema, P. J., Raijmakers, R., Lemeer, S., Mohammed, S., & Heck, A. J. (2009). Multiplex peptide stable isotope dimethyl labeling for quantitative proteomics. *Nat Protoc*, 4(4), 484-494. doi:10.1038/nprot.2009.21

- Borrmann, S., Straimer, J., Mwai, L., Abdi, A., Rippert, A., Okombo, J., . . . Clark, T. G. (2013). Genome-wide screen identifies new candidate genes associated with artemisinin susceptibility in *Plasmodium falciparum* in Kenya. *Sci Rep*, 3, 3318. doi:10.1038/srep03318
- Brancucci, N. M. B., Gerdt, J. P., Wang, C., De Niz, M., Philip, N., Adapa, S. R., . . . Marti, M. (2017). Lysophosphatidylcholine Regulates Sexual Stage Differentiation in the Human Malaria Parasite *Plasmodium falciparum*. *Cell*, 171(7), 1532-1544 e1515. doi:10.1016/j.cell.2017.10.020
- Bray, P. G., Mungthin, M., Ridley, R. G., & Ward, S. A. (1998). Access to hematin: the basis of chloroquine resistance. *Mol Pharmacol*, 54(1), 170-179. doi:10.1124/mol.54.1.170
- Bridgford, J. L., Xie, S. C., Cobbold, S. A., Pasaje, C. F. A., Herrmann, S., Yang, T., . . . Tilley, L. (2018). Artemisinin kills malaria parasites by damaging proteins and inhibiting the proteasome. *Nat Commun*, 9(1), 3801. doi:10.1038/s41467-018-06221-1
- Brock, P. M., Fornace, K. M., Parmiter, M., Cox, J., Drakeley, C. J., Ferguson, H. M., & Kao, R. R. (2016). *Plasmodium knowlesi* transmission: integrating quantitative approaches from epidemiology and ecology to understand malaria as a zoonosis. *Parasitology*, 143(4), 389-400. doi:10.1017/S0031182015001821
- Bruce, M. C., Alano, P., Duthie, S., & Carter, R. (1990). Commitment of the malaria parasite *Plasmodium falciparum* to sexual and asexual development. *Parasitology*, 100 Pt 2, 191-200. doi:10.1017/s0031182000061199
- Burkot, T. R., Farlow, R., Min, M., Espino, E., Mnzava, A., & Russell, T. L. (2019). A global analysis of National Malaria Control Programme vector surveillance by elimination and control status in 2018. *Malar J*, 18(1), 399. doi:10.1186/s12936-019-3041-2
- Camponovo, F., Ockenhouse, C. F., Lee, C., & Penny, M. A. (2019). Mass campaigns combining antimalarial drugs and anti-infective vaccines as seasonal interventions for malaria control, elimination and prevention of resurgence: a modelling study. *BMC Infect Dis*, 19(1), 920. doi:10.1186/s12879-019-4467-4
- Carter, R., & Chen, D. H. (1976). Malaria transmission blocked by immunisation with gametes of the malaria parasite. *Nature*, 263(5572), 57-60. doi:10.1038/263057a0
- Carter, R., Mendis, K. N., Miller, L. H., Molineaux, L., & Saul, A. (2000). Malaria transmission-blocking vaccines--how can their development be supported? *Nat Med*, 6(3), 241-244. doi:10.1038/73062
- Cerqueira, G. C., Cheeseman, I. H., Schaffner, S. F., Nair, S., McDew-White, M., Phyto, A. P., . . . Neafsey, D. E. (2017). Longitudinal genomic surveillance of *Plasmodium falciparum* malaria parasites reveals complex genomic architecture of emerging artemisinin resistance. *Genome Biol*, 18(1), 78. doi:10.1186/s13059-017-1204-4
- Chareonviriyaphap, T., Bangs, M. J., & Ratanatham, S. (2000). Status of malaria in Thailand. *Southeast Asian J Trop Med Public Health*, 31(2), 225-237. Retrieved from <https://www.ncbi.nlm.nih.gov/pubmed/11127318>
- Chenet, S. M., Akinyi Okoth, S., Huber, C. S., Chandrabose, J., Lucchi, N. W., Talundzic, E., . . . Udhayakumar, V. (2016). Independent Emergence of the *Plasmodium falciparum* Kelch Propeller Domain Mutant Allele C580Y in Guyana. *J Infect Dis*, 213(9), 1472-1475. doi:10.1093/infdis/jiv752
- Chin, W., Contacos, P. G., Collins, W. E., Jeter, M. H., & Alpert, E. (1968). Experimental mosquito-transmission of *Plasmodium knowlesi* to man and monkey. *Am J Trop Med Hyg*, 17(3), 355-358. doi:10.4269/ajtmh.1968.17.355
- Chitnis, C. E., Chaudhuri, A., Horuk, R., Pogo, A. O., & Miller, L. H. (1996). The domain on the Duffy blood group antigen for binding *Plasmodium vivax* and *P. knowlesi* malarial parasites to erythrocytes. *J Exp Med*, 184(4), 1531-1536. doi:10.1084/jem.184.4.1531
- Chitnis, C. E., Mukherjee, P., Mehta, S., Yazdani, S. S., Dhawan, S., Shakri, A. R., . . . Chauhan, V. S. (2015). Phase I Clinical Trial of a Recombinant Blood Stage Vaccine Candidate for *Plasmodium*

- falciparum Malaria Based on MSP1 and EBA175. *PLoS One*, 10(4), e0117820. doi:10.1371/journal.pone.0117820
- Cho, J., Park, J., Kim, E. E., & Song, E. J. (2020). Assay Systems for Profiling Deubiquitinating Activity. *Int J Mol Sci*, 21(16). doi:10.3390/ijms21165638
- Christoforidis, S., Miaczynska, M., Ashman, K., Wilm, M., Zhao, L., Yip, S.-C., . . . Zerial, M. (1999). Phosphatidylinositol-3-OH kinases are Rab5 effectors. *Nat Cell Biol*, 1(4), 249-252. doi:10.1038/12075
- Collins, W. E., & Jeffery, G. M. (2005). Plasmodium ovale: parasite and disease. *Clin Microbiol Rev*, 18(3), 570-581. doi:10.1128/CMR.18.3.570-581.2005
- Coppee, R., Jeffares, D. C., Miteva, M. A., Sabbagh, A., & Clain, J. (2019). Comparative structural and evolutionary analyses predict functional sites in the artemisinin resistance malaria protein K13. *Sci Rep*, 9(1), 10675. doi:10.1038/s41598-019-47034-6
- Coppi, A., Tewari, R., Bishop, J. R., Bennett, B. L., Lawrence, R., Esko, J. D., . . . Sinnis, P. (2007). Heparan sulfate proteoglycans provide a signal to Plasmodium sporozoites to stop migrating and productively invade host cells. *Cell Host Microbe*, 2(5), 316-327. doi:10.1016/j.chom.2007.10.002
- Cottrell, G., Musset, L., Hubert, V., Le Bras, J., Clain, J., & Atovaquone-Proguanil Treatment Failure Study, G. (2014). Emergence of resistance to atovaquone-proguanil in malaria parasites: insights from computational modeling and clinical case reports. *Antimicrob Agents Chemother*, 58(8), 4504-4514. doi:10.1128/AAC.02550-13
- Cowman, A. F., & Crabb, B. S. (2006). Invasion of red blood cells by malaria parasites. *Cell*, 124(4), 755-766. doi:10.1016/j.cell.2006.02.006
- Cowman, A. F., Healer, J., Marapana, D., & Marsh, K. (2016). Malaria: Biology and Disease. *Cell*, 167(3), 610-624. doi:10.1016/j.cell.2016.07.055
- Cox, F. E. (2002). History of human parasitology. *Clin Microbiol Rev*, 15(4), 595-612. doi:10.1128/cmr.15.4.595-612.2002
- Crabb, B. S., de Koning-Ward, T. F., & Gilson, P. R. (2010). Protein export in Plasmodium parasites: from the endoplasmic reticulum to the vacuolar export machine. *Int J Parasitol*, 40(5), 509-513. doi:10.1016/j.ijpara.2010.02.002
- Crosnier, C., Bustamante, L. Y., Bartholdson, S. J., Bei, A. K., Theron, M., Uchikawa, M., . . . Wright, G. J. (2011). Basigin is a receptor essential for erythrocyte invasion by Plasmodium falciparum. *Nature*, 480(7378), 534-537. doi:10.1038/nature10606
- Curd, F. H., Davey, D. G., & Rose, F. L. (1945). Studies on synthetic antimalarial drugs; some biguanide derivatives as new types of antimalarial substances with both therapeutic and causal prophylactic activity. *Ann Trop Med Parasitol*, 39, 208-216. Retrieved from <https://www.ncbi.nlm.nih.gov/pubmed/21013252>
- Daron, J., Boissière, A., Boundenga, L., Ngoubangoye, B., Houze, S., Arnathau, C., . . . Rougeron, V. (2020). Population genomic evidence of a Southeast Asian origin of Plasmodium vivax. doi:10.1101/2020.04.29.067439
- de Koning-Ward, T. F., Gilson, P. R., Boddey, J. A., Rug, M., Smith, B. J., Papenfuss, A. T., . . . Crabb, B. S. (2009). A newly discovered protein export machine in malaria parasites. *Nature*, 459(7249), 945-949. doi:10.1038/nature08104
- De Niz, M., Burda, P. C., Kaiser, G., Del Portillo, H. A., Spielmann, T., Frischknecht, F., & Heussler, V. T. (2017). Progress in imaging methods: insights gained into Plasmodium biology. *Nat Rev Microbiol*, 15(1), 37-54. doi:10.1038/nrmicro.2016.158
- De Niz, M., Meibalan, E., Mejia, P., Ma, S., Brancucci, N. M. B., Agop-Nersesian, C., . . . Marti, M. (2018). Plasmodium gametocytes display homing and vascular transmigration in the host bone marrow. *Sci Adv*, 4(5), eaat3775. doi:10.1126/sciadv.aat3775
- Delves, M., Plouffe, D., Scheurer, C., Meister, S., Wittlin, S., Winzeler, E. A., . . . Leroy, D. (2012). The activities of current antimalarial drugs on the life cycle stages of Plasmodium: a

- comparative study with human and rodent parasites. *PLoS Med*, 9(2), e1001169. doi:10.1371/journal.pmed.1001169
- Dhanao, B. S., Cogliati, T., Satish, A. G., Bruford, E. A., & Friedman, J. S. (2013). Update on the Kelch-like (KLHL) gene family. *Hum Genomics*, 7, 13. doi:10.1186/1479-7364-7-13
- Diallo, M. A., Yade, M. S., Ndiaye, Y. D., Diallo, I., Diongue, K., Sy, S. A., . . . Ndiaye, D. (2020). Efficacy and safety of artemisinin-based combination therapy and the implications of Pfkclch13 and Pfcoronin molecular markers in treatment failure in Senegal. *Sci Rep*, 10(1), 8907. doi:10.1038/s41598-020-65553-5
- Dondorp, A. M., Yeung, S., White, L., Nguon, C., Day, N. P., Socheat, D., & von Seidlein, L. (2010). Artemisinin resistance: current status and scenarios for containment. *Nat Rev Microbiol*, 8(4), 272-280. doi:10.1038/nrmicro2331
- Douglas, A. D., Baldeviano, G. C., Lucas, C. M., Lugo-Roman, L. A., Crosnier, C., Bartholdson, S. J., . . . Draper, S. J. (2015). A PfrH5-based vaccine is efficacious against heterologous strain blood-stage Plasmodium falciparum infection in aotus monkeys. *Cell Host Microbe*, 17(1), 130-139. doi:10.1016/j.chom.2014.11.017
- Draper, S. J., Sack, B. K., King, C. R., Nielsen, C. M., Rayner, J. C., Higgins, M. K., . . . Seder, R. A. (2018). Malaria Vaccines: Recent Advances and New Horizons. *Cell Host Microbe*, 24(1), 43-56. doi:10.1016/j.chom.2018.06.008
- Duffy, P. E., & Patrick Gorres, J. (2020). Malaria vaccines since 2000: progress, priorities, products. *npj Vaccines*, 5(1). doi:10.1038/s41541-020-0196-3
- Eaton, S., & Martin-Belmonte, F. (2014). Cargo sorting in the endocytic pathway: a key regulator of cell polarity and tissue dynamics. *Cold Spring Harb Perspect Biol*, 6(10), a016899. doi:10.1101/cshperspect.a016899
- Eilers, M., & Schatz, G. (1986). Binding of a specific ligand inhibits import of a purified precursor protein into mitochondria. *Nature*, 322(6076), 228-232. doi:10.1038/322228a0
- Elgoraish, A. G., Elzaki, S. E. G., Ahmed, R. T., Ahmed, A. I., Fadlalmula, H. A., Abdalgader Mohamed, S., . . . El-Sayed, B. B. (2019). Epidemiology and distribution of Plasmodium vivax malaria in Sudan. *Trans R Soc Trop Med Hyg*. doi:10.1093/trstmh/trz044
- Elmendorf, H. G., & Haldar, K. (1994). Plasmodium falciparum exports the Golgi marker sphingomyelin synthase into a tubovesicular network in the cytoplasm of mature erythrocytes. *J Cell Biol*, 124(4), 449-462. doi:10.1083/jcb.124.4.449
- Fidock, D. A., Nomura, T., Talley, A. K., Cooper, R. A., Dzekunov, S. M., Ferdig, M. T., . . . Wellems, T. E. (2000). Mutations in the P. falciparum digestive vacuole transmembrane protein PfCRT and evidence for their role in chloroquine resistance. *Mol Cell*, 6(4), 861-871. doi:10.1016/s1097-2765(05)00077-8
- Francis, S. E., Sullivan, D. J., Jr., & Goldberg, D. E. (1997). Hemoglobin metabolism in the malaria parasite Plasmodium falciparum. *Annu Rev Microbiol*, 51, 97-123. doi:10.1146/annurev.micro.51.1.97
- Frickel, E. M., Quesada, V., Muething, L., Gubbels, M. J., Spooner, E., Ploegh, H., & Artavanis-Tsakonas, K. (2007). Apicomplexan UCHL3 retains dual specificity for ubiquitin and Nedd8 throughout evolution. *Cell Microbiol*, 9(6), 1601-1610. doi:10.1111/j.1462-5822.2007.00896.x
- Friedman, J. S., Ray, J. W., Waseem, N., Johnson, K., Brooks, M. J., Hugosson, T., . . . Swaroop, A. (2009). Mutations in a BTB-Kelch protein, KLHL7, cause autosomal-dominant retinitis pigmentosa. *Am J Hum Genet*, 84(6), 792-800. doi:10.1016/j.ajhg.2009.05.007
- Fry, M., & Pudney, M. (1992). Site of action of the antimalarial hydroxynaphthoquinone, 2-[trans-4-(4'-chlorophenyl) cyclohexyl]-3-hydroxy-1,4-naphthoquinone (566C80). *Biochem Pharmacol*, 43(7), 1545-1553. doi:10.1016/0006-2952(92)90213-3
- Furukawa, M., He, Y. J., Borchers, C., & Xiong, Y. (2003). Targeting of protein ubiquitination by BTB-Cullin 3-Roc1 ubiquitin ligases. *Nat Cell Biol*, 5(11), 1001-1007. doi:10.1038/ncb1056

- Garoff, H., & Ansorge, W. (1981). Improvements of DNA sequencing gels. *Anal Biochem*, *115*(2), 450-457. Retrieved from <https://www.ncbi.nlm.nih.gov/pubmed/7304971>
- Garten, M., Nasamu, A. S., Niles, J. C., Zimmerberg, J., Goldberg, D. E., & Beck, J. R. (2018). EXP2 is a nutrient-permeable channel in the vacuolar membrane of Plasmodium and is essential for protein export via PTEX. *Nat Microbiol*, *3*(10), 1090-1098. doi:10.1038/s41564-018-0222-7
- Gehde, N., Hinrichs, C., Montilla, I., Charpian, S., Lingelbach, K., & Przyborski, J. M. (2009). Protein unfolding is an essential requirement for transport across the parasitophorous vacuolar membrane of Plasmodium falciparum. *Mol Microbiol*, *71*(3), 613-628. doi:10.1111/j.1365-2958.2008.06552.x
- Gibson, D. G., Young, L., Chuang, R. Y., Venter, J. C., Hutchison, C. A., 3rd, & Smith, H. O. (2009). Enzymatic assembly of DNA molecules up to several hundred kilobases. *Nat Methods*, *6*(5), 343-345. doi:10.1038/nmeth.1318
- Gilson, P. R., & Crabb, B. S. (2009). Morphology and kinetics of the three distinct phases of red blood cell invasion by Plasmodium falciparum merozoites. *Int J Parasitol*, *39*(1), 91-96. doi:10.1016/j.ijpara.2008.09.007
- Gnadig, N. F., Stokes, B. H., Edwards, R. L., Kalantarov, G. F., Heimsch, K. C., Kuderjavy, M., . . . Fidock, D. A. (2020). Insights into the intracellular localization, protein associations and artemisinin resistance properties of Plasmodium falciparum K13. *PLoS Pathog*, *16*(4), e1008482. doi:10.1371/journal.ppat.1008482
- Goldberg, D. E. (2005). Hemoglobin degradation. *Curr Top Microbiol Immunol*, *295*, 275-291. doi:10.1007/3-540-29088-5\_11
- Goldberg, D. E., Slater, A. F., Cerami, A., & Henderson, G. B. (1990). Hemoglobin degradation in the malaria parasite Plasmodium falciparum: an ordered process in a unique organelle. *Proc Natl Acad Sci U S A*, *87*(8), 2931-2935. doi:10.1073/pnas.87.8.2931
- Goodman, C. D., Buchanan, H. D., & McFadden, G. I. (2017). Is the Mitochondrion a Good Malaria Drug Target? *Trends Parasitol*, *33*(3), 185-193. doi:10.1016/j.pt.2016.10.002
- Gordo, I., Perfeito, L., & Sousa, A. (2011). Fitness effects of mutations in bacteria. *J Mol Microbiol Biotechnol*, *21*(1-2), 20-35. doi:10.1159/000332747
- Gorvel, J. P., Chavrier, P., Zerial, M., & Gruenberg, J. (1991). rab5 controls early endosome fusion in vitro. *Cell*, *64*(5), 915-925. doi:10.1016/0092-8674(91)90316-q
- Greenwood, B., Dicko, A., Sagara, I., Zongo, I., Tinto, H., Cairns, M., . . . Chandramohan, D. (2017). Seasonal vaccination against malaria: a potential use for an imperfect malaria vaccine. *Malar J*, *16*(1), 182. doi:10.1186/s12936-017-1841-9
- Greenwood, B. M., Fidock, D. A., Kyle, D. E., Kappe, S. H., Alonso, P. L., Collins, F. H., & Duffy, P. E. (2008). Malaria: progress, perils, and prospects for eradication. *J Clin Invest*, *118*(4), 1266-1276. doi:10.1172/JCI33996
- Grotendorst, C. A., Kumar, N., Carter, R., & Kaushal, D. C. (1984). A surface protein expressed during the transformation of zygotes of Plasmodium gallinaceum is a target of transmission-blocking antibodies. *Infect Immun*, *45*(3), 775-777. doi:10.1128/IAI.45.3.775-777.1984
- Group, W. K. G.-P. S. (2019). Association of mutations in the Plasmodium falciparum Kelch13 gene (Pf3D7\_1343700) with parasite clearance rates after artemisinin-based treatments-a WWARN individual patient data meta-analysis. *BMC Med*, *17*(1), 1. doi:10.1186/s12916-018-1207-3
- Gruring, C., Heiber, A., Kruse, F., Flemming, S., Franci, G., Colombo, S. F., . . . Spielmann, T. (2012). Uncovering common principles in protein export of malaria parasites. *Cell Host Microbe*, *12*(5), 717-729. doi:10.1016/j.chom.2012.09.010
- Gruring, C., Heiber, A., Kruse, F., Ungefehr, J., Gilberger, T. W., & Spielmann, T. (2011). Development and host cell modifications of Plasmodium falciparum blood stages in four dimensions. *Nat Commun*, *2*, 165. doi:10.1038/ncomms1169
- Guerra, C. A., Gikandi, P. W., Tatem, A. J., Noor, A. M., Smith, D. L., Hay, S. I., & Snow, R. W. (2008). The limits and intensity of Plasmodium falciparum transmission: implications for

- malaria control and elimination worldwide. *PLoS Med*, 5(2), e38. doi:10.1371/journal.pmed.0050038
- Gupta, V. A., & Beggs, A. H. (2014). Kelch proteins: emerging roles in skeletal muscle development and diseases. *Skelet Muscle*, 4, 11. doi:10.1186/2044-5040-4-11
- Guyatt, H. L., & Snow, R. W. (2004). Impact of malaria during pregnancy on low birth weight in sub-Saharan Africa. *Clin Microbiol Rev*, 17(4), 760-769, table of contents. doi:10.1128/CMR.17.4.760-769.2004
- Haase, S., Herrmann, S., Gruring, C., Heiber, A., Jansen, P. W., Langer, C., . . . Spielmann, T. (2009). Sequence requirements for the export of the Plasmodium falciparum Maurer's clefts protein REX2. *Mol Microbiol*, 71(4), 1003-1017. doi:10.1111/j.1365-2958.2008.06582.x
- Hammond, G. R., Machner, M. P., & Balla, T. (2014). A novel probe for phosphatidylinositol 4-phosphate reveals multiple pools beyond the Golgi. *J Cell Biol*, 205(1), 113-126. doi:10.1083/jcb.201312072
- Hanahan, D. (1983). Studies on transformation of Escherichia coli with plasmids. *J Mol Biol*, 166(4), 557-580. Retrieved from <https://www.ncbi.nlm.nih.gov/pubmed/6345791>
- Harashima, T., Anderson, S., Yates, J. R., 3rd, & Heitman, J. (2006). The kelch proteins Gpb1 and Gpb2 inhibit Ras activity via association with the yeast RasGAP neurofibromin homologs Ira1 and Ira2. *Mol Cell*, 22(6), 819-830. doi:10.1016/j.molcel.2006.05.011
- Hartwig, C. L., Rosenthal, A. S., D'Angelo, J., Griffin, C. E., Posner, G. H., & Cooper, R. A. (2009). Accumulation of artemisinin trioxane derivatives within neutral lipids of Plasmodium falciparum malaria parasites is endoperoxide-dependent. *Biochem Pharmacol*, 77(3), 322-336. doi:10.1016/j.bcp.2008.10.015
- Hawthorne, P. L., Trenholme, K. R., Skinner-Adams, T. S., Spielmann, T., Fischer, K., Dixon, M. W., . . . Gardiner, D. L. (2004). A novel Plasmodium falciparum ring stage protein, REX, is located in Maurer's clefts. *Mol Biochem Parasitol*, 136(2), 181-189. doi:10.1016/j.molbiopara.2004.03.013
- Hayward, R., Saliba, K. J., & Kirk, K. (2005). pfmdr1 mutations associated with chloroquine resistance incur a fitness cost in Plasmodium falciparum. *Mol Microbiol*, 55(4), 1285-1295. doi:10.1111/j.1365-2958.2004.04470.x
- Hehl, A. B., Lekutis, C., Grigg, M. E., Bradley, P. J., Dubremetz, J. F., Ortega-Barria, E., & Boothroyd, J. C. (2000). Toxoplasma gondii homologue of plasmodium apical membrane antigen 1 is involved in invasion of host cells. *Infect Immun*, 68(12), 7078-7086. Retrieved from <https://www.ncbi.nlm.nih.gov/pubmed/11083833>
- Henrici, R. C., van Schalkwyk, D. A., & Sutherland, C. J. (2019). Modification of pfap2mu and pfubp1 Markedly Reduces Ring-Stage Susceptibility of Plasmodium falciparum to Artemisinin In Vitro. *Antimicrob Agents Chemother*, 64(1). doi:10.1128/AAC.01542-19
- Henriques, G., Hallett, R. L., Beshir, K. B., Gadalla, N. B., Johnson, R. E., Burrow, R., . . . Sutherland, C. J. (2014). Directional selection at the pfmdr1, pfcrt, pfubp1, and pfap2mu loci of Plasmodium falciparum in Kenyan children treated with ACT. *J Infect Dis*, 210(12), 2001-2008. doi:10.1093/infdis/jiu358
- Henriques, G., Martinelli, A., Rodrigues, L., Modrzynska, K., Fawcett, R., Houston, D. R., . . . Cravo, P. (2013). Artemisinin resistance in rodent malaria--mutation in the AP2 adaptor mu-chain suggests involvement of endocytosis and membrane protein trafficking. *Malar J*, 12, 118. doi:10.1186/1475-2875-12-118
- Henriques, G., van Schalkwyk, D. A., Burrow, R., Warhurst, D. C., Thompson, E., Baker, D. A., . . . Sutherland, C. J. (2015). The Mu subunit of Plasmodium falciparum clathrin-associated adaptor protein 2 modulates in vitro parasite response to artemisinin and quinine. *Antimicrob Agents Chemother*, 59(5), 2540-2547. doi:10.1128/AAC.04067-14

- Hiller, N. L., Bhattacharjee, S., van Ooij, C., Liolios, K., Harrison, T., Lopez-Estrano, C., & Haldar, K. (2004). A host-targeting signal in virulence proteins reveals a secretome in malarial infection. *Science*, *306*(5703), 1934-1937. doi:10.1126/science.1102737
- Holland, C. A., & Kiechle, F. L. (2005). Point-of-care molecular diagnostic systems--past, present and future. *Curr Opin Microbiol*, *8*(5), 504-509. doi:10.1016/j.mib.2005.08.001
- Holmes, K. K., Bertozzi, S., Bloom, B. R., Jha, P., Gelband, H., DeMaria, L. M., & Horton, S. (2017). Major Infectious Diseases: Key Messages from Disease Control Priorities, Third Edition. In rd, K. K. Holmes, S. Bertozzi, B. R. Bloom, & P. Jha (Eds.), *Major Infectious Diseases*. Washington (DC).
- Huang, F., Takala-Harrison, S., Jacob, C. G., Liu, H., Sun, X., Yang, H., . . . Plowe, C. V. (2015). A Single Mutation in K13 Predominates in Southern China and Is Associated With Delayed Clearance of Plasmodium falciparum Following Artemisinin Treatment. *J Infect Dis*, *212*(10), 1629-1635. doi:10.1093/infdis/jiv249
- Hunt, P., Afonso, A., Creasey, A., Culleton, R., Sidhu, A. B., Logan, J., . . . Cravo, P. (2007). Gene encoding a deubiquitinating enzyme is mutated in artesunate- and chloroquine-resistant rodent malaria parasites. *Mol Microbiol*, *65*(1), 27-40. doi:10.1111/j.1365-2958.2007.05753.x
- Hunt, P., Martinelli, A., Modrzynska, K., Borges, S., Creasey, A., Rodrigues, L., . . . Cravo, P. (2010). Experimental evolution, genetic analysis and genome re-sequencing reveal the mutation conferring artemisinin resistance in an isogenic lineage of malaria parasites. *BMC Genomics*, *11*, 499. doi:10.1186/1471-2164-11-499
- Huotari, J., & Helenius, A. (2011). Endosome maturation. *EMBO J*, *30*(17), 3481-3500. doi:10.1038/emboj.2011.286
- Imai, N., White, M. T., Ghani, A. C., & Drakeley, C. J. (2014). Transmission and control of Plasmodium knowlesi: a mathematical modelling study. *PLoS Negl Trop Dis*, *8*(7), e2978. doi:10.1371/journal.pntd.0002978
- Ito, N., Watanabe-Matsui, M., Igarashi, K., & Murayama, K. (2009). Crystal structure of the Bach1 BTB domain and its regulation of homodimerization. *Genes Cells*, *14*(2), 167-178. doi:10.1111/j.1365-2443.2008.01259.x
- Itoh, K., Wakabayashi, N., Katoh, Y., Ishii, T., Igarashi, K., Engel, J. D., & Yamamoto, M. (1999). Keap1 represses nuclear activation of antioxidant responsive elements by Nrf2 through binding to the amino-terminal Neh2 domain. *Genes Dev*, *13*(1), 76-86. doi:10.1101/gad.13.1.76
- Janes, J. H., Wang, C. P., Levin-Edens, E., Vigan-Womas, I., Guillotte, M., Melcher, M., . . . Smith, J. D. (2011). Investigating the host binding signature on the Plasmodium falciparum PfEMP1 protein family. *PLoS Pathog*, *7*(5), e1002032. doi:10.1371/journal.ppat.1002032
- Janes, K. A. (2015). An analysis of critical factors for quantitative immunoblotting. *Sci Signal*, *8*(371), rs2. doi:10.1126/scisignal.2005966
- Jetten, T. H., Martens, W. J., & Takken, W. (1996). Model stimulations to estimate malaria risk under climate change. *J Med Entomol*, *33*(3), 361-371. doi:10.1093/jmedent/33.3.361
- Jonscher, E. (2018). Identification of proteins involved in host cell cytosol uptake in the human Malaria parasite Plasmodium falciparum, Universität Hamburg.
- Jonscher, E., Flemming, S., Schmitt, M., Sabitzki, R., Reichard, N., Birnbaum, J., . . . Spielmann, T. (2019). PfVPS45 Is Required for Host Cell Cytosol Uptake by Malaria Blood Stage Parasites. *Cell Host Microbe*, *25*(1), 166-173 e165. doi:10.1016/j.chom.2018.11.010
- Josling, G. A., & Llinas, M. (2015). Sexual development in Plasmodium parasites: knowing when it's time to commit. *Nat Rev Microbiol*, *13*(9), 573-587. doi:10.1038/nrmicro3519
- Jovic, M., Sharma, M., Rahajeng, J., & Caplan, S. (2010). The early endosome: a busy sorting station for proteins at the crossroads. *Histol Histopathol*, *25*(1), 99-112. doi:10.14670/HH-25.99
- Kadlecova, Z., Spielman, S. J., Loerke, D., Mohanakrishnan, A., Reed, D. K., & Schmid, S. L. (2017). Regulation of clathrin-mediated endocytosis by hierarchical allosteric activation of AP2. *J Cell Biol*, *216*(1), 167-179. doi:10.1083/jcb.201608071

- Kaksonen, M., & Roux, A. (2018). Mechanisms of clathrin-mediated endocytosis. *Nat Rev Mol Cell Biol*, *19*(5), 313-326. doi:10.1038/nrm.2017.132
- Kang, M. I., Kobayashi, A., Wakabayashi, N., Kim, S. G., & Yamamoto, M. (2004). Scaffolding of Keap1 to the actin cytoskeleton controls the function of Nrf2 as key regulator of cytoprotective phase 2 genes. *Proc Natl Acad Sci U S A*, *101*(7), 2046-2051. doi:10.1073/pnas.0308347100
- Kappe, S. H., Vaughan, A. M., Boddey, J. A., & Cowman, A. F. (2010). That was then but this is now: malaria research in the time of an eradication agenda. *Science*, *328*(5980), 862-866. doi:10.1126/science.1184785
- Kaslow, D. C. (1997). Transmission-blocking vaccines: uses and current status of development. *Int J Parasitol*, *27*(2), 183-189. doi:10.1016/s0020-7519(96)00148-8
- Kim, D. I., Jensen, S. C., Noble, K. A., Kc, B., Roux, K. H., Motamedchaboki, K., & Roux, K. J. (2016). An improved smaller biotin ligase for BioID proximity labeling. *Mol Biol Cell*, *27*(8), 1188-1196. doi:10.1091/mbc.E15-12-0844
- Klonis, N., Xie, S. C., McCaw, J. M., Crespo-Ortiz, M. P., Zaloumis, S. G., Simpson, J. A., & Tilley, L. (2013). Altered temporal response of malaria parasites determines differential sensitivity to artemisinin. *Proc Natl Acad Sci U S A*, *110*(13), 5157-5162. doi:10.1073/pnas.1217452110
- Koonin, E. V., Senkevich, T. G., & Chernos, V. I. (1992). A family of DNA virus genes that consists of fused portions of unrelated cellular genes. *Trends Biochem Sci*, *17*(6), 213-214. doi:10.1016/0968-0004(92)90379-n
- Korsinczky, M., Chen, N., Kotecka, B., Saul, A., Rieckmann, K., & Cheng, Q. (2000). Mutations in Plasmodium falciparum cytochrome b that are associated with atovaquone resistance are located at a putative drug-binding site. *Antimicrob Agents Chemother*, *44*(8), 2100-2108. doi:10.1128/aac.44.8.2100-2108.2000
- Kosh-Naucke, M. (2018). Identification of novel parasitophorous vacuole proteins in P. falciparum parasites using BioID, Universität Hamburg.
- Krishna, S., Bustamante, L., Haynes, R. K., & Staines, H. M. (2008). Artemisinins: their growing importance in medicine. *Trends Pharmacol Sci*, *29*(10), 520-527. doi:10.1016/j.tips.2008.07.004
- Krotoski, W. A., Collins, W. E., Bray, R. S., Garnham, P. C., Cogswell, F. B., Gwadz, R. W., . . . Stanfill, P. S. (1982). Demonstration of hypnozoites in sporozoite-transmitted Plasmodium vivax infection. *Am J Trop Med Hyg*, *31*(6), 1291-1293. doi:10.4269/ajtmh.1982.31.1291
- Krugliak, M., Zhang, J., & Ginsburg, H. (2002). Intraerythrocytic Plasmodium falciparum utilizes only a fraction of the amino acids derived from the digestion of host cell cytosol for the biosynthesis of its proteins. *Mol Biochem Parasitol*, *119*(2), 249-256. doi:10.1016/s0166-6851(01)00427-3
- Kumari, S., Mg, S., & Mayor, S. (2010). Endocytosis unplugged: multiple ways to enter the cell. *Cell Res*, *20*(3), 256-275. doi:10.1038/cr.2010.19
- Kurtovic, L., Boyle, M. J., Opi, D. H., Kennedy, A. T., Tham, W. H., Reiling, L., . . . Beeson, J. G. (2020). Complement in malaria immunity and vaccines. *Immunol Rev*, *293*(1), 38-56. doi:10.1111/imr.12802
- Kyhse-Andersen, J. (1984). Electrophoretic transfer of multiple gels: a simple apparatus without buffer tank for rapid transfer of proteins from polyacrylamide to nitrocellulose. *J Biochem Biophys Methods*, *10*(3-4), 203-209. Retrieved from <https://www.ncbi.nlm.nih.gov/pubmed/6530509>
- Laemmli, U. K. (1970). Cleavage of structural proteins during the assembly of the head of bacteriophage T4. *Nature*, *227*(5259), 680-685. Retrieved from <https://www.ncbi.nlm.nih.gov/pubmed/5432063>
- Lamarque, M. H., Roques, M., Kong-Hap, M., Tonkin, M. L., Rugarabamu, G., Marq, J. B., . . . Lebrun, M. (2014). Plasticity and redundancy among AMA-RON pairs ensure host cell entry of Toxoplasma parasites. *Nat Commun*, *5*, 4098. doi:10.1038/ncomms5098
- Laurens, M. B. (2020). RTS,S/AS01 vaccine (Mosquirix): an overview. *Hum Vaccin Immunother*, *16*(3), 480-489. doi:10.1080/21645515.2019.1669415

- Lazarus, M. D., Schneider, T. G., & Taraschi, T. F. (2008). A new model for hemoglobin ingestion and transport by the human malaria parasite *Plasmodium falciparum*. *J Cell Sci*, *121*(11), 1937-1949. doi:10.1242/jcs.023150
- Lennartz, F., Adams, Y., Bengtsson, A., Olsen, R. W., Turner, L., Ndam, N. T., . . . Jensen, A. T. (2017). Structure-Guided Identification of a Family of Dual Receptor-Binding PfEMP1 that Is Associated with Cerebral Malaria. *Cell Host Microbe*, *21*(3), 403-414. doi:10.1016/j.chom.2017.02.009
- Lim, L., & McFadden, G. I. (2010). The evolution, metabolism and functions of the apicoplast. *Philos Trans R Soc Lond B Biol Sci*, *365*(1541), 749-763. doi:10.1098/rstb.2009.0273
- Liu, B., Blanch, A. J., Namvar, A., Carmo, O., Tiash, S., Andrew, D., . . . Tilley, L. (2019). Multimodal analysis of *Plasmodium knowlesi*-infected erythrocytes reveals large invaginations, swelling of the host cell, and rheological defects. *Cell Microbiol*, *21*(5), e13005. doi:10.1111/cmi.13005
- Lord, S. J., Velle, K. B., Mullins, R. D., & Fritz-Laylin, L. K. (2020). SuperPlots: Communicating reproducibility and variability in cell biology. *J Cell Biol*, *219*(6). doi:10.1083/jcb.202001064
- Mahmoudi, S., & Keshavarz, H. (2017). Efficacy of phase 3 trial of RTS, S/AS01 malaria vaccine: The need for an alternative development plan. *Hum Vaccin Immunother*, *13*(9), 2098-2101. doi:10.1080/21645515.2017.1295906
- Malaria, G. E. N. P. f. C. P. (2016). Genomic epidemiology of artemisinin resistant malaria. *Elife*, *5*. doi:10.7554/eLife.08714
- Malleret, B., Claser, C., Ong, A. S., Suwanarusk, R., Sriprawat, K., Howland, S. W., . . . Renia, L. (2011). A rapid and robust tri-color flow cytometry assay for monitoring malaria parasite development. *Sci Rep*, *1*, 118. doi:10.1038/srep00118
- Marapana, D. S., Dagley, L. F., Sandow, J. J., Nebl, T., Triglia, T., Pasternak, M., . . . Cowman, A. F. (2018). Plasmepsin V cleaves malaria effector proteins in a distinct endoplasmic reticulum translocation interactome for export to the erythrocyte. *Nat Microbiol*, *3*(9), 1010-1022. doi:10.1038/s41564-018-0219-2
- Marcus, E. (2014). Credibility and reproducibility. *Cell*, *159*(5), 965-966. doi:10.1016/j.cell.2014.11.016
- Martell, J. D., Deerinck, T. J., Sancak, Y., Poulos, T. L., Mootha, V. K., Sosinsky, G. E., . . . Ting, A. Y. (2012). Engineered ascorbate peroxidase as a genetically encoded reporter for electron microscopy. *Nat Biotechnol*, *30*(11), 1143-1148. doi:10.1038/nbt.2375
- Marti, M., Baum, J., Rug, M., Tilley, L., & Cowman, A. F. (2005). Signal-mediated export of proteins from the malaria parasite to the host erythrocyte. *J Cell Biol*, *171*(4), 587-592. doi:10.1083/jcb.200508051
- Marti, M., Good, R. T., Rug, M., Knuepfer, E., & Cowman, A. F. (2004). Targeting malaria virulence and remodeling proteins to the host erythrocyte. *Science*, *306*(5703), 1930-1933. doi:10.1126/science.1102452
- Martzoukou, O., Amillis, S., Zervakou, A., Christoforidis, S., & Diallinas, G. (2017). The AP-2 complex has a specialized clathrin-independent role in apical endocytosis and polar growth in fungi. *Elife*, *6*. doi:10.7554/eLife.20083
- Maurer, G. (1902). Die Malaria perniciosa. *Centralblatt für Bakteriologie. Parasitenkunde und Infektionskrankheiten* *32*:695-719.
- Mbengue, A., Bhattacharjee, S., Pandharkar, T., Liu, H., Estiu, G., Stahelin, R. V., . . . Haldar, K. (2015). A molecular mechanism of artemisinin resistance in *Plasmodium falciparum* malaria. *Nature*, *520*(7549), 683-687. doi:10.1038/nature14412
- McMahon, H. T., & Boucrot, E. (2011). Molecular mechanism and physiological functions of clathrin-mediated endocytosis. *Nat Rev Mol Cell Biol*, *12*(8), 517-533. doi:10.1038/nrm3151
- McMillan, P. J., Millet, C., Batinovic, S., Maiorca, M., Hanssen, E., Kenny, S., . . . Tilley, L. (2013). Spatial and temporal mapping of the PfEMP1 export pathway in *Plasmodium falciparum*. *Cell Microbiol*, *15*(8), 1401-1418. doi:10.1111/cmi.12125

- Melnick, A., Ahmad, K. F., Arai, S., Polinger, A., Ball, H., Borden, K. L., . . . Licht, J. D. (2000). In-depth mutational analysis of the promyelocytic leukemia zinc finger BTB/POZ domain reveals motifs and residues required for biological and transcriptional functions. *Mol Cell Biol*, *20*(17), 6550-6567. doi:10.1128/mcb.20.17.6550-6567.2000
- Menard, D., Khim, N., Beghain, J., Adegnik, A. A., Shafiul-Alam, M., Amodu, O., . . . Consortium, K. (2016). A Worldwide Map of Plasmodium falciparum K13-Propeller Polymorphisms. *N Engl J Med*, *374*(25), 2453-2464. doi:10.1056/NEJMoa1513137
- Mercereau-Puijalon, O., & Menard, D. (2010). Plasmodium vivax and the Duffy antigen: a paradigm revisited. *Transfus Clin Biol*, *17*(3), 176-183. doi:10.1016/j.tracli.2010.06.005
- Merritt, R. W., Dadd, R. H., & Walker, E. D. (1992). Feeding behavior, natural food, and nutritional relationships of larval mosquitoes. *Annu Rev Entomol*, *37*, 349-376. doi:10.1146/annurev.en.37.010192.002025
- Mesen-Ramirez, P., Bergmann, B., Tran, T. T., Garten, M., Stacker, J., Naranjo-Prado, I., . . . Spielmann, T. (2019). EXP1 is critical for nutrient uptake across the parasitophorous vacuole membrane of malaria parasites. *PLoS Biol*, *17*(9), e3000473. doi:10.1371/journal.pbio.3000473
- Mesen-Ramirez, P., Reinsch, F., Blancke Soares, A., Bergmann, B., Ullrich, A. K., Tenzer, S., & Spielmann, T. (2016). Stable Translocation Intermediates Jam Global Protein Export in Plasmodium falciparum Parasites and Link the PTEX Component EXP2 with Translocation Activity. *PLoS Pathog*, *12*(5), e1005618. doi:10.1371/journal.ppat.1005618
- Meshnick, S. R., Thomas, A., Ranz, A., Xu, C. M., & Pan, H. Z. (1991). Artemisinin (qinghaosu): the role of intracellular heme in its mechanism of antimalarial action. *Mol Biochem Parasitol*, *49*(2), 181-189. doi:10.1016/0166-6851(91)90062-b
- Mikolajczak, S. A., Vaughan, A. M., Kangwanransan, N., Roobsoong, W., Fishbaugher, M., Yimamnuaychok, N., . . . Kappe, S. H. (2015). Plasmodium vivax liver stage development and hypnozoite persistence in human liver-chimeric mice. *Cell Host Microbe*, *17*(4), 526-535. doi:10.1016/j.chom.2015.02.011
- Miotto, O., Amato, R., Ashley, E. A., MacInnis, B., Almagro-Garcia, J., Amaratunga, C., . . . Kwiatkowski, D. P. (2015). Genetic architecture of artemisinin-resistant Plasmodium falciparum. *Nat Genet*, *47*(3), 226-234. doi:10.1038/ng.3189
- Miotto, O., Sekihara, M., Tachibana, S. I., Yamauchi, M., Pearson, R. D., Amato, R., . . . Mita, T. (2020). Emergence of artemisinin-resistant Plasmodium falciparum with kelch13 C580Y mutations on the island of New Guinea. *PLoS Pathog*, *16*(12), e1009133. doi:10.1371/journal.ppat.1009133
- Mok, S., Ashley, E. A., Ferreira, P. E., Zhu, L., Lin, Z., Yeo, T., . . . Bozdech, Z. (2015). Drug resistance. Population transcriptomics of human malaria parasites reveals the mechanism of artemisinin resistance. *Science*, *347*(6220), 431-435. doi:10.1126/science.1260403
- Mok, S., Stokes, B. H., Gnädig, N. F., Ross, L. S., Yeo, T., Amaratunga, C., . . . Fidock, D. A. (2021). Artemisinin-resistant K13 mutations rewire Plasmodium falciparum's intra-erythrocytic metabolic program to enhance survival. *Nat Commun*, *12*(1), 530. doi:10.1038/s41467-020-20805-w
- Mundwiler-Pachlatko, E., & Beck, H. P. (2013). Maurer's clefts, the enigma of Plasmodium falciparum. *Proc Natl Acad Sci U S A*, *110*(50), 19987-19994. doi:10.1073/pnas.1309247110
- Murphy, R. M., & Lamb, G. D. (2013). Important considerations for protein analyses using antibody based techniques: down-sizing Western blotting up-sizes outcomes. *J Physiol*, *591*(23), 5823-5831. doi:10.1113/jphysiol.2013.263251
- Murzin, A. G. (1992). Structural principles for the propeller assembly of beta-sheets: the preference for seven-fold symmetry. *Proteins*, *14*(2), 191-201. doi:10.1002/prot.340140206
- Mustiere, R., Vanelle, P., & Primas, N. (2020). Plasmodial Kinase Inhibitors Targeting Malaria: Recent Developments. *Molecules*, *25*(24). doi:10.3390/molecules25245949
- Nagano, M., Toshima, J. Y., & Toshima, J. (2015). [Rab GTPases networks in membrane traffic in Saccharomyces cerevisiae]. *Yakugaku Zasshi*, *135*(3), 483-492. doi:10.1248/yakushi.14-00246

- Nair, S., Li, X., Arya, G. A., McDew-White, M., Ferrari, M., Nosten, F., & Anderson, T. J. C. (2018). Fitness Costs and the Rapid Spread of kelch13-C580Y Substitutions Conferring Artemisinin Resistance. *Antimicrob Agents Chemother*, *62*(9). doi:10.1128/AAC.00605-18
- Nilsson, S. K., Childs, L. M., Buckee, C., & Marti, M. (2015). Targeting Human Transmission Biology for Malaria Elimination. *PLoS Pathog*, *11*(6), e1004871. doi:10.1371/journal.ppat.1004871
- Nobel-Media. (2015). The Nobel Prize in Physiology or Medicine 2015. Retrieved from <https://www.nobelprize.org/prizes/medicine/2015/press-release/>
- Noedl, H., Se, Y., Schaecher, K., Smith, B. L., Socheat, D., Fukuda, M. M., & Artemisinin Resistance in Cambodia 1 Study, C. (2008). Evidence of artemisinin-resistant malaria in western Cambodia. *N Engl J Med*, *359*(24), 2619-2620. doi:10.1056/NEJMc0805011
- Nussenzweig, R. S., Vanderberg, J., Most, H., & Orton, C. (1967). Protective immunity produced by the injection of x-irradiated sporozoites of plasmodium berghei. *Nature*, *216*(5111), 160-162. doi:10.1038/216160a0
- O'Donnell, R. A., Saul, A., Cowman, A. F., & Crabb, B. S. (2000). Functional conservation of the malaria vaccine antigen MSP-119 across distantly related Plasmodium species. *Nat Med*, *6*(1), 91-95. doi:10.1038/71595
- O'Neill, P. M., Barton, V. E., & Ward, S. A. (2010). The molecular mechanism of action of artemisinin—the debate continues. *Molecules*, *15*(3), 1705-1721. doi:10.3390/molecules15031705
- Obsomer, V., Dufrene, M., Defourny, P., & Coosemans, M. (2013). Anopheles species associations in Southeast Asia: indicator species and environmental influences. *Parasit Vectors*, *6*, 136. doi:10.1186/1756-3305-6-136
- Paaijmans, K. P., Blanford, S., Bell, A. S., Blanford, J. I., Read, A. F., & Thomas, M. B. (2010). Influence of climate on malaria transmission depends on daily temperature variation. *Proc Natl Acad Sci U S A*, *107*(34), 15135-15139. doi:10.1073/pnas.1006422107
- Pagola, S., Stephens, P. W., Bohle, D. S., Kosar, A. D., & Madsen, S. K. (2000). The structure of malaria pigment beta-haematin. *Nature*, *404*(6775), 307-310. doi:10.1038/35005132
- Payne, D. (1987). Spread of chloroquine resistance in Plasmodium falciparum. *Parasitol Today*, *3*(8), 241-246. doi:10.1016/0169-4758(87)90147-5
- Payne, R. O., Milne, K. H., Elias, S. C., Edwards, N. J., Douglas, A. D., Brown, R. E., . . . Draper, S. J. (2016). Demonstration of the Blood-Stage Plasmodium falciparum Controlled Human Malaria Infection Model to Assess Efficacy of the P. falciparum Apical Membrane Antigen 1 Vaccine, FMP2.1/AS01. *J Infect Dis*, *213*(11), 1743-1751. doi:10.1093/infdis/jiw039
- Payne, R. O., Silk, S. E., Elias, S. C., Miura, K., Diouf, A., Galaway, F., . . . Draper, S. J. (2017). Human vaccination against RH5 induces neutralizing antimalarial antibodies that inhibit RH5 invasion complex interactions. *JCI Insight*, *2*(21). doi:10.1172/jci.insight.96381
- Perez-Torrado, R., Yamada, D., & Defosse, P. A. (2006). Born to bind: the BTB protein-protein interaction domain. *Bioessays*, *28*(12), 1194-1202. doi:10.1002/bies.20500
- Peters, J. M., Chen, N., Gatton, M., Korsinczky, M., Fowler, E. V., Manzetti, S., . . . Cheng, Q. (2002). Mutations in cytochrome b resulting in atovaquone resistance are associated with loss of fitness in Plasmodium falciparum. *Antimicrob Agents Chemother*, *46*(8), 2435-2441. doi:10.1128/aac.46.8.2435-2441.2002
- Phyo, A. P., Nkhoma, S., Stepniewska, K., Ashley, E. A., Nair, S., McGready, R., . . . Nosten, F. (2012). Emergence of artemisinin-resistant malaria on the western border of Thailand: a longitudinal study. *The Lancet*, *379*(9830), 1960-1966. doi:10.1016/s0140-6736(12)60484-x
- Pillai-Kastoori, L., Schutz-Geschwender, A. R., & Harford, J. A. (2020). A systematic approach to quantitative Western blot analysis. *Anal Biochem*, *593*, 113608. doi:10.1016/j.ab.2020.113608
- Pinzon-Ortiz, C., Friedman, J., Esko, J., & Sinnis, P. (2001). The binding of the circumsporozoite protein to cell surface heparan sulfate proteoglycans is required for plasmodium sporozoite attachment to target cells. *J Biol Chem*, *276*(29), 26784-26791. doi:10.1074/jbc.M104038200

- Ponder, E. L., & Bogyo, M. (2007). Ubiquitin-like modifiers and their deconjugating enzymes in medically important parasitic protozoa. *Eukaryot Cell*, 6(11), 1943-1952. doi:10.1128/EC.00282-07
- Prag, S., & Adams, J. C. (2003). Molecular phylogeny of the kelch-repeat superfamily reveals an expansion of BTB/kelch proteins in animals. *BMC Bioinformatics*, 4, 42. doi:10.1186/1471-2105-4-42
- Price, R. N., Commons, R. J., Battle, K. E., Thriemer, K., & Mendis, K. (2020). Plasmodium vivax in the Era of the Shrinking P. falciparum Map. *Trends Parasitol*, 36(6), 560-570. doi:10.1016/j.pt.2020.03.009
- Price, R. N., Uhlemann, A.-C., Brockman, A., McGready, R., Ashley, E., Phaipun, L., . . . Krishna, S. (2004). Mefloquine resistance in Plasmodium falciparum and increased pfmdr1 gene copy number. *The Lancet*, 364(9432), 438-447. doi:10.1016/s0140-6736(04)16767-6
- Rahimi, B. A., Thakkinstian, A., White, N. J., Sirivichayakul, C., Dondorp, A. M., & Chokejindachai, W. (2014). Severe vivax malaria: a systematic review and meta-analysis of clinical studies since 1900. *Malar J*, 13, 481. doi:10.1186/1475-2875-13-481
- Regenass-Klotz (2009) Malaria. In: Tropenkrankheiten und Molekularbiologie. Birkhäuser Basel. [https://doi.org/10.1007/978-3-7643-8713-6\\_1](https://doi.org/10.1007/978-3-7643-8713-6_1)
- Rodrigues, C. D., Hannus, M., Prudencio, M., Martin, C., Goncalves, L. A., Portugal, S., . . . Mota, M. M. (2008). Host scavenger receptor SR-BI plays a dual role in the establishment of malaria parasite liver infection. *Cell Host Microbe*, 4(3), 271-282. doi:10.1016/j.chom.2008.07.012
- Rosenthal, P. J. (2013). The interplay between drug resistance and fitness in malaria parasites. *Mol Microbiol*, 89(6), 1025-1038. doi:10.1111/mmi.12349
- Rosenthal, P. J., John, C. C., & Rabinovich, N. R. (2019). Malaria: How Are We Doing and How Can We Do Better? *Am J Trop Med Hyg*, 100(2), 239-241. doi:10.4269/ajtmh.18-0997
- Ross, R. (2002). The role of the mosquito in the evolution of the malarial parasite: the recent researches of Surgeon-Major Ronald Ross, I.M.S. 1898. *Yale J Biol Med*, 75(2), 103-105. Retrieved from <https://www.ncbi.nlm.nih.gov/pubmed/12230308>
- Roux, K. J., Kim, D. I., & Burke, B. (2013). BioID: a screen for protein-protein interactions. *Curr Protoc Protein Sci*, 74, 19 23 11-19 23 14. doi:10.1002/0471140864.ps1923s74
- Rts, S. C. T. P. (2015). Efficacy and safety of RTS,S/AS01 malaria vaccine with or without a booster dose in infants and children in Africa: final results of a phase 3, individually randomised, controlled trial. *Lancet*, 386(9988), 31-45. doi:10.1016/S0140-6736(15)60721-8
- Rug, M., Cyrklaff, M., Mikkonen, A., Lemgruber, L., Kuelzer, S., Sanchez, C. P., . . . Cowman, A. F. (2014). Export of virulence proteins by malaria-infected erythrocytes involves remodeling of host actin cytoskeleton. *Blood*, 124(23), 3459-3468. doi:10.1182/blood-2014-06-583054
- Russo, I., Babbitt, S., Muralidharan, V., Butler, T., Oksman, A., & Goldberg, D. E. (2010). Plasmepsin V licenses Plasmodium proteins for export into the host erythrocyte. *Nature*, 463(7281), 632-636. doi:10.1038/nature08726
- Sabharanjak, S., Sharma, P., Parton, R. G., & Mayor, S. (2002). GPI-anchored proteins are delivered to recycling endosomes via a distinct cdc42-regulated, clathrin-independent pinocytic pathway. *Dev Cell*, 2(4), 411-423. doi:10.1016/s1534-5807(02)00145-4
- Saralamba, S., Pan-Ngum, W., Maude, R. J., Lee, S. J., Tarning, J., Lindegardh, N., . . . White, L. J. (2011). Intrahost modeling of artemisinin resistance in Plasmodium falciparum. *Proc Natl Acad Sci U S A*, 108(1), 397-402. doi:10.1073/pnas.1006113108
- Saridaki, T., Frohlich, K. S., Braun-Breton, C., & Lanzer, M. (2009). Export of PfSBP1 to the Plasmodium falciparum Maurer's clefts. *Traffic*, 10(2), 137-152. doi:10.1111/j.1600-0854.2008.00860.x
- Schmidt, H., Lee, Y., Collier, T. C., Hanemaaijer, M. J., Kirstein, O. D., Ouledi, A., . . . Lanzaro, G. C. (2019). Transcontinental dispersal of Anopheles gambiae occurred from West African origin via serial founder events. *Commun Biol*, 2, 473. doi:10.1038/s42003-019-0717-7

- Sharma, A. I., Shin, S. H., Bopp, S., Volkman, S. K., Hartl, D. L., & Wirth, D. F. (2020). Genetic background and PfKelch13 affect artemisinin susceptibility of PfCoronin mutants in *Plasmodium falciparum*. *PLoS Genet*, *16*(12), e1009266. doi:10.1371/journal.pgen.1009266
- Sherman, I. W. (1977). Amino acid metabolism and protein synthesis in malarial parasites. *Bull World Health Organ*, *55*(2-3), 265-276. Retrieved from <https://www.ncbi.nlm.nih.gov/pubmed/338183>
- Shortt, H. E., Garnham, P. C., & et al. (1948). The pre-erythrocytic stage of human malaria, *Plasmodium vivax*. *Br Med J*, *1*(4550), 547. doi:10.1136/bmj.1.4550.547
- Siddiqui, G., Srivastava, A., ARussell, A.S., Creek, D.J., (2017) Multi-omics Based Identification of Specific Biochemical Changes Associated With PfKelch13-Mutant Artemisinin-Resistant *Plasmodium falciparum*. *The Journal of Infectious Diseases*, *215*, 1435–1444. doi.org/10.1093/infdis/jix156
- Siddiqui, F. A., Boonhok, R., Cabrera, M., Mbenda, H. G. N., Wang, M., Min, H., . . . Cui, L. (2020). Role of *Plasmodium falciparum* Kelch 13 Protein Mutations in *P. falciparum* Populations from Northeastern Myanmar in Mediating Artemisinin Resistance. *mBio*, *11*(1). doi:10.1128/mBio.01134-19
- Silva, M., Ferreira, P. E., Otienoburu, S. D., Calcada, C., Ngasala, B., Bjorkman, A., . . . Veiga, M. I. (2019). *Plasmodium falciparum* K13 expression associated with parasite clearance during artemisinin-based combination therapy. *J Antimicrob Chemother*, *74*(7), 1890-1893. doi:10.1093/jac/dkz098
- Singh, B., & Daneshvar, C. (2013). Human infections and detection of *Plasmodium knowlesi*. *Clin Microbiol Rev*, *26*(2), 165-184. doi:10.1128/CMR.00079-12
- Singh, B., Kim Sung, L., Matusop, A., Radhakrishnan, A., Shamsul, S. S., Cox-Singh, J., . . . Conway, D. J. (2004). A large focus of naturally acquired *Plasmodium knowlesi* infections in human beings. *Lancet*, *363*(9414), 1017-1024. doi:10.1016/S0140-6736(04)15836-4
- Sinka, M. E., Bangs, M. J., Manguin, S., Rubio-Palis, Y., Chareonviriyaphap, T., Coetzee, M., . . . Hay, S. I. (2012). A global map of dominant malaria vectors. *Parasit Vectors*, *5*, 69. doi:10.1186/1756-3305-5-69
- Sirima, S. B., Cousens, S., & Druilhe, P. (2011). Protection against malaria by MSP3 candidate vaccine. *N Engl J Med*, *365*(11), 1062-1064. doi:10.1056/NEJMc1100670
- Smythe, W. A., Joiner, K. A., & Hoppe, H. C. (2008). Actin is required for endocytic trafficking in the malaria parasite *Plasmodium falciparum*. *Cell Microbiol*, *10*(2), 452-464. doi:10.1111/j.1462-5822.2007.01058.x
- Soltysik-Espanola, M., Rogers, R. A., Jiang, S., Kim, T. A., Gaedigk, R., White, R. A., . . . Avraham, S. (1999). Characterization of Mayven, a novel actin-binding protein predominantly expressed in brain. *Mol Biol Cell*, *10*(7), 2361-2375. doi:10.1091/mbc.10.7.2361
- Sorkin, A., & von Zastrow, M. (2009). Endocytosis and signalling: intertwining molecular networks. *Nat Rev Mol Cell Biol*, *10*(9), 609-622. doi:10.1038/nrm2748
- Spielmann, T., Gras, S., Sabitzki, R., & Meissner, M. (2020). Endocytosis in *Plasmodium* and *Toxoplasma* Parasites. *Trends Parasitol*, *36*(6), 520-532. doi:10.1016/j.pt.2020.03.010
- Spielmann, T., Hawthorne, P. L., Dixon, M. W., Hannemann, M., Klotz, K., Kemp, D. J., . . . Gardiner, D. L. (2006). A cluster of ring stage-specific genes linked to a locus implicated in cytoadherence in *Plasmodium falciparum* codes for PEXEL-negative and PEXEL-positive proteins exported into the host cell. *Mol Biol Cell*, *17*(8), 3613-3624. doi:10.1091/mbc.e06-04-0291
- Spring, M. D., Cummings, J. F., Ockenhouse, C. F., Dutta, S., Reidler, R., Angov, E., . . . Heppner, D. G., Jr. (2009). Phase 1/2a study of the malaria vaccine candidate apical membrane antigen-1 (AMA-1) administered in adjuvant system AS01B or AS02A. *PLoS One*, *4*(4), e5254. doi:10.1371/journal.pone.0005254
- Spycher, C., Klonis, N., Spielmann, T., Kump, E., Steiger, S., Tilley, L., & Beck, H. P. (2003). MAHRP-1, a novel *Plasmodium falciparum* histidine-rich protein, binds ferriprotoporphyrin IX and

- localizes to the Maurer's clefts. *J Biol Chem*, 278(37), 35373-35383. doi:10.1074/jbc.M305851200
- Srivastava, I. K., & Vaidya, A. B. (1999). A mechanism for the synergistic antimalarial action of atovaquone and proguanil. *Antimicrob Agents Chemother*, 43(6), 1334-1339. doi:10.1128/AAC.43.6.1334
- Stokes, B. H., Rubiano, K., Dhingra, S. K., Mok, S., Straimer, J., Gnädig, N. F., . . . Fidock, D. A. (2021). doi:10.1101/2021.01.05.425445
- Straimer, J., Gnädig, N. F., Stokes, B. H., Ehrenberger, M., Crane, A. A., & Fidock, D. A. (2017). Plasmodium falciparum K13 Mutations Differentially Impact Ozonide Susceptibility and Parasite Fitness In Vitro. *mBio*, 8(2). doi:10.1128/mBio.00172-17
- Straimer, J., Gnädig, N. F., Witkowski, B., Amaratunga, C., Duru, V., Ramadani, A. P., . . . Fidock, D. A. (2015). Drug resistance. K13-propeller mutations confer artemisinin resistance in Plasmodium falciparum clinical isolates. *Science*, 347(6220), 428-431. doi:10.1126/science.1260867
- Sturm, A., Amino, R., van de Sand, C., Regen, T., Retzlaff, S., Rennenberg, A., . . . Heussler, V. T. (2006). Manipulation of host hepatocytes by the malaria parasite for delivery into liver sinusoids. *Science*, 313(5791), 1287-1290. doi:10.1126/science.1129720
- Su, X. Z., Heatwole, V. M., Wertheimer, S. P., Guinet, F., Herrfeldt, J. A., Peterson, D. S., . . . Wellems, T. E. (1995). The large diverse gene family var encodes proteins involved in cytoadherence and antigenic variation of Plasmodium falciparum-infected erythrocytes. *Cell*, 82(1), 89-100. doi:10.1016/0092-8674(95)90055-1
- Takala-Harrison, S., Clark, T. G., Jacob, C. G., Cummings, M. P., Miotto, O., Dondorp, A. M., . . . Plowe, C. V. (2013). Genetic loci associated with delayed clearance of Plasmodium falciparum following artemisinin treatment in Southeast Asia. *Proc Natl Acad Sci U S A*, 110(1), 240-245. doi:10.1073/pnas.1211205110
- Tangpukdee, N., Duangdee, C., Wilairatana, P., & Krudsood, S. (2009). Malaria diagnosis: a brief review. *Korean J Parasitol*, 47(2), 93-102. doi:10.3347/kjp.2009.47.2.93
- Tebar, F., Sorkina, T., Sorkin, A., Ericsson, M., & Kirchhausen, T. (1996). Eps15 is a component of clathrin-coated pits and vesicles and is located at the rim of coated pits. *J Biol Chem*, 271(46), 28727-28730. doi:10.1074/jbc.271.46.28727
- Tilley, L., Straimer, J., Gnädig, N. F., Ralph, S. A., & Fidock, D. A. (2016). Artemisinin Action and Resistance in Plasmodium falciparum. *Trends Parasitol*, 32(9), 682-696. doi:10.1016/j.pt.2016.05.010
- Trager, W., & Jensen, J. B. (1976). Human malaria parasites in continuous culture. *Science*, 193(4254), 673-675. Retrieved from <https://www.ncbi.nlm.nih.gov/pubmed/781840>
- Triglia, T., Healer, J., Caruana, S. R., Hodder, A. N., Anders, R. F., Crabb, B. S., & Cowman, A. F. (2000). Apical membrane antigen 1 plays a central role in erythrocyte invasion by Plasmodium species. *Mol Microbiol*, 38(4), 706-718. Retrieved from <https://www.ncbi.nlm.nih.gov/pubmed/11115107>
- Tse, E. G., Korsik, M., & Todd, M. H. (2019). The past, present and future of anti-malarial medicines. *Malar J*, 18(1), 93. doi:10.1186/s12936-019-2724-z
- Tu, Y. (2011). The discovery of artemisinin (qinghaosu) and gifts from Chinese medicine. *Nat Med*, 17(10), 1217-1220. doi:10.1038/nm.2471
- Tu, Y. Y., Ni, M. Y., Zhong, Y. R., Li, L. N., Cui, S. L., Zhang, M. Q., . . . Liang, X. T. (1981). [Studies on the constituents of Artemisia annua L. (author's transl)]. *Yao Xue Xue Bao*, 16(5), 366-370. Retrieved from <https://www.ncbi.nlm.nih.gov/pubmed/7246183>
- Umlas, J., & Fallon, J. N. (1971). New thick-film technique for malaria diagnosis. Use of saponin stromatolytic solution for lysis. *Am J Trop Med Hyg*, 20(4), 527-529. Retrieved from <https://www.ncbi.nlm.nih.gov/pubmed/4105462>

- Uwimana, A., Legrand, E., Stokes, B. H., Ndikumana, J. M., Warsame, M., Umulisa, N., . . . Menard, D. (2020). Emergence and clonal expansion of in vitro artemisinin-resistant *Plasmodium falciparum* kelch13 R561H mutant parasites in Rwanda. *Nat Med*, 26(10), 1602-1608. doi:10.1038/s41591-020-1005-2
- van Bergen En Henegouwen, P. M. (2009). Eps15: a multifunctional adaptor protein regulating intracellular trafficking. *Cell Commun Signal*, 7, 24. doi:10.1186/1478-811X-7-24
- van den Heuvel, S. (2004). Protein Degradation: CUL-3 and BTB – Partners in Proteolysis. *Current Biology*, 14(2), R59-R61. doi:10.1016/j.cub.2003.12.044
- van der Pluijm, R. W., Imwong, M., Chau, N. H., Hoa, N. T., Thuy-Nhien, N. T., Thanh, N. V., . . . Dondorp, A. M. (2019). Determinants of dihydroartemisinin-piperaquine treatment failure in *Plasmodium falciparum* malaria in Cambodia, Thailand, and Vietnam: a prospective clinical, pharmacological, and genetic study. *The Lancet Infectious Diseases*, 19(9), 952-961. doi:10.1016/s1473-3099(19)30391-3
- van Dooren, G. G., Marti, M., Tonkin, C. J., Stimmler, L. M., Cowman, A. F., & McFadden, G. I. (2005). Development of the endoplasmic reticulum, mitochondrion and apicoplast during the asexual life cycle of *Plasmodium falciparum*. *Mol Microbiol*, 57(2), 405-419. doi:10.1111/j.1365-2958.2005.04699.x
- Varnai, P., Thyagarajan, B., Rohacs, T., & Balla, T. (2006). Rapidly inducible changes in phosphatidylinositol 4,5-bisphosphate levels influence multiple regulatory functions of the lipid in intact living cells. *J Cell Biol*, 175(3), 377-382. doi:10.1083/jcb.200607116
- Verdier, F., Le Bras, J., Clavier, F., Hatin, I., & Blayo, M. C. (1985). Chloroquine uptake by *Plasmodium falciparum*-infected human erythrocytes during in vitro culture and its relationship to chloroquine resistance. *Antimicrob Agents Chemother*, 27(4), 561-564. doi:10.1128/aac.27.4.561
- Volz, J. C., Yap, A., Sisquella, X., Thompson, J. K., Lim, N. T., Whitehead, L. W., . . . Cowman, A. F. (2016). Essential Role of the PfRh5/PfRipr/CyRPA Complex during *Plasmodium falciparum* Invasion of Erythrocytes. *Cell Host Microbe*, 20(1), 60-71. doi:10.1016/j.chom.2016.06.004
- Wang, J., Zhang, C. J., Chia, W. N., Loh, C. C., Li, Z., Lee, Y. M., . . . Lin, Q. (2015). Haem-activated promiscuous targeting of artemisinin in *Plasmodium falciparum*. *Nat Commun*, 6, 10111. doi:10.1038/ncomms10111
- Weiss, G. E., Crabb, B. S., & Gilson, P. R. (2016). Overlaying Molecular and Temporal Aspects of Malaria Parasite Invasion. *Trends Parasitol*, 32(4), 284-295. doi:10.1016/j.pt.2015.12.007
- Weiss, G. E., Gilson, P. R., Taechalerpaisarn, T., Tham, W. H., de Jong, N. W., Harvey, K. L., . . . Crabb, B. S. (2015). Revealing the sequence and resulting cellular morphology of receptor-ligand interactions during *Plasmodium falciparum* invasion of erythrocytes. *PLoS Pathog*, 11(2), e1004670. doi:10.1371/journal.ppat.1004670
- Wellems, T. E., & Plowe, C. V. (2001). Chloroquine-resistant malaria. *J Infect Dis*, 184(6), 770-776. doi:10.1086/322858
- White, N. (1999). Antimalarial drug resistance and combination chemotherapy. *Philos Trans R Soc Lond B Biol Sci*, 354(1384), 739-749. doi:10.1098/rstb.1999.0426
- White, N. J. (2004). Antimalarial drug resistance. *Journal of Clinical Investigation*, 113(8), 1084-1092. doi:10.1172/jci21682
- White, N. J. (2011). Determinants of relapse periodicity in *Plasmodium vivax* malaria. *Malar J*, 10, 297. doi:10.1186/1475-2875-10-297
- White, N. J., Hien, T. T., & Nosten, F. H. (2015). A Brief History of Qinghaosu. *Trends Parasitol*, 31(12), 607-610. doi:10.1016/j.pt.2015.10.010
- Wicht, K. J., Mok, S., & Fidock, D. A. (2020). Molecular Mechanisms of Drug Resistance in *Plasmodium falciparum* Malaria. *Annu Rev Microbiol*, 74, 431-454. doi:10.1146/annurev-micro-020518-115546

- William, T., Menon, J., Rajahram, G., Chan, L., Ma, G., Donaldson, S., . . . Yeo, T. W. (2011). Severe *Plasmodium knowlesi* malaria in a tertiary care hospital, Sabah, Malaysia. *Emerg Infect Dis*, *17*(7), 1248-1255. doi:10.3201/eid1707.101017
- Witkowski, B., Amaratunga, C., Khim, N., Sreng, S., Chim, P., Kim, S., . . . Menard, D. (2013). Novel phenotypic assays for the detection of artemisinin-resistant *Plasmodium falciparum* malaria in Cambodia: in-vitro and ex-vivo drug-response studies. *The Lancet Infectious Diseases*, *13*(12), 1043-1049. doi:10.1016/s1473-3099(13)70252-4
- World Health Organization. (2001). Antimalarial drug combination therapy. Report of a technical consultation. WHO. Geneva, Switzerland. WHO/CDS/RBM 2001.35.
- World Health Organization. (1996). A rapid dipstick antigen capture assay for the diagnosis of *falciparum* malaria. WHO Informal A rapid dipstick antigen capture assay for the diagnosis of *falciparum* malaria. WHO Informal Consultation on Recent Advances in Diagnostic Techniques and Vaccines for Malaria. *Bulletin of the World Health Organization*, *74*(1), 47–54.
- World Health Organization. (2019 b). Artemisinin resistance and artemisinin-based combination therapy efficacy: status report. World Health Organization. Retrieved from <https://apps.who.int/iris/handle/10665/274362>. Lizenz: CC BY-NC-SA 3.0 IGO
- World Health Organization. (2008). Bulletin of the World Health Organization. Volume 86, Number 2, February 2008, 81-160. Retrieved from <https://www.who.int/bulletin/volumes/86/2/07-050633/en/>
- World Health Organization. (2001). Drug resistance in malaria. WHO/CDS/CSR/DRS/2001.4. Retrieved from <https://www.who.int/csr/resources/publications/drugresist/malaria.pdf>
- World Health Organization. (2008). Global Malaria Control and Elimination: report of a technical review. Retrieved from <https://www.who.int/malaria/publications/atoz/9789241596756/en/>
- World Health Organization. (2018 b). Malaria vaccine: WHO position paper – January 2016. Vaccine. 2018 Jun 14;36(25):3576-3577. doi: 10.1016/j.vaccine.2016.10.047. Epub 2017 Apr 3.
- World Health Organization. (2017). WHO report of GACVAS, Safety monitoring of the RTS,S vaccine pilot implementation programme, Extract from report of GACVS meeting of 7-8 June 2017, published in the WHO Weekly Epidemiological Record of 14 July 2017
- World Health Organization. (2018 a). World Malaria Report 2018. Geneva. Licence: CC BY-NC-SA 3.0 IGO.
- World Health Organization. (2019 a). World malaria report 2019. Geneva. Licence: CC BY-NC-SA 3.0 IGO.
- World Health Organization. (2020). World malaria report 2020: 20 years of global progress and challenges. Geneva. Licence: CC BY-NC-SA 3.0 IGO.
- World Health Organization. (2020, 02.03.2021). Retrieved from [https://www.who.int/malaria/areas/diagnosis/rapid\\_diagnostic\\_tests/en/](https://www.who.int/malaria/areas/diagnosis/rapid_diagnostic_tests/en/)
- Wright, G. J., & Rayner, J. C. (2014). *Plasmodium falciparum* erythrocyte invasion: combining function with immune evasion. *PLoS Pathog*, *10*(3), e1003943. doi:10.1371/journal.ppat.1003943
- Wunderlich, J., Rohrbach, P., & Dalton, J. P. (2012). The malaria digestive vacuole. *Front Biosci (Schol Ed)*, *4*, 1424-1448. doi:10.2741/s344
- Xie, S. C., Ralph, S. A., & Tilley, L. (2020). K13, the Cytostome, and Artemisinin Resistance. *Trends Parasitol*, *36*(6), 533-544. doi:10.1016/j.pt.2020.03.006
- Yamauchi, L. M., Coppi, A., Snounou, G., & Sinnis, P. (2007). *Plasmodium* sporozoites trickle out of the injection site. *Cell Microbiol*, *9*(5), 1215-1222. doi:10.1111/j.1462-5822.2006.00861.x
- Yang, T., Yeoh, L. M., Tutor, M. V., Dixon, M. W., McMillan, P. J., Xie, S. C., . . . Cobbold, S. A. (2019). Decreased K13 Abundance Reduces Hemoglobin Catabolism and Proteotoxic Stress, Underpinning Artemisinin Resistance. *Cell Rep*, *29*(9), 2917-2928 e2915. doi:10.1016/j.celrep.2019.10.095
- Zekar, L., & Sharman, T. (2021). *Plasmodium Falciparum* Malaria. In *StatPearls*. Treasure Island (FL).

- 
- Zhang, D. D., Lo, S. C., Cross, J. V., Templeton, D. J., & Hannink, M. (2004). Keap1 is a redox-regulated substrate adaptor protein for a Cul3-dependent ubiquitin ligase complex. *Mol Cell Biol*, 24(24), 10941-10953. doi:10.1128/MCB.24.24.10941-10953.2004
- Zhang, M., Gallego-Delgado, J., Fernandez-Arias, C., Waters, N. C., Rodriguez, A., Tsuji, M., . . . Sullivan, W. J., Jr. (2017). Inhibiting the Plasmodium eIF2alpha Kinase PK4 Prevents Artemisinin-Induced Latency. *Cell Host Microbe*, 22(6), 766-776 e764. doi:10.1016/j.chom.2017.11.005
- Zhou, H. C., Gao, Y. H., Zhong, X., & Wang, H. (2009). Dynamin like protein 1 participated in the hemoglobin uptake pathway of Plasmodium falciparum. *Chin Med J (Engl)*, 122(14), 1686-1691. Retrieved from <https://www.ncbi.nlm.nih.gov/pubmed/19719972>
- Ziegelbauer, J., Shan, B., Yager, D., Larabell, C., Hoffmann, B., & Tjian, R. (2001). Transcription factor MIZ-1 is regulated via microtubule association. *Mol Cell*, 8(2), 339-349. doi:10.1016/s1097-2765(01)00313-6

## Publications

### **A Kelch13-defined endocytosis pathway mediates artemisinin resistance in malaria parasites.**

**Sarah Scharf\***, Jakob Birnbaum\*, Sabine Schmidt, Ernst Jonscher, Wieteke Anna Maria Hoeijmakers, Sven Flemming, Christa Geeke Toenhake, Marius Schmitt, Ricarda Sabitzki, Bärbel Bergmann, Ulrike Fröhlke, Paolo Mesén-Ramírez, Alexandra Blancke Soares, Hendrik Herrmann, Richárd Bártfai, Tobias Spielmann.

\* these authors contributed equally to this work

Science. (2020), 367(6473), 51-59. doi:10.1126/science.aax4735

### **Identification of novel IMC proteins and apical annuli homologues of the malaria parasite *Plasmodium falciparum***

Jan Stephan Wichers, Juliane Wunderlich, Dorothee Heincke, Samuel Pazicky, Jan Strauss, Marius Schmitt, Jessica Kimmel, Louisa Wilcke, **Sarah Scharf**, Heidrun von Thien, Paul-Christian Burda, Tobias Spielmann, Christian Löw, Michael Filarsky, Anna Bachmann, Tim W. Gilberger.

Cellular Microbiology. (2021), <https://doi.org/10.1101/2021.02.03.428885>doi

## **Danksagung**

An dieser Stelle möchte ich mich zuerst bei Dr. Tobias Spielmann bedanken. Vielen Dank, dass du mir die Möglichkeit gegeben hast meine Doktorarbeit in deiner Arbeitsgruppe durchzuführen, in der wir immer eine produktive und tolle Atmosphäre hatten. Außerdem weiß ich es sehr zu schätzen, dass du so viel Zeit, Energie und Wissen mit mir geteilt hast und dass du immer ein offenes Ohr hast. Ich bin dankbar an so einem spannenden Projekt gearbeitet zu haben das mir unglaublich viel Spaß gemacht hat. Es war eine sehr lehrreiche und spannende Zeit.

Des Weiteren möchte ich mich bei Prof. Dr. Tim Gilberger und Dr. Thomas Jacobs für die Co-Betreuung, Anregungen und Ideen bedanken. Außerdem danke ich Tim und Tobi für die Übernahme des Dissertationsgutachtens.

Außerdem bedanke ich mich herzlich bei der Claussen-Simon-Stiftung für die Förderung durch das DissertationPlus Stipendiums. Neben der finanziellen Unterstützung danke ich vor allem auch für die ideelle Förderung durch die Stiftung und all die spannenden und inspirierenden Workshops und Angebote, die mir die Möglichkeit gegeben haben, mich während meiner Doktorzeit nicht nur fachlich, sondern auch persönlich weiter zu entwickeln.

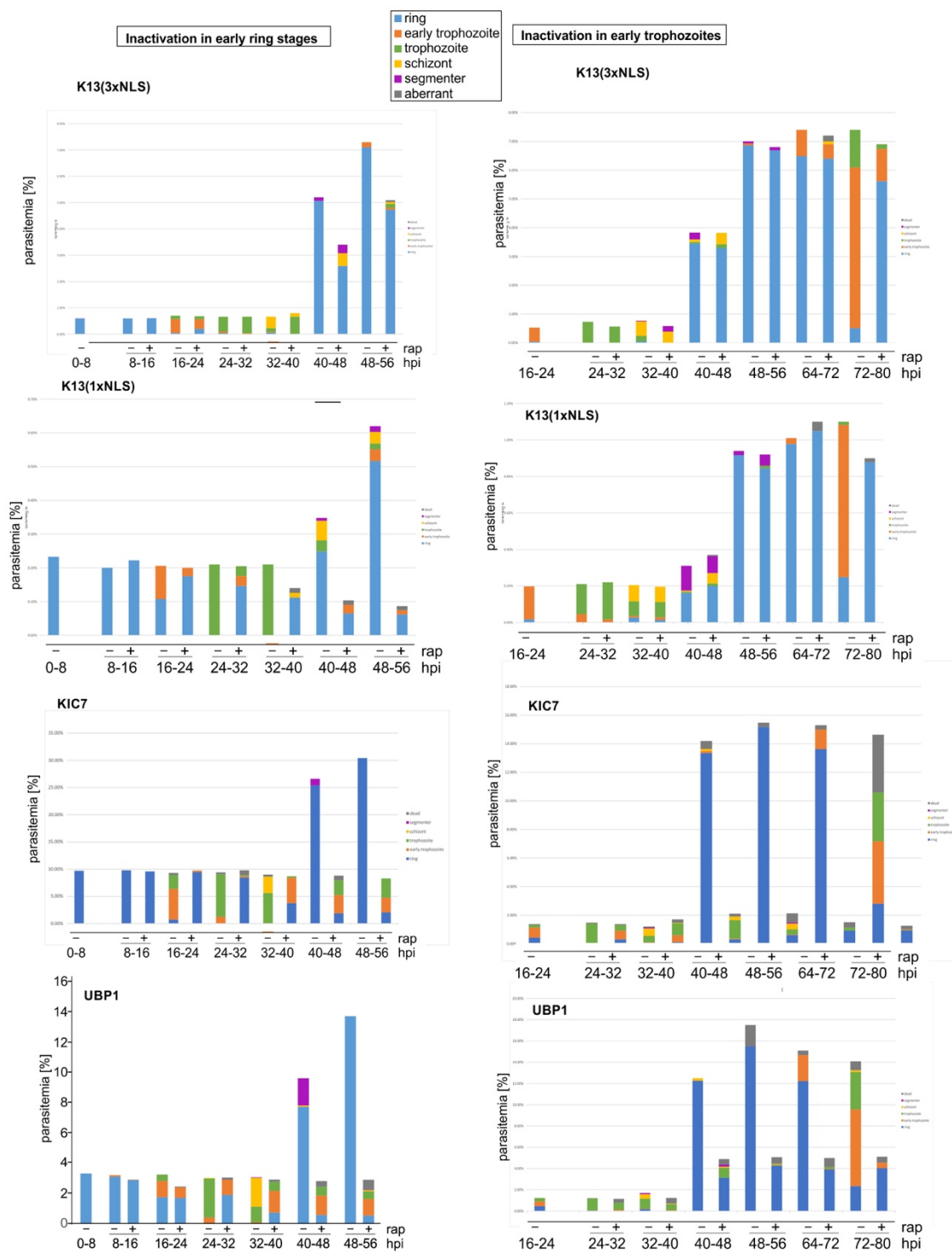
Darüber hinaus bedanke ich mich herzlich bei allen aktuellen und ehemaligen Mitgliedern der AG Spielmann und AG Gilberger die dazu beigetragen haben, dass die letzten Jahre immer einmalig und unvergesslich für mich sein werden. Vielen Dank, dass ich mit euch nicht nur Kollegen sondern auch Freunde gefunden habe und dass wir uns immer gegenseitig unterstützt haben. Ich werde die gemeinsamen stressigen Arbeitsphasen aber auch die Ausflüge und Partys mit euch immer in guter Erinnerung halten.

Abschließend geht ein besonderer Dank an meine Familie. Ich danke meinen Eltern und meiner Schwester, dass ihr mich immer in allem unterstützt und ihr immer für mich da seid. Außerdem danke ich dir, Denis, dass du immer an mich glaubst und dass du während den letzten Jahren immer an meiner Seite warst und mir den Rücken freigehalten hast.

# Appendix

## Appendix 1

Second independent experiment of stage-specific phenotypes after partial inactivation of Kelch13 (3xNLS) and full inactivation of Kelch13 (1xNLS), KIC7 and of UBP1.





Majority protein IDs	GeneDB Updated Product Name	Gene Symbol	log2 Ratio H/L normalized	log2 Ratio H/L normalized	average log2 Ratio normalized	K13C580 Y+BirA* -N exp1	K13C580 Y+BirA* -N exp2	K13C580 Y+BirA* -N exp1	K13C580 Y+BirA* -N exp2	K13+BirA * -CL exp1	K13+BirA * -CL exp2	K13+BirA * -N exp1	K13+BirA * -N exp2	K13C580 Y+BirA* -N exp1	K13C580 Y+BirA* -N exp2	Kelch13- C580Y #	Kelch13 #	Kelch13- C580Y #	
PF3D7_0408100	Plasmodium protein, unknown function	PlasmodiumDB33_ProteinProduct	0.628074	1.360564	0.994319	0.982188	0.002584												
PF3D7_1245800	conserved Plasmodium protein, unknown function	epsin, putative	NaN	NaN	#DIV/0!	0.969821	0.242874												
PF3D7_1247400	peptidyl-prolyl cis-trans isomerase FKBP35	FKBP35	0.769687	1.272228	1.020958	0.804245	0.48552												
PF3D7_0822900	conserved Plasmodium protein, unknown function		1.247624	1.417271	1.332448	0.984331	1												
PF3D7_0109000	photosensitized IMA-labeled protein PHIL1, putative	PHIL1	1.198871	1.464345	1.331608	0.023409	0.04651												
PF3D7_1470900	proteasome subunit beta type-2, putative		NaN	NaN	#DIV/0!	8.79E-09	0.00506												
PF3D7_1117800	conserved Plasmodium protein, unknown function		NaN	NaN	1.0443	0.891917	1												
PF3D7_1018200	serine/threonine protein phosphatase 8, putative	PPP8	NaN	NaN	#DIV/0!	0.346738	0.322078												
PF3D7_1345600	inner membrane complex protein		0.90458	0.345803	0.625192	0.002781	1.6E-05												
PF3D7_0103100	vacuolar protein sorting-associated protein 51, putative	VPS51	0.391878	0.913787	0.652882	1	0.002571												
PF3D7_0708400	heat shock protein 90	HSP90	0.271904	0.587511	0.428707	0.003026	0.120103												
PF3D7_0907200	GTPase-activating protein, putative		0.216983	NaN	0.216983	0.343347	1												
PF3D7_1329100	myosin C	MyoC	1.009132	1.164755	1.086944	0.725328	0.297986												
PF3D7_1329500	conserved Plasmodium protein, unknown function		1.10091	1.053973	1.077442	0.244342	1												
PF3D7_0721100	conserved Plasmodium protein, unknown function		-0.99706	NaN	-0.99706	1.05E-25	7.43E-21												
PF3D7_0405700	lysine decarboxylase, putative		1.573084	1.067304	1.320194	1	0.000496												
PF3D7_1449100	conserved Plasmodium protein, unknown function		NaN	0.519259	0.519259	5.31E-12	6.27E-18												
PF3D7_1455300	conserved Plasmodium protein, unknown function		NaN	NaN	#DIV/0!	0.00271	0.580771												
PF3D7_1402500	ubiquitin-40S ribosomal protein S27a, putative	ribosoma	NaN	NaN	#DIV/0!	0.885434	0.282303												
PF3D7_1141300	conserved Plasmodium protein, unknown function		1.538935	0.672704	1.105819	0.667636	0.135475												
PF3D7_0407800	conserved Plasmodium protein, unknown function		0.433494	0.672819	0.553156	3.15E-05	0.138151												
PF3D7_1411300	conserved Plasmodium protein, unknown function		1.10742	0.656922	0.882171	0.964093	0.001912												
PF3D7_1329000	DNA-directed RNA polymerase III subunit RPC1, putative		-0.17456	0.094202	-0.04018	9.72E-17	1.35E-12												
PF3D7_0423500	glideosome associated protein with multiple membrane null	GAPM2	0.934932	0.716078	0.825505	0.097981	0.013028												
PF3D7_0508800	single-stranded DNA-binding protein	SSB	NaN	NaN	#DIV/0!	0.854426	0.277681												
PF3D7_0731300	Plasmodium exported protein (PHISTb), unknown function	PFGL74	-0.392333	0.648575	0.128124	1	1												
PF3D7_1435600	conserved Plasmodium protein, unknown function		NaN	1.793407	1.793407	0.008122	0.967961												
PF3D7_1121300	tyrosine kinase-like protein	TKL2	0.840201	0.622954	0.731578	0.000959	0.353156												
PF3D7_1133100	conserved Plasmodium protein, unknown function		0.428035	0.475836	0.451936	1.27E-28	1.31E-21												
PF3D7_1015600	heat shock protein 60	HSP60	0.497331	0.882571	0.689951	1	0.098815												
PF3D7_0526200	ADP-ribosylation factor GTPase-activating protein, putative	ARF-GAP	0.939302	1.103891	1.021596	0.013061	0.761886												
PF3D7_1027700	centrin-3	CEN3	NaN	1.167928	1.167928	0.02976	0.050423												
PF3D7_0914500	conserved Plasmodium protein, unknown function		NaN	2.166308	2.166308	0.43489	0.108503												
PF3D7_0704100	conserved Plasmodium membrane protein, unknown function		0.482332	0.581691	0.532012	0.29662	0.563461												
PF3D7_1136500	casein kinase 1	CK1	1.153416	0.488977	0.321197	1	2.73E-05												

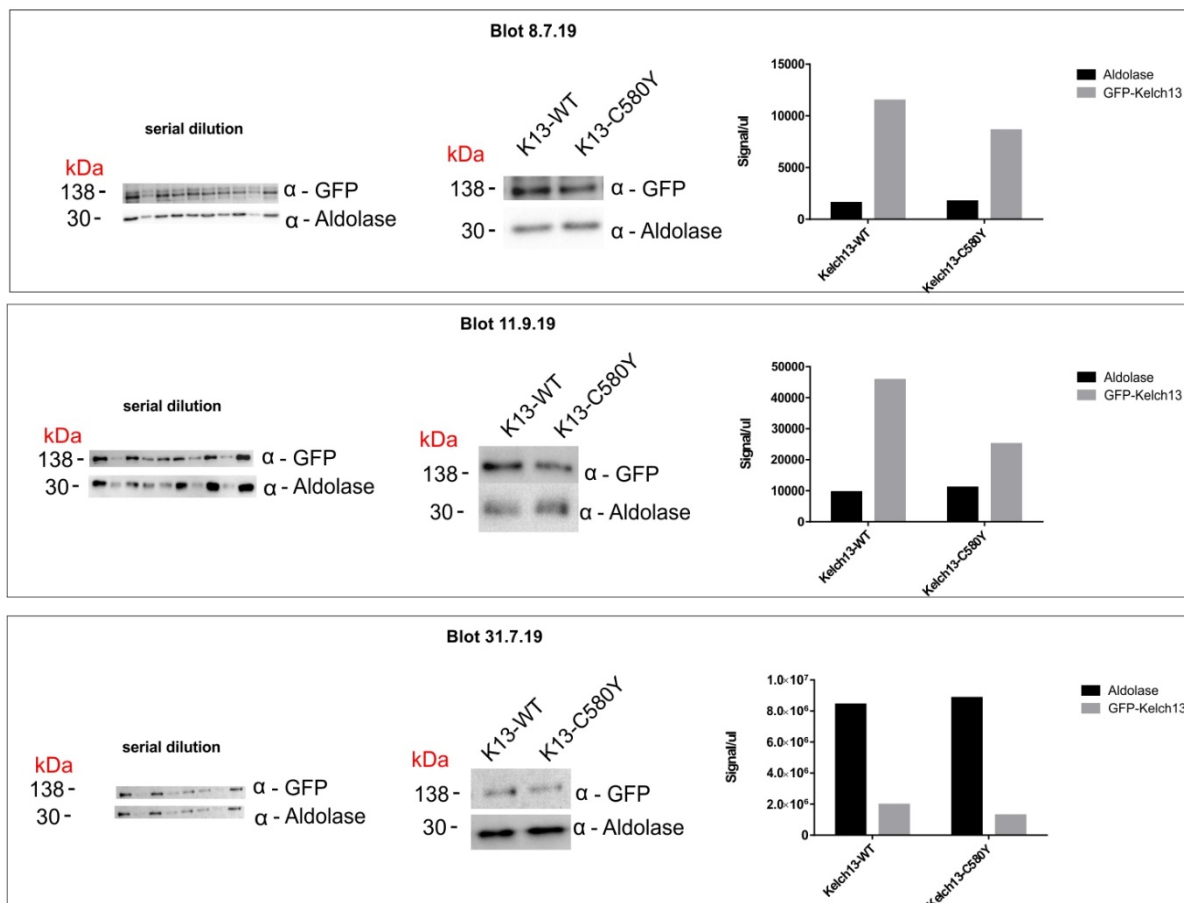


Majority protein IDs	PlasmoDB33_ProteinProduct	GeneDB Updated Product Name	Gene Name or Symbol	log2 ratio H/L normalized	log2 H/L ratio normalized	average log2 ratio normalized	K13C580 Y+BirA* N exp1 significance	K13C580 Y+BirA* N exp2 significance	K13C580 Y+BirA* N exp1 significance	K13C580 Y+BirA* N exp2 significance	K13+BirA* CL exp1 significance	K13+BirA* CL exp2 significance	K13+BirA* N exp1 significance	K13+BirA* N exp2 significance	Kelch13-580Y # significance	Kelch13 # significance	Kelch13-580Y # significance	
PF3D7_0727000	vacuolar protein sorting-associated protein 53, putative	VP53	VP53	-0.15382	1.485277	0.665721	0.006668	0.266914										
PF3D7_0304400	60S ribosomal protein L44	RPL44	RPL44	0.217851	0.658174	0.438012	0.46393	0.009513										
PF3D7_1145400	dynamitin-like protein	DYN1	DYN1	0.037312	0.925632	0.481472	0.653446	0.655259										
PF3D7_0321500	peptidase, putative	PEP	PEP	-0.18758	1.181509	0.496967	4.68E-05	0.665575										
PF3D7_1251500	ATP-dependent RNA helicase DRS1, putative	DRS1	DRS1	0.131194	NaN	0.131194	0.009116	0.162876										
PF3D7_1032100	mRNA-decapping enzyme subunit 1, putative	DCP1	DCP1	0.990955	0.305592	0.648274	1	1										
PF3D7_1014300	conserved protein, unknown function	CP1	CP1	-0.28481	1.959599	0.837395	1	0.000198										
PF3D7_0903500	conserved Plasmodium protein, unknown function	CP2	CP2	0.848798	-0.33239	0.258203	1	1										
PF3D7_0703500	erythrocyte membrane-associated antigen	EMA	EMA	0.878529	0.131835	0.505182	1.28E-22	1.22E-13										
PF3D7_0618200	conserved Plasmodium protein, unknown function	CP3	CP3	NaN	NaN	NaN	0.594266	9.61E-05										
PF3D7_0532100	early transcribed membrane protein 5	ETM5	ETM5	NaN	NaN	NaN	0.11657	0.008068										
PF3D7_1440700	adaptor complexes medium subunit family	ACM	ACM	-0.82884	1.326769	0.248962	4.95E-25	1.47E-11										
PF3D7_0418200	eukaryotic translation initiation factor 3 subunit M, putative	EIF3M	EIF3M	-0.23118	1.399312	0.584068	0.376311	0.063387										
PF3D7_1429900	ADP-dependent DNA helicase RecQ	WRN	WRN	1.792481	0.059014	0.925747	1.33E-10	5.95E-10										
PF3D7_0303200	HAD superfamily protein, putative	HAD	HAD	0.15558	0.92703	0.540294	1	0.645432										
PF3D7_1438600	conserved protein, unknown function	CP4	CP4	0.062398	1.296474	0.679436	1	1										
PF3D7_1457300	conserved Plasmodium protein, unknown function	CP5	CP5	-0.61116	1.98593	0.687385	0.284415	0.001622										
PF3D7_0813200	CS domain protein, putative	CS	CS	-0.33297	NaN	-0.33297	0.002044	1										
PF3D7_1416900	prefoldin subunit 2, putative	PFD2	PFD2	-0.46365	1.302333	0.419342	0.002944	0.991991										
PF3D7_0423600	conserved Plasmodium protein, unknown function	CP6	CP6	NaN	NaN	NaN	0.176117	0.001402										
PF3D7_1425900	conserved Plasmodium protein, unknown function	CP7	CP7	-0.33998	0.380164	0.02009	0.008916	0.839497										
PF3D7_1250800	DNA repair protein rhp16, putative	RHP16	RHP16	0.021906	1.739517	0.880712	1	1										
PF3D7_1457700	large ribosomal subunit nuclear export factor, putative	NEF	NEF	1.29443	NaN	1.29443	1.12E-06	1										
PF3D7_0411100	conserved Plasmodium protein, unknown function	CP8	CP8	1.064745	NaN	1.064745	0.439008	0.139078										



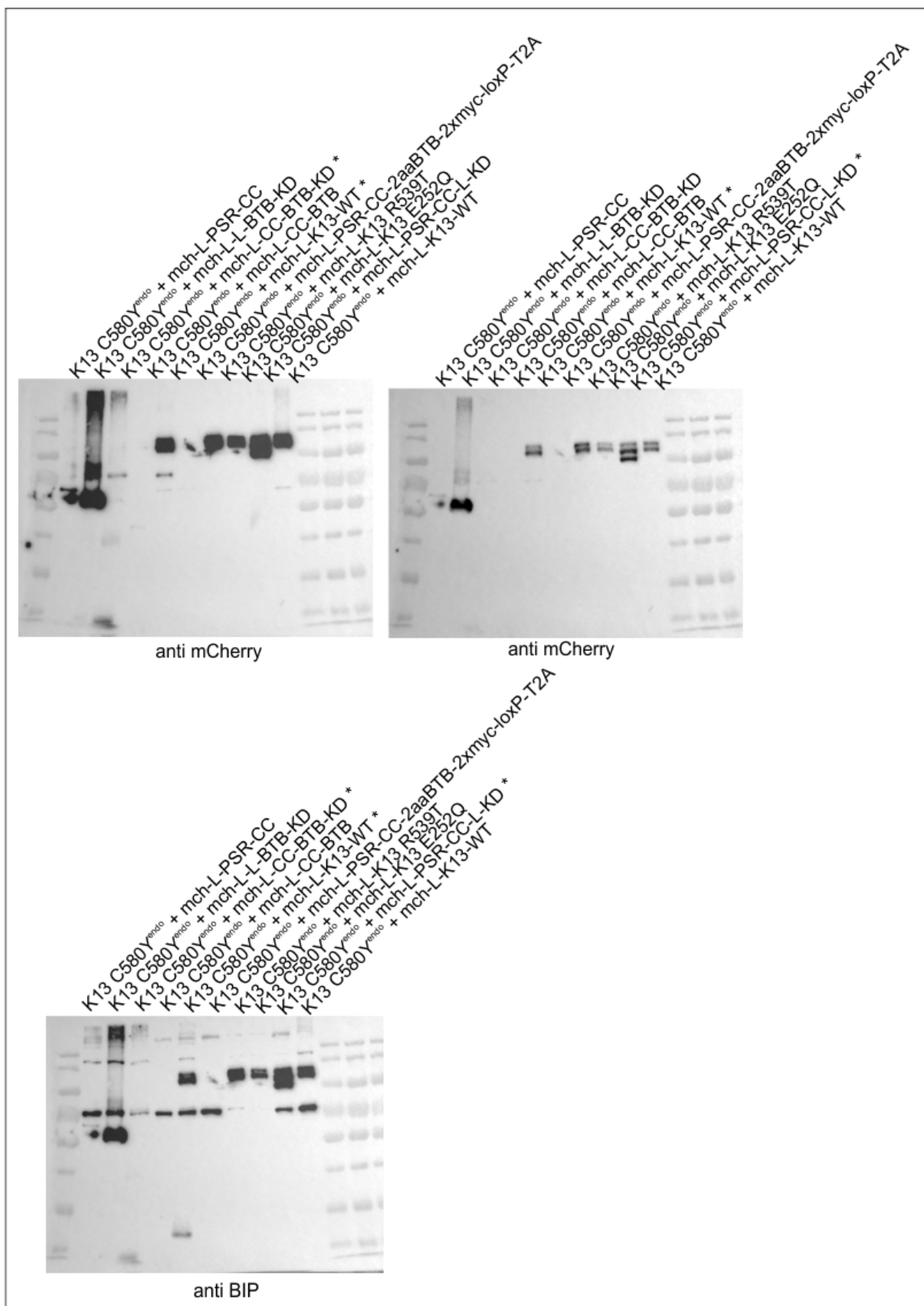
## Appendix 3

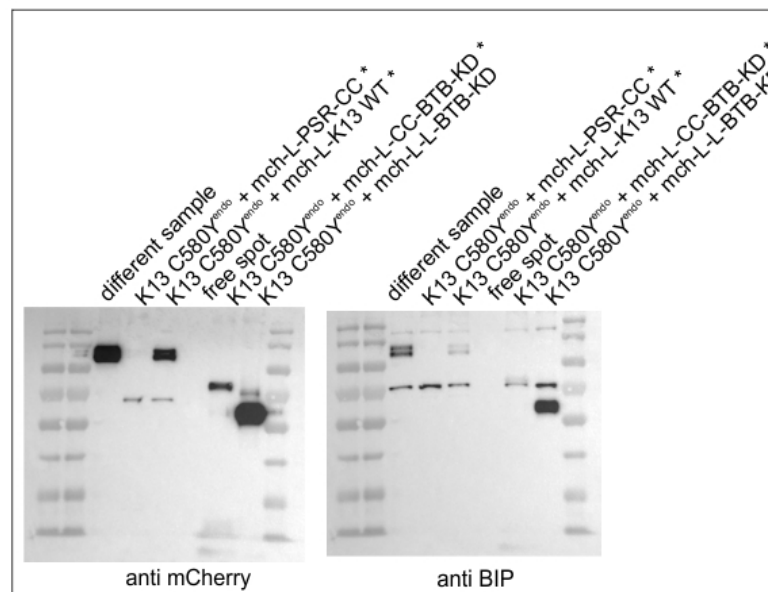
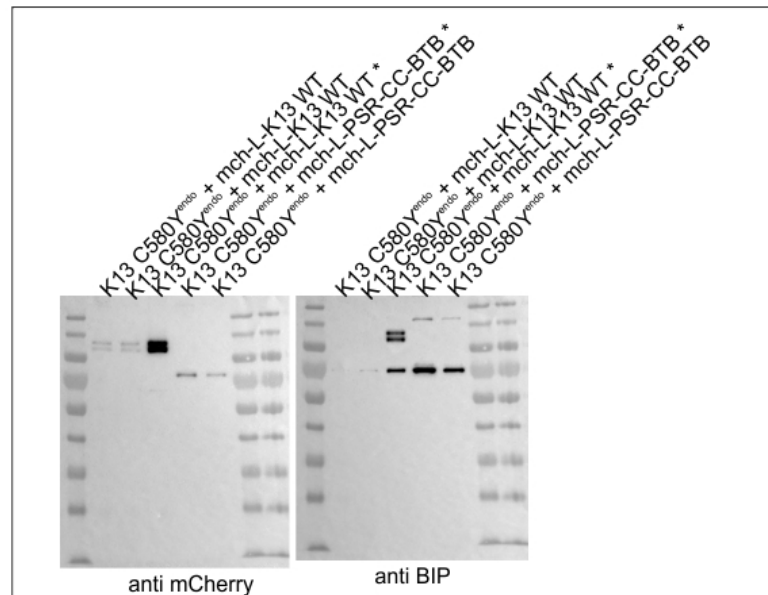
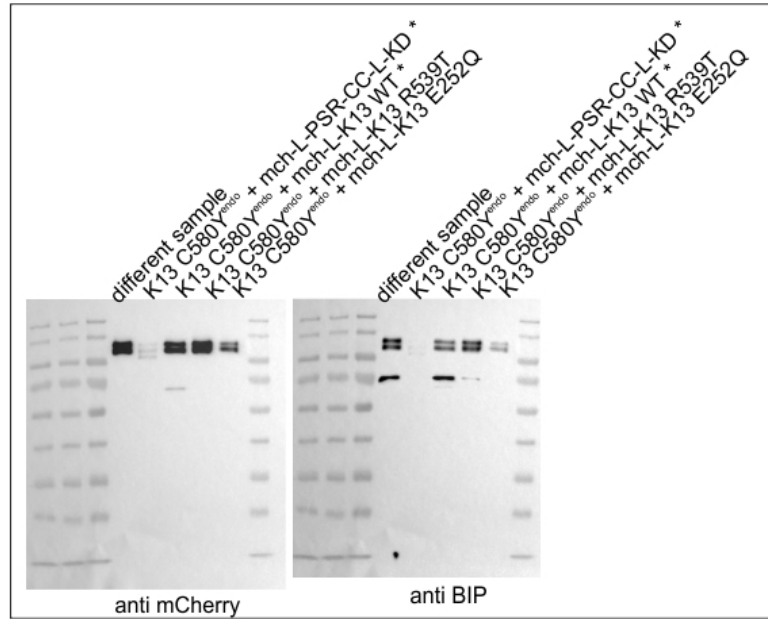
Immunoblots used for quantification of the abundance of K13WT<sup>endo</sup> and K13C580Y<sup>endo</sup>.



## Appendix 4

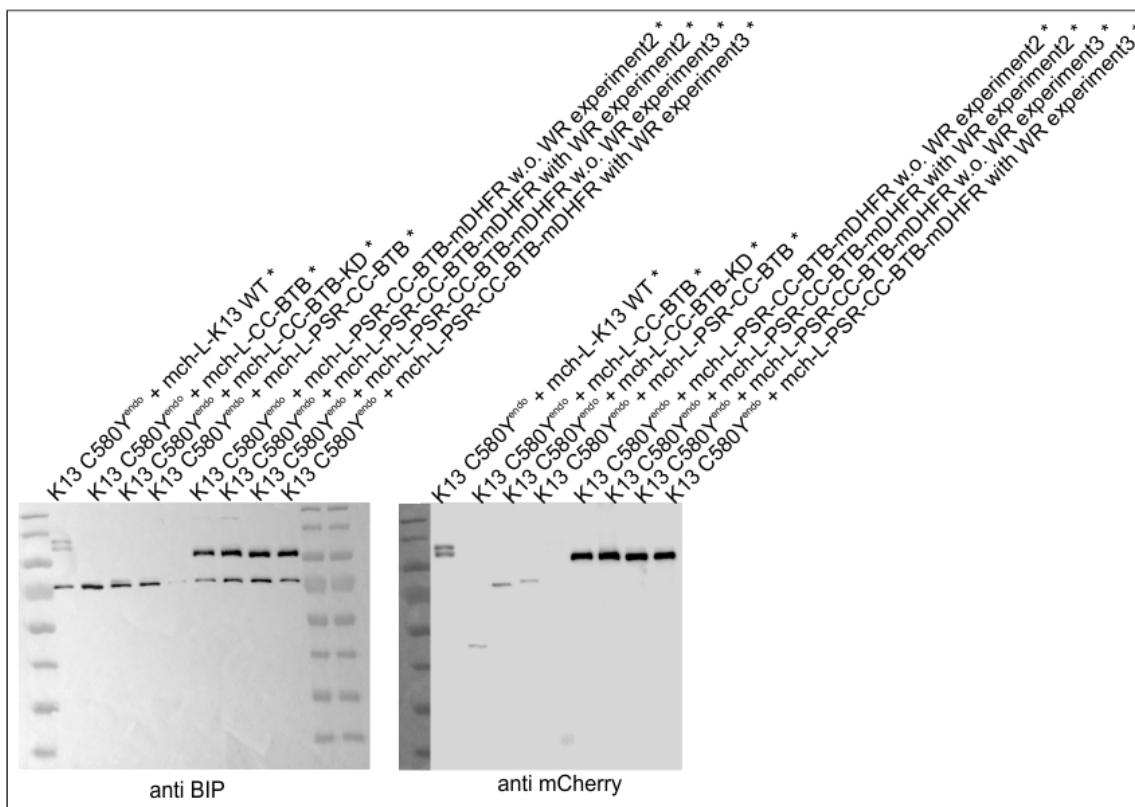
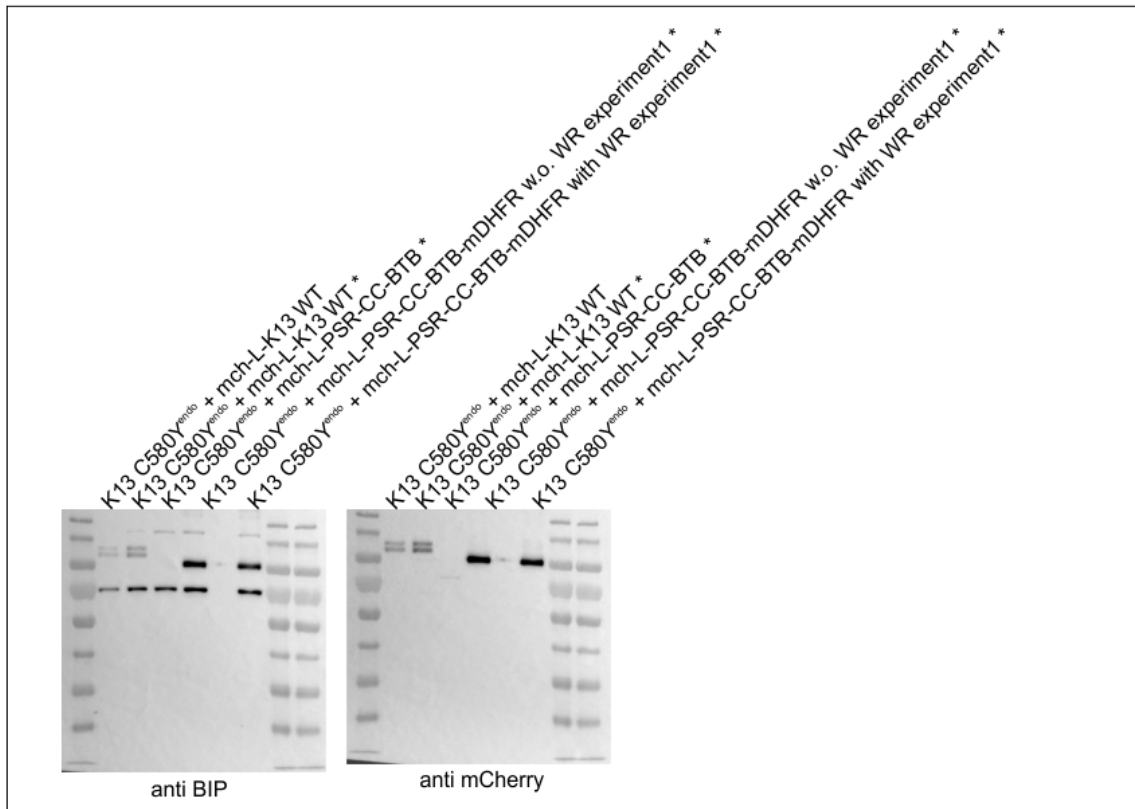
Immunoblots used for quantification of the abundance of different Kelch13 domain constructs.





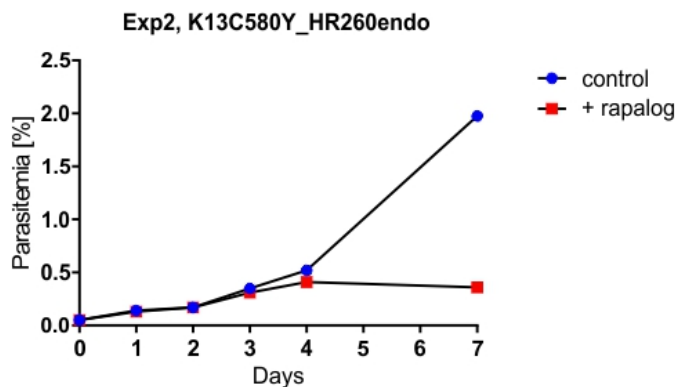
## Appendix 5

Immunoblots used for quantification of the effect of mDHFR domain on relative cellular abundance of episomal Kelch13 constructs lacking the Kelch domain.



## Appendix 6

Second replica of parasite growth as determined by flow cytometry of the K13C580Y\_HR260<sup>endo</sup> parasites grown in the presence (+rapalog) and absence (control) of rapalog.



## Appendix 7

Oligonucleotides used in this thesis.

Oligonucleotides for cloning

primer name	sequence
C580Y_recod.Sarah_NheI fw	caggagcaggagcaggagcaatattaagtagagctagcATGGAAGGAGAAAA GTAAAAACAAAAGCAAATAG
C580Y_recod.Sarah_XmaI rv	CGAACATTAAGCTGCCATATCCCTCGACCCGGGTTATCATA TATTTGCTATTA AAACTGAGTGACCAAATCTAGG
C580Y-sequ. 1321 fw	CCATTCCCATTAGTATTTTGTATAG
C580Y-sequ. 1687 fw	GAAAGCATGGGTAGAGGTAGCACC
K13 recod2_314_rv	GCTGCCATATCCCTCGACCCGGGTTAATTATTAATGTTCT TGATAAATTAC
K13 PSR fw_NheI_nmd3	CGTATATCATTTTAAAGATAAActcagggctagcATGGAAGGAGAA AAAGTAAAAACAAAAGC
K13 312 rv_PmeI_2xmyc	CTTCCTCACTAATAAGTTTTTGTTCGTTTAAACCATTATTAA ATGTTCTTGATAAATTACTTGG
PSR 107AA fw	ggagcaggagcaatattaagtagagctagcATGTCAAAGATAATATAGGA AATAAATATTTAAATAAATTATTAATAAAAAAAAAAAG
K13 BTB rv	CATTAAGCTGCCATATCCCTCGACCCGGGTTTAAATACCATA AAATTCTGCTTCTTTTAAAC
Cre 721 fw	gcaagagcaggagtaagtataccagaaataatgcaagcaggaggatggacaaatgtaaataag taatgaattatataagaatttagatagtgaaacaggagcaatggttaagattatta
Cre 820_T2A_BSD fw	ggagcaatggttaagattatagaagatggagatggagaaggaagaggaagttattataacatgtgg agatgtagaagaaatccaggaccaATGGCCAAGCCTTTGTCTCAAGAAG AATCC
BSD_T2A-NLS rv	cttttttcttaggagccatTGGACCTGGATTTTCTTCAACATCACCACA AGTCAACAAGAACCTCTACCTTCACCGCCCTCCACACAT AACCAGAGGGCAGCAATTCACGAATCCC
CAM-mch fw	GATTTATATTTTATAATAATAAATACCTAATAGAAATATAT CAGGATCCGAGCTCatggtgagcaagggcaggaggataacatgg
skip flox K13 rv	GTTTTTATTTTATAAATTTTTTAATCTATTATTAATAATA TATTTGCTATTA AAACTGAGTGACCAAATCTAG

Cre 767 fw	ggacaaatgtaaatatagtaatg
FKBP 31 rv	cctcttttggaaatgtcttccatc
nmd3_fw_skipflox_neu	catataaacacaaatgatggttttccctcaatttcGATcttaagactagtcctaggAGATCTt attattattacatGTTGAAATATAAATTTCAAAAAAAAAATGATCAC
K13 recod Sarah_WT_fw	CTTTAAATACTCCTAGATCATCAGCTATGTGTGTGCGCTTTTG ATAATAAAATTTATG
K13 recod Sarah_WT_rv	CATAAATTTTATTATCAAAGCGACACACATAGCTGATGAT CTAGGAGTATTTAAAG
K13 recod Sarah_3primeUTR_fw	CTCAGTTTTAATAGCAAATATATGATAAgcggccgcATTTAAT AATAGATTAATAAATTATAAAAAATAAAAAC
3primeUTR_rv_XbaI_skipflox	GTGAATTGTAATACGACTCACTATAGAATTCTAGATTTAAT AAATATGTTCTTATATATAATG
skip flox K13 recod.S._NotI_rv	GTTTTTATTTTTATAATTTTTTAATCTATTATTAATgcggcc gcTTATCATATATTTGCTATTTAAACTG
skipflox_xmaI_fw	cagcatggtgtaattaaattaaCCCGGGTcggaggatggcagcttaatgttc
Skipflox_Pb3UTR_rv_nmd3	gtaataataataAGATCTcctaggactagcttaagATCgaaattgaaggaaaaccatc atgtgtttatag
K13 BTB fw	ggagcaggagcaatattaagtagagctagcATGATTGATATTAATGTTGGTG GAGCTATTTTTG
K13 BTB rv	CATTAAGCTGCCATATCCCTCGACCCGGGTTAATACCATA AAATTCTGCTTCTTTTAAAC
K13 coiled coiled fw	caggagcaatattaagtagagctagcATGAGTGATTTTGAAAATATGGTA GG
K13 coiled coil rv	CATTAAGCTGCCATATCCCTCGACCCGGGCATAGTTTCAGT AGCAATATTTGCATC
T2A_loxP_recod.rv	GCTGCCATATCCCTCGACCCGGGTAAACCAGGGTTCTCCTC AACGTCACCGCAAGTAAGAAGTGAACCACGACCCCTCACCG GaAAGTTTTGTGTAGTGAATTGAGTAACTTGAATAAAGG
loxP_2xmyc_recod._rv	GAATTGAGTAACTTGAATAAAGGTCCTCCTCTGAAATTAAC TTCTGCTCTCCAAGGCTTCTCCTCACTAATAAGTTTTTGTTCG TTTAAACCATATCAATCATAGTTTCAGTAGC
K13HR Jakob_NheI_fw_neu	caggagcaggagcaatattaagtagagctagcATGGAAGGAGAAAAAGTAA AAACAAAAGCAAATAGTATC
K13_BTBT Domäne_fw_Linker	ggagcaggagcaatattaagtagagctagcATTGATATTAATGTTGGTGGAG CTATTTTTG
L-5xGGGGS-BTB_fw	gcaggagcaatattaagtagagctagcGGAGGTGGAGGTAGTGGAGGCGG AGGTAGCGGAGGCGGTGGGAGTGGTGGAGGCGGAAGTGG CGGTGGAAGCATTGATATTAATGTTGGTGGGA
K13R539Tgenomic.seq_fw_neu	GAAGAAATAATTGTGGTGTACGTCAAATGGTACAATTTAT TGTATTGGGGGATATGATGGC
K13R539Tgenomic.seq_rv_neu	GAAGAGCCATCATATCCCCCAATACAATAAATTGTACCATT TGACGTAACACCACAATTATTTCTTC
K13 coiled coiled genom.seq. fw	ggagcaatattaagtagagctagcATGAGTGATTTTGAAAATATGGTAGG TG
E252Q genomic seq. rv	CGTACTCTTTCCATTTGTAGTTCCTTCTTATC
E252Q genomic seq. fw	GATAAGAAAGAACTACAAATGGAAAGAGTACG
K13PSR_rv	GCCATATCCCTCGACCCGGGTACATAGTTTCAGTAGCAAT ATTTGCATC
C580Y_recod.Sarah_NheI fw	caggagcaggagcaggagcaatattaagtagagctagcATGGAAGGAGAAAA GTAAAAACAAAAGCAAATAG
C580Y_recod.Sarah_XmaI rv	CGAACATTAAGCTGCCATATCCCTCGACCCGGGTATCATA TATTTGCTATTAAACTGAGTGACCAAATCTAGG
C580Y-sequ. 1321 fw	CCATTCCCATTAGTATTTTGTATAG
C580Y-sequ. 1687 fw	GAAAGCATGGGTAGAGGTAGCACC
K13_Pl.spec.seq._fw_Link	gcaggagcaatattaagtagagctagcATGGAAGGAGAAAAAGTAAAAAC AAAAG

K13_Pl.spec.seq._rv_Linker	gctagcccttcaaaccctgggtcctcaaacggttcaTTTTTACCATTCCCATTAGT ATTTTG
K13_BTBDomäne_fw_Linker	ggagcaggagcaatattaagtagagctagcATTGATATTAATGTTGGTGGAG CTATTTTTG
K13_kelch domains rv	CTGCCATATCCCTCGACCCGGGTTATATATTTGCTATTA ACGGAGTGACCAAATC
K13_Pl.spec.seq._fw_Linker	gcaggagcaatattaagtagagctagcATGGAAGGAGAAAAAGTAAAAAC AAAAG
K13_BTBrv	GCTGCCATATCCCTCGACCCGGGTTATAATGGGAATGGTAA AAATTTAATACC
BTB fw AflIII HpaI	GGGATAGTGAGTTATTTAGAATTATACTTAACTTCTTAAGA AATCCGTTAACTATACCCATACCAAAAAGATTTAAGTGAAA GTGAAGCCTTGTTG
Kelch codon adjust fw	CTGCTGCTGGTGGTGGAGGTGCAGGTAGAcctaggATGGAGG GTGAGAAGGTTAAGACTAAAG
Kelch codon adjust rv neu	CAGTATTGATTGCTAACATTTGAaggcctataacttcgtatagcatacattata cgaagtattataTGActcgaggatggcagctaatgttcgttttctattata
Kelch codon adjust seq fw	CAACGTAAACGACACATACGAG
Kelch codon adjust_Jakob seq_1595 fw	GCGGAGTAACCTCTAACGGAAGG
Sadelta260_C580Y_NEW_fw	gctatttagtgacactatagaataactcgcggccgcTAAACGTATGATAGGGAA TCTGGTGGTAACAGCAATAG
Sadelta260_C580Y_NEW_rv	CCTCTTCTGATATTAACCTTCTGCTCGTTTAAACTATTAATG TTCTTGATAAATTAATG

## Standard Oligonucleotides for sequencing

primer name	sequence
Crt fw	CCGTTAATAATAAATACACGCAGTC
FKBP 253 fw	TCACCAGATTATGCATACGGTG
FKBP 276 fw	CAGGCCATCCTGGCATCATC
FKBP 39 rv	TTGACCTCTTTTGGAAATGTACG
FKBP 82 rv	CTTCCATCTTCAAGCATTCCAG
GFP 272 as	CCTTCGGGCATGGCACTC
GFP 633 fw	GCCCTTTCGAAAGATCCC
GFP 85 rv	ACCTTCACCCTCTCCACTGAC
mCherry 620 fw	CTCCACAACGAGGACTACACC
mCherry 88 rv	GGCCGTTACGGAGCCCTCC
2xmyc-as	TAAATCTTCTCGCTTATGAG
2xmyc-sense	GAGCAGAAGTTAATATC
pArl sense 55	GGAATTGTGAGCGGATAACAATTCACACAGG
pARLminus rv	CAGTTATAAATACAATCAATTGG
SF3A2-5'UTR-955-fw	GTACATATATACATATAC

